Synthesis and Evaluation of Small Molecule Generators of Redox-Active Reactive Species

A thesis

Submitted in partial fulfillment of the requirements

of the degree of

Doctor of Philosophy

By

Vinayak S. Khodade

ID: 20113106

INDIAN INSTITUTE OF SCIENCE EDUCATION AND RESEARCH, PUNE

2016

Dedicated to…

My Parents

And

My Beloved Family

भारतीय विज्ञान शिक्षा एवं अनुसंधान संस्थान, पुणे
INDIAN INSTITUTE OF SCIENCE EDUCATION AND RESEARCH (IISER), PUNE
Autonomous Institution, Ministry of Human Resource Development, Govt. of India)
Dr. Homi Bhabha Road, Pashan, Pune – 411 008

Dr. Harinath Chakrapani
Associate Professor
Department of Chemistry,
IISER Pune

CERTIFICATE

Certified that, the work incorporated in the thesis entitled, "**Synthesis and Evaluation of Small Molecule Generators of Redox-Active Reactive Species**" submitted by **Vinayak S. Khodade** was carried out by the candidate, under my supervision. The work presented here or any part of it has not been included in any other thesis submitted previously for the award of any degree or diploma from any other University or institution.

Date: **Dr. Harinath Chakrapani**

(Research Advisor)

Fax: +91 20 2589 9790 • Ph: +91 20 2590 8090 • Email: harinath@iiserpune.ac.in

DECLARATION

I declare that this written submission represents my ideas in my own words and where others' ideas have been included; I have adequately cited and referenced the original sources. I also declare that I have adhered to all principles of academic honesty and integrity and have not misrepresented or fabricated or falsified any idea/data/fact/source in my submission. I understand that violation of the above will be cause for disciplinary action by the Institute and can also evoke penal action from the sources which have thus not been properly cited or from whom proper permission has not been taken when needed.

Date: **Vinayak S. Khodade**

Pune, India. **ID: 20113106**

Table of Contents

General Remarks

- ^{1}H NMR spectra were recorded on JEOL ECX 400 MHz spectrometer using tetramethylsilane (TMS) as an internal standard. Chemical shifts are expressed in ppm units downfield to TMS.
- ^{13}C NMR spectra were recorded on JEOL ECX 100 MHz spectrometer.
- Mass spectra were obtained using a HRMS-ESI-Q-Time of Flight LC-MS (Synapt G2, Waters) or MALDI TOF/TOF Analyser (Applied Biosystems 4800 Plus).
- FT-IR spectra were obtained using NICOLET 6700 FT-IR spectrophotometer as KBr disc or Bruker Alpha-FT-IR spectrometer and reported in cm^{-1}.
- All reactions were monitored by Thin-Layer Chromatography carried out on precoated Merck silica plates (F254, 0.25 mm thickness); compounds were visualized by UV light.
- All reactions were carried out under nitrogen or argon atmosphere with dry freshly prepared solvents under anhydrous conditions and yields refer to chromatographically homogenous materials unless otherwise stated.
- All evaporations were carried out under reduced pressure on Büchi and Heildoph rotary evaporator below 45 °C unless otherwise specified.
- Silica gel (60-120) and (100-200) mesh were used for column chromatography.
- Materials were obtained from commercial suppliers and were used without further purification.
- Semi-preparative HPLC purification was performed using high performance liquid chromatography (HPLC), Dionex ICS-3000 model.
- HPLC analysis data was obtained using Agilent Technologies 1260 Infinity, C18 (5 μm, 4.6 × 250 mm).
- NO was detected using Sievers Nitric Oxide Analyzer (NOA 280i).
- Spectrophotometric and fluorimetric measurements were performed using Thermo Scientific Varioscan microwell plate reader.
- Cyclic voltammetry (CV) analysis was performed using a Basi Epsilon-EC-Ver 2.00.71-USB Bioanalytical systems.

Abbreviations

ACN – Acetonitrile

AcOH – Acetic acid

Ac_2O – Acetic Anhydride

au – Arbitrary unit

bs – Broad singlet

^tBuOH – Tertiary-Butanol

$CDCl_3$ – Chloroform-D

$CHCl_3$ – Chloroform

CV – Cyclic Voltammetry

dd – Doublet of doublet

DCM – Dichloromethane

DMAP – *N*, *N*-Dimethylaminopyridine

DMF – *N*, *N*'-Dimethyl formamide

DMSO – Dimethyl Sulfoxide

DNA – Deoxyribonucleic acid

dt – doublet of triplet

DT-D – DT-Diaphorase

δ – Delta (in PPM)

E. coli – *Escherichia coli*

eq. – Equivalents

E_{Red} – Reduction Potential

ESI – Electron spray ionization

FACS – Fluorescence Activated Cell Sorting

g – Gram

GSH – Glutathione

h – Hours

H_2O – Water

HPLC – High Performance Liquid Chromatography

HRMS – High-Resolution Mass Spectrometry

Hz – Hertz

IC_{50} – Half maximal inhibitory concentration

IR – Infrared

J – Coupling constant

LB – Luria-Bertani

λ_{ex} – Excitation wavelength

λ_{em} – Emission wavelength

m – Multiplet

Me – Methyl

mg – Milligram

MIC – Minimum inhibitory concentration

min – Minutes

MHz – Megahertz

mL – millilitre

mM – Millimolar

mmol – millimoles

mp – Melting point

MALDI – Matrix-Assisted Laser Desorption Ionization

M. smeg – Mycobacterium Smegmatis

Mtb – Mycobacterium tuberculosis

MTT – 3-(4,5-Dimethylthiazol-2-yl)-2,5-Diphenyltetrazolium Bromide

μM – Micromolar

NADPH – Reduced nicotinamide-adenine-dinucleotide phosphate

$NaHCO_3$ – Sodium bicarbonate

$NaNO_2$ – Sodium nitrite

Na_2SO_4 – Sodium sulphate

NMR – Nuclear Magnetic Resonances

NO – Nitric oxide

NO_2^- – Nitrite

NO_3^- – Nitrate

NOA – Nitric Oxide Analyzer

NTR – Nitroreductase

OD – Optical density

$^{\bullet}OH$ – Hydroxyl radical

$O_2^{\bullet-}$ – Superoxide radical

$ONOO^-$ – Peroxynitrite

PBS – Phosphate Buffered Saline

Pd – Palladium

$Pd(PPh_3)_4$ – Tetrakis(triphenylphosphine)palladium(0)

pH – Potential of hydrogen

Ph – Phenyl

ppm – Parts per million

% – Percent

ROS – Reactive Oxygen Species

RT – Room temperature

s – Singlet

t – Triplet

THF – Tetrahydrofuran

TLC – Thin Layer Chromatography

TMS – Tetramethylsilane

TRIS – Tris(hydroxymethyl)aminomethane

μg – Microgram

μmol– Micromolar

μL – Microliter

Zn – Zinc

Acknowledgements

First and foremost, I would like to express my deepest and sincerest gratitude to my enthusiastic supervisor, Dr. Harinath Chakrapani. My PhD has been an amazing experience and I thank Harinath wholeheartedly, not only for his tremendous academic support, but also for giving me so many wonderful opportunities. He has been supportive since the days I began working in his lab. I admire his lessons on independent thinking, perfection, soft skills and many more, in shaping up the researcher in me. It is my great fortune to work in his group, and explore the most attractive field in chemistry under his guidance. I believe this experience will be unforgettable for my whole life.

I sincerely thank Prof. K. N. Ganesh, Director IISER-Pune for providing world class research facilities. Also, I am thankful to all the faculty members in the department of chemistry for providing their research facilities, interactive scientific discussions and teaching me various courses.

I am very grateful to my research advisory committee members Dr. S. K. Asha from National Chemical Laboratory, Pune and Dr. M. Jeganmohan from IISER, Pune for their valuable suggestions and feedback during RAC evaluations. I would like to acknowledge Dr. Srinivas Hotha and his group for their help during TLC-MS and LC-MS analysis. I would like to thank Dr. M. Jayakannan and his students for helping me to carryout fluorescence experiments.

I would like to thank our collaborator, Dr. Amit Singh and Prashant Shukla from IISc Bangalore for their efforts of studying the role of hydrogen sulfide in bacteria. I also thank Dr. Sidharth Chopra and Isha Soni from CDRI, Lucknow for providing anti-MRSA activity. I am also hugely appreciative to Dr. Kundan Sengupta from Department of Biology, IISER-Pune, who has helped me during our initial working days to carry out biological experiments. I must acknowledge his students Devika Ranade, Ayantica

Sengupta, and Apoorva Kulkarni for their supportive and helping nature. My special mention goes to our collaborator Dr. Radha Rangrajan, Vitas Pharma Hyderabad and Ankita Sengupta for helping us to setup the microbiology lab.

Words cannot suffice the deep gratitude I feel towards my lab mates for their love, help, support, suggestions, criticism and memorable moments given throughout my life at IISER. I take this opportunity to say my sincere thank to my seniors Dr. Satish Malwal, Dr. A. T. Dharmaraja and Dr. Kavita Sharma for their support and encouragement. I extend my sincere gratitude to my present lab mates Kundan Pardeshi, Ravikumar, Preeti Chauhan, Ajay Sharma, Amogh Kulkarni, Prerona Bora and Anand Kumar for their continuous support, patience and scientific discussions. Among the members, I got opportunities to work with Preeti, Ajay, Sharathchandra, Charu Jain, Sushama and Abhijeet. More than they learned from me, I benefitted a lot from them. I cannot forget the members those who worked for short duration in the lab but really helped me by their own way including Dr. Ritu Mamgain, Dr. Viraj Gala, Rohan Kumbhare and R. K. Sankar. “Dr. Harianth laboratory” will always remain an unforgettable episode in my entire life.

I want to thank Swati (MALDI-TOF), Nayana (HRMS), Deepali and Nitin (NMR) for their help. I am indebted to many other friends for providing a stimulating and fun filled environment in IISER Pune, especially, Rohan Yadav, Dinesh Chauhan, Trimbak Mete, Prabhakar Pawar, Pramod Sabale and all other friends. I am forever grateful to my Appa Niwas friends Babasaheb Dabhade, Sharad Dawange, Harshal Chaudhari and Pritish Wadage. I want to thank my friends Dhanaji Khodade, Yashwant Diwekar and Vaibhav Andhalkar for their support and encouragement. Thank you all for your friendship, stimulating advice, constructive criticism and positive outlook that played a pivotal role in shaping my life during these past five years.

It would have not possible for me to complete my doctoral work without the support from my family. I have highest gratitude to my father (Shahaji Khodade) and mother (Tarabai Khodade). It is due to their unconditional trust, timely encouragement, endless patience and unstinting sacrifice; I am able to reach this position. I am deeply indebted to my sister (Priyanka) and brother (Sachin) for their unconditional support and encouragement. I would like to acknowledge with tremendous and deep thank to my life partner, Ujwala. Through her untiring love, support, encouragement and unwavering belief in me, I have been able to complete this long dissertation journey. Thank you, Ujwala for always being my pillar, my joy and my guiding light.

I am thankful to Council of Scientific and Industrial Research (CSIR), Government of India for financial support during the course of PhD.

Vinayak S. Khodade

Abstract

Chemically reactive species derived from oxygen, nitrogen and sulfur are produced in nearly all living cells and play important roles in numerous physiological processes. Recently, several studies have demonstrated that reactive oxygen species (ROS), reactive nitrogen species (RNS) which includes peroxynitrite ($ONOO^-$) and hydrogen sulfide (H_2S) are involved in host-pathogen interaction and antibiotic action. However, the precise role of these redox-active reactive species in bacteria remains poorly characterized. This is, in part, due to transient nature of these reactive species. In order to study the precise role of these reactive species in bacteria, their reliable sources would be useful. Although numerous methodologies for generating ROS, $ONOO^-$ and H_2S have been reported, they are typically associated with various limitations such as poor cell permeability and lack of specificity. Here, we propose to design and develop small molecules that can reliably generate each of these reactive species independently within cells and study their roles in bacterial growth inhibition and antibiotic resistance.

First, in order to generate ROS within bacteria, a series of natural product-inspired benzo[*b*]phenanthridine-5,7,12-triones were synthesized and studied. These compounds were found to generate ROS only in the presence of a bioreductive enzyme and were capable of enhancing ROS in *Staphylococcus aureus* (*S. aureus*). Several ROS generators from this series showed moderate to potent inhibitory activity against drug-resistant strain of *S. aureus* suggesting that antibiotic resistance in certain bacteria can be targeted by perturbing bacterial redox-homeostasis.

Next, we designed and synthesized a bioreductively activated $ONOO^-$ generator, in which a superoxide generating 1,4-naphthoquinone scaffold is strategically linked to a diazeniumdiolate-based nitric oxide donor. Using an array of experiments, the ability of this small molecule to generate $ONOO^-$ upon reaction with a bioreductive enzyme was demonstrated. The superiority of this compound to enhance $ONOO^-$ levels in both cell-free as well as within cells was demonstrated. Our results support the utility of this compound to study the role of $ONOO^-$ in bacteria.

Lastly, in order to selectively generate H_2S within bacteria, bis(4-nitrobenzyl)sulfanes were designed and synthesized as nitroreductase (NTR) activated H_2S donors. These compounds were

found to be metabolized by NTR to produce H_2S. The suitability of these compounds to enhance H_2S levels in both Gram-positive as well as Gram-negative bacteria was demonstrated. The tools developed here are well suited to interrogate the role of H_2S in antibiotic resistance.

In summary, our results address important problems associated with site-specific delivery of ROS, $ONOO^-$ and H_2S within cells and we anticipate that these small molecules can be used as tools to understand the precise roles of these reactive species in antibiotic resistance.

Chapter 1: Introduction of Redox-active Reactive Species

1.1. Redox-active reactive species

Redox-active reactive species are chemically reactive molecules containing N, O and S with potential to alter redox homeostasis in cells. These reactive species are broadly classified into three categories namely reactive oxygen species (ROS), reactive nitrogen species (RNS) and reactive sulfur species (RSS) (Figure 1.1).[1] Historically, these reactive species were considered toxic due to their extremely high reactivity and off target effects, but recent studies demonstrated their importance in cell signaling pathways.[2-5] These species are produced endogenously during normal cellular functions as a response to various stimuli.[6] At moderate concentrations, they act as regulatory mediators in signaling processes. However, at elevated concentrations, these reactive species are hazardous for living organisms and can damage cellular constituents such as DNA, proteins and lipids. Hence, elevated levels of these reactive species have been implicated in various diseases including cancer, cardiovascular diseases and neurodegenerative disease.[7-8]

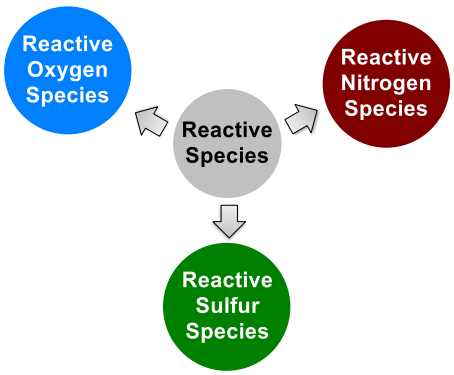

Figure 1.1. Classification of reactive species

1.1.1. Reactive oxygen species

ROS is a collective term that has been used for oxygen-derived free radicals such as superoxide ($O_2^{\bullet -}$), hydroxyl ($^{\bullet}OH$), peroxyl ($RO_2^{\bullet}$) and alkoxyl ($RO^{\bullet}$) radicals, as well as oxygen-derived non-radical species such as hydrogen peroxide (H_2O_2). In biological systems, ROS are constantly generated through a variety of pathways including both enzyme-catalyzed reactions and non-enzymatic reactions. The mitochondrial electron-transport chain (ETC) is the main source of ROS.[9] Leakage of electrons from mitochondrial ETC leads to partial reduction of molecular

oxygen to form $O_2^{\bullet-}$ (Scheme 1.1). It has been estimated that 0.2% to 2.0% of O_2 consumed by mitochondria generates $O_2^{\bullet-}$.[10-11]

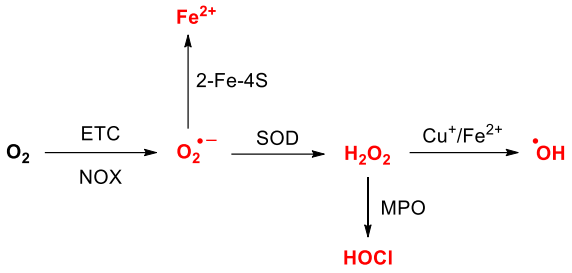

Scheme 1.1. ROS generation in biological system; ETC: electron transport chain, NOX: NADPH oxidase, SOD: superoxide dismutase, MPO: myeloperoxidase

Under physiological conditions, $O_2^{\bullet-}$ is dismutated into H_2O_2 by an enzyme superoxide dismutase.[12] The trace amount of metal ions such as copper (I) or iron (II) can react with H_2O_2 to form highly reactive $^{\bullet}OH$ (Scheme 1.1).[13] Furthermore, an enzyme myeloperoxidase catalyzes formation of HOCl from H_2O_2. Together, these reactive species at high concentrations can attack a diverse range of biological targets and exert cytotoxic effects.

1.1.2. Reactive Nitrogen species

RNS is a collective term that includes nitric oxide (NO), peroxynitrite ($ONOO^-$), nitroxyl (HNO), nitrogen dioxide radical ($NO_2^{\bullet}$) and other oxides of nitrogen.[14] Under biological system, NO is produced during metabolism of L-arginine to L-citrulline by nitric oxide synthase (NOS) (Scheme 1.2).[15]

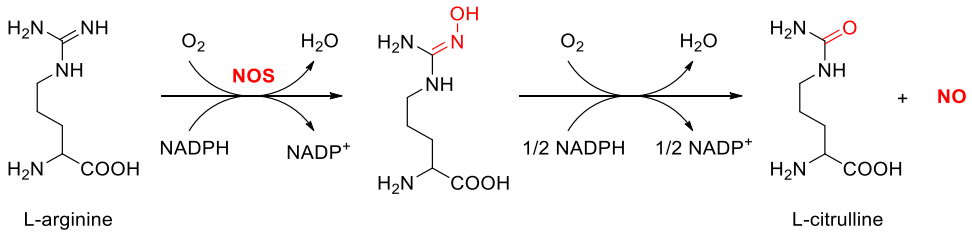

Scheme1.2. Biosynthesis of NO catalysed by NOS

The rapid reaction of NO with free radicals has been considered as major source of RNS. For example, NO can react with $O_2^{\bullet-}$ at diffusion-controlled rate (~1×10^{10} $M^{-1}s^{-1}$) to form peroxynitrite ($ONOO^-$), a short-lived RNS (Scheme 1.3).[16] Under biological system,

$ONOO^-$ rapidly reacts with carbon dioxide (under physiological conditions CO_2 exist in CO_3^{2-}) to form nitrosoperoxycarbonate ($ONOOCO_2^-$), which then rapidly decomposes to produce nitrogen dioxide radical ($^{\bullet}NO_2$) and carbonate radical ($CO_3^{\bullet-}$) (Scheme 1.3).[22]

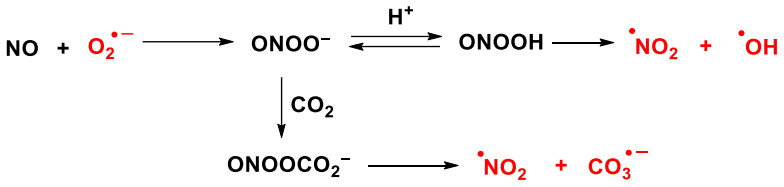

Scheme1.3. Generation of RNS from NO

In addition, $ONOO^-$ can undergo protonation to its conjugated acid peroxynitrous acid (ONOOH), which then undergoes homolytic cleavage to produce $^{\bullet}OH$ and $^{\bullet}NO_2$ (Scheme 1.3).[17] Furthermore, NO can undergo oxidation in the presence of oxygen to form N_2O_3, a powerful nitrosating agent. Under physiological conditions, N_2O_3 undergoes decomposition to form nitrosonium ion (NO^+), which can nitrosylate nucleophiles such as thiols, secondary amines and phenols.[18]

1.1.3. Reactive Sulfur Species

Likewise, oxygen and nitrogen forms ROS and RNS, sulfur can also form RSS.[19] Hydrogen sulfide (H_2S) is a prototypical example of RSS. Due to its ability to oxidize and reduce biomolecules, H_2S is recognized as redox-active RSS. It is endogenously produced from L-cysteine by two pyridoxal 5'-phosphate dependent-enzymes, cystathionine β-synthase (CBS) and cystathionine γ-lyase (CSE) (Scheme 1.4). Additionally, cysteine aminotransferase (CAT) and 3-mercaptopyruvate sulfurtransferase (3-MST) together generates H_2S.[20-34]

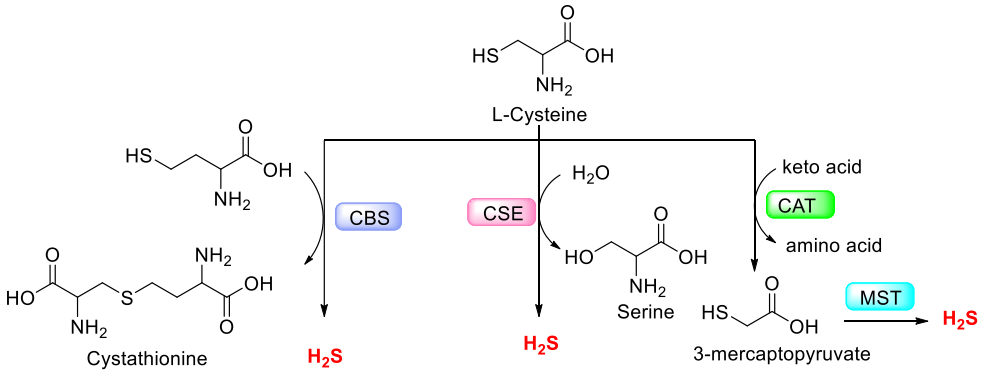

Scheme1.4. H_2S biosynthesis

Sulfur can exist in various oxidation states ranging from -2 to +6 and possibly including fractional oxidation states and this property of sulphur give rise to formation of various RSS upon reaction with ROS and RNS.[21] In thiolate form, sulfur undergoes oxidation with ROS to produce sulfenic acid (Scheme 1.5). This acid may be reduced into a disulfide by reaction with thiols or further oxidized to sulfinic acid by ROS (Scheme 1.5). Furthermore, ROS can react with thiol side chain of cysteine to form thiyl radical. This radical species can undergo oxidation with oxygen to produce sulfoxyl radical (Scheme1.5). Thiol residues of cysteine can also react with NO to form nitrososthiol. These chemically reactive forms of thiols are categorized into reactive sulfur species.

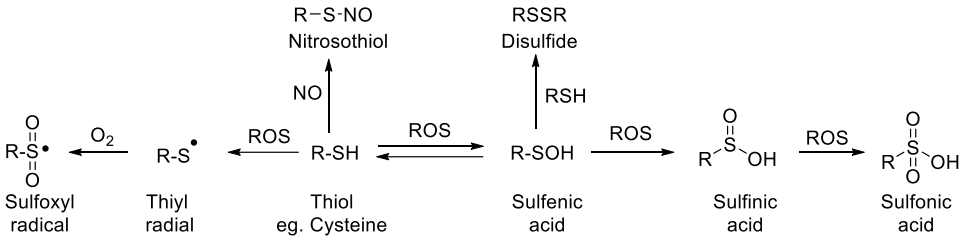

Scheme 1.5. Generation of various reactive sulfur species from a thiol

1.2. Reactive species in cell signaling

1.2.1. ROS in cell signaling

Traditionally, ROS were considered as toxic by-products of oxygen metabolism, but growing evidence indicates that controlled generation of ROS contributes to physiological intracellular signaling events.[3,22-23] ROS act as signaling molecules when present in low concentration.ROS mediated signaling occurs through oxidative modification of specific cysteine residues on proteins. Oxidation of cysteine residues leads to reversible modification of enzymatic activity. Furthermore, post-translational modifications of signaling proteins such as phosphorylation have been shown to be regulated in part through a redox-mediated mechanism. Thus, several *in vitro* and *in vivo* evidences demonstrate the importance of ROS mediated cell signaling for cellular homeostasis.

1.2.2. RNS in cell signaling

NO acts as a signaling molecule in diverse physiological functions ranging from vasodilation to immune response.[24-26] When NO is produced in low concentrations, it rapidly diffuses and reacts with biomolecules and exert cell regulatory effects. Many of the physiological functions

exhibited by NO are mediated by activation of soluble guanylate cyclase (sGC).[27-28] NO binds to iron in heme group of sGC and activates the enzyme whereby cyclic guanosine monophosphate (cGMP) is produced. cGMP is a secondary messenger and it activates cGMP-based protein kinases, phosphodiesterases and cyclic nucleotide gated ion channels.[29] However, when NO is produced in high concentrations, it can react with $O_2^{\bullet-}$ to produce $ONOO^-$. Due to strong oxidizing and nitrating ability of $ONOO^-$, it was only considered as a toxic molecule; recent studies have however demonstrated the importance of peroxynitrite-mediated signaling, which occurs at sub-lethal concentrations.[30-32] $ONOO^-$ regulates an array of signaling cascade by mechanism involving activation of many different protein kinases. For example, $ONOO^-$ mediated conversion of cGMP to 8-nitro-cyclic guanosine monophosphate (8-nitro-cGMP) has been reported to be involved in autophagy (Scheme 1.6).[33] Autophagy is a process in which cellular components undergo lysosomal degradation to eliminate defective and superfluous elements. Autophagy is also associated with the innate immune response to clear bacterial infections.

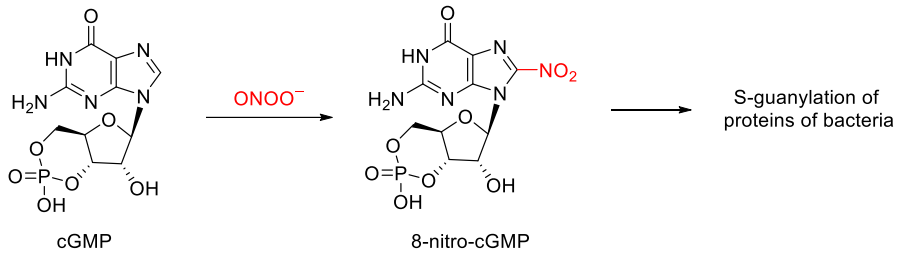

Scheme 1.6. $ONOO^-$ mediated nitration of cGMP to 8-nitro-cGMP during autophagy

Upon detection of invading pathogens, macrophage cell surface receptors initiate signaling process leading to generation of $O_2^{\bullet-}$ and NO, which then combine with each other to form $ONOO^-$. This reactive species nitrates cGMP to form 8-nitro-cGMP which then promotes S-guanylation of proteins at the bacterial cell surface escaping the phagosome in the cytosol and initiates Lys63-linked ubiquitination leading to the recruitment of the autophagic machinery.[30,34] After forming autophagosome, the entrapped bacteria are targeted to lysosomal degradation.

1.2.3. H_2S in cell signaling

H_2S is recognized as one of the three gasotransmitters in mammals along with NO and CO. It is involved in a myriad of cell signaling processes that trigger physiological events ranging from

vasodilation to cell proliferation.[35] One of the modes by which H_2S signals is by modification of cysteine residues on target proteins. It reacts with sulfhydryl group of cysteine and convert into –SSH group. This modified cysteine residue is highly reactive and increases the catalytic activity of targeted proteins. S-sulfydration in the proteins has been considered as common post-translational modification in H_2S biology.[36] H_2S activates K_{ATP} channel that regulate the dilation of blood vessels. Furthermore, sulfhydration of calcium-activated potassium channels (IK_{Ca}) and K_{ATP} channels by H_2S induces vasorelaxation in cells.[37]

1.3. Reactive species in redox-homeostasis

Redox–active reactive species also play important roles in maintaining cellular redox-homeostasis.[38] Under physiologic conditions, cells maintain redox balance through generation and elimination of ROS and RNS.[5] The balance between ROS generation and elimination is maintained by many complex mechanisms. ROS scavenging enzymes such as SOD, catalase, glutathione peroxidase and glutathione reductase scavenge elevated levels of ROS and/or RNS.[39-40] Furthermore, small antioxidant molecules such as GSH, ascorbic acid and vitamin E directly scavenge ROS.[41] However, an increase in ROS production or dysfunction of any of these antioxidant mechanisms can disrupt redox homeostasis, leading to an overall increase of intracellular ROS levels and can lead oxidative stress. Under oxidative stress, these reactive species can damage the important cellular constituents and ultimately leading to cell death. The toxic effect of these ROS and RNS are described in the following sections.

1.3.1. DNA damage

ROS can induce DNA damage leading to the single or double-strand breaks, base modifications, and DNA cross-linking.[42] ROS can react with both purine and pyrimidine bases and sugar backbone. Among the nucleobases, guanine is more susceptible to oxidative attack by ROS due to its low reduction potential.[43] Among ROS, $^{\bullet}OH$ is the principal ROS that targets the DNA. It can react with guanine to produces 8-hydroxy-guanine (Scheme 1.7). Similarly, $^{\bullet}OH$ can react with thymine to form thymine radical, which induces mutations in DNA. The oxidative damage to the sugar backbone, through proton abstraction has also been known to cause single and double-strand breaks (Scheme 1.7).

Similarly, NO and $ONOO^-$ can react with DNA bases and induces single and double-strand breaks.[44] $ONOO^-$ can react with is 8-oxoguanine (oxidized product of guanine) to produce

cyanuric acid and oxazolone. $ONOO^-$ can also nitrate guanine to from 8-nitroguanine which leads to formation of abasic sites. $ONOO^-$ may attack the sugar phosphate backbone by abstracting a hydrogen atom from the deoxyribose moiety, resulting in the opening of the sugar ring and the generation of DNA strand breaks.

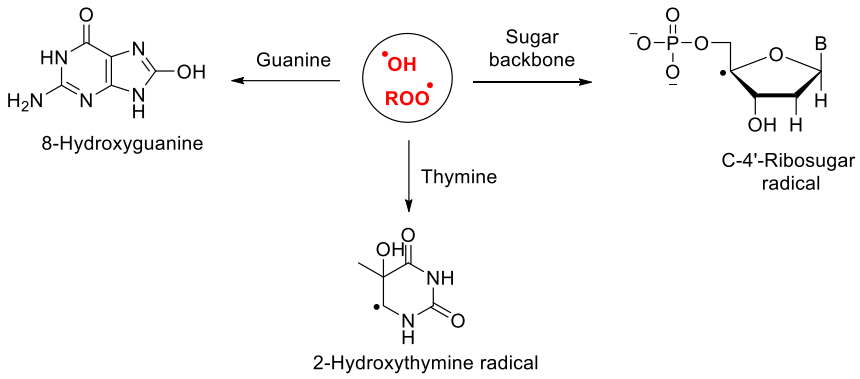

Scheme1.7. Oxidative DNA damage by ROS

1.3.2. Protein modification

ROS can mediate a diverse array of reversible and irreversible redox modification to proteins. Thiol side chain of cysteine residue in proteins is the most vanuerable target of ROS. The reaction of H_2O_2 with thiol of the cysteine containing proteins oxidizes to sulfenic acids. This in turn can undergo further oxidations by second and third equivalent of H_2O_2 to form sulfinic and then sulfonic acid. Furthermore, $^{\bullet}OH$ can also react with thiol containing amino acids such as cysteine and methionine which affects the protein structure and functions.[45-48]

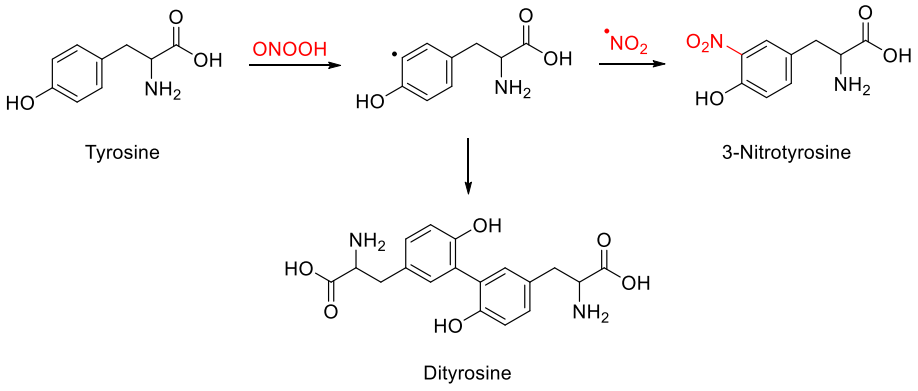

Scheme 1.8. Peroxynitrite mediated tyrosine nitration and dityrosine formation

Similar to ROS, $ONOO^-$ also modifies proteins structure and alters their function. For example, $ONOO^-$ can nitrate the tyrosine residues in the protein and alter its function (Scheme 1.8).[49-50]

Protein tyrosine nitration can result in dramatic changes in protein structure and can affect biological activity. Nitration of tyrosine residue may inhibit its phosphorylation or adenylation, important for protein function. Furthermore, peroxynitrite at lower concentration can mediate tyrosine dimerisation (Scheme 1.8). $ONOO^-$ can also oxidize methionine, tryptophan and histidine residues in proteins.[51] Furthermore, it can directly oxidize low molecular weight free thiol such as GSH.[52]

1.3.1. Lipid peroxidation

Lipids are most susceptible to attack by ROS and RNS. Hydroxy radical can abstract the proton from lipids to generate lipids radicals, which can further attack the subsequent lipid molecules and propagate as a chain reaction (Scheme 1.9).[53] The lipid peroxidation reaction leads to formation of many toxicological products such as malondialdehyde (MDA), 4-hydroxy-2-nonenal (4-HNE) and 2-alkenals. Furthermore, ROS reaction with polyunsaturated fatty acid residues of phospholipids can produce highly toxic ROS such as peroxyl radical, alkoxyl radicals and hydroperoxids.[54] Peroxidation of membrane lipids leads to loss of membrane fluidity and elasticity, impaired cellular functioning and even cell rupture.

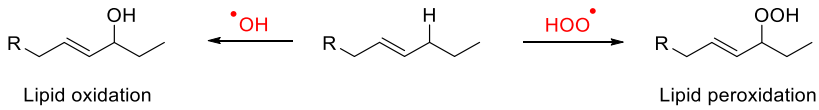

Scheme 1.9. Oxidative reactions of ROS with lipids

Thus, excessive ROS/RNS can attack lipids, proteins and DNA, leading to severe and irreversible oxidative damage, which ultimately lead to cell death. Therefore maintaining redox-balance is crucial for cellular homeostasis and survival.

1.4. Reactive species during immune response

Due to high reactivity of ROS/RNS, the mammalian immune system deploys these species during invasion by pathogens.[55-56] Immune cells such as macrophages and neutrophils engulf pathogens into phagosome, and then trigger a process called as respiratory burst. During this process, phagocytes elevate O_2 uptake, which triggers the recruitment of NADPH oxidase (NOX-2) in phagosome membrane. The active form of NOX-2 transfers electrons from cytosolic NADPH to O_2 to release $O_2^{\bullet -}$ in the phagosome (Figure 1.2).[57] Under acidic conditions of

phagosome, $O_2^{\bullet-}$ is rapidly dismutated into H_2O_2, which further reacts with metal ion such as Fe(II) by a Fenton reaction to from a highly reactive $^{\bullet}OH$. Furthermore, H_2O_2 can be converted into highly reactive ROS, HOCl by myeloperoxidase (Figure 1.2).[58] These reactive species reacts non-discriminately with contents of the phagosome and causes arrest the growth and multiplication of pathogens.

In addition to NOX2-dependent production of ROS, macrophages also produce RNS that can contribute to microbial killing. Macrophages activate inducible nitric oxide synthase (iNOS), which synthesize NO from L-arginine and NADPH (Figure 1.2).[59-60] NO is hydrophobic in nature as results, it can diffuse across the phagosome membrane to react with ROS.[61] As described earlier in section 1.1.2, NO can react with $O_2^{\bullet-}$ in a diffusion-controlled rate to form $ONOO^-$, a highly reactive nitrogen species (Figure 1.2). Furthermore, NO in luminal environment can undergo either spontaneous or catalytic conversion to a range of RNS such as $^{\bullet}NO_2$, N_2O_3, dinitrosyl iron complexes, nitrosothiols and nitroxyl (HNO).[62] Together, these reactive species interact with microbial targets such as nucleic acids, proteins, lipids and thiols. The oxidative damage to biomolecules impairs their functions and ultimately leads to pathogen death.

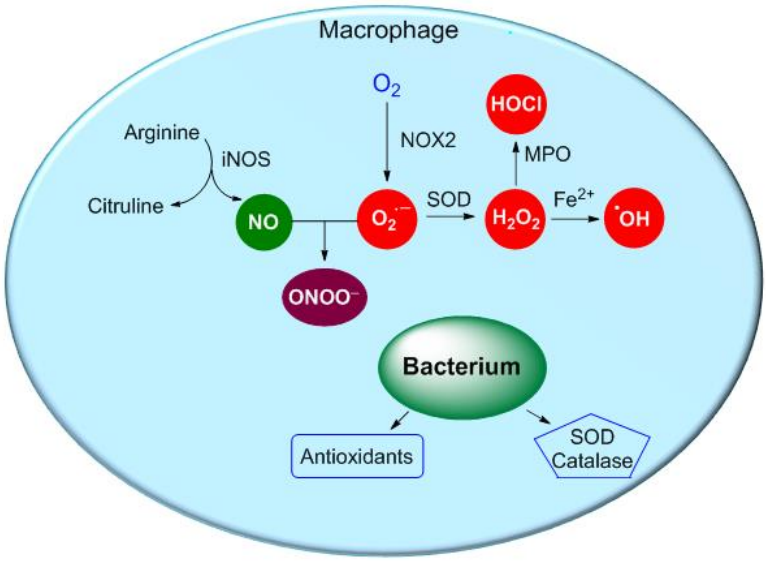

Figure 1.2. ROS/RNS generation during phagocytosis and defensive mechanism of microorganism

Although most of the bacteria are successfully internalized and eliminated by phagocytes, certain bacteria have developed survival strategies that interfere with the internalization and phagosome

maturation process.[63] For example, *Mycobacterium tuberculosis* survives within macrophages by arresting phagosomal maturation. Bacteria also produce several antioxidants that scavenge these reactive species and reduce their cytotoxic effects. Additionally, bacteria counter the phagocytes mediated oxidative and nitrosative stress by expressing ROS/RNS detoxifying enzymes such as SOD, catalase and peroxiredoxins (Figure 1.2).[64] Furthermore, bacteria protect from the cytotoxic effects of antimicrobial peptides by actively degrading these peptides. In this way, bacteria use one or more of these protective mechanisms to survive and replicate inside phagocytes, which results into infections.

1.5. Antibiotic resistance

In order to overcome these infections, several antibiotics were developed and these infections were successfully treated. However, due to misuse and overuse of antibiotics, bacteria have developed resistance to these antibiotics. For example, staphylococcal infections were successfully treated using penicillin in 1940s. However, in the late 1940s and 1950s, *Staphylococcus aureus* (*S. aureus*) developed resistance to penicillin. In order to treat these penicillin-resistant strains of *S. aureus*, methicillin was introduced. However, in 1961, the first strain of methicillin resistant *S. aureus* (MRSA) was observed.[65] Vancomycin was then introduced into clinical practice for the treatment of MRSA infections but cases of vancomycin resistant *S. aureus* (VRSA) were also reported (Figure 1.3). The emergence of resistance to vancomycin has now become a major concern for global public health.[66-67]

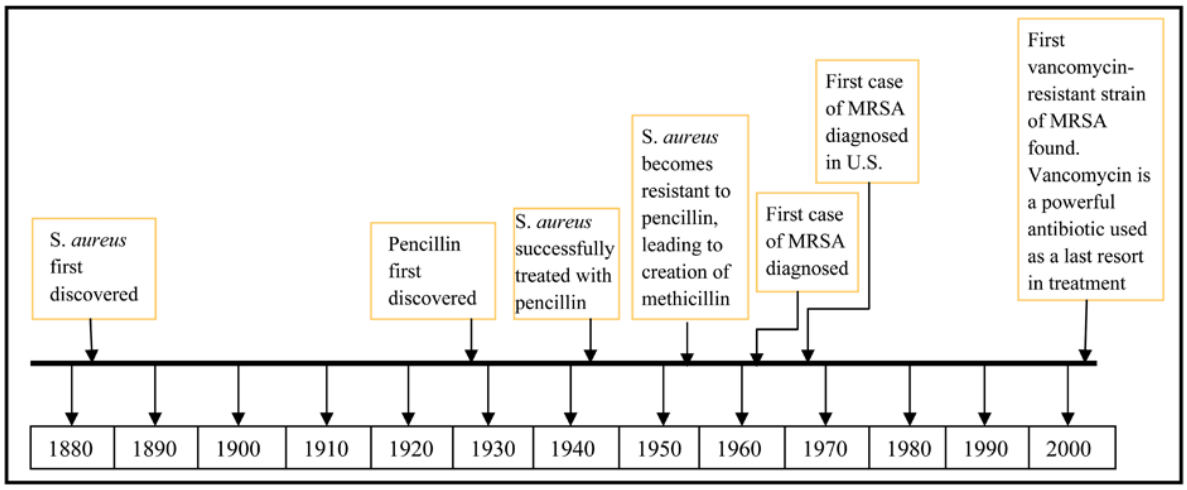

Figure 1.3. Timeline of MRSA (Figure adapted from Angles 2009, Combating Methicillin-Resistant *Staphylococcus aureus*)

Therefore, there is an urgent need of synthesis of new classes of antibiotics and finding new cellular targets. The traditional antibiotic drug discovery has been relied on the modification of existing antibiotics. However this strategy is not very successful because only two new classes of antibiotics (oxazolidinone and lipopeptides) were developed in the last decade for clinical application. These results indicate that the success rate of discovering new antibiotics using conventional approaches is limited and we have to reconsider our antibiotic discovery approaches.

1.6. Strategies to combat MRSA

Traditional approaches to combat bacterial infection were primarily rely on the disruption of bacterial growth cycle by preventing the synthesis of key components of bacterial processes such as cell wall synthesis, DNA replication and protein synthesis. Although these strategies were highly effective, they resulted in selective pressure with antimicrobial resistance as an inevitable consequence of their use. Therefore, there is an urgent need to identify novel antibacterial targets and develop new agents effective against multi-resistant strains that do not rapidly succumb to resistance. The following section provides an overview of some of the current approaches being used to develop alternative antimicrobial therapies to combat MRSA infections.

1.6.1. Quorum sensing and development of its inhibitors

Quorum sensing (QS) is a process of cell-to-cell communication that allows bacteria to share information about cell density and adjust gene expression accordingly.[68] Staphylococci have developed quorum-sensing systems that enable cell-to-cell communication in order to improve their ability to cause variety of human disease. Quorum sensing involves the production, detection and response to extracellular signaling molecules called autoinducers (AIs).[69] AIs accumulate in the environment as the bacterial population density increases and bacteria monitor this information to track changes in their cell numbers and collectively alter gene expression. Quorum sensing controls genes that direct activities that are beneficial.

1.6.2. Mechanism of quorum sensing in *S. aureus*

Staphylococcus aureus uses a canonical two-component QS system encoded by the accessory gene regulator (*agr*) locus. The expression of *agr* was found to contribute to staphylococcal pathogenesis in several infection models.[70] The *agr* locus is composed of two divergent transcripts, RNAII (encoding *agrB, agrD, agrC* and *agrA*) and RNAIII, which act to suppress

cell wall-associated protein production and enhance secreted exoprotein production in response to high cell density. The AgrD synthesizes autoinducing peptide (AIP) as a precursor, which then processed by the AgrB to mature AIP and transported it out of the cell (Figure 1.4). When the AIP accumulates in extracellular medium, it binds to membrane-bound histidine kinase AgrC, which autophosphorylates at a conserved histidine and transfers the phosphate group to an aspartate on the response regulator AgrA (Figure 1.4). Phosphorylated AgrA binds upstream of P2 promoter to autoinduce *agr* operon. In addition to activating the P2 promoter, phosphorylated AgrA also activates the divergently encoded P3 promoter. The P3 promoter controls expression of RNAIII. The RNAIII post-transcriptionally activates virulence factor production. Most of the effects of QS on regulation of virulence in *S. aureus* are mediated through direct and indirect regulation by RNAIII.[70]

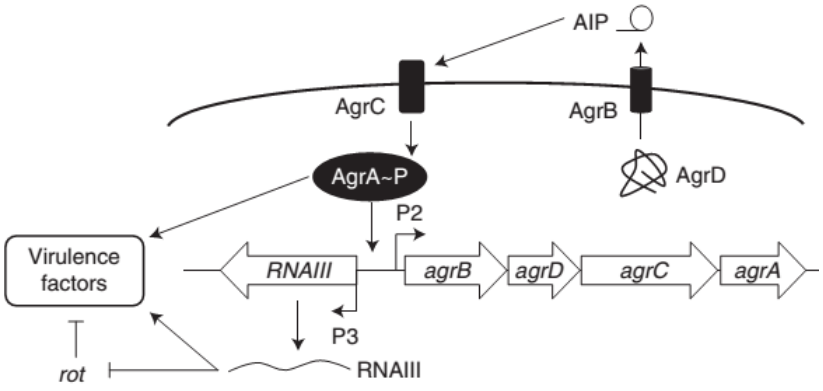

Figure 1.4. *S. aureus* Agr QS system (Figure adapted from *Cold Spring Harb. Perspect. Med.* **2012**, *2*, a012427)

1.6.3. Quorum sensing inhibitors

Recently, compounds that inhibit quorum sensing have received considerable attention as a potentially novel class of antimicrobial agents.[71-72] Pharmacologic inhibition of quorum sensing is a particularly attractive approach for the prevention or treatment of chronic infections with high bacterial cell density. It has been hypothesized that the development of resistance to these quorum sensing inhibitors would be minimized, because they would target virulence mechanisms and not growth.[73] Potential strategies to inhibit quorum sensing include inhibiting receptor function, reducing production or release of functional autoinducer, stimulating autoinducer degradation or inhibiting autoinducer-receptor binding. In the past decade, the scientific research

has focused on the synthesis and characterization of autoinducer analogs as QS inhibitors. Several synthetic and natural product small molecule analogues such as savirin, benzbromarone and a benzo-1,4-dioxane analogue (Figure 1.5) have shown inhibitory activity against *agr*.[74] These compounds were identified from extensive random screening programs and each inhibits AIP-induced production of RNAIII transcripts and thus virulence factors such as α-hemolysin and lipase. Savirin has been reported to prevent the development of dermonecrotic ulcers following infection with *agr* bacteria in an experimental mouse model of skin and soft tissue infection. Benzbromarone has been reported to reduce abscess formation in mouse models and provided protection against *agr*II and *agr*III *S. aureus* infection.

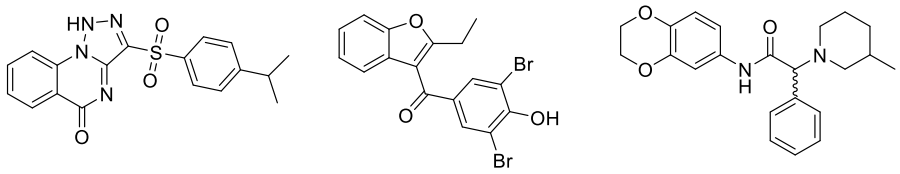

Figure 1.5. Structures of the small molecule *agr* inhibitors

Although quorum sensing inhibitors have proven to be active antipathogenic agents *in vitro* and in several *in vivo* models, it is still unknown whether these compounds will be useful in humans. Furthermore, several fundamental mechanisms by which the different QS systems in *Staphylococcus spp*. exert their regulatory functions and how they are inhibited by QSIs are still poorly understood.

1.6.4. Anti-virulence strategies

In the recent years, there is a growing body of evidence indicating that inhibiting virulence factor production can significantly attenuate infection.[75] Antivirulence agents do not kill bacteria as antibiotics do but inhibit the production of disease-causing virulence factors and toxins. These agents interfere with the ability of the bacteria to recognize host signals that alert the bacteria that they are at the site of infection and activate specific virulence factors that are needed to establish infection.[76] By preventing the expression of virulence, the bacteria are less able to colonize in the host. As this strategy does not directly kill the bacteria, there is presumably less evolutionary pressure for the development of resistant clones than with traditional antibiotics. In addition, a boost in the form of a low-dose conventional antibiotic in combination with an antivirulence agent may become successful strategy against more invasive infections.

Bacteria use an array of virulence factors to cause disease in the human host. These factors include adhesins, which bind to host cells and facilitate colonization; toxins, which kill or change signal transduction in mammalian cells; and specialized secretion systems to deliver effectors. Virulence factor production in *S. aureus* is regulated by a quorum-sensing mechanism, predominantly under the control of the accessory gene regulator (*agr*) operon.[77-78] The *agr* operon is the most important operon for virulence. Inhibition of the *agr* system by small molecules has been considered as important antivirulence strategy.[73]

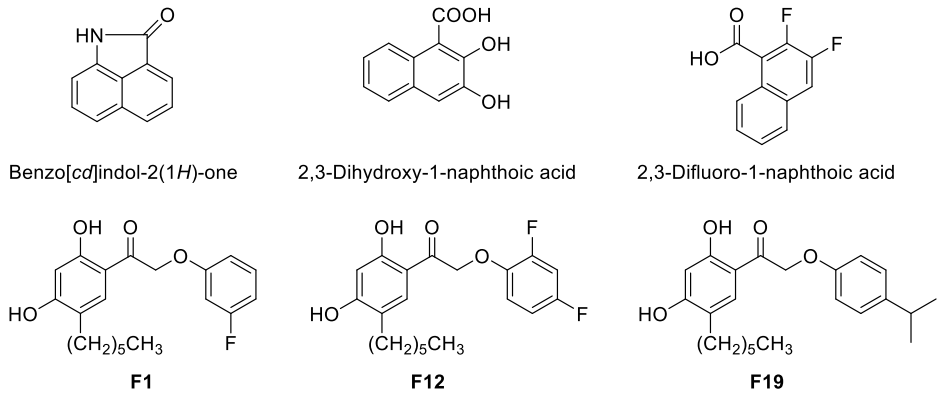

Figure 1.6. Chemical structures of antivirulence agents against MRSA

Recently, Viswanathan and coworker have developed small-molecule biaryl hydroxyketone compounds (Figure 1.6) that target response regulator AgrA and inhibit its interaction with promoter P3, inhibiting the production of toxins and virulence factors.[79] Based on the most efficacious compound, a series of biaryl hydroxyketones were synthesized and F12 was identified as the most efficacious antivirulence agent. F12 demonstrated 98% MRSA rabbit erythrocyte hemolysis inhibition at a concentration of 1 μg/ml.[80] Topical therapy of compounds F1 and F12 in a MRSA murine wound infection model promoted wound healing. F1, F12 and F19 also showed significant survival benefits in a MRSA insect larva model.[81] The combination therapy of these quorum-quenching agents with cephalothin has shown additional survival benefits. Furthermore, these QS inhibitors have been found to sensitize MRSA to β-lactam antibiotics.

Although it is assumed that anti-virulence drugs will produce a milder evolutionary pressure for the development of antimicrobial resistance, it is unlikely that resistance will not develop over time. The rapid rate of bacterial evolution enables a pathogen to change to an alternative route to

the one being targeted to achieve infection. Furthermore, as none of these anti-virulence strategies has been applied in a broad-scale clinical trial, it is difficult to determine the potential side effects.

1.7. Redox-active reactive species and antibiotic resistance

Recently, several studies have demonstrated that redox-active reactive species plays crucial role in either antibiotic mediated bacterial cell death or protection of bacteria from antibiotics. The following sections describe various roles of these redox-active reactive species in antibiotics action and bacterial responses to antibiotics.

1.7.1. ROS in antibiotic action

Recent studies have demonstrated that ROS play important role in antibiotic action. For example, Kohanski *et al*. proposed that oxidative stress is a common contributing factor to antibiotic toxicity, in addition to their primary targets. They have demonstrated that bactericidal antibiotics induce highly deleterious $^{\bullet}OH$ formation in bacteria, which ultimately contribute to bacterial cell death (Figure 1.7).[82] Although this view has been challenged by few independent researchers,[83-84] extensive body of evidence indicates that metabolic perturbations resulting from the interactions of antibiotics with their targets contribute to antibiotic lethality through generation of ROS and other toxic molecules.

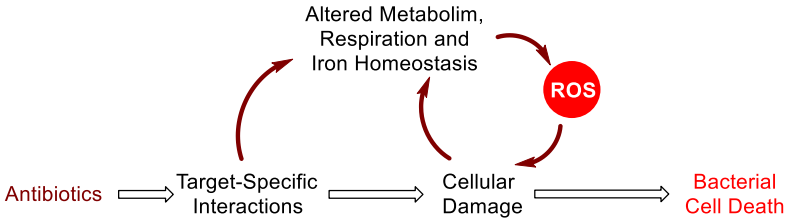

Figure 1.7. Bactericidal antibiotics interactions with their target trigger stress responses that induce redox-related physiological alterations resulting in the formation of ROS, which further contribute to cellular damage and death.

Independent evidence that support the hypothesis of ROS generation during antibiotic actions was demonstrated by Shen *et al*. in *S. aureus* upon treatment with fosfomycin, a broad-spectrum antibacterial agent. Using hydroxyphenyl fluorescein (HPF), they have demonstrated that treatment of *S. aureus* with fosfomycin results in the generation of $^{\bullet}OH$. Fosfomycin also enhances the activity of neutrophils by inducing NOX-2 that leads to generation of ROS such as

$O_2^{\bullet-}$ and H_2O_2. Furthermore, recent work by Hwang *et al*. showed that oxidative stress induced by silver ion enhances the lethality of ampicillin and kanamycin suggesting the synergetic effects of ROS with antibiotics. Thus, these studies demonstrate the importance of ROS during antibiotic mediated bacterial cell death.

1.7.2. NO as cytoprotective against antibiotics

During past two decades, NO has been recognized as one of the most versatile players in the immune system for controlling infectious diseases. Upon engulfing invading pathogens by the innate immune cells, inducible nitric oxide synthase (iNOS) produces flux of NO, which then rapidly reacts with ROS to produce highly reactive RNS. These reactive species causes an upsurge in oxidative and nitrosative stress within pathogens and induce cytotoxic effects. In contrast, recent studies demonstrate that endogenously produced NO in bacteria have cytoprotective role against oxidative stress and antibiotics.[85-86] Bacterial NOS (bNOS) generate NO inside bacteria upon exposure of antibiotics or attack by immune cells. In 2005, Shatalin and coworkers have showed that that bacterial NO production in *Bacillus antracis* (*B. anthracis*) is crucial for survival in macrophages during the initial hours post infection. Furthermore, NO generated in *B. anthracis* can act as virulence factor by *S*-nitrosylating host proteins leading to macrophage death.[87] NO produced in *Bacillus subtilis* and *S. aureus* also protects against killing by H_2O_2. In addition, recently it has been demonstrated that bNOS deficient strains of MRSA were less virulent and more sensitive to vancomycin, suggesting the role of this gaseous molecule in antibiotic resistance.

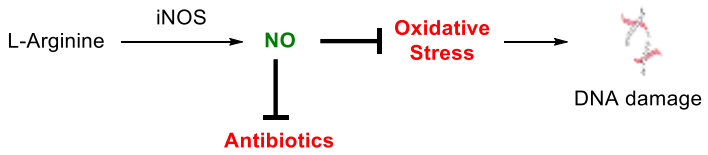

Figure 1.8. Bacterial NO protect the cell from ROS and antibiotics

Thus, the aforementioned results demonstrate the importance of endogenous NO during protection of bacteria from the oxidative stress and antibiotics (Figure 1.8). However, the cytoprotective role of bacterial NO appears controversial because NO in the presence of ROS is known to produce $ONOO^-$, which is highly deleterious species. Therefore, studying bacterial

response to $ONOO^-$ during antibiotic mediated cell death would be useful for understanding the role of this reactive species in antibiotic resistance.

1.7.3. H_2S, a universal defense against antibiotics

Recently, Shatalin *et al*. have demonstrated that endogenously produced H_2S in bacteria serves as a universal defense against antibiotics by attenuating oxidative stress.[88] They showed H_2S generation in four clinically relevant bacteria, namely *E. coli, S. aureus, B. anthracis,* and *P. aeruginosa* and inhibition of H_2S biosynthesis enzymes using chemical inhibitors as well as mutant strains that deficient in H_2S biosynthesis enzymes resulted in suppression of H_2S production. Furthermore, the mutant strains that are deficient in H_2S biosynthesis enzymes were more sensitive to antibiotics than wild type. However, an addition of NaHS (H_2S source) suppressed the antibiotic sensitivity. Similarly, H_2S biosynthesis enzyme deficient strains were more sensitive to H_2O_2 than wild type. In addition, ROS detoxifying ability of 3MST mutant strain of *E. coli* was reduced.

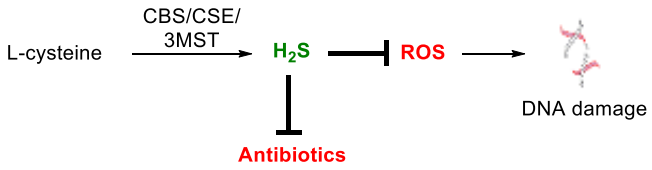

Figure 1.9. Bacterial H_2S protect the cell from ROS and antibiotics

These results demonstrate the importance of endogenous H_2S during protection from oxidative stress and antibiotic (Figure 1.9) and suggests the involvement of this gaseous molecule in antibiotic resistance.[89]

1.8. Direction of Research

The aforementioned sections describe the importance of redox-active reactive species in antibiotic action possibly through induction of oxidative stress or protection of bacteria by deploying bacterial NO and H_2S (Figure 1.10).[89] These studies indicate that the cross-talk among NO, H_2S and ROS plays critical role during antibiotics action and protection of bacteria from oxidative stress induced by antibiotics, which might be linked to resistance. However, cross-talk among these reactive species is not well understood, in part, due to their transient nature under biological system. Therefore, deeper understanding of these redox-active reactive species in bacterial response to antibiotics would be useful for designing new strategies to manage bacterial infections. In order to precisely study the role of these reactive species in bacteria, their reliable sources that can independently generate each of these reactive species are required. Although numerous methodologies for generating ROS, NO, $ONOO^-$ and H_2S have been reported, they are associated with certain limitations such as poor cell permeability, lack of specificity and lack of controlled generation. Therefore, we propose to design and develop new donors of ROS, $ONOO^-$ and H_2S that can independently generate each of these reactive species in bacteria and study their roles in antimicrobial resistance.

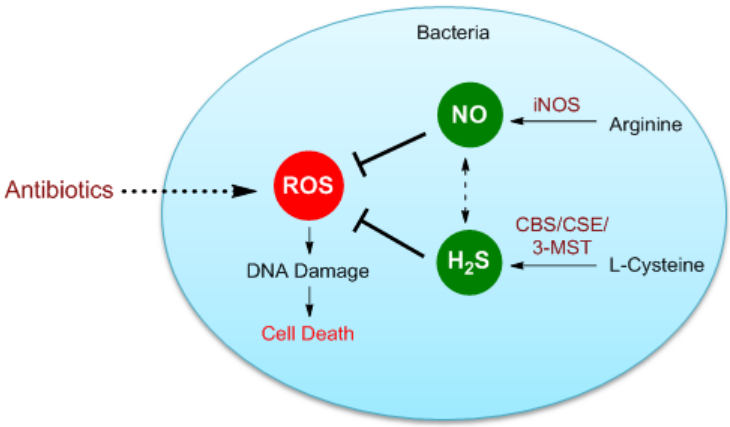

Figure 1.10. ROS generation during antibiotic action and bacterial protection from oxidative stress by producing H_2S and NO

This thesis contains four chapters. In Chapter 1, we describe an overview of redox-active reactive species and their various biological roles.

In chapter 2.1, we present design and synthesis of natural product-inspired benzo[*b*]phenanthridine-5,7,12-triones as bioreductively activated ROS generators. The ability of these redox-active compounds to inhibit the growth of *S. aureus* has also been described. In Chapter 2.2, we describe the structure-activity relationship studies of benzo[*b*]phenanthridine-5,7,12-trione for improving selectivity index and increasing aqueous solubility of lead compound.

In Chapter 3, we present design and synthesis of a novel small molecule that generates concurrent flux of NO and $O_2^{\bullet-}$ upon bioreduction. The ability of this small molecule to generate peroxynitrite in both cell-free as well as in cells is presented.

Lastly, in chapter 4, we present synthesis and evaluation of nitroreductase activated H_2S donors that selectively enhance H_2S levels in bacteria and not in macrophages.

Altogether, the results presented in this thesis address important problems associated with site-specific generation of redox-active reactive species. Also, these approaches may be used as tools to study roles of these reactive species in antibiotic resistance.

References

(1) Lü, J.-M.; Lin, P. H.; Yao, Q.; Chen, C. *J. Cell. Mol. Med.* **2010**, *14*, 840.

(2) Rhee, S. G. *Science* **2006**, *312*, 1882.

(3) Finkel, T. *J. Cell Biol.* **2011**, *194*, 7.

(4) dickinson, B. C.; Chang, C. J. *Nat. Chem. Biol.* **2011**, *7*, 504.

(5) Kamata, H.; Hirata, H. *Cell. Signal.* **1999**, *11*, 1.

(6) Schieber, M.; Chandel, Navdeep S. *Curr. Biol.*, *24*, R453.

(7) Pham-Huy, L. A.; He, H.; Pham-Huy, C. *Int. J. Biomed. Sci.* **2008**, *4*, 89.

(8) Uttara, B.; Singh, A. V.; Zamboni, P.; Mahajan, R. T. *Curr. Neuropharmacol.* **2009**, *7*, 65.

(9) Turrens, J. F. *J. Physiol.* **2003**, *552*, 335.

(10) Quinlan, C. L.; Perevoshchikova, I. V.; Hey-Mogensen, M.; Orr, A. L.; Brand, M. D. *Redox Biol.* **2013**, *1*, 304.

(11) Saybaşili, H.; Yüksel, M.; Haklar, G.; Yalçin, A. S. *Antioxid. Redox Signal.* **2001**, *3*, 1099.

(12) Faraci, F. M.; Didion, S. P. *Arterioscler. Thromb. Vasc. Biol.* **2004**, *24*, 1367.

(13) Goldstein, S.; Meyerstein, D.; Czapski, G. *Free Radic. Biol. Med.* **1993**, *15*, 435.

(14) Patel, R. P.; McAndrew, J.; Sellak, H.; White, C. R.; Jo, H.; Freeman, B. A.; Darley-Usmar, V. M. *Biochim. Biophys. Acta* **1999**, *1411*, 385.

(15) Griffith, O. W.; Stuehr, D. J. *Annu. Rev. Physiol.* **1995**, *57*, 707.

(16) Beckman, J. S.; Beckman, T. W.; Chen, J.; Marshall, P. A.; Freeman, B. A. *Proc. Natl. Acad. Sci. USA* **1990**, *87*, 1620.

(17) Szabo, C.; Ischiropoulos, H.; Radi, R. *Nat. Rev. Drug. Discov.* **2007**, *6*, 662.

(18) Brown, G. C.; Borutaite, V. *Biochem. Soc. Trans.* **2006**, *34*, 953.

(19) Gruhlke, M. C. H.; Slusarenko, A. J. *Plant Physiol. Biochem.* **2012**, *59*, 98.

(20) Kolluru, G. K.; Shen, X.; Bir, S. C.; Kevil, C. G. *Nitric Oxide* **2013**, *35*, 5.

(21) Paulsen, C. E.; Carroll, K. S. *Chem. Rev.* **2013**, *113*, 4633.

(22) D'Autreaux, B.; Toledano, M. B. *Nat. Rev. Mol. Cell. Biol.* **2007**, *8*, 813.

(23) Ray, P. D.; Huang, B.-W.; Tsuji, Y. *Cell. Signal.* **2012**, *24*, 981.

(24) Bogdan, C. *Nat Immunol.* **2001**, *2*, 907.

(25) Massion, P. B.; Feron, O.; Dessy, C.; Balligand, J.-L. *Circ. Res.* **2003**, *93*, 388.

(26) Rosselli, M.; Keller, R.; Dubey, R. *Hum. Reprod. Update* **1998**, *4*, 3.

(27) Bellamy, T. C.; Wood, J.; Garthwaite, J. *Proc. Natl. Acad. Sci. USA* **2002**, *99*, 507.

(28) Friebe, A.; Koesling, D. *Circ. Res.* **2003**, *93*, 96.

(29) Francis, S. H.; Busch, J. L.; Corbin, J. D. *Pharmacol. Rev.* **2010**, *62*, 525.

(30) Sawa, T.; Zaki, M. H.; Okamoto, T.; Akuta, T.; Tokutomi, Y.; Kim-Mitsuyama, S.; Ihara, H.; Kobayashi, A.; Yamamoto, M.; Fujii, S.; Arimoto, H.; Akaike, T. *Nat. Chem. Biol.* **2007**, *3*, 727.

(31) Ito, C.; Saito, Y.; Nozawa, T.; Fujii, S.; Sawa, T.; Inoue, H.; Matsunaga, T.; Khan, S.; Akashi, S.; Hashimoto, R.; Aikawa, C.; Takahashi, E.; Sagara, H.; Komatsu, M.; Tanaka, K.; Akaike, T.; Nakagawa, I.; Arimoto, H. *Mol. Cell* **2013**, *52*, 794.

(32) Akaike, T.; Nishida, M.; Fujii, S. *J. Biochem.* **2013**, *153*, 131.

(33) Rawet-Slobodkin, M.; Elazar, Z. *Mol. Cell* **2013**, *52*, 767.

(34) Jain, A.; Lamark, T.; Sjøttem, E.; Bowitz Larsen, K.; Atesoh Awuh, J.; Øvervatn, A.; McMahon, M.; Hayes, J. D.; Johansen, T. *J. Biol. Chem.* **2010**, *285*, 22576.

(35) Li, L.; Rose, P.; Moore, P. K. *Annu. Rev. Pharmacol. Toxicol.* **2011**, *51*, 169.

(36) Paul, B. D.; Snyder, S. H. *Nat. Rev. Mol. Cell Biol.* **2012**, *13*, 499.

(37) Mustafa, A. K.; Sikka, G.; Gazi, S. K.; Steppan, J.; Jung, S. M.; Bhunia, A. K.; Barodka, V. M.; Gazi, F. K.; Barrow, R. K.; Wang, R.; Amzel, L. M.; Berkowitz, D. E.; Snyder, S. H. *Circ. Res.* **2011**, *109*, 1259.

(38) Trachootham, D.; Lu, W.; Ogasawara, M. A.; Valle, N. R.-D.; Huang, P. *Antioxid. Redox Signal.* **2008**, *10*, 1343.

(39) Valko, M.; Rhodes, C. J.; Moncol, J.; Izakovic, M.; Mazur, M. *Chem. Biol. Interact.* **2006**, *160*, 1.

(40) Brigelius-Flohé, R. In *Biol. Chem.* **2006**; Vol. 387, p 1329.

(41) Galano, A.; Alvarez-Idaboy, J. R. *RSC Adv.* **2011**, *1*, 1763.

(42) COOKE, M. S.; EVANS, M. D.; DIZDAROGLU, M.; LUNEC, J. *FASEB J.* **2003**, *17*, 1195.

(43) Kawanishi, S.; Hiraku, Y.; Oikawa, S. *Mutat. Res.* **2001**, *488*, 65.

(44) Inoue, S.; Kawanishi, S. *FEBS Lett.* **1995**, *371*, 86.

(45) Finkel, T.; Holbrook, N. J. *Nature* **2000**, *408*, 239.

(46) Imlay, J. A. *Nat. Rev. Microbiol.* **2013**, *11*, 443.

(47) Winterbourn, C. C. *Nat. Chem. Biol.* **2008**, *4*, 278.

(48) Stadtman, E. R. *Free Radic. Res.* **2006**, *40*, 1250.

(49) Gunaydin, H.; Houk, K. N. *Chem. Res. Toxicol.* **2009**, *22*, 894.

(50) Sawa, T.; Akaike, T.; Maeda, H. *J. Biol. Chem.* **2000**, *275*, 32467.

(51) Alvarez, B.; Ferrer-Sueta, G.; Freeman, B. A.; Radi, R. *J. Biol. Chem.* **1999**, *274*, 842.

(52) Quijano, C.; Alvarez, B.; Gatti, R. M.; Augusto, O.; Radi, R. *Biochem. J.* **1997**, *322*, 167.

(53) Girotti, A. W. *J. Lipid Res.* **1998**, *39*, 1529.

(54) Zhong, H.; Yin, H. *Redox Biol.* **2015**, *4*, 193.

(55) Fang, F. C. *mBio.* **2011**, *2*, e00141.

(56) Flannagan, R. S.; Cosio, G.; Grinstein, S. *Nat. Rev. Microbiol.* **2009**, *7*, 355.

(57) Quinn, M. T.; Gauss, K. A. *J. Leukoc. Biol.* **2004**, *76*, 760.

(58) Lau, Y. L.; Chan, G. C. F.; Ha, S. Y.; Hui, Y. F.; Yuen, K. Y. *Clin. Infect. Dis.* **1998**, *26*, 226.

(59) Bogdan, C.; Röllinghoff, M.; Diefenbach, A. *Immunol. Rev.* **2000**, *173*, 17.

(60) Bermudez, L. E. *Clin. Exp. Immunol.* **1993**, *91*, 277.

(61) Webb, J. L.; Harvey, M. W.; Holden, D. W.; Evans, T. J. *Infect. Immun.* **2001**, *69*, 6391.

(62) Fang, F. C. *Nat. Rev. Microbiol.* **2004**, *2*, 820.

(63) Garrity-Ryan, L.; Kazmierczak, B.; Kowal, R.; Comolli, J.; Hauser, A.; Engel, J. N. *Infect. Immun.* **2000**, *68*, 7100.

(64) John, G. S.; Brot, N.; Ruan, J.; Erdjument-Bromage, H.; Tempst, P.; Weissbach, H.; Nathan, C. *Proc. Natl. Acad. Sci. U.S.A.* **2001**, *98*, 9901.

(65) Jevons, M. P. *Br. Med. J.* **1961**, *1*, 124.

(66) Rossolini, G. M.; Arena, F.; Pecile, P.; Pollini, S. *Curr. Opin. Pharmacol.* **2014**, *18*, 56.

(67) Laxminarayan, R.; Duse, A.; Wattal, C.; Zaidi, A. K. M.; Wertheim, H. F. L.; Sumpradit, N.; Vlieghe, E.; Hara, G. L.; Gould, I. M.; Goossens, H.; Greko, C.; So, A. D.; Bigdeli, M.; Tomson, G.; Woodhouse, W.; Ombaka, E.; Peralta, A. Q.; Qamar, F. N.; Mir, F.; Kariuki, S.; Bhutta, Z. A.; Coates, A.; Bergstrom, R.; Wright, G. D.; Brown, E. D.; Cars, O. *Lancet Infect. Dis.* **2013**, *13*, 1057.

(68) Waters, C. M.; Bassler, B. L. *Annu. Rev. Cell Dev. Biol.* **2005**, *21*, 319.

(69) Miller, M. B.; Bassler, B. L. *Annu. Rev. Microbiol.* **2001**, *55*, 165.

(70) Rutherford, S. T.; Bassler, B. L. *Cold Spring Harb. Perspect. Med.* **2012**, *2*, a012427.

(71) Williams, P. *Expert Opin. Ther. Targets* **2002**, *6*, 257.

(72) Rasmussen, T. B.; Givskov, M. *Int. J. Med. Microbiol.* **2006**, *296*, 149.

(73) Cegelski, L.; Marshall, G. R.; Eldridge, G. R.; Hultgren, S. J. *Nat. Rev. Microbiol.* **2008**, *6*, 17.

(74) Gordon, C. P.; Williams, P.; Chan, W. C. *J. Med. Chem.* **2013**, *56*, 1389.

(75) Shoham, M. *Future Med. Chem.* **2011**, *3*, 775.

(76) Rasko, D. A.; Sperandio, V. *Nat. Rev. Drug. Discov.* **2010**, *9*, 117.

(77) Novick, R. P.; Projan, S. J.; Kornblum, J.; Ross, H. F.; Ji, G.; Kreiswirth, B.; Vandenesch, F.; Moghazeh, S. *Mol. Gen. Genet.* **1995**, *248*, 446.

(78) Date, S. V.; Modrusan, Z.; Lawrence, M.; Morisaki, J. H.; Toy, K.; Shah, I. M.; Kim, J.; Park, S.; Xu, M.; Basuino, L.; Chan, L.; Zeitschel, D.; Chambers, H. F.; Tan, M.-W.; Brown, E. J.; Diep, B. A.; Hazenbos, W. L. W. *J. Infect. Dis.* **2014**, *209*, 1542.

(79) Khodaverdian, V.; Pesho, M.; Truitt, B.; Bollinger, L.; Patel, P.; Nithianantham, S.; Yu, G.; Delaney, E.; Jankowsky, E.; Shoham, M. *Antimicrob. Agents Chemother.* **2013**, *57*, 3645.

(80) Yu, G.; Kuo, D.; Shoham, M.; Viswanathan, R. *ACS Comb. Sci.* **2014**, *16*, 85.

(81) Kuo, D.; Yu, G.; Hoch, W.; Gabay, D.; Long, L.; Ghannoum, M.; Nagy, N.; Harding, C. V.; Viswanathan, R.; Shoham, M. *Antimicrob. Agents Chemother.* **2015**, *59*, 1512.

(82) Kohanski, M. A.; Dwyer, D. J.; Hayete, B.; Lawrence, C. A.; Collins, J. J. *Cell*, *130*, 797.

(83) Keren, I.; Wu, Y.; Inocencio, J.; Mulcahy, L. R.; Lewis, K. *Science* **2013**, *339*, 1213.

(84) Liu, Y.; Imlay, J. A. *Science* **2013**, *339*, 1210.

(85) Gusarov, I.; Nudler, E. *Proc. Natl. Acad. Sci. U.S.A.* **2005**, *102*, 13855.

(86) Gusarov, I.; Shatalin, K.; Starodubtseva, M.; Nudler, E. *Science (New York, N.Y.)* **2009**, *325*, 1380.

(87) Shatalin, K.; Gusarov, I.; Avetissova, E.; Shatalina, Y.; McQuade, L. E.; Lippard, S. J.; Nudler, E. *Proc. Natl. Acad. Sci. U.S.A.* **2008**, *105*, 1009.

(88) Shatalin, K.; Shatalina, E.; Mironov, A.; Nudler, E. *Science* **2011**, *334*, 986.

(89) Luhachack, L.; Nudler, E. *Curr. Opin. Microbiol.* **2014**, *21*, 13.

Chapter 2.1: Design, Synthesis and Evaluation of Benzo[*b*]phenanthridine-5,7,12-trione as Reactive Oxygen Species Generators

2.1.1. Introduction

Maintaining redox-homeostasis is crucial for normal cellular function. Reactive oxygen species (ROS) play an important role in maintaining redox-homeostasis at lower concentrations.[1,2] However, an elevated level of these reactive species can cause oxidative damage to macromolecules (DNA, proteins, and lipids) and their irreparable damage could lead to cell death.[3] The intracellular ROS level is tightly regulated by many complex mechanisms but due to excessive ROS production or reduced physiological activity of antioxidant defense systems induces oxidative stress. An enhanced levels of ROS is harmful to the cells, however, potentiating these ROS in certain cells has been considered as possible drug design strategy.[4] For example, several ROS inducing compounds have been demonstrated to possess anticancer activity in a number of cancer models.[5] A naturally occurring ROS inducing compound β-lapachone displayed potent inhibitory activity against pancreatic cancer cells (Figure 2.1.1).[6,7] The natural product piperlongumine has been reported to induce ROS generation in cancer cells and this compound has shown potent growth-inhibitory properties in a variety of cancer cell lines and various animal models (Figure 2.1.1).[8-10]

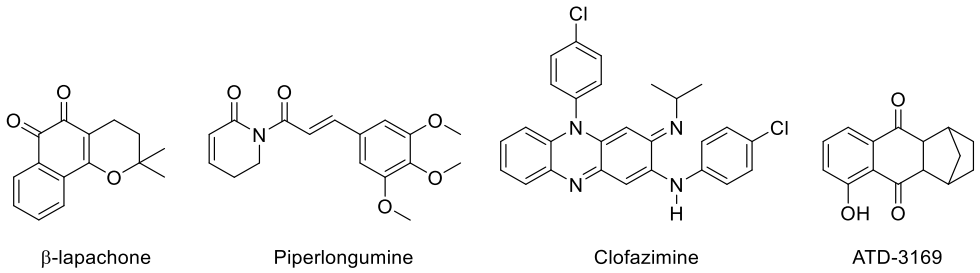

Figure 2.1.1. ROS inducing anticancer and antibacterial agents

Similarly, perturbing redox-homeostasis in bacteria has been considered as a potential antibacterial strategy. Clofazimine (CLF) is a commercial drug used for the treatment of leprosy, a chronic infection caused by *Mycobacterium leprae* (Figure 2.1.1). The proposed mechanism of action for CLF includes generation of intracellular ROS and induction of oxidative stress.[11] In addition, various small molecule ROS generators (developed in our research group) have shown antimycobacterial activity. For example, ATD-3169, a ROS generator is reported to induce oxidative stress in *Mycobacterium tuberculosis* (*Mtb*) and found to inhibit growth of multidrug

resistant strain of *Mtb*.[12,13] Furthermore, it has been demonstrated that ROS can sensitize bacteria to a number of antibiotics. Silver ion induces ROS generation in gram-negative bacteria and potentiates the activity of traditional antibiotics.[14] Although ROS has been reported to sensitize bacteria to antibiotics and acts as an adjuvant, only limited sources of reliable ROS generators are available. Therefore, we proposed to develop ROS generators that can reliably enhance intracellular ROS level and exploit their therapeutic potential against bacteria.

We proposed to synthesize ROS generator based on redox-active natural products, because these compounds have the ability to induce oxidative stress and they are evolutionary optimized as drug-like molecules. Microorganisms secrete these secondary metabolites in order to keep competitors in check.[15] For example, *Streptomyces venezuelae* ISP5230 produces quinone based redox-active natural product jadomycins under nutrient limited condition. Jadomycins have shown important biological activities such as antibacterial, antifungal and anticancer.[16,17] Several members of jadomycin family have been reported to induce DNA-damage in the presence of Cu(II), presumably through ROS generation.[18,19]

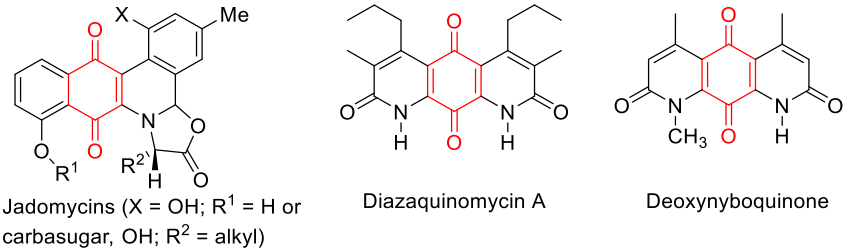

Figure 2.1.2. Structures of ROS generating redox-active natural products

Diazaquinomycins (Figure 2.1.2), another class of redox-active compound isolated from *Streptomyces species* have shown inhibitory activity against *Mtb*.[20,21] Deoxynyboquinone (Figure 2.1.2), a derivative of diazaquinomycins, has shown potent anti-tumor activity and its efficacy is, in part, dependent on ROS generation.[22,23] Therefore, we proposed to synthesize ROS generators based on these redox-active natural products. Although natural products are a rich source of new drug candidates, their utility is sometimes limited by the complexity of synthesis. For example, jadomycin B synthesis has been achieved in >20 steps with 5 % overall yield.[24] Similarly, deoxynyboquinone synthesis was reported in seven linear steps that heavily involved Pd-mediated cross-coupling reactions.[22] Thus, a preferable route is to use certain structural aspects of these compounds to identify simpler scaffolds with comparable or superior biological

function. We considered retaining aromatic ring from jadomycin and amide adjoining quinone and aromatic ring from deoxynyboquinone for efficient ROS generation. Compound **5** was proposed as potential candidate of ROS generator. We predicted that **5** can undergo reduction with 1e⁻ reductase to its semiquinone (intermediate I), which then can react with molecular oxygen to produce superoxide and oxidized quinone. Similarly, **5** can undergo reduction with 2e⁻ reductase to from hydroquinone (intermediate II), which then can react with molecular oxygen to produce $O_2^{\bullet -}$. During this oxidation **5** will be regenerated and would be available for next cycle of ROS generation (Scheme 2.1.1).

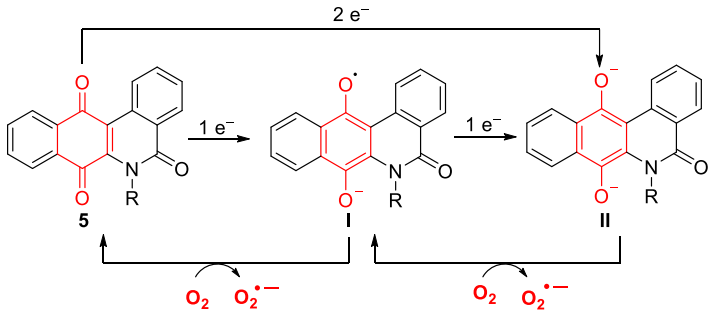

Scheme 2.1.1. Proposed mechanism of superoxide generation from **5**

2.1.2. Retrosynthetic analysis

The retrosynthetic analysis of benzo[*b*]phenanthridine-5,7,12(6*H*)-trione is illustrated in Scheme 2.1.2. We envisioned that benzo[*b*]phenanthridine-5,7,12(6*H*)-trione could be obtained by oxidation of hemiaminal. We intended to construct heterocyclic ring B through a 6π-electron electrocyclic ring closure followed by hydration and oxidation. The imine can be obtained by the reaction of aldehyde with primary amine. The aldehyde compound could be achieved by Stille coupling of 2-bromo-l,4-naphthoquinone with arylstannane.

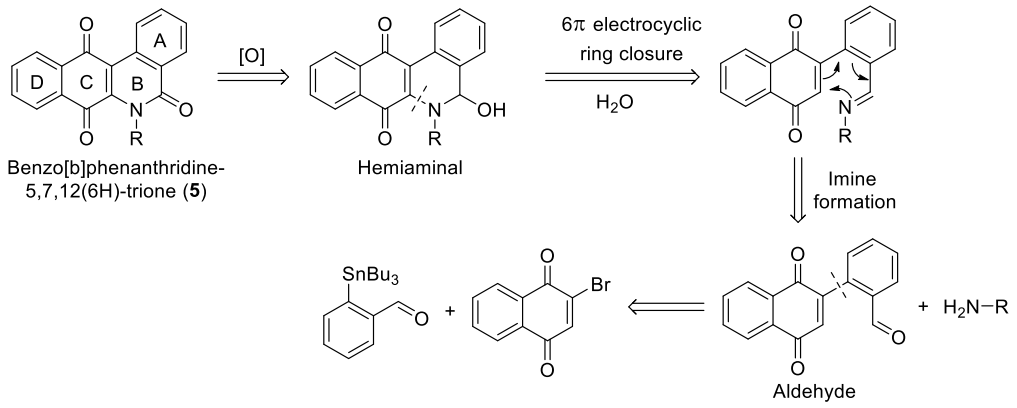

Scheme 2.1.2. Retrosynthetic analysis of benzo[*b*]phenanthridine-5,7,12(6*H*)-trione **5**

2.1.2. Results and Discussion

2.1.2.1. Synthesis and characterization

The benzo[*b*]-phenanthridine-5,7,12(6*H*)-trione **5** was synthesized in four steps. Stanylation of 2-(2-bromophenyl)-1,3-dioxane **1** with tributyltin chloride afforded stannane derivative **2** in 76% yield. Palladium-catalyzed Stille coupling of **2** with 2-bromo-1,4-naphthoquinone in the presence of CuI afforded **3** in 65% yield. Acid-mediated deprotection of 1,3-dioxolane **3** provided aldehyde **4** in 79% yield (Scheme 2.1.3).

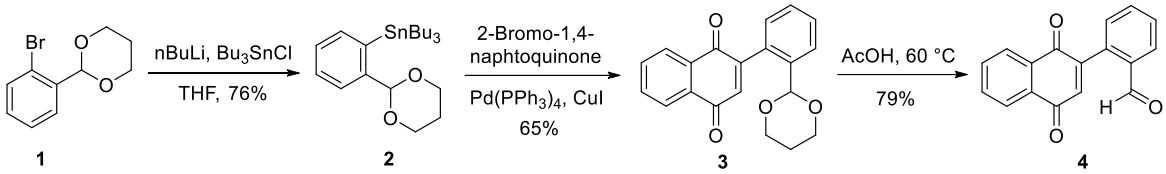

Scheme 2.1.3. Synthesis of **4**

Table 2.1.1. Synthesis of 5a-5n by the reaction of 4 with a primary amine

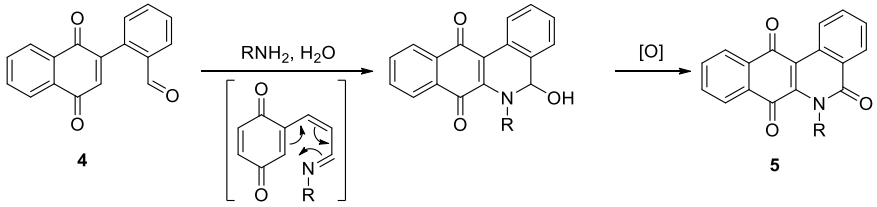

Entry	R	Compound	% Yield
1	Me	**5a**	73
2	Et	**5b**	50
3	^{n}Pr	**5c**	45
4	Cyclohexyl	**5d**	23
5	Allyl	**5e**	21
6	Propargyl	**5f**	20
7	CH_2CO_2Me	**5g**	39
8	Bn	**5h**	39
9	2-CF_3-C_6H_4-CH_2	**5i**	14
10	4-Cl-C_6H_4-CH_2	**5j**	20
11	4-OMe-C_6H_4-CH_2	**5k**	17
12	4-NO_2-C_6H_4-CH_2	**5l**	22
13	4-CF_3-C_6H_4-CH_2	**5m**	47
14	(3,4,5-triOMe)-C_6H_4-CH_2	**5n**	13

Finally, aldehyde **4** was reacted with methylamine in an open container to afford hemiaminal derivative, which can be oxidized to benzo[*b*]phenanthridine-5,7,12(6*H*)-trione derivative (**5a**). However, during this reaction, oxidized compound **5a** was directly obtained as a major product (Table 2.1.1, entry 1). Under similar conditions, a reaction of various aliphatic primary amines such as ethylamine, propylamine and cyclohexylamine with aldehyde **4** provided compounds **5b-5d** in moderate yields (Table 2.1.1, entries 2-4). Similarly, allylamine and propargylamine were independently reacted with aldehyde **4** to afford compound **5e** and **5f** in moderate yield. A reaction of glycine methyl ester with **4** afforded **5g** in 39% yield. A reaction of benzylamine with **4** provided **5h** in 37% yield. This one-pot methodology was also found to be compatible with electron donating and withdrawing substituted benzylamines. The substituted benzylamine such as 2-(trifluromethyl)benzylamine, 4-chlorobenzylamine, 4-methoxybenzylamine, 4-nitrobenzylamine, 4-(trifluromethyl)benzylamine and 3,4,5-trimethoxybenzylamine were independently reacted with aldehyde **4** to produce corresponding benzo[*b*]phenanthridine-5,7,12(6*H*)-trione derivatives **5i-5n** (Table 2.1.1, entries 9-14). However, the reaction of aromatic amine such as aniline did not produce the desired product but instead gave an inseparable mixture of products. Also, our several attempts for making (R = H) derivative by the reaction of ammonia with aldehyde **4** were unsuccessful and instead gave inseparable mixture of products.

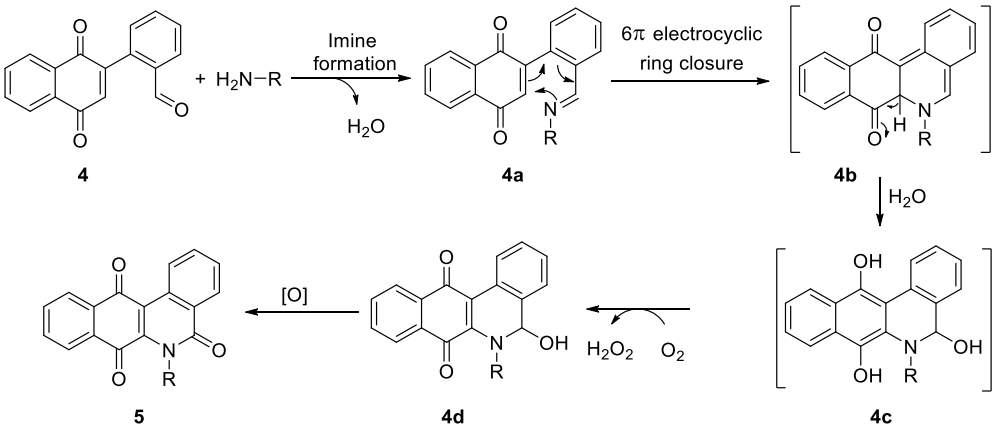

Scheme 2.1.4. Proposed reaction mechanism for synthesis of **5**

Next a possible reaction mechanism was proposed as depicted in scheme 2.1.4. A reaction of amine with aldehyde forms imine **4a**, which can undergo 6π electrocyclic-ring closure followed by hydration to form hemiaminal **4c**. The hydroquinone **4c** is unstable and hence it can undergo oxidation to form quinone and generates hydrogen peroxide. We proposed that, H_2O_2 generated

during this reaction could oxidize hemiaminal to **5** (Scheme 2.1.4). A mechanism of hydrogen peroxide mediated oxidation of hemiaminal to benzo[*b*]phenanthridine-5,7,12(6*H*)-trione was supported by conducting a reaction in the presence of authentic hydrogen peroxide. When the reaction mixture of **4** and propargylamine was supplemented with H_2O_2, the yield of **5f** was found to be increased from 20 to 37% yield. Thus, we have developed one-pot methodology through which the redox-active compounds were synthesized in four steps with good overall yields.

2.1.2.2. Reduction potential measurement

Next, the propensity of **5a-5n** to undergo reduction with bioreductive enzymes were predicted by measuring one electron reduction potential using cyclic voltammetric analysis. A quinone with a reduction potential in the range of -0.7 to -1.1 V has been reported to be a candidate for reduction by enzymes such as NADPH: cytochrome P450 reductase.[25] Cyclic voltammetric analysis revealed that $1e^-$ reduction potential (E_{red}) of **5a-5n** were -1.0 to -1.21 V (Table 2.1.2), which appears appropriate for reduction by bioreductive enzymes. In addition, the one electron reduction potential values suggest that there no is strong effect of nitrogen substituent on reduction potentials of these compounds.

Table 2.1.2. One electron reduction potential of 5a-5n

Entry	R	Compound	$-E_{red}$
1	Me	**5a**	1.04
2	Et	**5b**	1.09
3	^{n}Pr	**5c**	1.07
4	Cyclohexyl	**5d**	1.11
5	Allyl	**5e**	1.05
6	Propargyl	**5f**	1.00
7	CH_2CO_2Me	**5g**	1.21
8	Bn	**5h**	1.14
9	2-CF_3-C_6H_4-CH_2	**5i**	1.07
10	4-Cl-C_6H_4-CH_2	**5j**	1.04
11	4-OMe-C_6H_4-CH_2	**5k**	1.08
12	4-NO_2-C_6H_4-CH_2	**5l**	1.02
13	4-CF_3-C_6H_4-CH_2	**5m**	1.04
14	(3,4,5-triOMe)-C_6H_4-CH_2	**5n**	1.10

2.1.2.3. Superoxide generation

The ability of **5a-5n** to generate superoxide was tested using a luminol based chemiluminescence assay.[26] In this assay, the reaction of luminol with superoxide leads to nitrogen extrusion and simultaneous formation of excited state species of 3-aminobenzene-1,2-dicarboxylate (Scheme 2.1.5). Returning of the excited state species to ground state emits light (luminescence) and the emission is recorded as a measure of superoxide generated during the reaction. In this assay, DT-diaphorase (DT-D) was used as model bioreductive enzyme along with NADPH as co-factor.

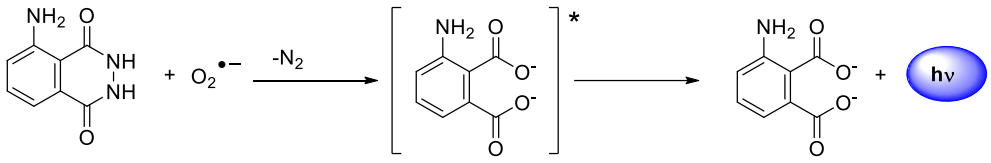

Scheme 2.1.5. Reaction of luminol with superoxide radical

When **5a** was incubated with luminol in pH 7.4 buffer, no evidence of superoxide generation was found. However, when **5a** was exposed to DT-D and NADPH in the presence of luminol, chemiluminescence was observed (Figure 2.1.3), confirming the intermediacy of superoxide. When, a similar experiment was conducted with other derivatives **5b-5n**, a similar result was recorded (Figure 2.1.3). The aliphatic amine derivatives (**5a-5f**) produced higher levels of $O_2^{\bullet-}$ than benzylamine derivatives. Thus, this result confirmed the ability of these compounds to undergo reduction with bioreductive enzymes to produce superoxide.

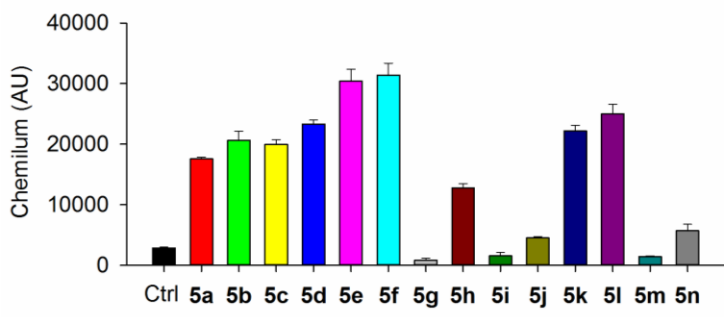

Figure 2.1.3. Measurement of $O_2^{\bullet-}$ generated during incubation of **5a-5n** (25 μM) with DT-D in pH-7.4 buffer at 37 °C using luminol assay. Ctrl is **5a** was incubated in pH 7.4 buffer in the absence of DT-D.

2.1.2.4. Antibacterial activity against *S. aureus*

Having demonstrated the superoxide generation from **5a-5n** in the presence of bioreductive enzyme, next the potential of these compounds to inhibit the growth *Staphylococcus aureus* (*S.*

aureus) was tested. *S. aureus* is gram-positive bacteria and it causes skin and soft-tissue infections. The infection caused by this bacterium was successfully treated using a number of antibiotics. However, over a period of time *S. aureus* has developed resistance to traditional antibiotics. The condition has become even worse when recently it was reported that it has acquired resistance to antibiotics of last line which include vancomycin, linezolid and daptomycin.[27,28] Therefore, there is urgent need for the development of new antibacterial drugs with novel structure and a mechanism of action possibly different from that of current first-line antibiotics.

Table 2.1.3. Calculated partition coefficients (ClogP) and MIC against MSSA of 5a-5n

Entry	Compound	ClogP[a]	MIC (μg/mL)[b]
1	**5a**	2.63	1.0
2	**5b**	3.16	>32
3	**5c**	3.69	>32
4	**5d**	4.66	>32
5	**5e**	3.40	>32
6	**5f**	2.73	0.5
7	**5g**	2.82	>32
8	**5h**	4.40	>32
9	**5i**	5.28	>32
10	**5j**	5.11	>32
11	**5k**	4.32	32
12	**5l**	4.14	8.0
13	**5m**	5.28	>32
14	**5n**	3.70	8.0
15	Fosfomycin	-	8
16	Vancomycin	-	0.5

[a]Calculated using Chembiodraw Ultra 13.0

[b]MIC values were provided by Dr. Radha Rangrajan, Vitas Pharma, Hyderabad

The potential of these redox-active compounds **5a-5n** to inhibit the growth of methicillin sensitive *S. aureus* (MSSA) and methicillin resistant *S. aureus* (MRSA) was tested using a microdilution method according to Clinical and Laboratory Standards Institute (CLSI) guidelines. The antibacterial activities are expressed as MICs, which is the lowest concentration of a compound required for the inhibition of bacterial growth. Vancomycin and fosfomycin were

used as positive control in this study. The results of the *in vitro* antibacterial evaluation revealed methyl derivative **5a** exhibited potent inhibitory activity against MSSA with MIC 1 μg/mL (Table 2.1.3, entry 1). However, compounds **5b-5e** were found to be inactive at 32 μg/mL, suggesting that increasing carbon chain length of alkyl substituent at nitrogen reduces the inhibitory activity. On the other hand, propargylamine derivative **5f** exhibited potent antibacterial activity against MSSA with MIC 0.5 μg/mL (Table 2.1.3, entry 6), which was comparable with vancomycin. The glycine-methyl ester derivative **5g** and benzylamine derivative **5h** were also tested, however these compounds were found to be inactive against MSSA (Table 2.1.3, entries 7 and 8). However, 4-nitrobenzyl derivative **5l** and 3,4,5-trimethoxybenzyl derivative **5n** exhibited moderate antibacterial activity with MICs 8 μg/mL. Benzyl derivatives **5i-5k** and **5m** did not show inhibitory activity against MSSA at 32 μg/mL. Although all derivatives (**5a-5n**) were found to generate superoxide in the presence of bioreductive enzyme, only few derivatives were found active against MSSA suggesting that along with ROS generation some other properties of these compounds might be contributing to antibacterial activity. We speculated that, the cell permeability of these compounds might have some effects on antibacterial activity. In order to test this hypothesis, partition coefficients (ClogP), a measure of cell permeability, of **5a-5n** was calculated using Chembiodraw Ultra 13.0 and correlation between ClogP and MICs was studied. Our preliminary analysis revealed that the compound having ClogP < 3 exhibited good inhibitory activity against MSSA. For example, compound **1a** and **1f** has ClogP value 2.63 and 2.73 respectively and both the compounds showed good inhibitory activity. While the ClogP of **5b-5e** is greater than 3 and these compounds were found to be inactive against MSSA at 32 μg/mL. However, in case of benzylamine derivatives we did not find a clear relationship between ClogP and MICs. Amongst the compounds tested, **5f** was found to be a better inhibitor of MSSA with MIC 0.5 μg/mL and identified as a lead compound for further studies.

2.1.2.5. ROS generation studies in buffer

Due to short-half life of ROS under physiological conditions, unambiguous detection of ROS warrants multiple assay technologies. Hence, several independent assays were used to confirm the ROS generation from **5f** in cell-free system. First, a time course of superoxide generation was measured using a luminol-based chemiluminescence assay.[26] When **5f** was incubated in pH 7.4 buffer, no evidence of superoxide generation was found in the absence of bioreductive enzyme (Figure 2.1.4A). Whereas, when **5f** was exposed to DT-D, an immediate increase in the

chemiluminescence was observed as a read out for the intermediacy of superoxide under these conditions (Figure 2.1.4A).

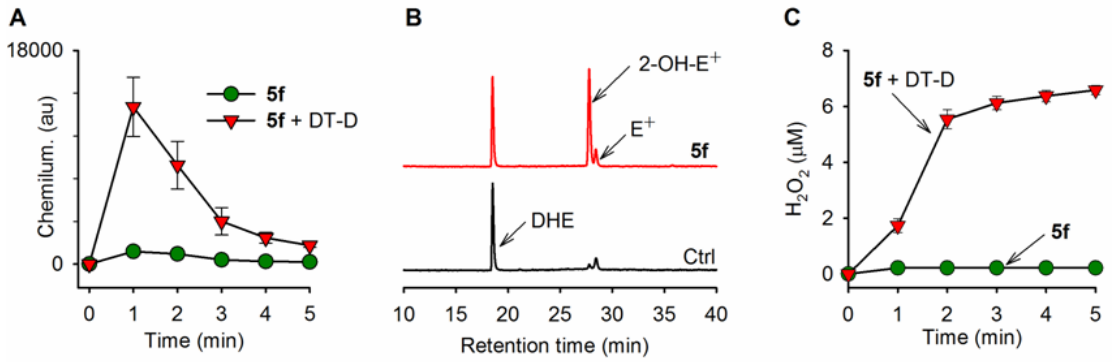

Figure 2.1.4. ROS generation by compound **5f** in pH 7.4 buffer (A) Time course of $O_2^{\bullet-}$ generation was measured using a luminol-based chemiluminescence assay in the presence of DT-D (B) $O_2^{\bullet-}$ generated during incubation of **5f** with DT-D was estimated using a dihydroethidium (DHE) assay. $O_2^{\bullet-}$ specifically react with DHE to produce 2-hydroxyethidium (2-OH-E^+); Ethidium (E^+) is formed by non-specific oxidation of DHE and is indicative of a general increase in oxidative species. Ctrl is **5f** in pH 7.4 buffer (C) H_2O_2 produced during incubation of **5f** (2 μg/mL) with DT-D for 5 min was quantified by an Amplex Red-based fluorescence assay.

Next, a HPLC-based dihydroethidium (DHE) assay was used to infer the superoxide generation independently. In this assay, $O_2^{\bullet-}$ specifically reacts with DHE to produce 2-hydroxyethidium (2-OH-E^+) (Scheme 2.1.6). DHE also reacts non-specifically with other ROS and forms ethidium (E^+) dye.[29,30] Both of these oxidized products can be detected using HPLC attached with a fluorescence detector.[31]

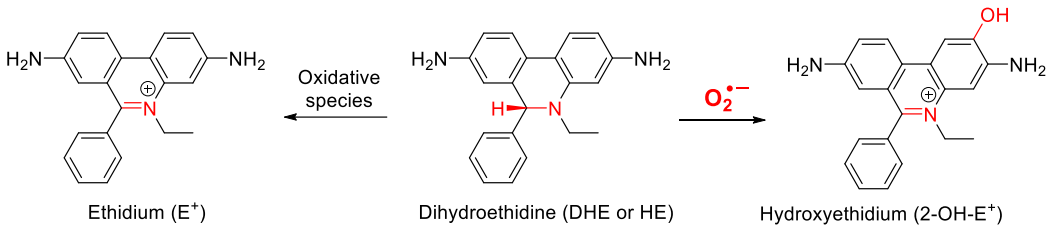

Scheme 2.1.6. A scheme for formation of 2-OH-E^+ and E^+ during reaction of DHE with ROS

An authentic sample of DHE was injected into HPLC and we observed a peak at 18.5 min corresponding to DHE (Figure 2.1.4B). When **5f** was incubated with DHE under comparable

conditions, chromatogram indicated superoxide and ROS were not generated in the absence of bioreductive enzyme. However, when **5f** and DHE were incubated with DT-D in pH 7.4 phosphate buffer, a new peak at 27.7 min corresponding to 2-OH-E^+ was observed indicating the superoxide is a major product formed under these conditions, and a small peak at 28.4 min was identified as E^+ as an evidence for the formation of other oxidative species in minor proportions (Figure 2.1.4B). Together, these experiments confirmed the superoxide generation from **5f** under physiological conditions.

Next, the ability of **5f** to generate H_2O_2, a one electron reduction product of $O_2^{\bullet-}$, was measured using the Amplex Red assay. In this assay, H_2O_2 reacts stoichiometrically with non-fluorescent dye Amplex Red in the presence of horse radish peroxidase (HRP) and produces resorufin, a highly fluorescent dye. During this reaction, HRP catalyzes the hydroxyl radical formation from H_2O_2, which then reacts with Amplex Red to produce resorufin (Scheme 2.1.7).[32] This assay has been extensively used for quantitative measurement of H_2O_2 in cell-free as well as extracellular medium. ROS generator **5f** was incubated in pH 7.4 buffer under ambient aerobic conditions and at one minute interval Amplex Red reagent was added. The resulting mixture was incubated for 30 min and fluorescence was measured using 96-well plate reader. We did not find evidence for H_2O_2 generation in the absence of DT-D (Figure 2.1.4C), suggesting the stability of compound under this condition. However, when **5f** was incubated with DT-D, we found an increase in H_2O_2 level over 5 minute durations (Figure 2.1.4C). Taken together these experiments confirmed the ability of **5f** to produce ROS in the presence of a model bioreductive enzyme.

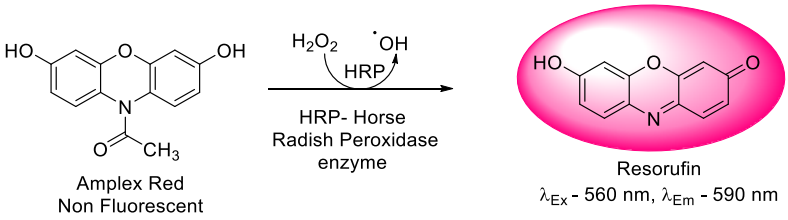

Scheme 2.1.7. Oxidation of non-fluorescent Amplex Red by H_2O_2 to fluorescent resorufin in the presence of HRP enzyme

2.2.2.6. ROS generation studies in *S. aureus*

The ability of **5f** to permeate bacterial cells and generate ROS was measured using three independent assays. First, a HPLC based DHE assay was conducted for intracellular superoxide

detection.[30] In this assay, the reaction of DHE with superoxide produces 2-hydroxyethidium (2-OH-E^+) as an exclusive product, which elutes at 27.7 min and a non-specific oxidation of DHE leads to the formation of ethidium E^+, which elutes at 28.4 min. We incubated *S. aureus* with DHE for 60 min and bacterial culture was centrifuged to remove the extracellular dye by discarding supernatant followed by washing bacterial pellet with phosphate buffer. The bacterial pallet was then lysed in acetonitrile using probe sonicator and the organic layer was analyzed using HPLC attached with fluorescence detector. The HPLC analysis revealed that the presence of minor quantities of peaks corresponding to 2-OH-E^+ and E^+ indicating the basal level of ROS in bacteria (Figure 2.1.5A). However, when *S. aureus* was co-incubated with **5f** and DHE, the formation of new peak at 27.7 min corresponding to 2-OH-E^+ was observed (Figure 2.1.5A). When *S. aureus* was incubated with increasing concentration of **5f,** we observed a dose dependent increase in the peak intensity for 2-OH-E^+ confirming the ability of compound to enhance $O_2^{\bullet-}$ levels in bacteria (Figure 2.1.5A).

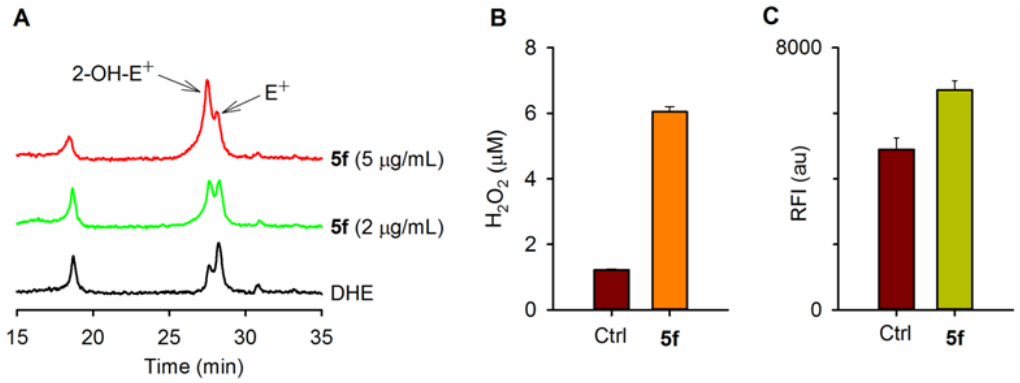

Figure 2.1.5. ROS generation by **5f** in *S. aureus* (A) $O_2^{\bullet-}$ generated during incubation of *S. aureus* with **5f** was estimated using a dihydroethidium (DHE) assay (B) Estimation of H_2O_2 generated during incubation of *S. aureus* with **5f** (2 µg/mL) was estimated using an Amplex Red fluorescence assay (C) Increase in intracellular oxidative species upon treatment of *S. aureus* with **5f** was determined by a 2,7-dichlorodihydrofluoresceindiacetate (H_2DCF-DA)-based fluorescence assay and DMSO (0.5%) was used as control.

Having demonstrated the superoxide generation in *S. aureus*, we evaluated **5f** for their ability to generate H_2O_2, a scavenged product of superoxide radical. The intracellular H_2O_2 measurement is challenging due to lack of reliable method for its detection. However, H_2O_2 diffuses out of the bacterial cell and extracellular H_2O_2 has been considered as surrogates of an increased

intracellular ROS.[33] The extracellular H_2O_2 was measured using Amplex-Red assay.[32] Unlike other ROS, H_2O_2 is relatively stable reactive species under physiological conditions; hence it can be quantified using Amplex-Red assay. A calibration curve with known concentrations of H_2O_2 was generated and used for the quantification of H_2O_2 generated from **5f** in *S. aureus*. When *S. aureus* was incubated with **5f** at 2 μg/mL (6.38 μM), we found 6.0 μM of extracellular H_2O_2 (Figure 2.1.5B), confirming the efficiency of this compound to generate H_2O_2 in bacteria.

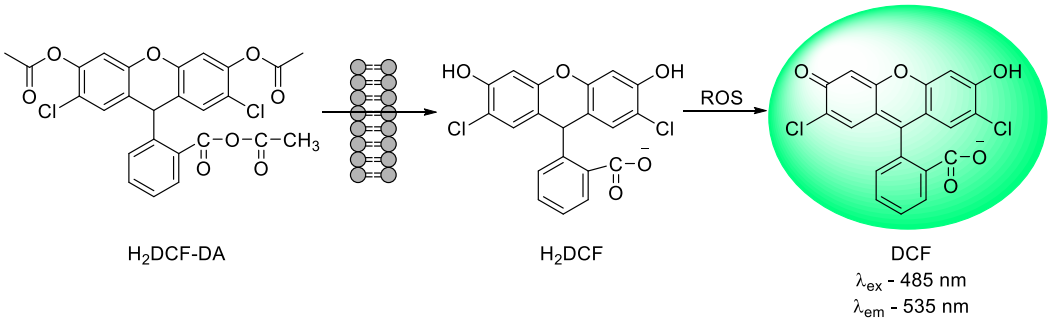

Scheme 2.1.8. Oxidation of non-fluorescent H_2DCF-DA by ROS to fluorescent dye, DCF

Hydrogen peroxide itself is not very toxic to bacterial cell however its secondary products such as hydroxy radical (•OH) and hypochlorite are highly reactive towards biomolecules (DNA, proteins, and lipids). Under biological system, •OH can be formed by reaction of metal ion such as Fe^{2+} with H_2O_2.[34] We evaluated **5f** for their ability to generate •OH in *S. aureus*. The direct detection of •OH is challenging due to its short half-life.[35,36] Therefore, 2,7-dichlorodihydrofluorescein-diacetate (H_2DCF-DA)-based fluorescence assay was used to infer the •OH generation. H_2DCF-DA is a weakly fluorescent cell permeable dye, which reacts efficiently with •OH radical and to some extent with H_2O_2 to produce fluorescent molecule DCF (Scheme 2.1.8).[37] When *S. aureus* was co-incubated with ROS generator **5f** and H_2DCF-DA, a significant increase in the fluorescence intensity was observed confirming the •OH generation (Figure 2.1.5C). Taken together, our data establishes that **5f** was capable of increasing intracellular ROS at concentrations that are relevant to growth inhibition.

2.1.2.7. Mechanistic studies

Having demonstrated the ROS generation in *S. aureus*, next the involvement of ROS in bacterial cell death was studied. At elevated levels, ROS can cause oxidative damage to different macromolecules like proteins, DNA and lipids leading to loss of their functions and ultimately

result into cell death. Amongst ROS, ˙OH is the most reactive oxygen species and it can damage DNA leading to single and double-strand breaks.[38] These double-strand breaks can be lethal if not repaired prior to cell division. Hence bacteria activate several repair-pathways to repair damaged DNA in a timely manner. Symptomatic of one such repair pathway is the expression of *RecA*, a repair protein crucial to homologous recombination.[39] Our collaborator (Dr. Radha Rangrajan, Vitas Pharma, Hyderabad) assessed ROS-mediated DNA damage in MSSA upon treatment of **5f** by measuring the expression level of *RecA* using reverse transcription polymerase chain reaction (RT-PCR) analysis. When MSSA was incubated with **5f** for 2h, an increased expression level of *RecA* was found (data is not shown), suggesting activation of DNA damage repair response. Thus, this experiment confirmed the ROS-mediated DNA damage in *S. aureus*. Furthermore, our collaborator examined the effect of **5f** on the viable colony count of MSSA in the presence of thiourea, a ˙OH scavenger. The growth inhibition of **5f** was reduced in the presence of thiourea, suggesting that quenching the ROS in the cell reduces the antibacterial effect of the compound. These data provide further support for a ROS based mechanism contributing to antibacterial activity.

Thus, the antibacterial activity of **5f** may be attributed to a mechanism involving ROS. Although, from the library of compounds **5a-5n** many compounds were found to generate ROS in the presence of DT-D but only **5a** and **5f** were found to be potent inhibitor of MSSA. This suggests that ROS alone does not play important role in the killing of the MSSA. Our future efforts would be towards understanding the detail mechanism of action of these ROS generators.

2.1.2.8. Antibacterial activity against clinical isolates of MRSA

Next, the efficacy of **5f** to inhibit the growth of drug resistant strain of *S. aureus*, MRSA was tested by our collaborator (Dr. Radha Rangrajan, Vitas Pharma, Hyderabad).Vancomycin was selected as the positive control as it is a well-known antibacterial agent that is often used as a last resort drug in the treatment of drug-resistant infections. First, the inhibitory potential of **5f** was tested against laboratory strain of MRSA (ATCC 33591). The lead compound **5f** exhibited good anti-MRSA activity with MIC value 0.5 μg/mL. The inhibitory activity of lead compound was assessed against an array of clinically relevant multidrug-resistant MRSA strains. Compound **5f** retained its antimicrobial activity against MRSA isolates with MICs ranging from 0.06-0.5 μg/mL suggesting that **5f** activity against patient-derived strains was conserved.

2.1.2.9. Cytotoxicity study

Finally, the lead **5f** was tested for its toxicity towards mammalian cells to determine if this compound targets bacteria and not mammalian cells, a critical aspect of developing new antibacterial agents. The growth inhibitory potential of **5f** was evaluated against A549 human lung carcinoma cells using a standard cell viability assay. The cell viability assay revealed that the growth inhibitory activity (GI_{50}) of **5f** was 8.6 μM against A549 cancer cell line. The selectivity index SI (GI_{50}/MIC) for MRSA B19506 was nearly 45, while the SI for MRSA 7419 and MRSA 7425 was 22. The cytotoxicty assay revealed the necssesity of imroving the selectivity index of this compound for further development.

2.1.3. Conclusion

In this Chapter 2.1, we have presented the design and synthesis of natural product-inspired benzo[*b*]-phenanthridine-5,7,12(6*H*)-triones as bioreductively activated ROS generators. These small molecules were found to undergo reduction with a model bioreductive enzyme, DT-diaphorase to generate ROS such as superoxide, H_2O_2 and hydroxyl radical. ROS generation from these compounds in the presence of bioreductive enzyme was demonstrated using multiple assays. The potential of these redox-active compounds to inhibit the growth of *S. aureus* was tested and many of the compounds (**5a**, **5l** and **5n**) showed moderate to good inhibitory activity against MSSA. The redox-active compound **5f** (0.5 μg/mL) was identified as lead compound and it has shown potent inhibitory activity against MRSA and clinical isolates of MRSA. We demonstrated the ability of **5f** to enhance intracellular ROS level using two independent assays, DHE assay (for superoxide) and H_2DCF-DA assay (oxidative species). Although derivatives (**5b-5e**, **5g-5j** and **5m**) showed ROS generation, but were found to be ineffective in inhibiting growth of *S. aureus* suggesting that mechanism of action is not solely dependent on ROS generation. However, our viable colony count experiment in the presence of thiourea suggested the contribution of ROS in cells death. Taken together, we identified redox-active compound **5f** as a potent MRSA inhibitor with a unique mechanism of action that involves enhancement of ROS levels in cells.

2.1.4. Experimental Section

(2-(1,3-Dioxan-2-yl)phenyl)tributylstannane (2)

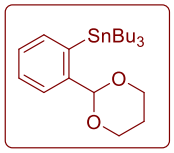

To a solution of 2-(2-bromophenyl)-1,3-dioxane (5 g, 20.57 mmol) in THF (80 mL) at -78 °C, *n*-BuLi in hexane (2.5 M, 9.87 mL, 24.68 mmol) was added dropwise. The mixture was stirred at -78 °C for 1h. Bu_3SnCl (6.67 mL, 24.68 mmol) was slowly added into the reaction mixture at -78 °C, and the mixture was stirred at -78 °C for 1 h. The reaction mixture was diluted with ethyl acetate (60 mL) followed by addition of saturated aqueous $NaHCO_3$ (60 mL). The mixture was stirred at 0 °C for 30 min. After separation, aqueous layer was extracted with ethyl acetate twice. The combined organic layer was washed with brine, dried over sodium sulfate and filtered. The filtrate was evaporated under reduced pressure. The crude residue was purified by column chromatography using 2% EtOAc/pet ether as the eluent to afford (2-(1,3-dioxan-2-yl)phenyl)tributylstannane(6.91 g, 74%) as a colorless liquid.^{1}H NMR (400 MHz, $CDCl_3$): δ 7.54 (d, *J* = 7.3 Hz, 1H), 7.47 (dd, *J* = 7.2, 1.3 Hz, 1H), 7.31 (td, *J* = 7.5, 1.6 Hz, 1H), 7.25 (td, *J* = 7.5, 1.6 Hz, 1H), 5.42 (s, 1H), 4.25 (dd, *J* = 10.7, 5.0 Hz, 2H), 3.95 (td, *J* = 12.3, 2.4 Hz, 2H), 2.30–2.15 (m, 1H), 1.57–1.44 (m, 7H), 1.32 (sextet, *J* = 7.3 Hz, 6H), 1.08–0.98 (m, 6H), 0.88 (t, *J* = 7.3 Hz, 9H); ^{13}C NMR (100 MHz, $CDCl_3$): δ 144.9, 139.8, 136.7, 128.2, 128.0, 126.1, 102.8, 67.3, 29.2, 27.6, 25.6, 13.8, 11.0; MALDI: calcd. For $C_{22}H_{38}OSn$ $[M+K]^+$: 493.1531; Found: 493.0167.

2-(2-(1,3-Dioxan-2-yl)phenyl)naphthalene-1,4-dione (3)

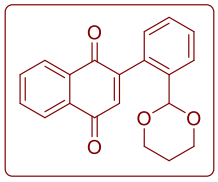

To a suspension of 2-bromo-1,4-naphthoquinone (2.5 g, 10.55 mmol), (2-(1,3-dioxan-2-yl)phenyl)tributylstannane (7.17 g, 15.82 mmol) and CuI (401.7 mg, 2.11 mmol) in THF (80 mL), $Pd(PPh_3)_4$ (609.3 mg, 0.52 mmol) were added. The mixture was stirred at 70°C for 16h. After completion of reaction (TLC analysis), the mixture was cooled down to 0°C, diluted with ethyl acetate, and quenched with aqueous sodium bicarbonate. The mixture was stirred for 30 min at 0 °C. After separation, aqueous layer was extracted with ethyl acetate twice, and combined organic layer was washed with brine, dried over sodium sulfate, filtered and then filtrate evaporatedunder reduced pressure. The crude compound was purified using silica gel chromatography using 10 % EtOAc/pet ether as eleunt to afford 2-(2-(1,3-dioxan-2-yl)phenyl)naphthalene-1,4-dione (2.20 g, 65%) as a yellow solid: mp 126-128 ºC; FT-IR (ν_{max}, cm^{-1}): 1743, 1654, 1541; ^{1}H NMR (400 MHz, $CDCl_3$): δ 8.15–8.10 (m, 2H), 7.76 (dd, *J* = 5.7, 3.3 Hz, 2H), 7.69 (d, *J* = 7.6 Hz, 1H), 7.45 (t, *J* = 7.6 Hz,

1H), 7.39 (t, *J* =7.6 Hz, 2H), 7.23 (s, 1H), 6.92 (s, 1H), 5.43 (s, 1H), 4.01 (broad s, 2H), 3.72 (t, *J* = 11.3 Hz, 2H), 2.03 (m, 1H), 1.29 (d, *J* = 13.6 Hz, 1H); ^{13}C NMR (100 MHz, $CDCl_3$): δ 185.3, 184.0, 151.0, 136.0, 135.0, 133.9, 133.8, 132.4, 132.2, 132.1, 129.8, 129.6, 128.7, 126.8, 126.6,126.1, 100.1, 67.1, 25.6; HRMS (ESI): calcd. For $C_{20}H_{16}O_4$ $[M+H]^+$: 321.1127; Found: 321.1131.

2-(1,4-Dioxo-1,4-dihydronaphthalen-2-yl)benzaldehyde (4)

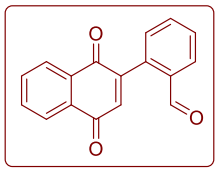

2-(2-(1,3-dioxan-2-yl)phenyl)naphthalene-1,4-dione (2.8 g, 1.74 mmol) was dissolved in acetic acid (80 %, 80 mL) and the resulting mixture was stirred at 60 °C for 5 h. The reaction mixture was diluted with ethyl acetate (30 mL) and quenched with aqueous sodium bicarbonate. The mixture was extracted with ethyl acetate (30 mL × 3). The combined organic layer was washed with brine, dried over sodium sulfate, filtered and then filtrate was concentrated under reduced pressure. The crude residue was purified using silica gel column chromatography using 10% EtOAc/pet ether as eluent, compound **4** (2.1 g, 92%) was obtained as a yellow solid: mp 135-137 ºC; FT-IR (ν_{max}, cm^{-1}): 2856, 1649, 1589, 1565; ^{1}H NMR (400 MHz, $CDCl_3$): δ 9.93 (s, 1H), 8.13–8.08 (m, 2H), 7.93 (d, *J* = 7.2 Hz, 1H), 7.76–7.64 (m, 4H), 7.37 (d, *J* = 6.9 Hz, 1H), 6.91 (s, 1H); ^{13}C NMR (100 MHz, $CDCl_3$): δ 191.5, 184.9, 183.6, 150.8, 135.1, 134.6, 134.5, 134.1, 134.0, 133.9, 133.2, 132.5, 132.4, 130.5, 130.1, 127.1, 126.3; HRMS (ESI): calcd. For $C_{17}H_{10}O_3$ $[M+H]^+$: 263.0708; Found: 263.0714

General procedure for synthesis of compounds (5a- 5n): To a solution of aldehyde **4** (0.76 mmol) in THF (20 mL), the amine (0.76 mmole) was added and the reaction mixture was stirred at room temperature for 2-3 days (monitored by TLC). The resulting solution was evaporated under reduced pressure and the crude material was purified using silica gel column chromatography, eluted with 3-8% EtOAc/pet ether to afford pure product.

6-Methylbenzo[*b*]phenanthridine-5,7,12(6*H*)-trione (5a)

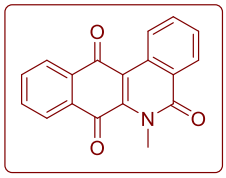

Starting from **4** (200 mg, 0.76 mmol), **5a** (160 mg, 73%) was isolated as a yellow solid: mp 163-165 °C; FT-IR (ν_{max}, cm^{-1}): 1679, 1659, 1479; ^{1}H NMR (400 MHz, $CDCl_3$): δ 9.30 (d, *J* = 8.3 Hz, 1H), 8.45 (dd, *J* = 8.0, 1.2 Hz, 1H), 8.09 (dd, *J* = 7.6, 1.2 Hz, 1H), 8.00 (dd, *J* = 7.4, 1.2 Hz, 1H), 7.85–7.68 (m, 3H), 7.62 (td, *J* = 8.04, 0.76 Hz, 1H), 3.91 (s, 3H); ^{13}C NMR (100 MHz, $CDCl_3$): δ 183.5, 181.6,

162.8, 142.2, 134.5, 133.8, 133.5, 132.7, 132.0, 131.9, 130.0, 128.5, 128.2, 127.2, 126.5, 126.3, 117.0, 35.7; HRMS (ESI): calcd. For $C_{18}H_{11}NO_3$ $[M+H]^+$: 290.0817; Found: 290.0803.

6-Ethylbenzo[*b*]phenanthridine-5,7,12(6*H*)-trione (5b)

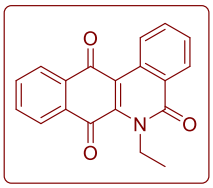

Starting from **4** (300 mg, 1.14 mmol), **5b** (142 mg, 50%) was isolated as a yellow solid: mp 168-170 °C; FT-IR (ν_{max}, cm^{-1}): 1741, 1706, 1693, 1676; ^{1}H NMR (400 MHz, $CDCl_3$) δ 9.30 (d, *J* = 8.5 Hz, 1H), 8.47 (d, *J* = 8.2 Hz, 1H), 8.11 (d, *J* = 7.5 Hz, 1H), 8.01 (d, *J* = 7.5 Hz, 1H), 7.80–7.62 (m, 4H), 4.50 (q, *J* = 6.8 Hz, 2H), 1.55 (t, *J* = 6.9 Hz, 3H); ^{13}C NMR (100 MHz, $CDCl_3$): δ 183.6, 181.7, 162.5, 142.3, 134.4, 133.7, 133.6, 132.7, 132.3, 131.9, 130.0, 128.5, 128.2, 127.5, 126.4, 126.3, 117.2, 43.6, 15.0; HRMS (ESI): calcd. For $C_{19}H_{13}NO_3$ $[M+H]^+$: 304.0974; Found: 304.0985.

6-Propylbenzo[*b*]phenanthridine-5,7,12(6*H*)-trione (5c)

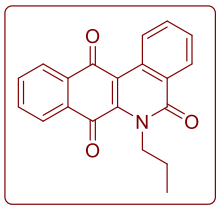

Starting from **4** (100 mg, 0.38 mmol), **5c** (55 mg, 45%) was isolated as a yellow solid: mp 158-160 °C; FT-IR (ν_{max}, cm^{-1}): 1670, 1647, 1458; ^{1}H NMR (400 MHz, $CDCl_3$): δ 9.31 (d, *J* = 8.3 Hz, 1H), 8.48 (dd, *J* = 8.0, 1.3 Hz, 1H), 8.12 (dd, *J* = 7.3, 1.3 Hz, 1H), 8.0 (dd, *J* = 7.3, 1.4 Hz, 1H), 7.62-7.82 (m, 4H), 4.45 (t, *J* = 7.7 Hz, 2H), 1.90 (sextet, *J* = 7.6 Hz, 2H), 1.03 (t, *J* = 7.4 Hz, 3H); ^{13}C NMR (100 MHz, $CDCl_3$): δ 183.7, 181.8, 162.7, 142.2, 134.4, 133.8, 133.6, 132.7, 132.3, 131.9, 130.0, 128.5, 128.3, 127.4, 126.4, 117.2, 49.0, 23.1, 11.5; HRMS (ESI): calcd. For $C_{20}H_{15}NO_3$ $[M+H]^+$: 318.1130; Found: 318.1131.

6-Cyclohexylbenzo[*b*]phenanthridine-5,7,12(6*H*)-trione (5d)

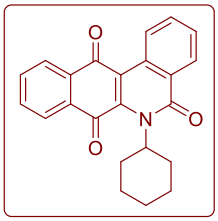

Starting from **4** (200 mg, 0.76 mmol), **5d** (62 mg, 23%) was isolated as a yellow solid: mp 224-226 °C; FT-IR (ν_{max}, cm^{-1}): 2923, 1671, 1652, 1592; ^{1}H NMR (400 MHz, $CDCl_3$): δ 9.31 (dd, *J* = 0.4, 8.4 Hz, 1H), 8.44 (dd, *J* = 8.0, 1.1 Hz, 1H), 8.15 (dd, *J* = 7.6, 1.2 Hz, 1H), 8.03 (dd, *J* = 7.3, 1.3 Hz, 1H), 7.81–7.62 (m, 4H), 4.25 (tt, *J* = 11.7, 3.4 Hz, 1H), 2.71 (q, *J* = 11.7 Hz, 2H), 1.98 (d, *J* = 12.4 Hz, 2H), 1.88 (broad, 2H), 1.69 (broad, 1H), 1.41-1.30 (m, 3H); ^{13}C NMR (100 MHz, $CDCl_3$): δ 183.5, 182.3, 163.1, 145.5, 134.3, 133.6, 132.7, 132.6, 131.6, 130.0, 128.5, 128.4, 127.9, 126.5,

126.4, 118.3, 65.4, 30.2, 26.7, 25.4; HRMS (ESI): calcd. For $C_{23}H_{19}NO_3$ $[M+H]^+$: 358.1439; Found: 358.1385.

6-Allylbenzo[*b*]phenanthridine-5,7,12(6*H*)-trione (5e)

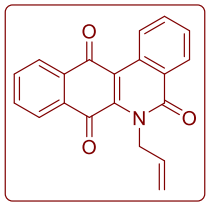

Starting from **4** (200 mg, 0.76 mmol), **5e** (50 mg, 21%) was isolated as a yellow solid: mp 162-164 °C; FT-IR (ν_{max}, cm^{-1}): 1674, 1647, 1385, 1050, 766; ^1H NMR (400 MHz, $CDCl_3$): δ 9.32 (d, *J* = 8.4 Hz, 1H), 8.49 (d, *J* = 7.8 Hz, 1H), 8.13 (d, *J* = 7.4 Hz, 1H), 8.00 (d, *J* = 7.4 Hz, 1H), 7.83–7.63 (m, 4H), 6.07 (ddt, *J* = 22.2, 10.4, 5.1 Hz, 1H), 5.28 (d, *J* = 5.1 Hz, 2H), 5.21 (dd, *J* = 13.3, 9.8 Hz, 2H); ^{13}C NMR (100 MHz, $CDCl_3$): δ 183.7, 181.7, 162.5, 141.9, 134.5, 133.9, 133.6, 132.7, 132.3, 131.9, 130.1, 128.6, 128.5, 127.4, 126.5, 126.4, 117.7, 48.3; HRMS (ESI): calcd. For $C_{20}H_{13}NO_3$ $[M+H]^+$: 316.0974; Found: 316.0967.

6-(Prop-2-ynyl)benzo[*b*]phenanthridine-5,7,12(6*H*)-trione (5f)

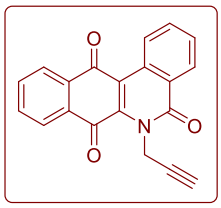

Starting from **4** (200 mg, 0.76 mmol), **5f** (48 mg, 20%) was isolated as a yellow solid: mp 187-189 °C; FT-IR (ν_{max}, cm^{-1}): 2370, 2326, 1677, 1647; ^1H NMR (400 MHz, $CDCl_3$): δ 9.34 (d, *J* = 8.5 Hz, 1H), 8.52 (dd, *J* = 8.0, 1.3 Hz, 1H), 8.15 (dd, *J* = 7.6, 1.1 Hz, 1H), 8.09 (dd, *J* = 7.5, 1.3 Hz, 1H), 7.86–7.65 (m, 4H), 5.51 (d, *J* = 2.4 Hz, 2H), 2.24 (t, *J* = 2.4 Hz, 1H); ^{13}C NMR (100 MHz, $CDCl_3$): δ 183.6, 181.4, 162.0, 140.8, 134.6, 134.2, 133.8, 132.7, 132.0, 131.8, 130.4, 128.8, 128.6, 127.2, 126.6, 118.2, 79.7, 72.3, 35.9; HRMS (ESI): calcd. For $C_{20}H_{11}NO_3$ $[M+H]^+$: 314.0817; Found: 314.0841.

6-(Methylcarbomethoxy)[*b*]phenanthridin-6(5*H*,7*H*,12*H*)-yl)acetate (5g)

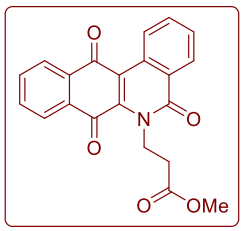

Starting from **4** (200 mg, 0.76 mmol), **5g** (103 mg, 39%) was isolated as a yellow solid: mp 226-228 °C; FT-IR (ν_{max}, cm^{-1}): 1758, 1677, 1585, 1058; ^1H NMR (400 MHz, $CDCl_3$): δ 9.34 (d, *J* = 8.4 Hz, 1H), 8.54–8.44 (m, 1H), 8.19–8.10 (m, 1H), 8.06–7.98 (m, 1H), 7.87–7.62 (m, 4H), 5.40 (s, 2H), 3.81 (s, 3H); ^{13}C NMR (100 MHz, $CDCl_3$): δ 183.7, 181.5, 169.2, 162.4, 140.0, 134.7, 134.2, 133.7, 132.7, 130.0, 131.6, 130.3, 128.9, 128.6, 127.2, 126.7, 126.5, 52.6, 47.5; HRMS (ESI): calcd. For $C_{20}H_{13}NO_5$ $[M+H]^+$: 348.0872; Found: 348.0868.

6-Benzylbenzo[*b*]phenanthridine-5,7,12(6*H*)-trione (5h)

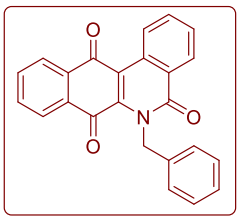

Starting from **4** (200 mg, 0.76 mmol), **5h** (110 mg, 39%) was isolated as a brown solid: mp 192-194 °C; FT-IR (ν_{max}, cm^{-1}): 1671, 1649, 1423, 1054, 978; ^{1}H NMR (400 MHz, $CDCl_3$): δ 9.35 (d, *J* = 8.5 Hz, 1H), 8.54 (d, *J* = 8.0 Hz, 1H), 8.10 (d, *J* = 7.7 Hz, 1H), 7.85 (t, *J* = 8.3 Hz, 2H), 7.75–7.62 (m, 3H), 7.28–7.12 (m, 5H), 5.99 (s, 2H); ^{13}C NMR (100 MHz, $CDCl_3$): δ 183.6, 181.6, 162.7, 141.9, 137.9, 134.3, 134.0, 133.5, 132.5, 132.2, 131.9, 130.1, 128.7, 128.6, 127.3, 127.2, 127.1, 126.3, 126.2, 117.9, 48.8; HRMS (ESI): calcd. For $C_{24}H_{15}NO_3$ $[M+H]^+$: 388.0945; Found: 388.0885.

6-(2-(Trifluoromethyl)benzyl)benzo[*b*]phenanthridine-5,7,12(6*H*)-trione (5i)

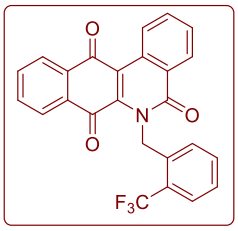

Starting from **4** (200 mg, 0.76 mmol), **5i** (45 mg, 14%) was isolated as a yellow solid: mp 230-232 °C; FT-IR (ν_{max}, cm^{-1}): 1676, 1658, 1458, 1311; ^{1}H NMR (400 MHz, $CDCl_3$): δ 9.38 (d, *J* = 8.5 Hz, 1H), 8.55 (d, *J* = 7.0 Hz, 1H), 8.14 (d, *J* = 7.4 Hz, 1H), 7.93 (d, *J* = 7.5 Hz, 1H), 7.90–7.84 (m, 1H), 7.78–7.64 (m, 4H), 7.38–7.30 (m, 2H), 6.95 (d, *J* = 7.4 Hz, 1H), 5.90 (s, 2H); ^{13}C NMR (100 MHz, $CDCl_3$): δ 183.8, 180.8, 162.7, 141.4, 136.6, 134.7, 134.3, 133.8, 132.7, 132.1, 131.8, 130.4, 128.9, 128.7, 127.3, 126.8, 126.7, 126.5, 126.4, 125.6, 118.0, 48.7; HRMS (ESI): calcd. For $C_{25}H_{14}{}^{19}F_3NO_3$ $[M+H]^+$: 434.1004; Found: 434.0986.

6-(4-Chlorobenzyl)benzo[*b*]phenanthridine-5,7,12(6*H*)-trione (5j)

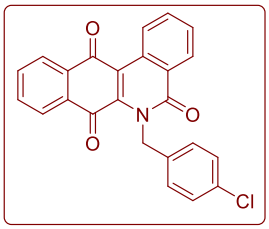

Starting from **4** (200 mg, 0.76 mmol), **5j** (60 mg, 20%) was isolated as a yellow solid: mp 203-205 °C; FT-IR (ν_{max}, cm^{-1}): 1667, 1654, 1588, 1490, 1056; ^{1}H NMR (400 MHz, $CDCl_3$): δ 9.34 (d, *J* = 8.4 Hz, 1H), 8.52 (d, *J* = 8.0 Hz, 1H), 8.12 (d, *J* = 7.5 Hz, 1H), 7.90 (d, *J* = 7.4 Hz, 1H), 7.85 (t, *J* = 7.8 Hz, 1H), 7.78–7.64 (m, 3H), 7.22 (d, *J* = 8.4 Hz, 2H), 7.14 (d, *J* = 8.3 Hz, 2H), 5.90 (s, 2H); ^{13}C NMR (100 MHz, $CDCl_3$): δ 183.5, 181.5, 162.7, 136.3, 134.5, 134.1, 133.6, 132.9, 132.5, 132.0, 131.8, 130.3, 128.7, 128.5, 127.3, 126.4, 126.3, 118.1, 48.8; HRMS (ESI): calcd. For $C_{24}H_{14}{}^{35}ClNO_3$ $[M+H]^+$: 400.0740; Found: 400.0730.

6-(4-Methoxybenzyl)benzo[*b*]phenanthridine-5,7,12(6*H*)-trione (5k)

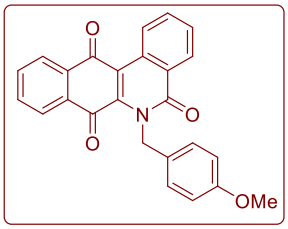

Starting from **4** (200 mg, 0.76 mmol), **5k** (50 mg, 17%) was isolated as a brown solid: mp 219-221 °C; FT-IR (ν_{max}, cm-^{1}): 1683, 1651, 1515; ^{1}H NMR (400 MHz, $CDCl_3$): δ 9.34 (d, *J* = 8.4 Hz, 1H), 8.54 (d, *J* = 8.0 Hz, 1H), 8.10 (d, *J* = 7.5 Hz, 1H), 7.89 (d, *J* = 7.6 Hz, 1H), 7.86–7.81 (m, 1H), 7.76–7.63 (m, 3H), 7.14 (d, *J* = 8.6 Hz, 2H), 6.76 (d, *J* = 8.6 Hz, 2H), 5.96 (s, 2H), 3.71 (s, 3H); ^{13}C NMR (100 MHz, $CDCl_3$): δ 183.6, 181.9, 162.8, 158.6, 142.1, 134.3, 134.0, 133.6, 132.6, 132.4, 131.9, 130.1, 128.9, 128.7, 128.6, 127.4, 126.4, 126.2, 55.3, 48.0; HRMS (ESI): calcd. For $C_{25}H_{17}NO_4$ $[M+H]^+$: 396.1236; Found: 396.1234.

6-(4-Nitrobenzyl)benzo[*b*]phenanthridine-5,7,12(6*H*)-trione (5l)

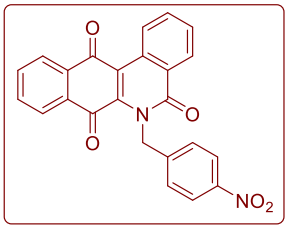

Starting from **4** (200 mg, 0.76 mmol), **5l** (70 mg, 22%) was isolated as a yellow solid: mp 152-154 °C; FT-IR (ν_{max}, cm^{-1}): 1674, 1646, 1510; ^{1}H NMR (400 MHz, DMSO-*d*$_6$): δ 9.33 (s, 1H), 8.48 (s, 1H), 8.11 (s, 3H), 8.87– 8.36 (m, 5H), 7.20 (s, 2H), 5.86 (s, 2H); ^{13}C NMR (100 MHz, DMSO-*d*$_6$): δ 184.0, 181.0, 162.5, 147.4, 146.6, 143.0, 135.0, 134.7, 134.4, 132.5, 130.6, 128.7, 128.2, 127.6, 127.0, 126.8, 126.4, 123.8, 116.7, 51.1; HRMS (ESI): calcd. For $C_{24}H_{14}N_2O_4$ $[M+H]^+$: 411.0981; Found: 411.0971.

6-(4-(Trifluoromethyl)benzyl)benzo[*b*]phenanthridine-5,7,12(6*H*)-trione (5m)

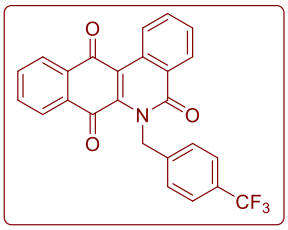

Starting from **4** (200 mg, 0.76 mmol), **5m** (155 mg, 47%) was isolated as a yellow solid: mp 219-221 °C; FT-IR (ν_{max}, cm-1): 1674, 1658, 1416, 1162, 1068; ^{1}H NMR (400 MHz, $CDCl_3$): δ 9.35 (d, *J* = 8.4 Hz, 1H), 8.51 (d, *J* = 8.0 Hz, 1H), 8.12 (d, *J* = 7.7 Hz, 1H), 7.90 (d, *J* = 7.6 Hz, 1H), 7.86 (t, *J* = 7.8 Hz, 1H), 7.76–7.65 (m, 3H), 7.52 (d, *J* = 8.0 Hz, 2H), 7.32 (d, *J* = 8.0 Hz, 2H), 5.92 (s, 2H); ^{13}C NMR (100 MHz, $CDCl_3$): δ 183.6, 181.3, 162.8, 142.0, 141.1, 134.7, 134.2, 133.8, 132.6, 132.0, 130.4, 128.9, 128.7, 127.3, 127.0, 126.5, 126.4, 125.6, 125.5, 118.2, 49.5; HRMS (ESI): calcd. For $C_{25}H_{14}{}^{19}F_3NO_3$ $[M]^+$: 433.1004; Found: 433.1000.

6-(3,4,5-Trimethoxybenzyl)benzo[*b*]phenanthridine-5,7,12(6*H*)-trione (5n)

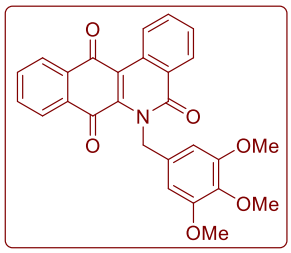

Starting from **4** (200 mg, 0.76 mmol), **5n** (45 mg, 13%) was isolated as a yellow solid: mp 200-202 °C; FT-IR (ν_{max}, cm^{-1}): 1669, 1649, 1588, 1419, 1050; ^{1}H NMR (400 MHz, $CDCl_3$) δ 9.34 (d, *J* = 8.2 Hz, 1H), 8.53 (d, *J* = 8.1 Hz, 1H), 8.10 (d, *J* = 7.7 Hz, 1H), 7.88-7.83 (m, 2H), 7.76–7.63 (m, 3H), 6.41 (s, 2H), 5.93 (s, 2H), 3.73 (s, 3H), 3.71 (s, 6H); ^{13}C NMR (100 MHz, $CDCl_3$): 183.5, 181.8, 162.8, 153.3, 142.2, 137.2, 134.5, 134.0, 133.7, 133.6, 132.6, 132.3, 131.8, 130.2, 128.7, 128.6, 127.3, 126.5, 126.0, 117.8, 104.8, 60.8, 56.1, 48.5; HRMS (ESI): calcd. For $C_{27}H_{21}NO_6$ $[M+H]^+$: 478.1278; Found: 478.1232.

2.1.4.3. Cyclic voltammetry

CV analysis was performed using a Basi Epsilon –EC-Ver 2.00.71- USB Bioanalytical system. A three-electrode setup was used: Pt wire auxiliary electrode, platinum disc working electrode, and $Ag/AgNO_3$ reference electrode. All potential values were calibrated against the saturated calomel electrode (SCE) by measuring the oxidation of ferrocene as a reference ($E°$ (Fc^+/Fc) = 0.424 V vs SCE). The working electrode was polished with 0.05 μM alumina (BASi polishing solution) on a felt pad and washed with de-ionized water and rinsed using acetonitrile. All electrochemical samples were purged with N_2 for 5 min and were measured under a nitrogen atmosphere. The supporting electrolyte of 0.1 M tetrabutylammoniumhexafluorophosphate ($TBAPF_6$) and 0.5 mM stock solution of the compound was prepared in MeCN.

2.1.4.4. Superoxide detection using luminol assay

A luminol stock solution (4 mM) was prepared by dissolving 7.1 mg of luminol in 10 mL of 30 mM sodium hydroxide solution and stored under ice. A stock solution of **5a-5n** 2.5 mM was prepared in DMSO and 1 mM NADPH was prepared in phosphate buffer pH 7.4. The enzyme stock solution was prepared by dissolving 1.5 mg of the lyophilized human DT-diaphorase (Sigma, ≥100 units; wherein 1 unit is 1.0 μmole cytochrome C reduced per min/mg) in PB pH 7.4. 20 μL of this enzyme solution was further diluted to 100 μL and was used in the subsequent reactions. To a 96-microwell plate the reaction mixture was prepared in quadruplicate by dissolving 2 μL of **5a-5n**, 20 μL of NADPH solution, 5 μL of luminol solution, and 2 μL of the enzyme solution in 171 μL of phosphate buffer pH 7.4. The resulting mixture was incubated at

37 °C and luminescence from reaction mixture was measured using microtiter plate reader at 1 minute interval for 4 minutes.

2.1.4.5. Minimum Inhibitory Concentration Determination

The Minimum Inhibitory Concentration (MIC) assay is used to determine the inhibitory potential of a compound against bacterial pathogens. To determine the MIC, the microbroth dilution technique is commonly used as recommended by National Committee for Clinical Laboratory Standards.[40] For this, a fixed bacterial inoculum (5×10^5 CFU/mL) is added into a series of test wells in a microtitre plate that contain various concentrations of compound under test. Following a period of incubation (37 °C, 18-20 hours), the wells are examined for growth. The lowest concentration of antibiotic that inhibits growth of the organism, as detected visually is designated as the MIC.

2.1.4.6. ROS Generation in buffer

2.1.4.6.A. Dihydroethidium (DHE) assay for superoxide detection

A stock solution of dihydroethidium (1.2 mg, 10 mM) was prepared in DMSO (380 μL) and stored in the dark at -20 ℃. A stock solution of **5f** (2 mg/mL) was prepared in DMSO. Stock solution of 1 mM NADPH was prepared in PB pH 7.4. The enzyme stock solution was prepared by dissolving 1.5 mg of the lyophilized human DT-Diaphorase (Sigma, ≥100 units; wherein 1 unit is 1.0 μmole cytochrome C reduced per min/mg) in PB pH 7.4. 20 μL of this enzyme solution was further diluted to 100 μL and was used in the subsequent reactions. The reaction mixture was prepared by dissolving of **5f** (2 μL, 200 μg/mL or 500 μg/mL), NADPH solution (20 μL, 1 mM), dihydroethidium (1 μL, 10 mM) and 2 μL of the enzyme solution in PB pH 7.4 (175 μL). The reaction mixture was incubated at 37 ˚C for 10 minutes. The resulting mixture was filtered (0.22 μm) and injected (50 μL) in an Agilent high performance liquid chromatography (HPLC). The mobile phase was H_2O/ CH_3CN containing 0.1 % trifluroacetic acid. The stationary phase was a C_{18} reverse-phase column (5μm, 4.6 × 250 mm). Fluorescence detection at 510 nm (excitation) and 595 nm (emission) was used to monitor this compound. Hydroethidium, ethidium and hydroxyethidium were separated by a linear increase in CH_3CN concentration from 10% to 70% in 46 min at a flow rate of 0.5 mL/ min. The elution was monitored by a variable UV detector at 210 and 350 nm and a fluorescence detector with excitation and emission at 510 and 595 nm, respectively.

2.1.4.6.B. Hydrogen peroxide estimation using Amplex Red assay

A stock solution of **5f** (2.5 mM) was prepared in DMSO and 1 mM NADPH was prepared in PB pH 7.4. The enzyme stock solution was prepared by dissolving 1.5 mg of the lyophilized human DT-Diaphorase (Sigma, ≥100 units; wherein 1 unit is 1.0 μmole cytochrome C reduced per min/mg) in PB pH 7.4. 20 μL of this enzyme solution was further diluted to 100 μL and was used in the subsequent reactions. The reaction mixture was prepared by adding **5f** (1 μL, 2.5 mM), NADPH (20 μL, 1 mM), DT-Diaphorase (2 μL stock as previously prepared) in phosphate buffer of pH 7.4 (27 μL).[41] To the reaction mixture, 50 μL of a premixed solution of 10-acetyl-3,7-dihydroxyphenoxazine or Amplex Red® (prepared by following manufacturer's protocol from Invitrogen) was added. The resulting mixture was incubated at 37 °C and fluorescence (excitation 550 nm; emission 590 nm) from reaction mixture was measured using microtiter plate reader at 1 minute interval for 5 minutes.

2.1.4.7. ROS generation by 5f in *S. aureus*

2.1.4.7.A. Intracellular superoxide detection using DHE assay

S. aureus was cultured in 5 mL of Cation Adjusted Mueller-Hinton Broth (CAMHB) medium at 37 ºC to obtain O.D. of 0.5. This bacterial solution was incubated with dihydroethidium (50 μM) and **5f** (2 and 5 μg/mL) at 37 ºC for 1 h under dark conditions. The suspension was centrifuged to aspirate out excess of compound and dihydroethidium in the medium. The bacterial pellet was washed with phosphate buffer pH 7.4.[30,42] The resulting pellet was re-suspended with acetonitrile and cells were lysed using a probe sonication for 3 min on ice. The cell lysate was then removed by centrifugation and the supernatant acetonitrile was separated and stored at -20 ºC before injecting in HPLC. The HPLC method used was as described previously.

2.1.4.7.B. Extracellular H_2O_2 estimation

Staphylococcus aureus was cultured in 5 mL of Cation Adjusted Mueller-Hinton Broth (CAMHB) medium at 37 ºC for ~2 hrs to obtain O.D. of 0.1. This bacterial solution (50 μL) was treated with **5f** in DMSO (1%) so that the final concentration was 2 μg/mL and incubated at 37 ºC for 60 min. 50 μL of a premixed solution of Amplex Red® (prepared by following manufacturer's protocol from Invitrogen) was added and incubated at RT for 25 min before measuring the fluorescence using a microtiter plate reader (excitation 550 nm; emission 590 nm).[12,32,33,43] A calibration curve with known concentrations of hydrogen peroxide was generated

in CAMHB medium and was used to quantify hydrogen peroxide produced during incubation of test compound. Data presented are an average of three independent experiments.

Table S2. Calibration curve of H_2O_2 in of Cation Adjusted Mueller-Hinton Broth using amplex red assay

H_2O_2 in μM	RFI	Corrected	S.D.
0	131.81	0.00	9.40
1	182.74	50.93	11.17
5	392.86	261.06	25.97
10	650.33	518.52	17.86
20	1250.21	1118.40	54.53
30	1823.99	1692.18	64.65
40	2252.44	2120.64	34.68
50	2501.92	2370.11	29.42
60	2711.42	2579.62	11.76

RFI: Relative fluorescence intensity

2.1.4.7.C. Estimation of intracellular oxidative species using H_2DCF-DA

An overnight culture of MSSA 29213 was diluted 1:100 with fresh Cation Adjusted Mueller Hinton Broth (CAMHB) and allowed to grow until an OD_{625} of 0.3 was reached. This culture was split into multiple tubes of 2 ml each. To each tube, 20 μl of 100X DMSO stocks of **5f** was added, such that a series of final concentrations ranging from 0.5 μg/mL to 0.03 μg/mL was obtained in triplicate. The culture tubes with compound were incubated for 1 hour and normalized to an OD_{625} of 1. 1 mL of the normalized culture was then centrifuged, washed twice with PBS and re-suspended in 500 μl of PBS. This was further diluted 1:10. To 135 μl of the diluted culture 15 μl of 100 μM 2,7-dichlorodihydrofluorescein-diacetate(H_2DCF-DA) was added per well of a 96-well black plate. The plate was incubated for 2 hours at 37 °C. Fluorescence was measured at an excitation wavelength of 485 nm and emission wavelength of 535 nm. Fluorescence intensity of treated verses untreated cells was compared.

2.1.4.7.A. Cytotoxicity Assay

To test the effect of **5f** on the growth of mammalian cells, a cytotoxicity assay was performed as per published protocols.[44] In brief, 10,000 A549 (lung cell carcinoma) cells were seeded in a 96-well plate and grown for 24 hours at 37°C in a humidified atmosphere of 5% CO_2 and 95% air in F12K medium supplemented with 10% heat-inactivated fetal bovine serum, 1.5 g Sodium

bicarbonate/L, 100 µg/mL of Penicillin and 10 µg/mL of Streptomycin. The next day, cells were washed with PBS and different concentrations of **5f** were added in serum free media in triplicate. Following 72 hours of incubation, MTT (3-(4, 5-Dimethyl-2-thiazolyl)-2, 5-diphenyl-2H-tetrazolium bromide) was added to a final concentration of 1 mg/mL for 5 hours. At the end of the incubation period, the media were removed by gently inverting the plate. DMSO was added to the wells to solubilize the formazan crystals and absorbance was read at 595 nm in a plate reader. The absorbance of treated vs. untreated cells was compared. % survival vs. concentration of **5f** was plotted to determine the GI_{50} concentration.

2.1.5. Spectral charts

^{1}H NMR Spectrum (400 MHz, $CDCl_3$) of **2**

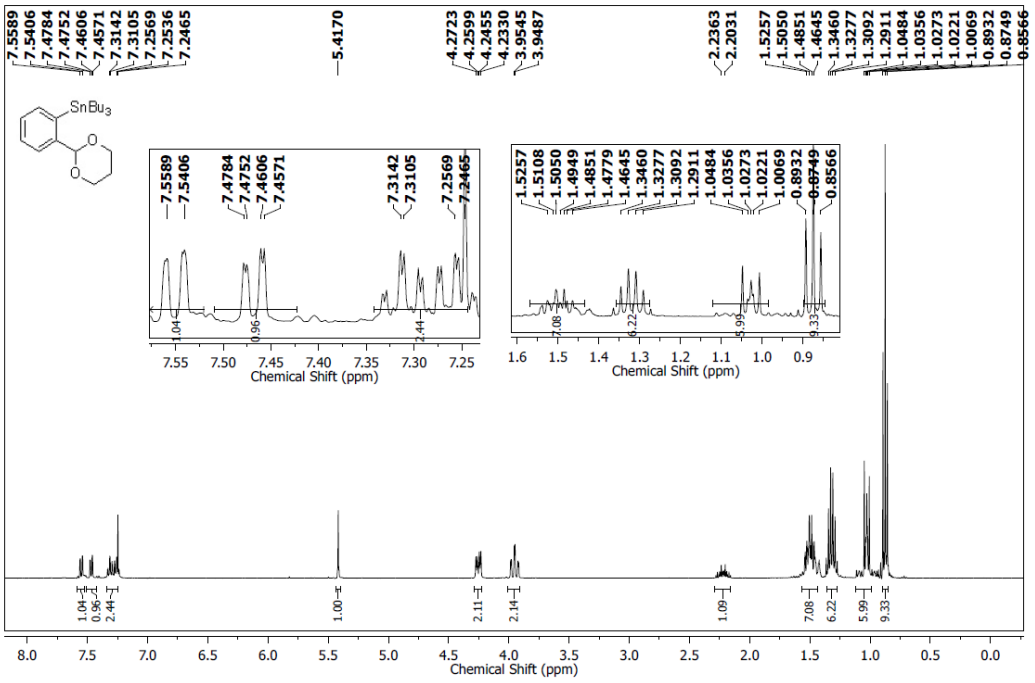

^{13}C NMR Spectrum (100 MHz, $CDCl_3$) of **2**

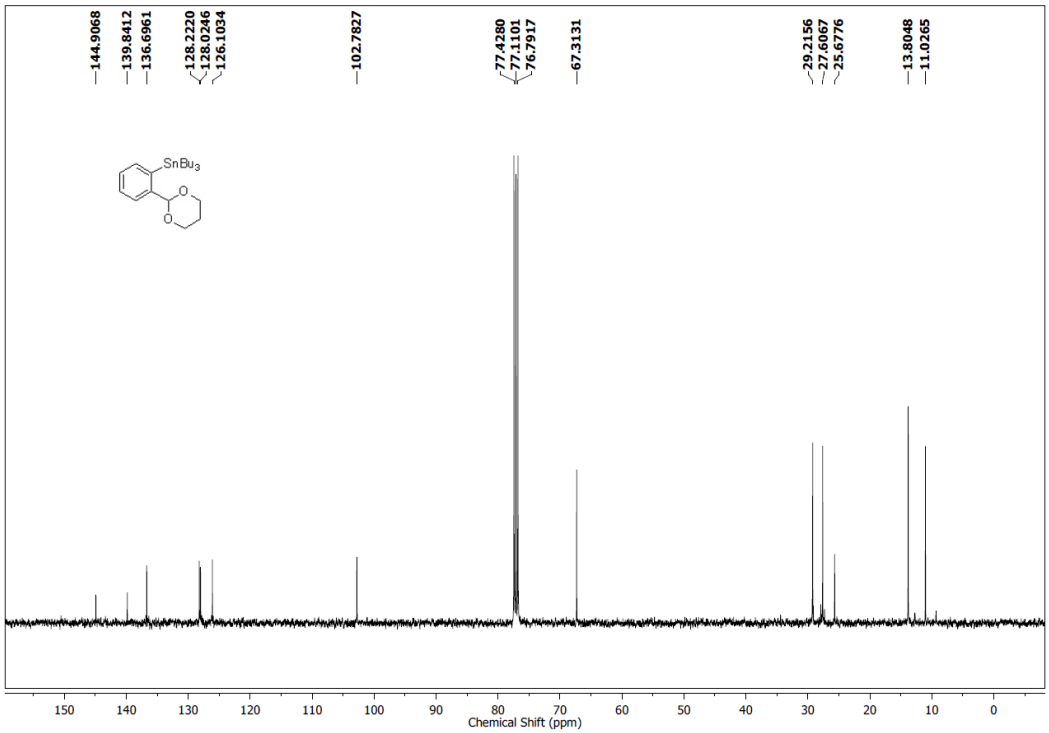

^{1}H NMR Spectrum (400 MHz, $CDCl_3$) of **3**

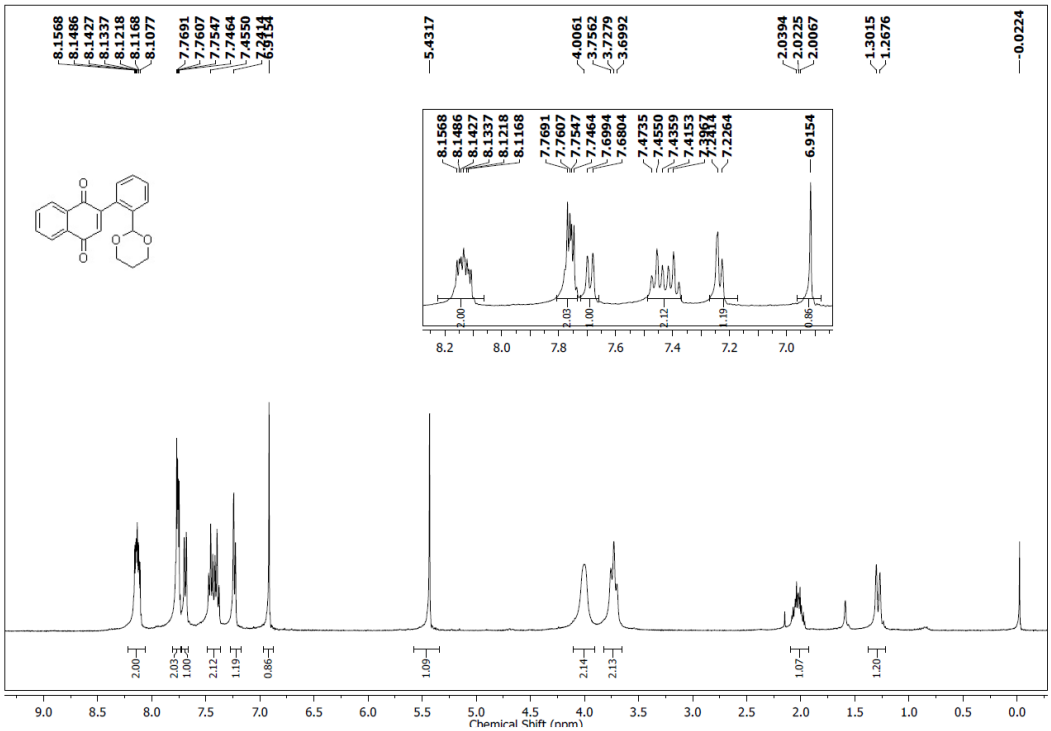

^{13}C NMR Spectrum (100 MHz, $CDCl_3$) of **3**

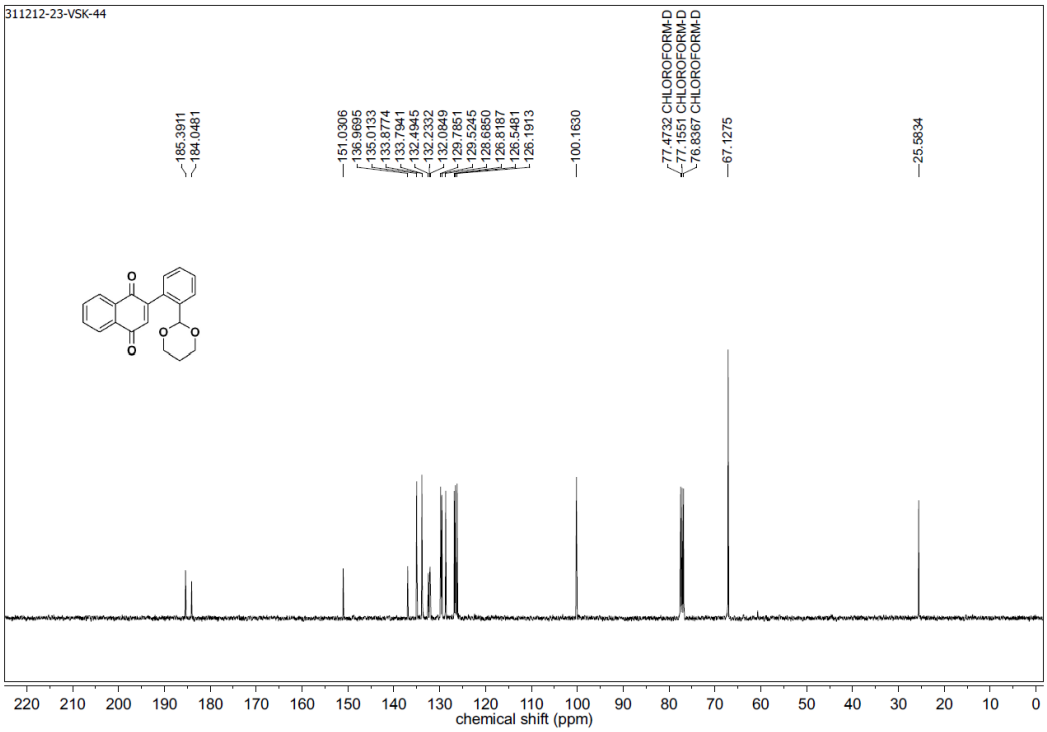

^{1}H NMR Spectrum (400 MHz, $CDCl_3$) of **4**

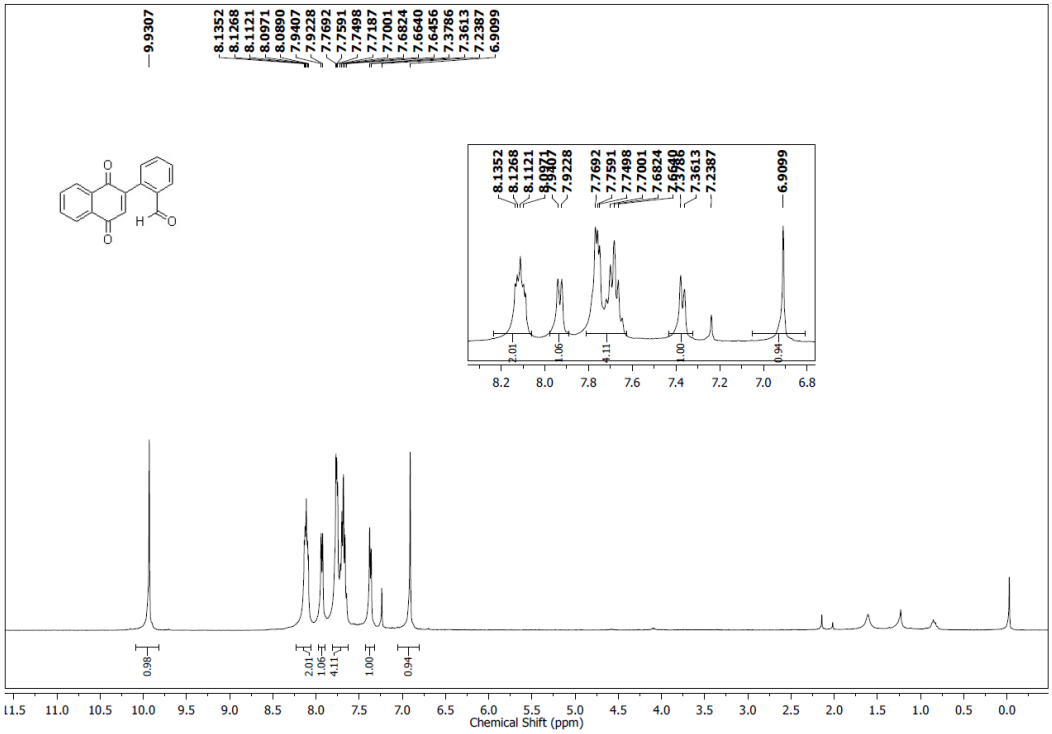

^{13}C NMR Spectrum (100 MHz, $CDCl_3$) of **4**

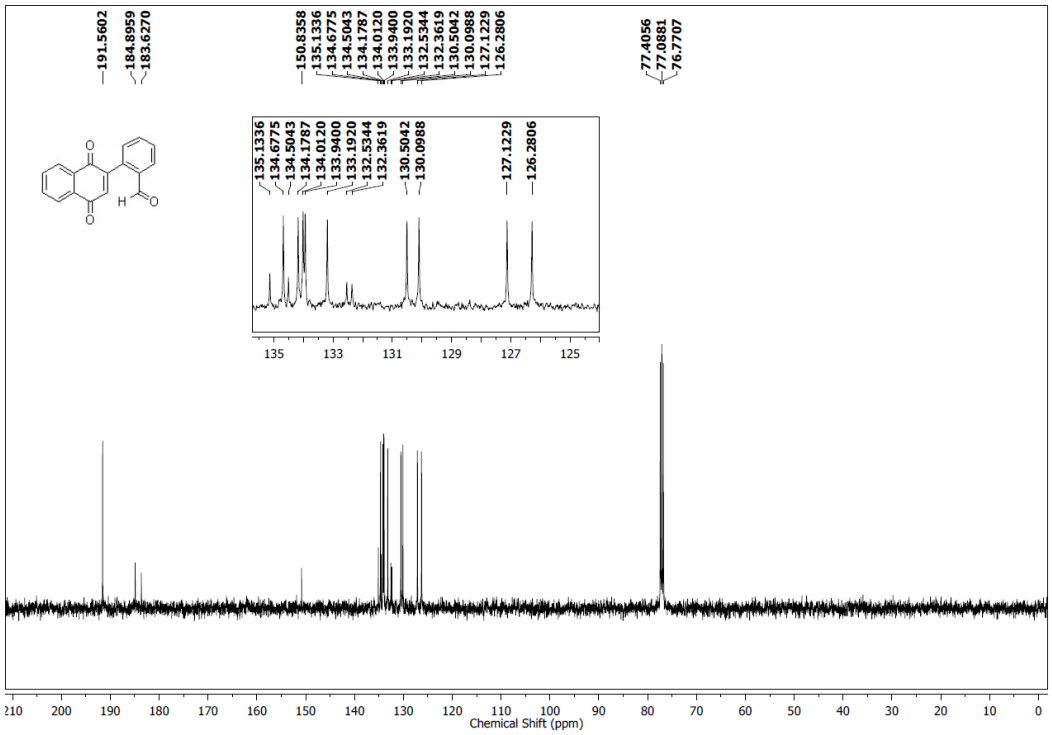

^{1}H NMR Spectrum (400 MHz, $CDCl_3$) of **5a**

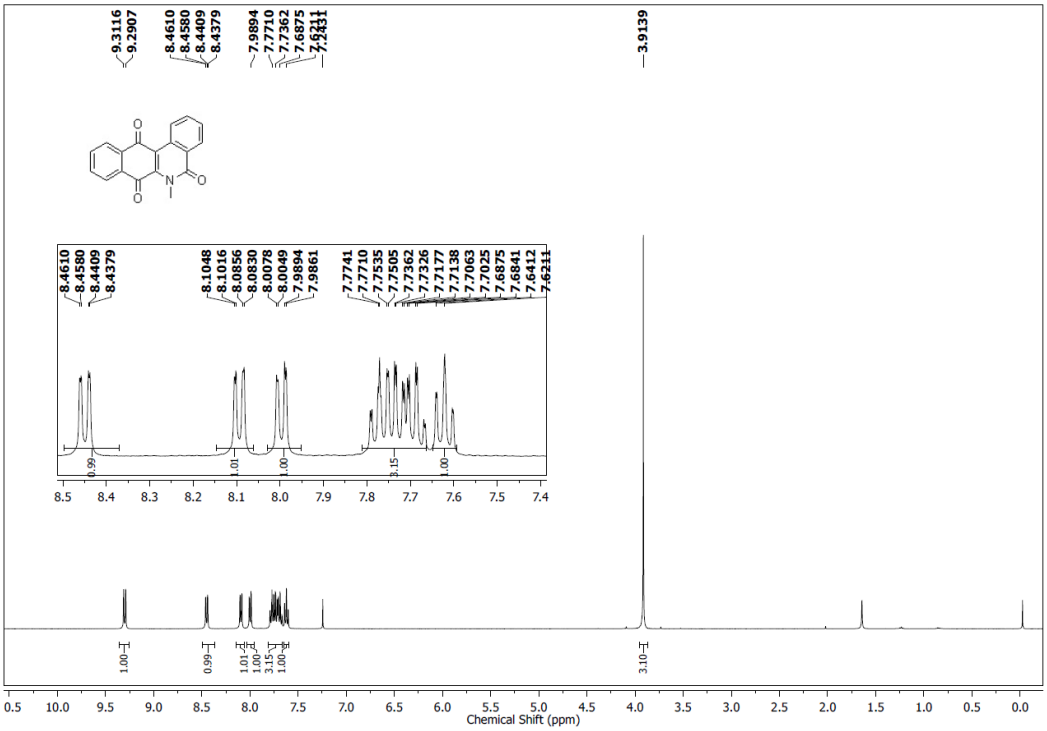

^{13}C NMR Spectrum (100 MHz, $CDCl_3$) of **5a**

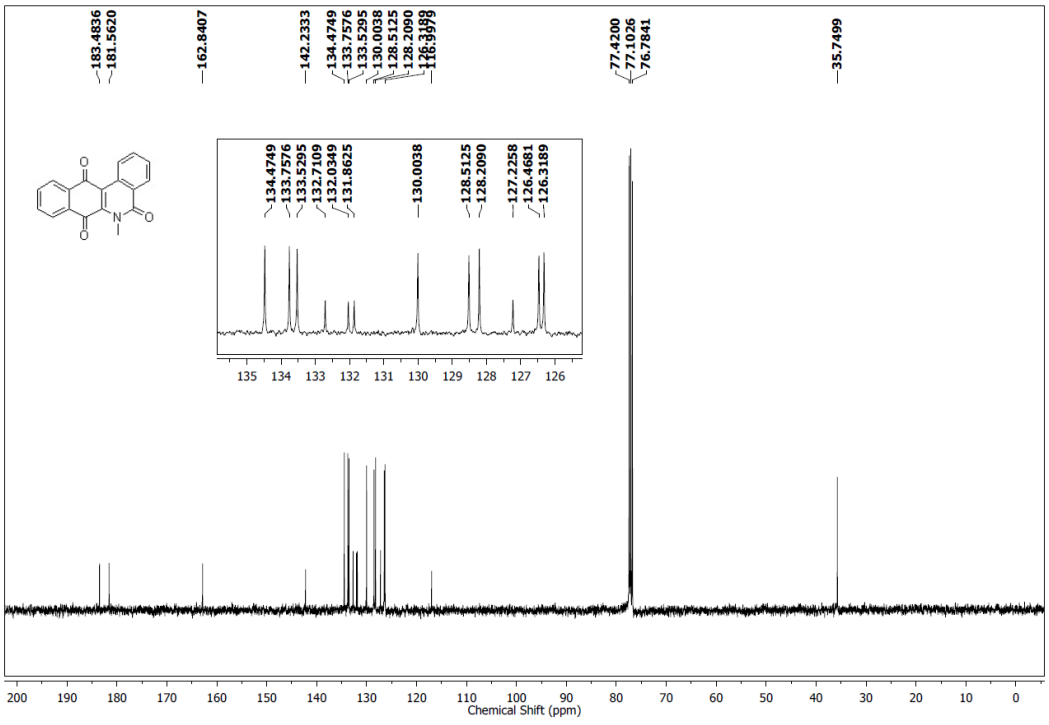

^{1}H NMR Spectrum (400 MHz, $CDCl_3$) of **5b**

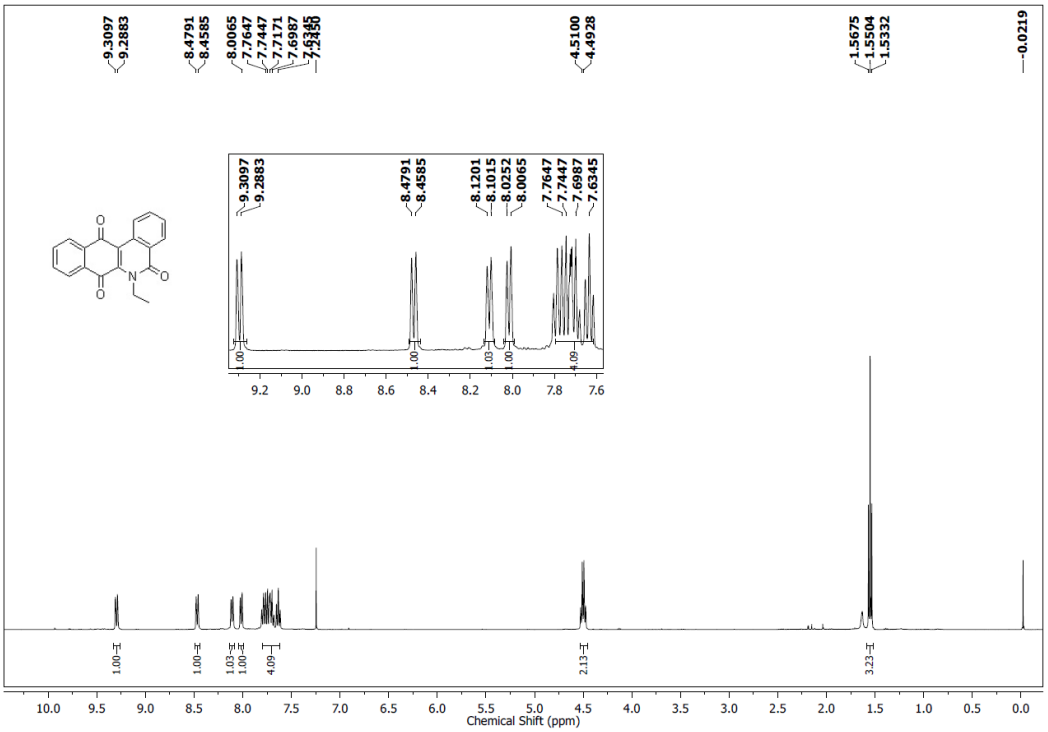

^{13}C NMR Spectrum (100 MHz, $CDCl_3$) of **5b**

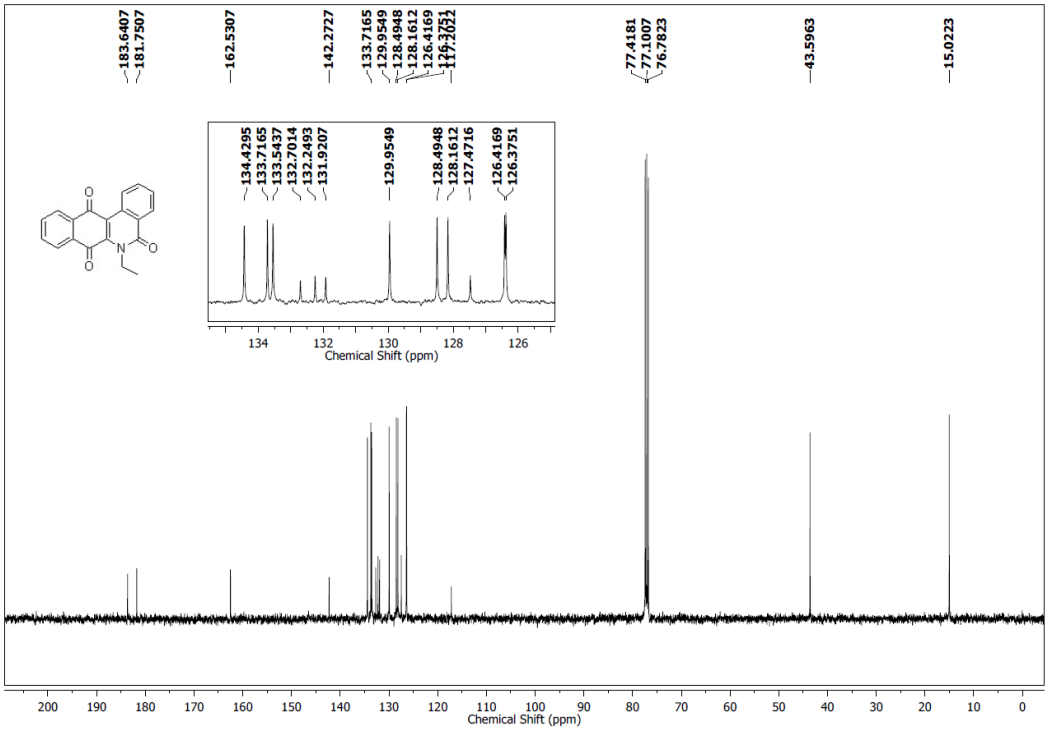

^{1}H NMR Spectrum (400 MHz, $CDCl_3$) of **5c**

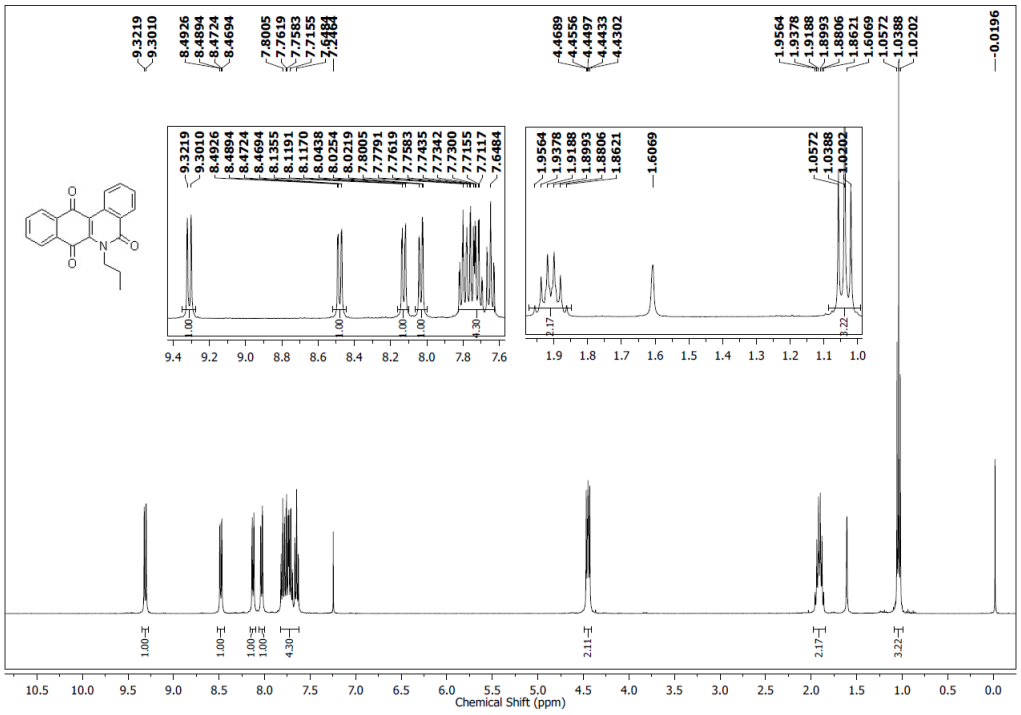

^{13}C NMR Spectrum (100 MHz, $CDCl_3$) of **5c**

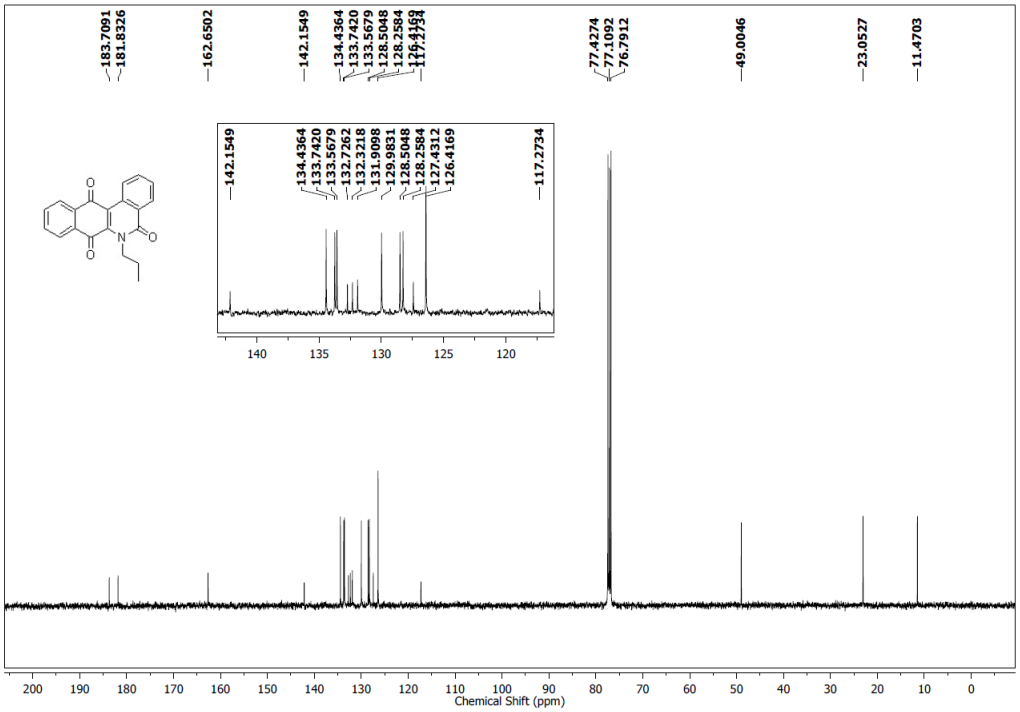

^{1}H NMR Spectrum (400 MHz, $CDCl_3$) of **5d**

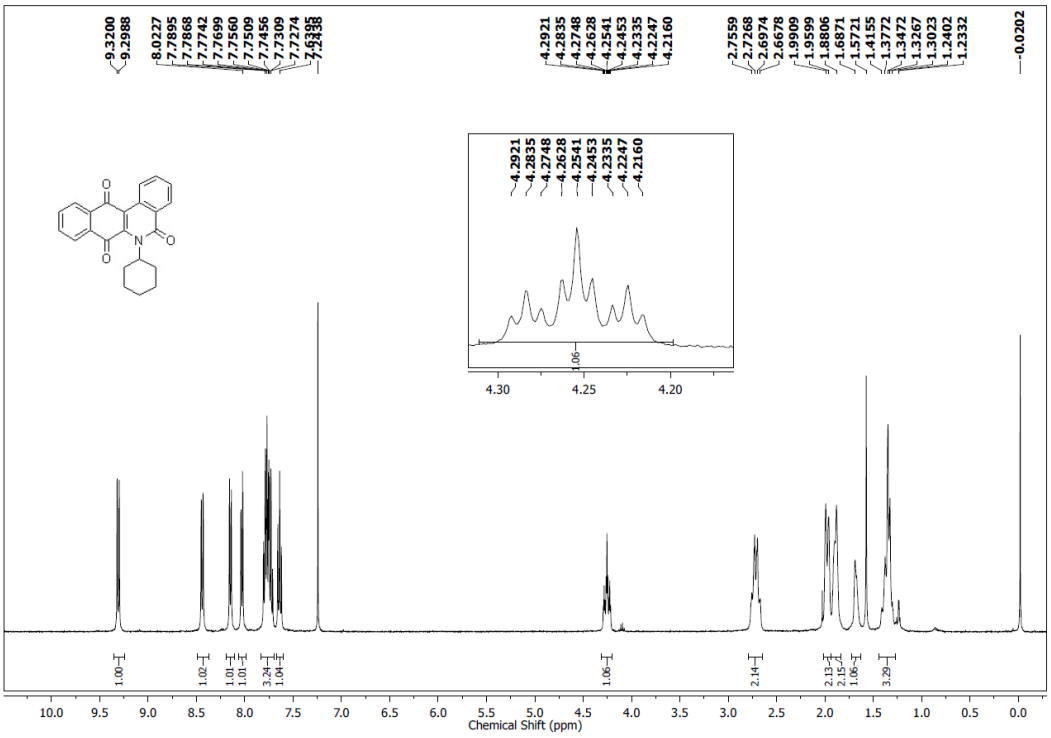

^{13}C NMR Spectrum (100 MHz, $CDCl_3$) of **5d**

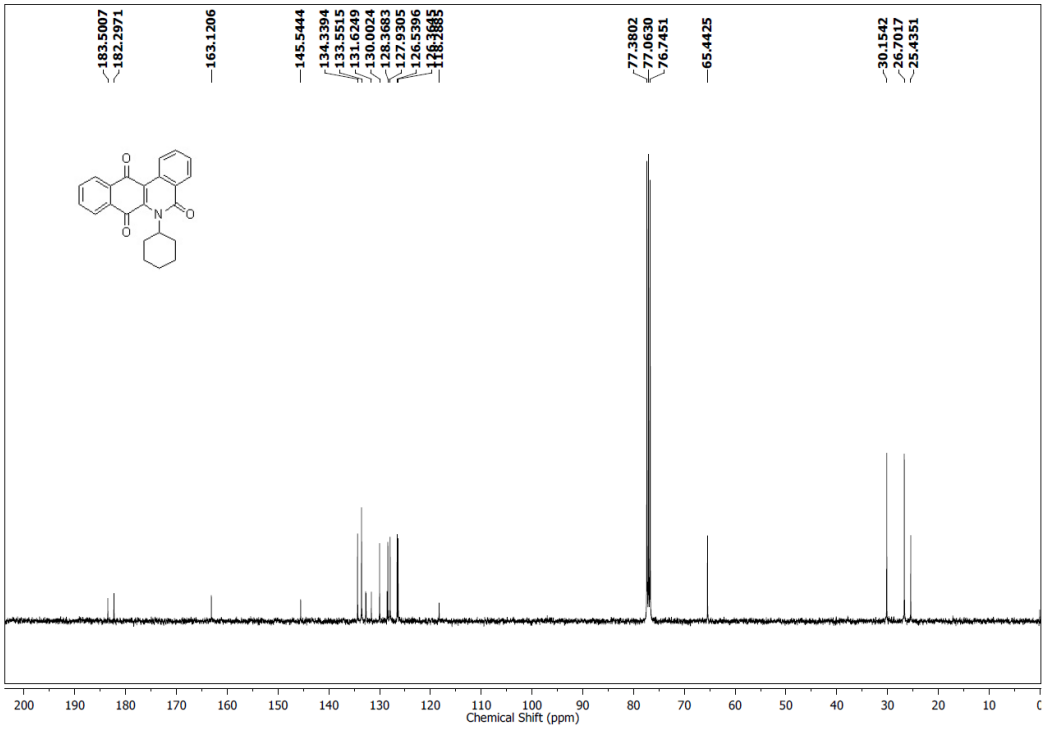

^{1}H NMR spectrum (400 MHz, $CDCl_3$) of **5e**

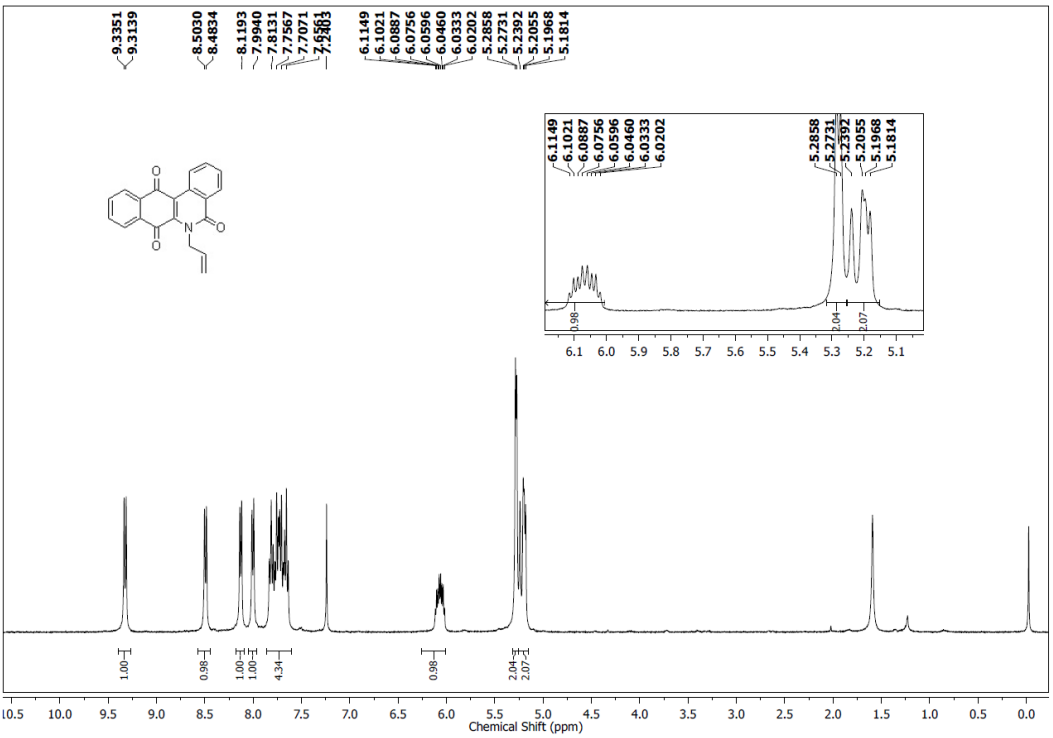

^{13}C NMR spectra (100 MHz, $CDCl_3$) of **5e**

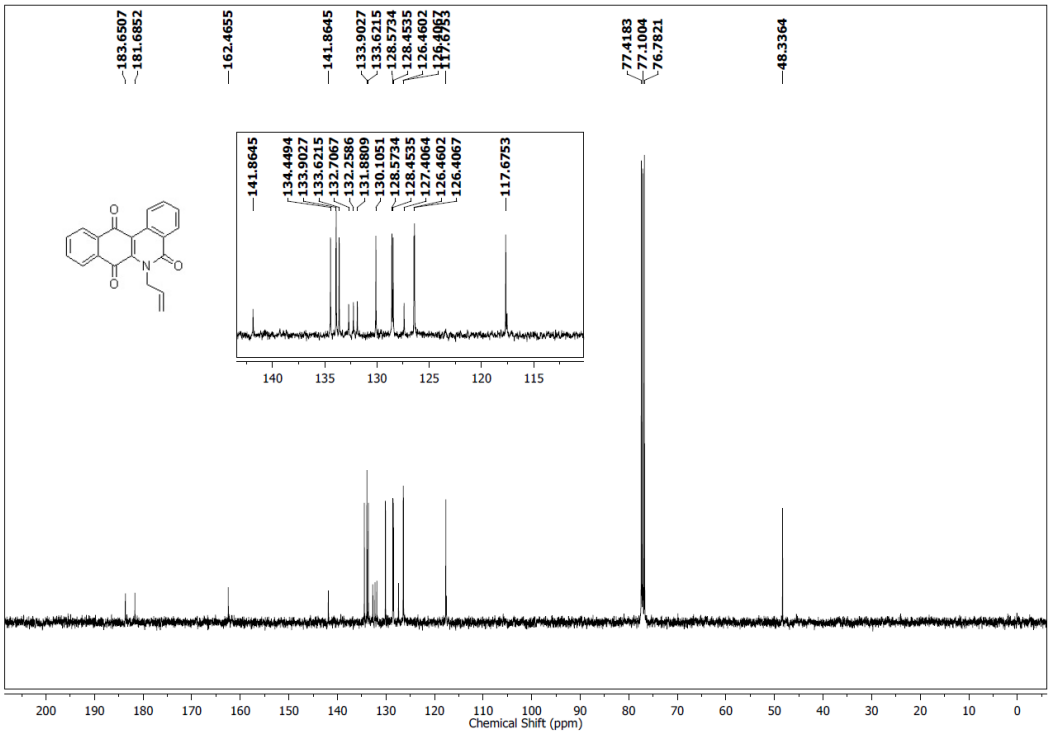

^{1}H NMR spectrum (400 MHz, $CDCl_3$) of **5f**

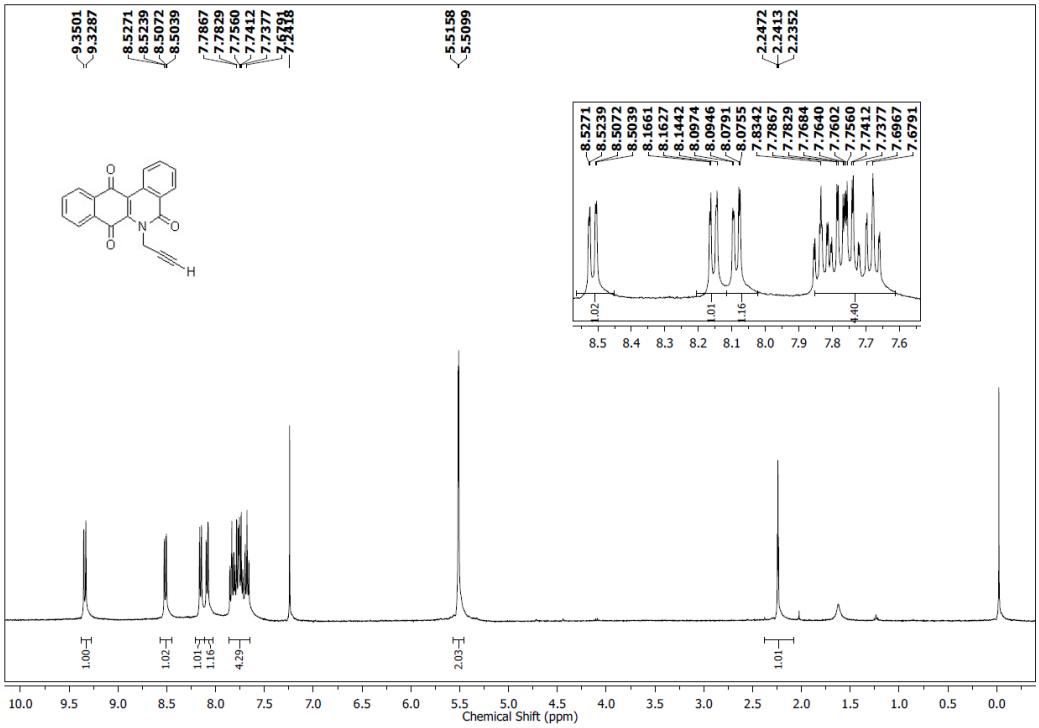

^{13}C NMR spectrum (100 MHz, $CDCl_3$) of **5f**

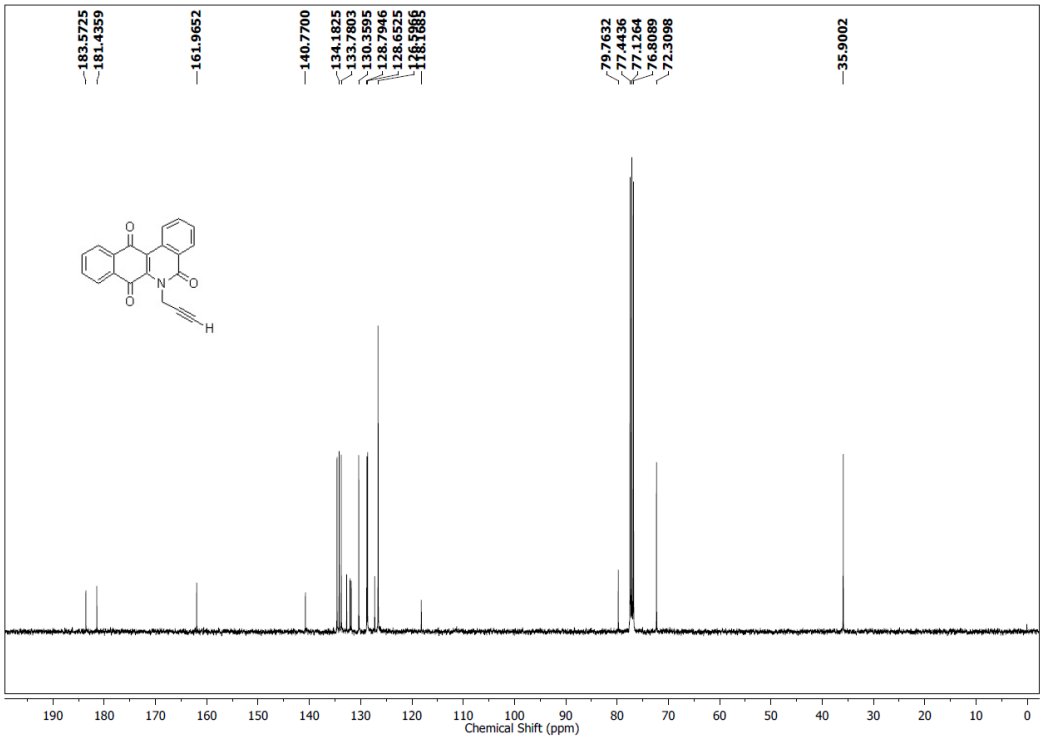

^{1}H NMR spectrum (400 MHz, $CDCl_3$) of **5g**

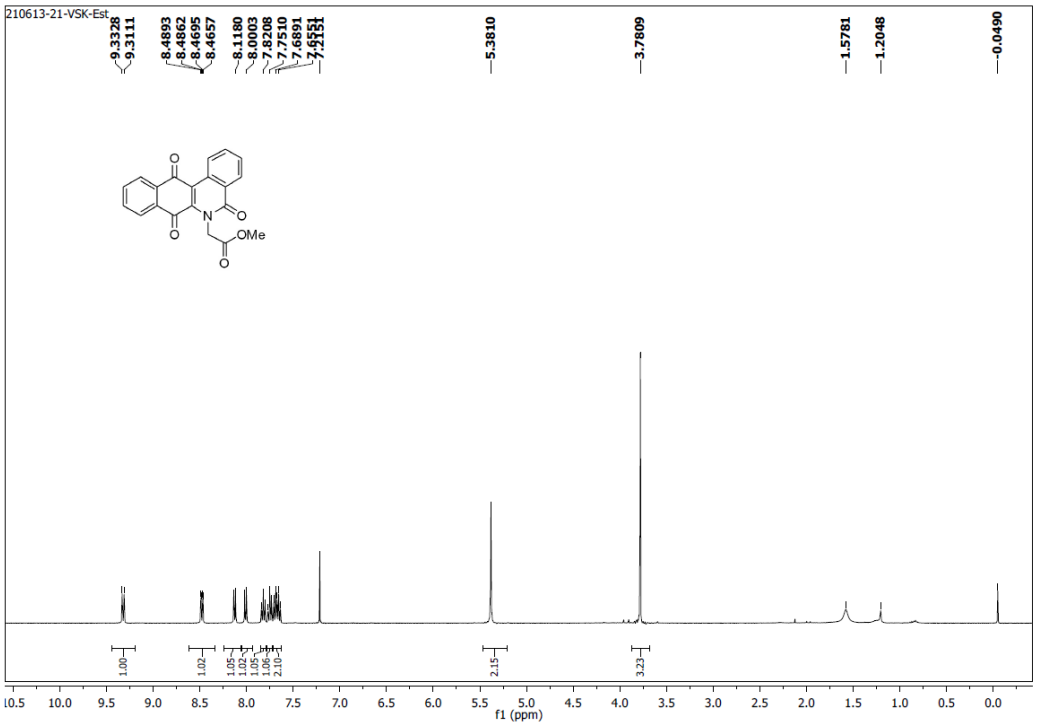

^{13}C NMR spectrum (100 MHz, $CDCl_3$) of **5g**

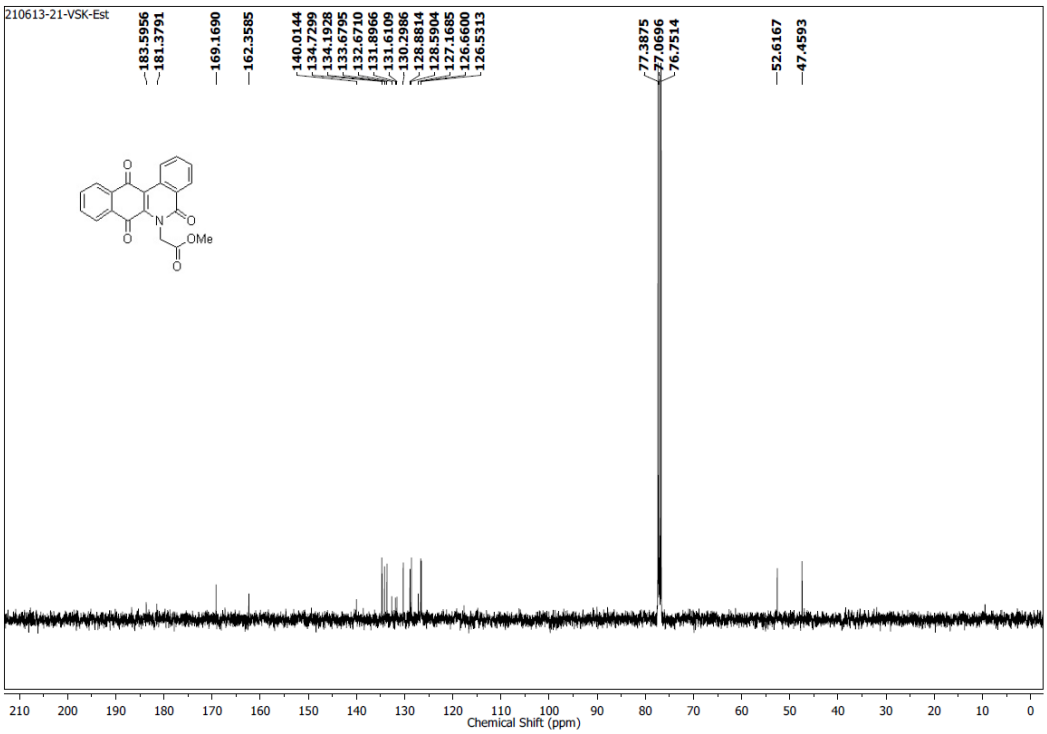

^{1}H NMR spectrum (400 MHz, $CDCl_3$) of **5h**

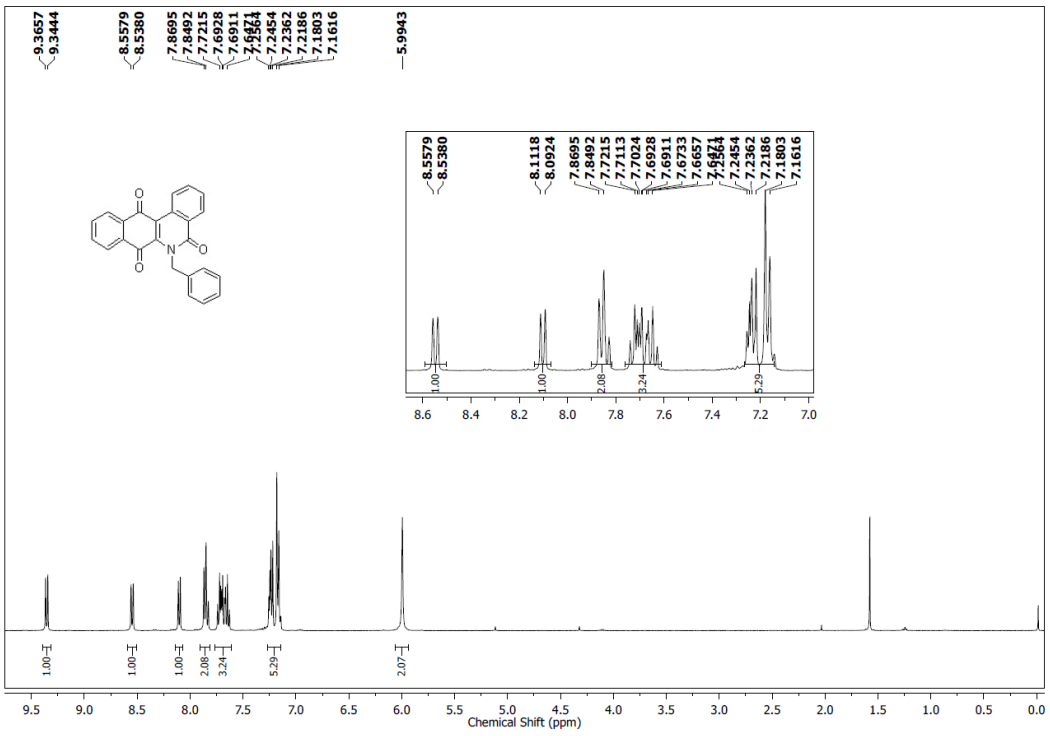

^{13}C NMR spectrum (100 MHz, $CDCl_3$) of **5h**

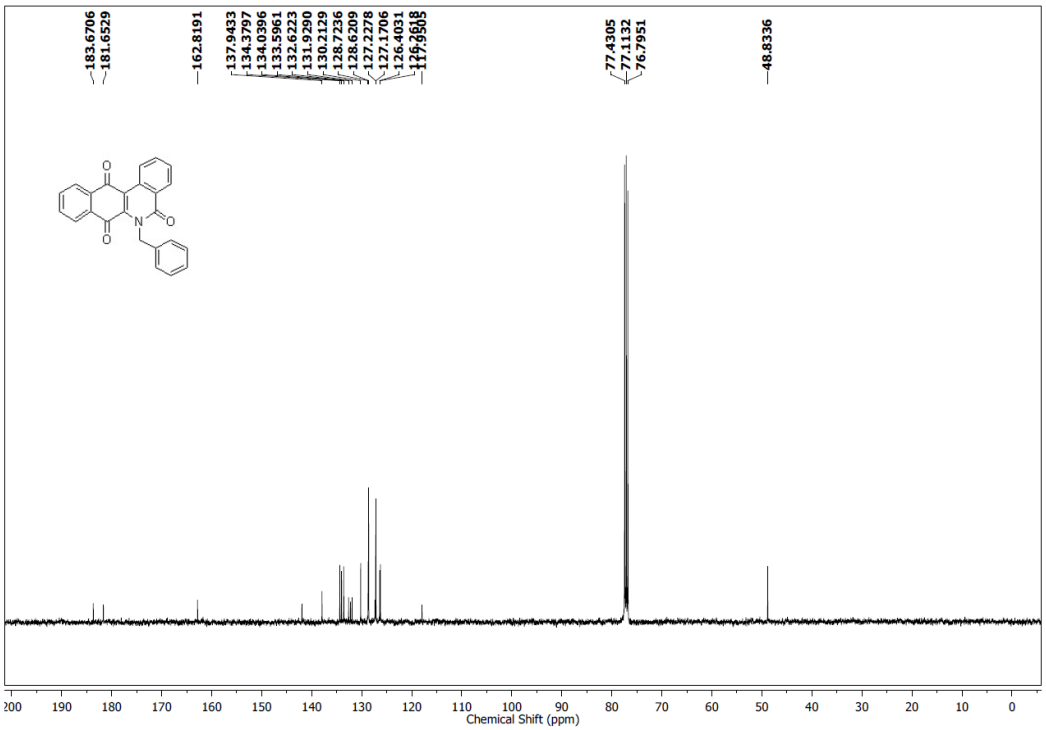

^{1}H NMR spectrum (400 MHz, $CDCl_3$) of **5i**

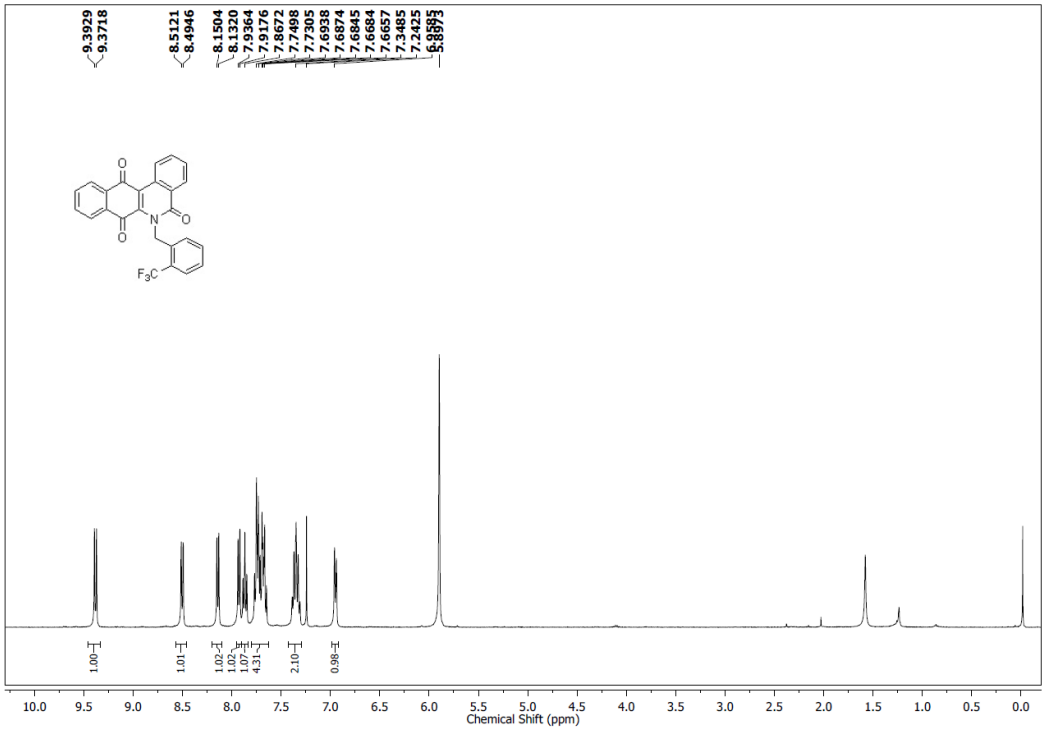

^{13}C NMR spectrum (100 MHz, $CDCl_3$) of **5i**

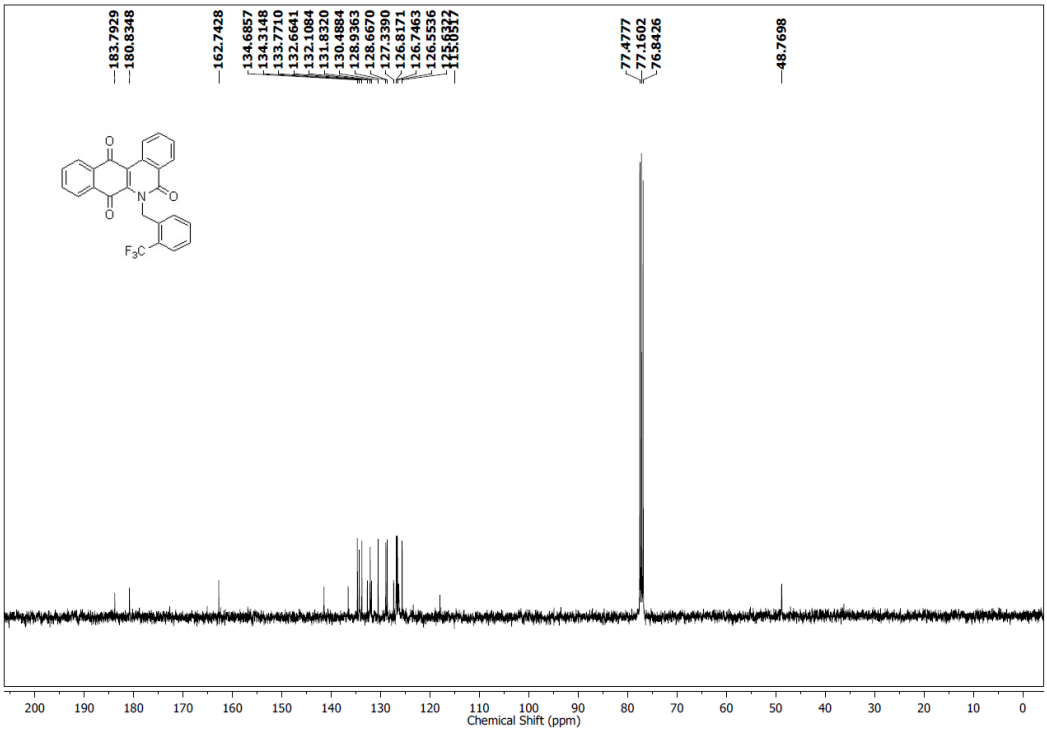

^{1}H NMR spectrum (400 MHz, $CDCl_3$) of **5j**

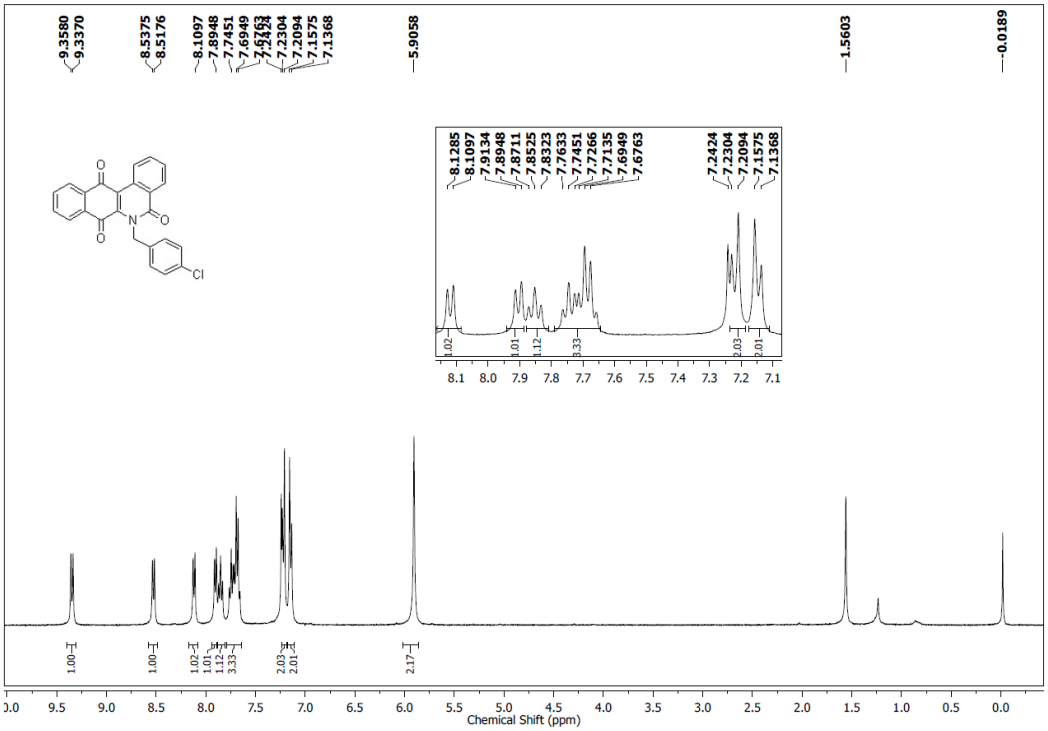

^{13}C NMR spectrum (100 MHz, $CDCl_3$) of **5j**

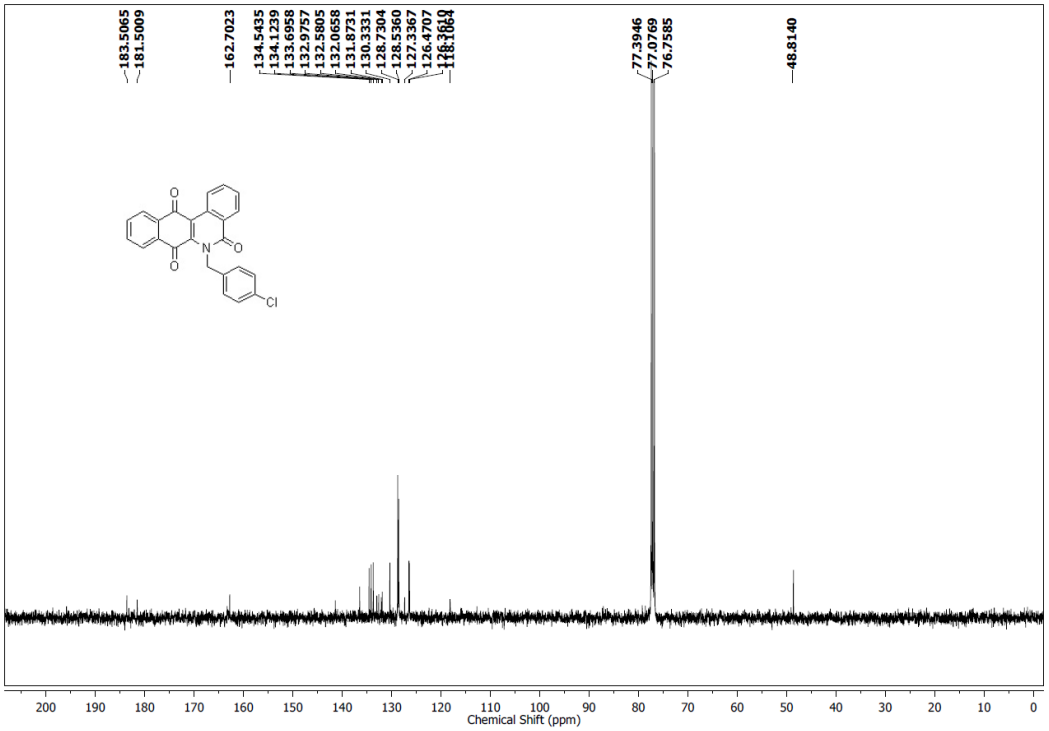

^{1}H NMR spectrum (400 MHz, $CDCl_3$) of **5k**

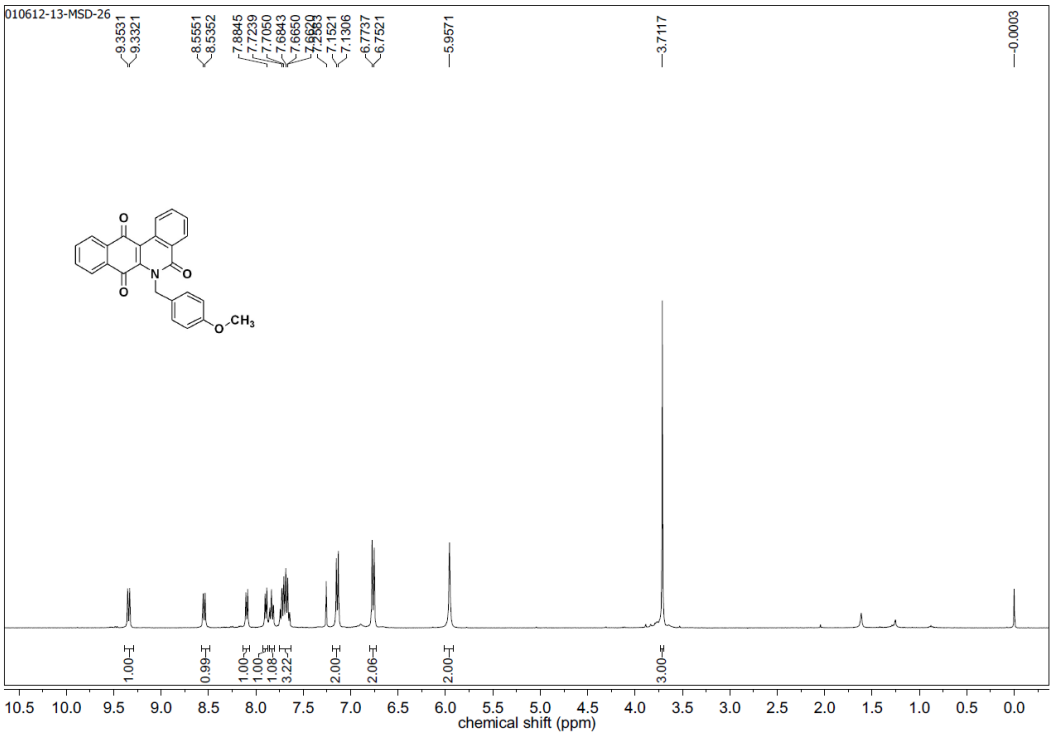

^{13}C NMR spectrum (100 MHz, $CDCl_3$) of **5k**

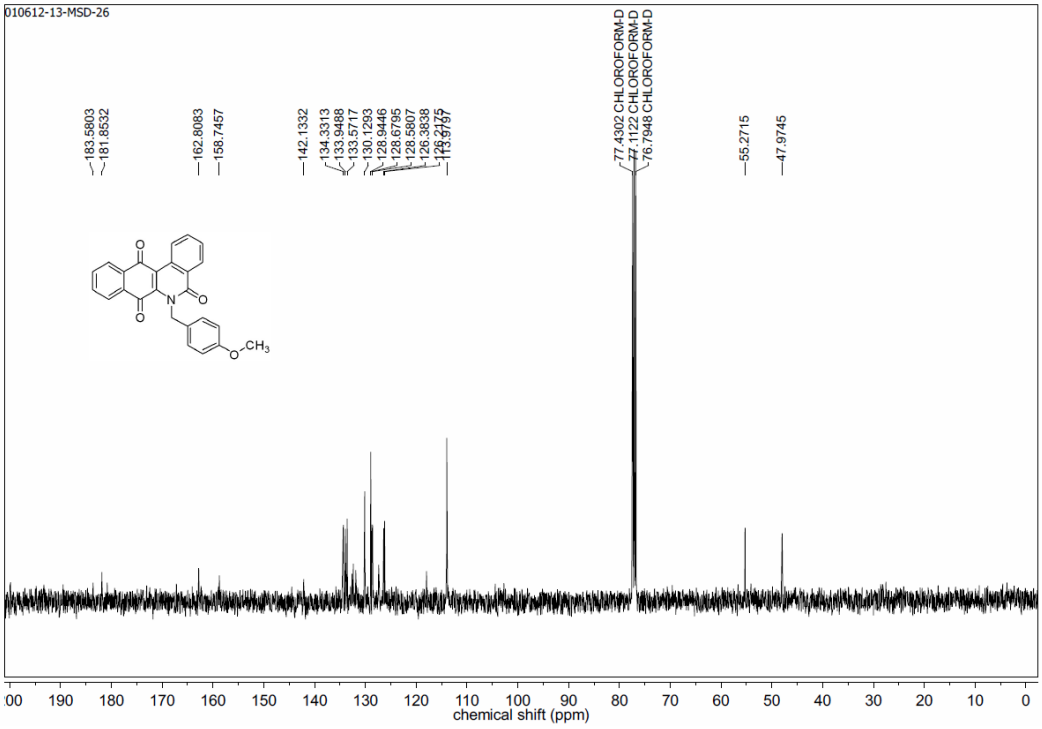

^{1}H NMR spectrum (400 MHz, DMSO-d_6) of **5l**

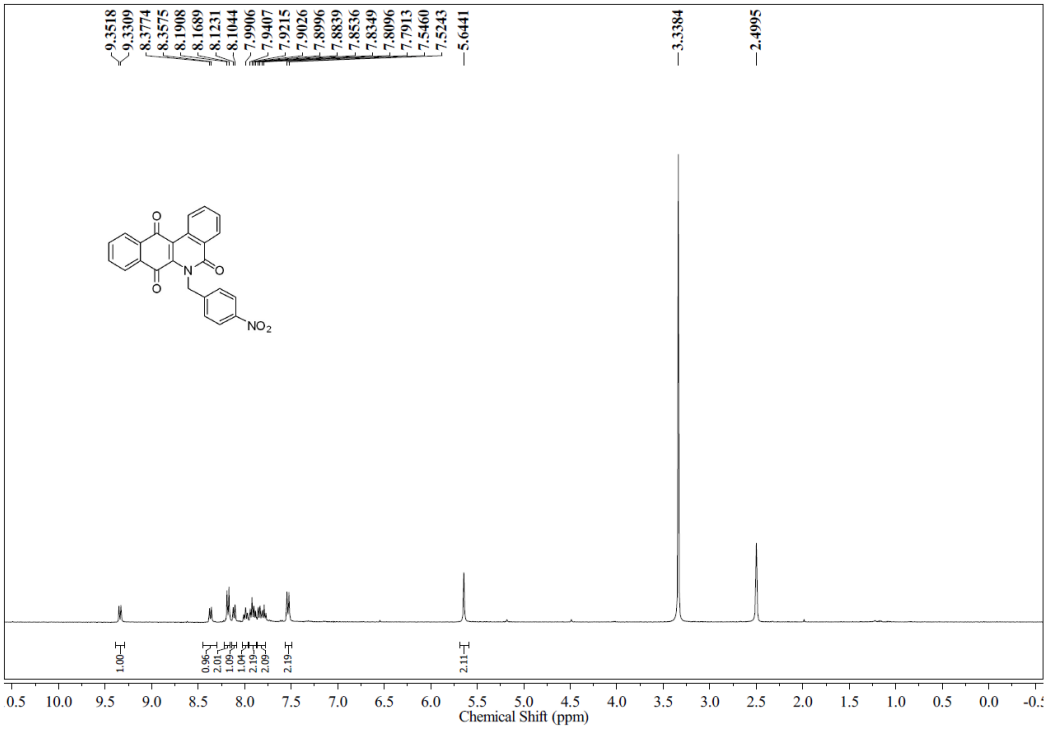

^{13}C NMR spectrum (100 MHz, DMSO-d_6) of **5l**

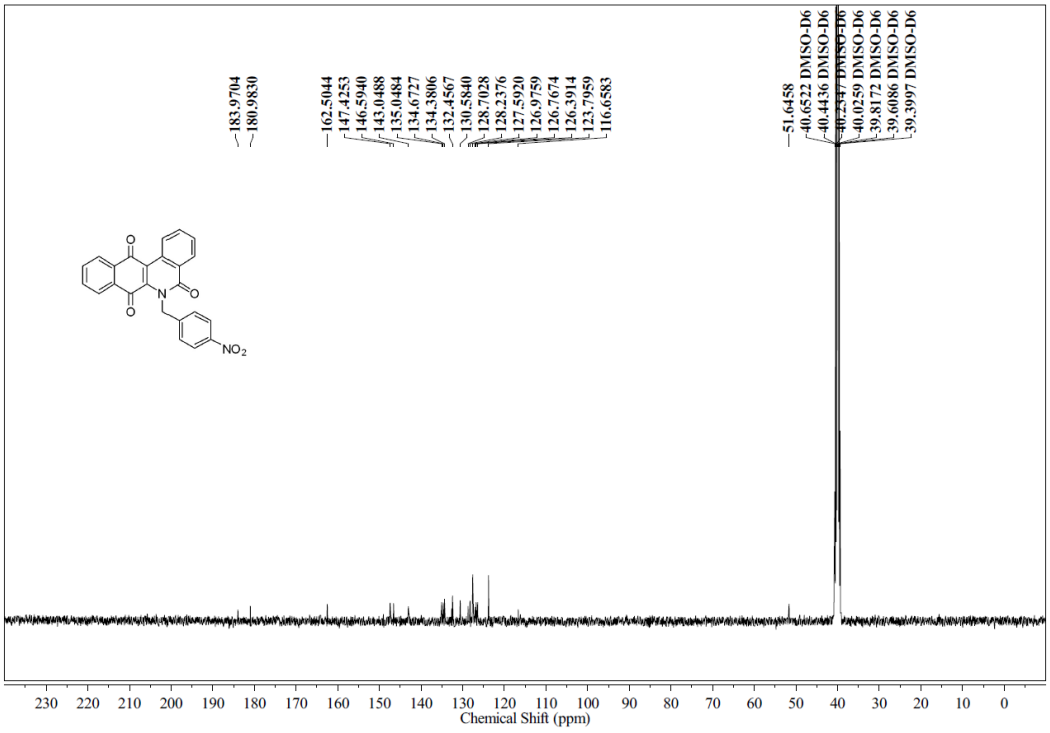

^{1}H NMR spectrum (400 MHz, $CDCl_3$) of **5m**

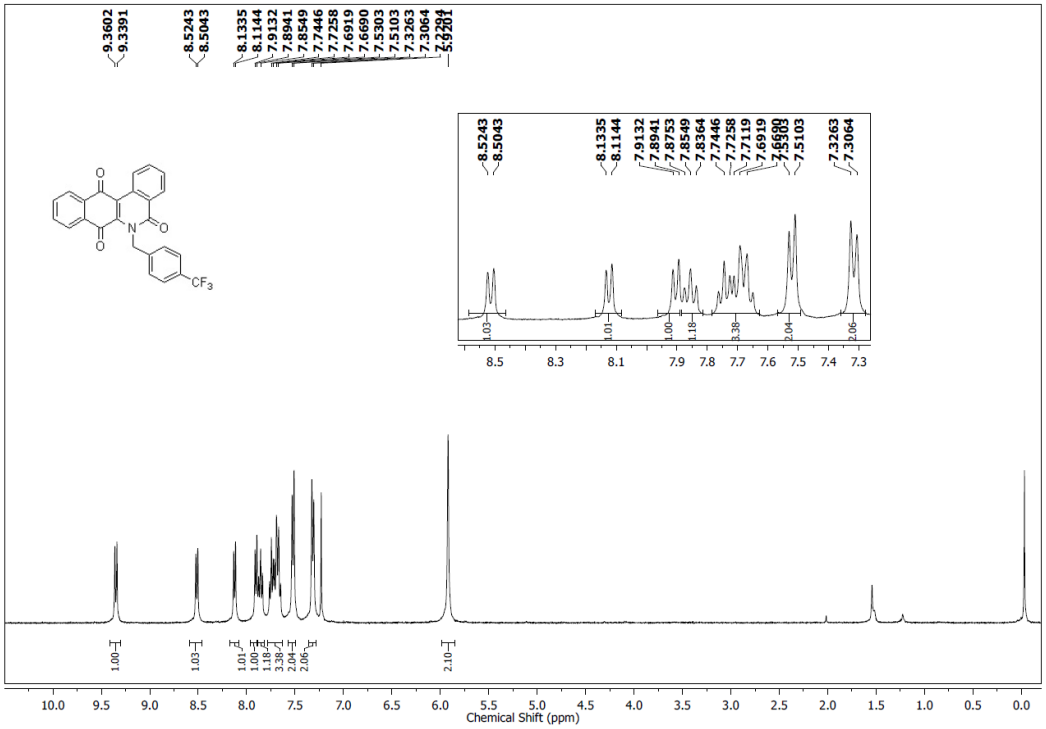

^{13}C NMR spectrum (100 MHz, $CDCl_3$) of **5m**

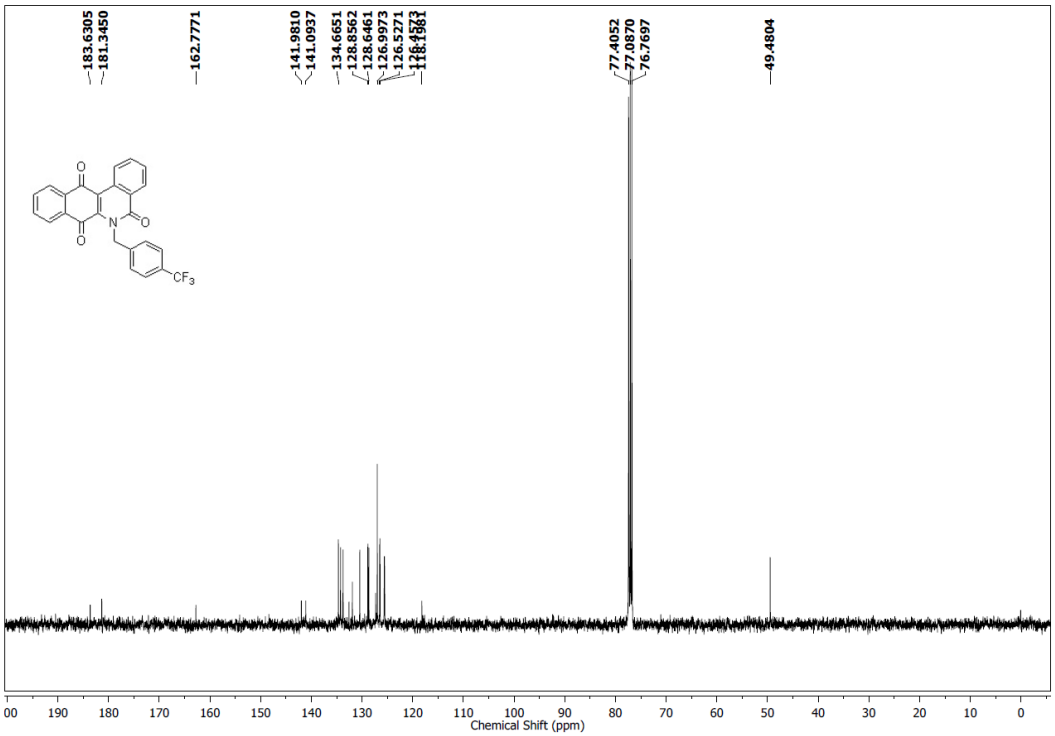

^{1}H NMR spectrum (400 MHz, $CDCl_3$) of **5n**

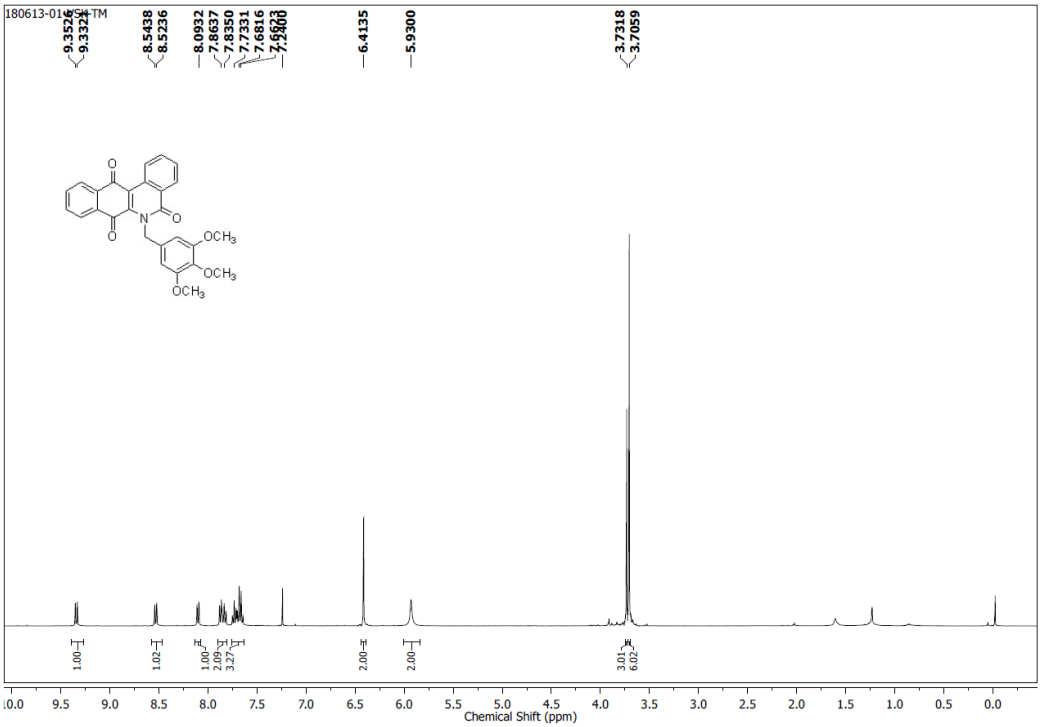

^{13}C NMR spectrum (100 MHz, $CDCl_3$) of **5n**

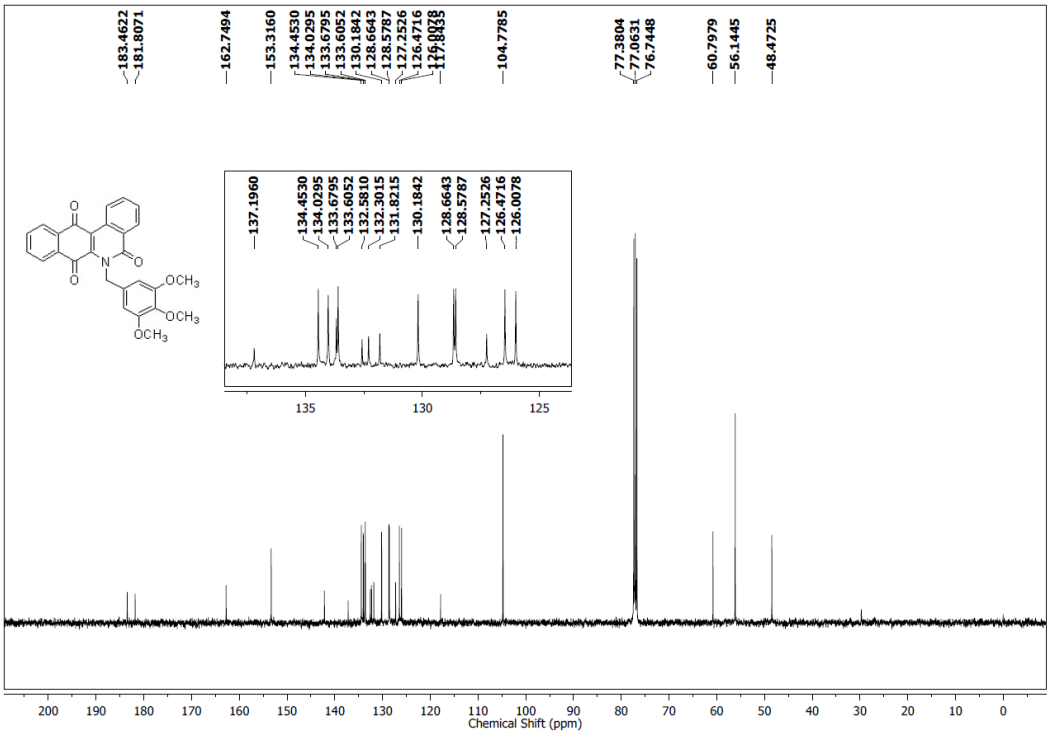

2.1.6. References

(1) Trachootham, D.; Lu, W.; Ogasawara, M. A.; Valle, N. R.-D.; Huang, P. *Antioxid. Redox Signal.* **2008**, *10*, 1343.

(2) Oktyabrsky, O. N.; Smirnova, G. V. *Biochemistry (Moscow)* **2007**, *72*, 132.

(3) Valko, M.; Leibfritz, D.; Moncol, J.; Cronin, M. T. D.; Mazur, M.; Telser, J. *Int. J. Biochem. Cell Biol.* **2007**, *39*, 44.

(4) Trachootham, D.; Alexandre, J.; Huang, P. *Nat. Rev. Drug Discov.* **2009**, *8*, 579.

(5) Pelicano, H.; Carney, D.; Huang, P. *Drug Resist. Updates* **2004**, *7*, 97.

(6) Li, L. S.; Bey, E. A.; Dong, Y.; Meng, J.; Patra, B.; Yan, J.; Xie, X.-J.; Brekken, R. A.; Barnett, C. C.; Bornmann, W. G.; Gao, J.; Boothman, D. A. *Clin. Cancer Res.* **2011**, *17*, 275.

(7) Li, J. Z.; Ke, Y.; Misra, H. P.; Trush, M. A.; Li, Y. R.; Zhu, H.; Jia, Z. *Toxicol. Appl. Pharm.* **2014**, *281*, 285.

(8) Raj, L.; Ide, T.; Gurkar, A. U.; Foley, M.; Schenone, M.; Li, X.; Tolliday, N. J.; Golub, T. R.; Carr, S. A.; Shamji, A. F.; Stern, A. M.; Mandinova, A.; Schreiber, S. L.; Lee, S. W. *Nature* **2011**, *475*, 231.

(9) Dhillon, H.; Chikara, S.; Reindl, K. M. *Toxicol. Rep.* **2014**, *1*, 309.

(10) Adams, D. J.; Dai, M.; Pellegrino, G.; Wagner, B. K.; Stern, A. M.; Shamji, A. F.; Schreiber, S. L. *Proc. Natl. Acad. Sci. USA* **2012**, *109*, 15115.

(11) Yano, T.; Kassovska-Bratinova, S.; Teh, J. S.; Winkler, J.; Sullivan, K.; Isaacs, A.; Schechter, N. M.; Rubin, H. *J. Biol. Chem.* **2011**, *286*, 10276.

(12) Dharmaraja, A. T.; Alvala, M.; Sriram, D.; Yogeeswari, P.; Chakrapani, H. *Chem. Commun.* **2012**, *48*, 10325.

(13) Tyagi, P.; Dharmaraja, A. T.; Bhaskar, A.; Chakrapani, H.; Singh, A. *Free Radic. Biol. Med.* **2015**, *84*, 344.

(14) Morones-Ramirez, J. R.; Winkler, J. A.; Spina, C. S.; Collins, J. J. *Sci. Transl. Med.* **2013**, *5*, 190ra81.

(15) Price-Whelan, A.; Dietrich, L. E. P.; Newman, D. K. *Nat. Chem. Biol.* **2006**, *2*, 71.

(16) Borissow, C. N.; Graham, C. L.; Syvitski, R. T.; Reid, T. R.; Blay, J.; Jakeman, D. L. *Chem. Bio. Chem.* **2007**, *8*, 1198.

(17) Zheng, J.-T.; Rix, U.; Zhao, L.; Mattingly, C.; Adams, V.; Chen, Q.; Rohr, J.; Yang, K.-Q. *J. Antibiot.* **2005**, *58*, 405.

(18) Cottreau, K. M.; Spencer, C.; Wentzell, J. R.; Graham, C. L.; Borissow, C. N.; Jakeman, D. L.; McFarland, S. A. *Org. Lett.* **2010**, *12*, 1172.

(19) Hall, S. R.; Blundon, H. L.; Ladda, M. A.; Robertson, A. W.; Martinez-Farina, C. F.; Jakeman, D. L.; Goralski, K. B. *Pharmacol. Res. Perspect.* **2015**, *3*, e00110.

(20) O¯mura, S.; Nakagawa, A.; Aoyama, H.; Hinotozawa, K.; Sano, H. *Tetrahedron Lett.* **1983**, *24*, 3643.

(21) Mullowney, M. W.; Hwang, C. H.; Newsome, A. G.; Wei, X.; Tanouye, U.; Wan, B.; Carlson, S.; Barranis, N. J.; Ó hAinmhire, E.; Chen, W.-L.; Krishnamoorthy, K.; White, J.; Blair, R.; Lee, H.; Burdette, J. E.; Rathod, P. K.; Parish, T.; Cho, S.; Franzblau, S. G.; Murphy, B. T. *ACS Infect. Dis.* **2015**, *1*, 168.

(22) Bair, J. S.; Palchaudhuri, R.; Hergenrother, P. J. *J. Am. Chem. Soc.* **2010**, *132*, 5469.

(23) Parkinson, E. I.; Hergenrother, P. J. *Acc. Chem. Res.* **2015**, *48*, 2715.

(24) Shan, M.; Sharif, E. U.; O'Doherty, G. A. *Angew. Chem. Int. Ed.* **2010**, *49*, 9492.

(25) Hillard, E. A.; de Abreu, F. C.; Ferreira, D. C. M.; Jaouen, G.; Goulart, M. O. F.; Amatore, C. *Chem. Commun.* **2008**, 2612.

(26) Trung Pham, H.; Marquetty, C.; Pasquier, C.; Hakim, J. *Anal. Biochem.* **1984**, *142*, 467.

(27) Klevens, R.; Morrison, M. A.; Nadle, J.; et al. *J. Am. Med. Assoc.* **2007**, *298*, 1763.

(28) Rodvold, K. A.; McConeghy, K. W. *Clin. Infect. Dis.* **2014**, *58*, S20.

(29) Georgiou, C. D.; Papapostolou, I.; Grintzalis, K. *Nat. Protoc.* **2008**, *3*, 1679.

(30) Zielonka, J.; Vasquez-Vivar, J.; Kalyanaraman, B. *Nat. Protoc.* **2008**, *3*, 8.

(31) Zhao, H.; Joseph, J.; Fales, H. M.; Sokoloski, E. A.; Levine, R. L.; Vasquez-Vivar, J.; Kalyanaraman, B. *Proc. Natl. Acad. Sci. USA* **2005**, *102*, 5727.

(32) Zhou, M.; Diwu, Z.; Panchuk-Voloshina, N.; Haugland, R. P. *Anal. Biochem.* **1997**, *253*, 162.

(33) Dharmaraja, A. T.; Chakrapani, H. *Org. Lett.* **2014**, *16*, 398.

(34) Haber, F.; Weiss, J. *Proc. Royal Soc. Lond. A***1934**, *147*, 332.

(35) Wardman, P. *Free Radic.Biol. Med.* **2007**, *43*, 995.

(36) Wrona, M.; Patel, K.; Wardman, P. *Free Radic. Biol. Med.* **2005**, *38*, 262.

(37) Wu, D.; Yotnda, P. *J. Vis. Exp.* **2011**, 3357.

(38) Imlay, J. A. *Nat. Rev. Micro.* **2013**, *11*, 443.

(39) Chen, Z.; Yang, H.; Pavletich, N. P. *Nature* **2008**, *453*, 489.

(40) Hogg, N.; Darley-Usmar, V. M.; Wilson, M. T.; Moncada, S. *FEBS Lett.* **1993**, *326*, 199.

(41) Sharma, K.; Iyer, A.; Sengupta, K.; Chakrapani, H. *Org. Lett.* **2013**, *15*, 2636.

(42) Zhao, H.; Joseph, J.; Fales, H. M.; Sokoloski, E. A.; Levine, R. L.; Vasquez-Vivar, J.; Kalyanaraman, B. *Proc. Natl. Acad. Sci.*, **2005**, *102*, 5727.

(43) Khodade, V. S.; Dharmaraja, A. T.; Chakrapani, H. *Bioorg. Med. Chem. Lett.* **2012**, *22*, 3766.

(44) Nakashio, A.; Fujita, N.; Rokudai, S.; Sato, S.; Tsuruo, T. *Cancer Res.* **2000**, *60*, 5303.

Chapter 2.2: Structure-Activity Relationships Studies of Benzo[*b*]phenanthridine-5,7,12-trione as MRSA Inhibitors

2.2.1. Introduction

The increasing prevalence of antibiotic resistant strains of *Staphylococcus aureus* (*S. aureus*) such as methicillin resistant *S. aureus* (MRSA) and vancomycin resistant *S. aureus* (VRSA) have now become a major public health problem globally.[1-2] Unfortunately, the discovery of new antibiotics has lagged far behind the growing emergence of antibiotic resistance.[3] Therefore, there is an urgent need for new antibacterial agents with novel modes of action.[4] Recently, it has been reported that bactericidal antibiotics (e.g., ampicillin, kanamycin and norfloxacin) induce highly deleterious hydroxyl radical formation in bacteria, which ultimately contribute to bacterial cell death.[5-6] Although this hypothesis was challenged by few independent reports,[7-8] recent studies have demonstrated that bactericidal antibiotics induce complex redox alterations that contribute to cellular damage and death.[9] Therefore, enhancing intracellular ROS level has been considered as potential strategy to target bacterial infection. For example, fosfomycin has been reported to induce hydroxyl radical generation in *S. aureus* to kill the bacterial cells.[10] Fosfomycin also enhanced the extracellular killing of *S. aureus* in macrophages, which was mediated by ROS through the oxidative burst process. In addition, photodynamic therapy has been reported to be a promising strategy for the treatment of some infections.[11] In this therapy, photosensitizers generate toxic levels of ROS, especially singlet oxygen ($^1O_2$), upon exposure to light which causes irreparable bimolecular damages leading to cell death. In chapter 2.1, we have described the development of natural-product inspired bioreductively activated ROS generators as MRSA inhibitors. Using these redox-active compounds, we have demonstrated that antibiotic resistance in certain bacteria can be targeted by perturbing bacterial redox-homeostasis. For example, the redox-active lead compound that we have identified in chapter 2.1, **5f**, displayed potent inhibitory activity against MRSA.[12] Although **5f** possessed high inhibitory activity against MRSA, it also exhibited cytotoxicity in mammalian cells at comparable concentrations. In addition, this compound has poor aqueous solubility. Thus, our next target was to tune the **5f** structure in order to enhance the solubility and improve the selectivity index towards bacterial cells. In light of that, we proposed to systematically explore the structure activity relationship (SAR) of benzo[*b*]phenanthridine-5,7,12-trione and overcome observed challenges without compromising on the potency while inhibiting MRSA. We considered retaining the ROS

generating quinone core (Figure 2.2.1, highlighted in green) and systematically modifying the substituents of the parent compound. First, we proposed to synthesize 2-aryl-3-amino-1,4-naphthoquinones **8**, in which the electron donating amine substituted with the electron withdrawing amide functional group of **5**, this could shed light on the importance of amide adjoining quinone and aromatic ring A on anti-MRSA activity (Figure 2.2.1).

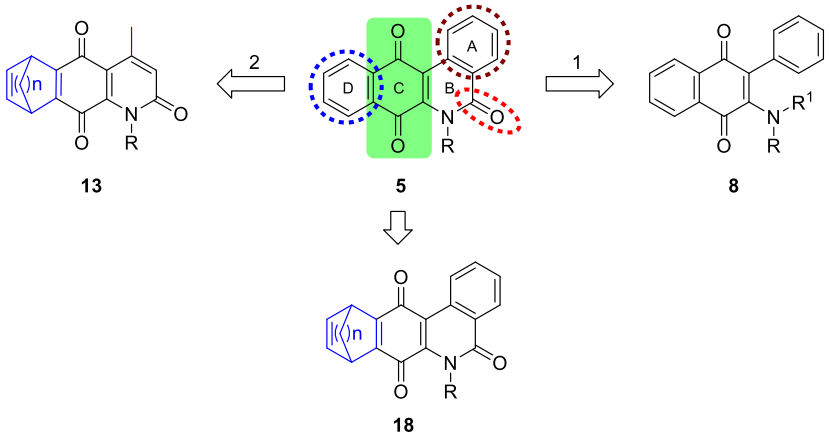

Figure 2.2.1. Schematic representation of the systematic structural modifications to the benzo[*b*]phenanthridine-5,7,12-trione (**5**)

Next, the role of aromatic ring A and D needed to be investigated for its participation in anti-MRSA activity. The scaffold **13** was proposed in which aromatic ring A was replaced with 4-methyl group and aromatic ring D was replaced with bridged bicyclic ring. We considered replacing aromatic ring D with bicyclic ring because it has been reported that the ROS generation from quinone can be tuned by changing its substituents. Finally, we wanted to determine the importance of aromatic ring A for anti-MRSA activity. Therefore, compound **18** was proposed in which the aromatic ring A was retained and aromatic ring D was replaced with bicyclic ring.

2.2.2. Results and Discussion

2.2.2.1. Synthesis and characterization

In order to test whether an amide adjoining quinone and aromatic ring A is essential for antibacterial activity, we proposed to synthesize 2-aryl-3-amino-1,4-naphthoquinones. The titled compounds were obtained in two steps from 2-bromo-1,4-naphthoquinone, which in turn was prepared by oxidative bromination of 1-naphthol using N-bromosuccinimide in acetic acid in

74% yield (Scheme 2.2.1).[13-14] Pd(II)-catalyzed Suzuki coupling of 2-bromo-1,4-naphthoquinone with phenylboronic acid produced 2-phenyl-1,4-naphthoquinone **7** in 90% yield.[15]

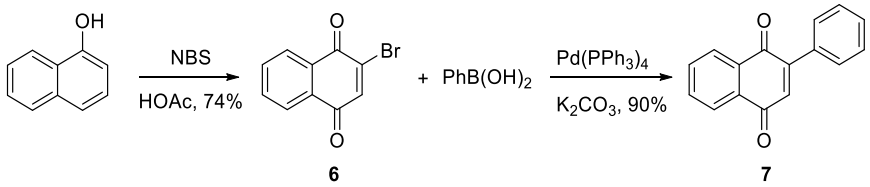

Scheme 2.2.1. Synthesis of 2-phenyl-1,4-naphthoquinone **7**

Table 2.2.1. Synthesis of 2-aryl-3-amino-1,4-naphthoquinones (**8a-8m**)

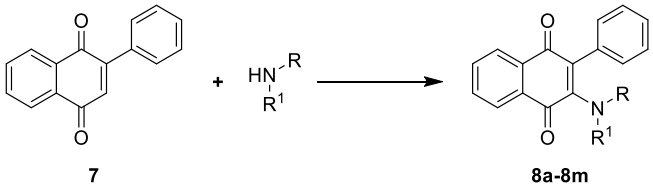

Entry	R^1	R	Product	% Yield
1	H	H[a]	**8a**	50
2	H	^{n}Pr[a]	**8b**	64
3	H	^{n}Bu[a]	**8c**	78
4	H	$CH_2CH_2NMe_2$[a]	**8d**	72
5	H	Allyl[a]	**8e**	60
6	H	Bn[a]	**8f**	80
7	H	4-OMe-C_6H_4-CH_2[a]	**8g**	81
8	H	4-Cl-C_6H_4-CH_2[a]	**8h**	63
9	H	Ph[b]	**8i**	53
10	H	4-OMePh[b]	**8j**	58
11	H	4-NO_2Ph[b]	**8k**	25
12	R^1RNH = Pyrrolidine[a]		**8l**	77
13	R^1RNH = Piperidine[a]		**8m**	86

[a]Reaction was conducted in dioxane at RT.

[b]Reaction was conducted in acetic acid and water (1:1) at 90 °C.

Finally, 2-phenyl-1,4-napthoquinone was reacted with ammonia to afford **8a** in 50% yield.[16] Similarly, a reaction of different primary amines such as ^{n}propylamine, ^{n}butylamine, and *N*,*N*-dimethyaminoethylamine with **7** produced **8b-8d** in yields ranging from 64% to 78% (Table 2.2.1, entries 2-4). The allylamine derivative **8e** and benzylamine derivative **8f** was prepared in

60% and 80% yield, respectively (Table 2.2.1, entries 5 and 6). Furthermore, the reaction condition employed here was also found to be compatible with electron-donating and electron-withdrawing substituted benzylamines. 4-Methoxybenzyl and 4-chlorobenzyl derivatives were prepared in good yields. When aniline was reacted with **7** at RT, no evidence of product formation was observed. However, when the reaction mixture was heated at 90 °C, **8i** was obtained in 60% yield.[17] Using similar reaction conditions, aniline derivatives **8j** and **8k** were synthesized in 58% and 25% yield, respectively (Table 2.2.1, entries 10 and 11). The reaction of secondary amine such as pyrrolidine and piperidine with **7** afforded **8l** and **8m** in 77% and 86% yield, respectively (Table 2.2.1, entries 12 and 13). All the synthesized compounds were purified using silica gel column chromatography. The purity of **8a-8m** was determined using a HPLC analysis and was estimated to be > 95% pure.

2.2.2.2. Antibacterial activity against *S. aureus*

All the newly synthesized compounds **8a-8m** were evaluated for their *in vitro* antibacterial activity against methicillin sensitive *S. aureus* (MSSA) using conventional microdilution method. The results of antibacterial studies revealed that none of the compounds from this series showed inhibitory activity at 32 μg/mL against MSSA. This result confirmed the necessity of amide adjoining between quinone and aromatic ring A for anti-bacterial activity. Therefore, we decided to retain the amide group in benzo[*b*]phenanthridine-5,7,12-triones.

2.2.2.3. Synthesis of Benzo[*b*]phenanthridine-5,7,12-trione analogues

Having demonstrated the importance of amide adjoining quinone and aromatic ring A, we proceeded to investigate the role of aromatic ring A and D for anti-MRSA activity. We proposed to synthesize scaffold **13** in which aromatic ring A was replaced with 4-methyl group and aromatic ring D was replaced with bicyclic ring. The general scheme for the preparation of **13a-13e** is described in Schemes 2.2.2 and Scheme 2.2.3. The synthesis commenced with the amidation of the readily available 2,5-dimethoxyaniline with *tert*-butyl acetoacetate to give amide **9** in 86% yield.[18] Next, **9** was subjected to cyclization in the presence of H_2SO_4 to afford **10a** in 87% yield.[19] The synthesized intermediate **10a** was reacted with different alkyl halides in the presence of sodium hydride to afford *N*-alkyl isomers **10b-10e** in moderate yields ranging from 33% to 63%.[18,20] During this alkylation, *O*-alkyl derivatives **11b-11e** were also obtained as

byproducts (Scheme 2.2.2). The *N*-alkyl and *O*-alkyl isomers were separated using silica gel column chromatography and their structure was confirmed using ^{1}H and ^{13}C NMR spectroscopy.

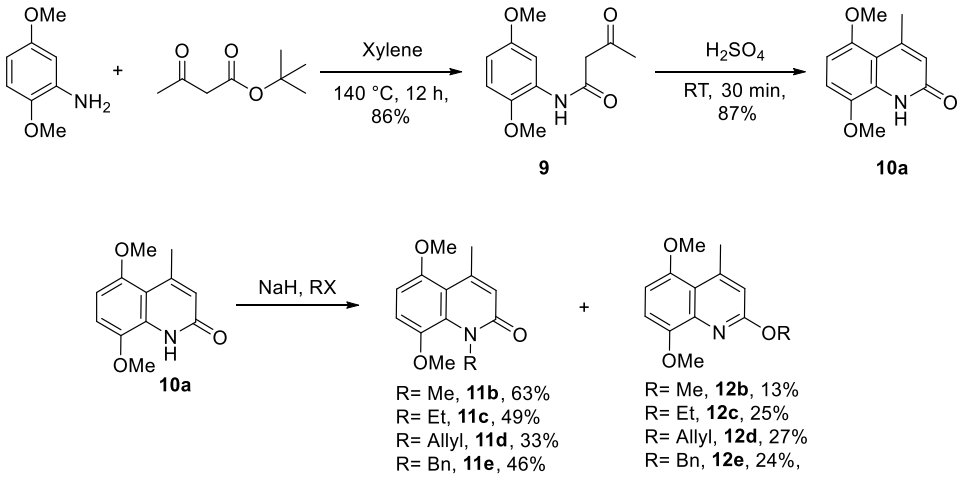

Scheme 2.2.2. Synthesis of **11b**-**11e** and **12b**-**12e**

Next, 5,8-dimethoxy-4-methylquinolin-2(1*H*)-one **10a** was oxidized using ceric ammonium nitrate in acetonitrile/water at RT to afford 4-methylquinoline-2,5,8(1*H*)-trione (Scheme 2.2.3).[21-22] The resulting quinone intermediate was not further purified, but used directly in the subsequent reaction due to its low stability. A Diels-Alder reaction of 4-methylquinoline-2,5,8(1H)-trione with 1,3-cyclohexadiene afforded oxidized compound **13a** in 26% yield (calculated from **10a**) after column chromatography. Similarly, oxidation of *N*-methyl derivative **11b** using ceric ammonium nitrate produced quinone intermediate, which was then subjected to [4+2] cycloaddition reaction with 1,3-cyclohexadiene to afford **13b** in 26% yield (Scheme 2.2.3).

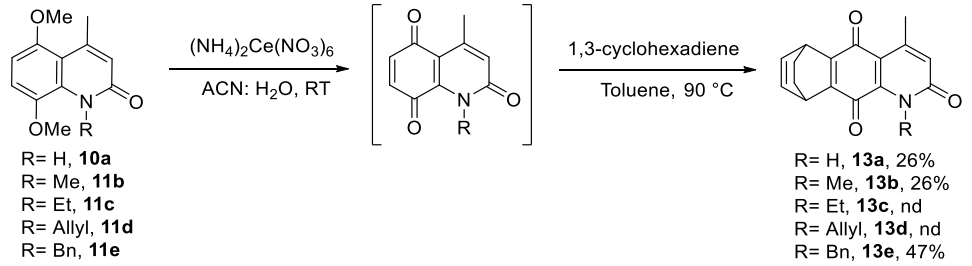

Scheme 2.2.3. Synthesis of *N*-alkyl-4-methyl-6,9-dihydro-6,9-ethano -benzo[*g*]quinoline-2,5,10(1*H*)-triones.

Similarly, derivatives **11c** and **11d** were oxidized to the corresponding quinone derivatives, which were then reacted independently with 1,3-cyclohexadiene. Due to unstable nature of

oxidized compounds, several attempts isolating these compounds was unsuccessful. A Diels-Alder reaction of 1,3-cyclohexadiene with quinone intermediate obtained from **11e** afforded **13e** in 47% yield (Scheme 2.2.3). The quinone intermediates obtained from the oxidation of **10a** and **11b-11e** were also reacted with cyclopentadiene. However, due to formation of a number of inseparable products during the reaction, we were unable to isolate desired products.

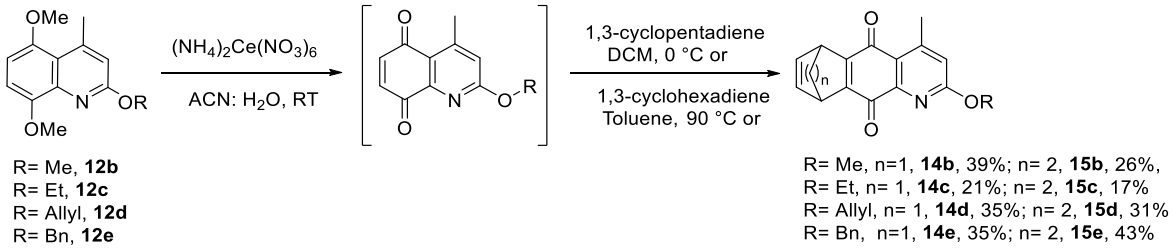

Scheme 2.2.4. Synthesis of *O*-alkyl-4-methyl-6,9-dihydro-6,9-methano/ethano-benzo[*g*]quinoline-2,5,10(1*H*)-triones

Next, *O*-methyl derivative **12b** was oxidized using ceric ammonium nitrate to 2-methoxy-4-methylquinoline-5,8-dione. A Diels-Alder reaction of this quinone intermediate with 1,3-cyclopentadiene produced **14b** in 39 % yield (Scheme 2.2.4). Under similar conditions, quinone compounds obtained from oxidation of **12c-12e** were reacted with 1,3-cyclopentadiene to afford **14c**-**14e** in moderate yields (Scheme 2.2.4). Next, the quinone compound obtained from the oxidation of **12b** was subjected to Diels-Alder reaction with 1,3-cyclohexadiene to afford **15b** in 26% yield (Scheme 2.2.4). Similarly, derivatives **15c-15e** were prepared by a cycloaddition reaction of 1,3-cyclohexadiene with quinone intermediates obtained from **12c-12e** with yields ranging from 17%-43%.

Next, we proceeded to synthesize 6-alkyl-8,11-dihydro-8,11-ethanobenzo[*b*]phenanthridine-5,7,12(6*H*)-trione **18** for investigating the importance of aromatic ring D on anti-MRSA activity. As demonstrated in Scheme 2.2.5, our synthetic step toward **18** commenced with amidation of commercially available 2,5-dimethoxyaniline with 2-iodobenzoyl chloride to form *N*-(2,5-dimethoxyphenyl)-2-iodobenzamide **16** in excellent yield. Potassium *tert*-butoxide mediated intermolecular cross-coupling of **16** in the presence of 1, 10-phenanthroline afforded **17a** in good yield (Scheme 2.2.5).[23] The intermediate **17a** was then reacted with different alkyl halides such as methyl iodide and allyl bromide in the presence of sodium hydride to afford *N*-alkyl

derivatives **17b** and **17c** in good yields. During this alkylation, *O*-alkyl derivatives were formed in a minor portion.

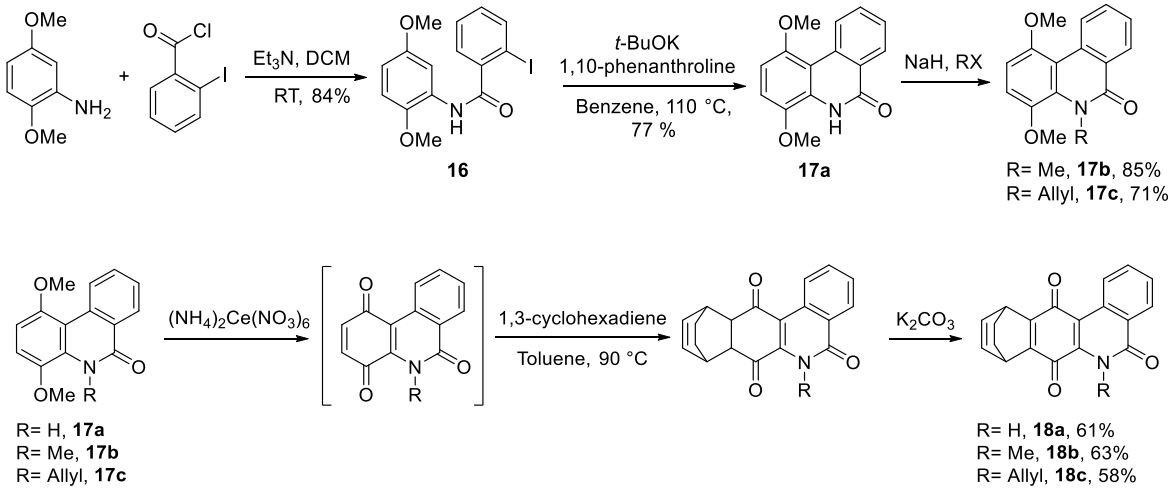

Scheme 2.2.5. Synthesis of **18a-18c**

Finally, **17a** was oxidized using ceric ammonium nitrate to form quinone intermediate, which was then reacted with 1,3-cyclohexadiene to afford oxidized compound **18a**, but during this reaction unoxidized compound was obtained (scheme 2.2.5). We attempted to isolate this unoxidized compound, but our several efforts were unsuccessful due to formation of number of inseparable products during purification. Therefore, we proposed to oxidize this compound using base treatment. It has been reported that under basic conditions, protons adjacent to quinone undergo enolization to hydroquinone, which then undergoes oxidation under aerobic condition to form quinone.[24] Indeed, when this intermediate was treated with K_2CO_3, we obtained **18a** in 61% yield. Similarly, **17b** and **17c** were oxidized to the corresponding quinone intermediates, which was reacted with 1,3-cyclohexadiene followed by treatment with potassium carbonate to afford **18b** and **18c** in 63% and 58% yield, respectively. Thus, we have synthesized a series of redox-active compounds in good yields via systematic structural modifications to understand the SAR of **5** in inhibiting MRSA.

2.2.2.4. Reduction potential measurement

Quinones are known to generate ROS through a bioreduction/oxidation process mediated by bioreductive enzymes.[25-26] One electron reduction of quinone generates unstable semiquinone, which can transfer electron to oxygen to produce superoxide radical and parent quinone. It has

been postulated that the ROS generation ability of quinone is dependent on its reduction potentials.[27] Therefore, we measured the reduction potentials of these redox-active compounds using cyclic voltammetry. The reduction potential measurement was carried out in the aprotic solvent acetonitrile with tetrabutylammonium hexa-flurophosphate ($TBAPF_6$) as supporting electrolyte. First, the one electron reduction potential ($-E_{red}$) of 1-alkyl-4-methyl-6,9-dihydro-6,9-ethanobenzo[*g*]quinoline-2,5,10(1*H*)-triones were measured.

Table 2.1.2. One electron reduction potential of **13a-13e**, **14b-14e**, **15b-15e** and **18a-18c**

Entry	Compound	$-E_{red}$ (V)
1	**13a**	1.25
2	**13b**	1.28
3	**13e**	1.29
4	**14b**	1.28
5	**14c**	1.29
6	**14d**	1.32
7	**14e**	1.27
8	**15b**	1.20
9	**15c**	1.24
10	**15d**	1.22
11	**15e**	1.25
12	**18a**	1.23
13	**18b**	1.30
14	**18c**	1.30

Cyclic voltammetry analysis revealed that E_{red} of **13a, 13b** and **13e** were in the range -1.25 to -1.28 V, suggesting no major effect of *N*-alkyl substituents on the reduction potential of these derivatives. Next, we tested whether by changing an electron withdrawing amide group to electron donating 2-alkoxy group influenced their reduction potential. The one electron reduction potential of 2-alkoxy-4-methyl-6,9-dihydro-6,9-methano-benzo[*g*]quinoline-2,5,10(1*H*)-triones **14b-14e** was found in the range of -1.27 to -1.32 V, suggesting that electron donating substituent reduces their reduction potential. However, in case of 2-alkoxy-4-methyl-6,9-dihydro-6,9-ethano-benzo[*g*]quinoline-2,5,10(1*H*)-trione **15b-15d**, the E_{red} values (-1.20 to -1.25 V) were

higher than **14b-14e**, indicating that the sterric effect of bicyclic ring on attached to quinone increases their reduction potential. The E_{red} for **18a-18c** were in the range of -1.27 to 1.29 V. Thus, the cyclic voltammetry analysis suggested that the one electron reduction potential of these derivatives were appropriate for the reduction by bioreductive enzymes.

2.2.2.5. Antibacterial activity against *S. aureus*

The newly synthesized redox-active compounds were evaluated for their *in vitro* antibacterial activity against Gram-positive *S. aureus* (ATCC 29213) by microdilution method. The minimum inhibitory concentrations (MIC) are presented in Table 2.2.2. Vancomycin and Fosfomycin were used as positive control in this study.

Table 2.2.3. Calculated partition coefficients (ClogP) and MIC against MSSA (ATCC 29213)

Entry	Compound	ClogP	MIC μg/mL
1	**13a**	1.87	2
2	**13b**	2.02	1
3	**13e**	3.51	8
4	**14b**	3.33	1
5	**14c**	4.16	2
6	**14d**	4.40	>64
7	**14e**	4.69	>64
8	**15b**	4.19	>64
9	**15c**	4.72	>64
10	**15d**	4.96	>64
11	**15e**	5.56	>64
12	**18a**	2.76	0.12
13	**18b**	2.92	0.12
14	**18c**	3.70	0.5
15	Vancomycin		0.5
16	Fosfomycin		8

The antibacterial study revealed that *N*-alkyl derivatives **13a** and **13b** exhibited good inhibitory activity against MSSA with MICs 2 μg/mL and 1 μg/mL, respectively (Table 2.2.3, entries 1 and

2). However, benzyl derivative **13e** showed moderate antibacterial activity with MIC 8 μg/mL, suggesting that increasing the steric at *N*-1 position reduces the antibacterial activity. The *O*-alkyl derivatives **14b** and **14c** exhibited high inhibitory activity with MICs 1 μg/mL and 2 μg/mL, respectively (Table 2.2.3, entries 4 and 5). However, **14d** and **14e** were found to be inactive against MSSA, suggesting that introducing the bulky substituent at the 2-position markedly diminishes the potency. *O*-alkyl-4-methyl-6,9-dihydro-6,9-ethano-benzo[*g*]quinoline-2,5,10(1*H*)-triones **15b-15e** were then evaluated against MSSA (Table 2.2.3, entries 8-11). Unfortunately, none of the compound from this series showed inhibitory activity against MSSA. These results suggested that replacement of the aromatic ring-A with methyl group and aromatic ring-D with bulky bicyclic ring system results in a dramatic loss of the antibacterial activity. In addition, it is noteworthy to mention that by changing the amide group to 2-alkoxy-pyridine reduced antibacterial activity. Subsequently, we prepared compounds **18a**–**18c** to assess whether retaining aromatic ring-A have any beneficial effects on improving the potency of these compounds. The antibacterial studies demonstrated that **18a** exhibited excellent inhibitory activity with MIC 0.12 μg/mL, representing a 66-fold increase in potency relative to vancomycin (Table 2.2.3, entry 12). Similarly, methyl derivative **18b** showed comparable inhibitory activity with lead compound **5f**. The allyl derivative **18c** demonstrated the significant increase in the activity with MIC 0.12 μg/mL (Table 2.2.3, entry 14).

Next, the correlation between ClogP, a measure of cell permeability, and antibacterial activity was studied. It has been reported that the physical characteristic such as lipophilicity and hydrophilicity of the drug governs the biological activity.[28-29] The partition coefficient is frequently used to define the lipophilic character of a compound. The partition coefficient log*P* (ClogP) was calculated using ChemBioDraw Ultra 2014. The compound having low lipophilicity exhibited good inhibitory activity against MSSA. For example, *N*-alkyl derivatives **13a-b** and **13e** possessed ClogP value < 4 and have shown moderate to potent inhibitory activity. However, 2-alkoxy derivatives **15b-15e** possessed ClogP > 4 and were found to be inactive against MSSA at 64 μg/mL. In general, the *O*-alkyl derivatives showed stronger lipophilicity than *N*-alkyl derivatives. On the basis of the structural features and the antibacterial activity data, the SARs are summarized below. Generally, the *N*-alkyl derivatives **13** series showed comparable inhibitory potency against MSSA with lead compound **5f**. The aromatic ring A of this scaffold is important for antibacterial potency. The poor antibacterial potency of *O*-alkyl derivatives **13d-**

13e and **15b-15e** suggest that changing amide group to pyridine is not favorable for improving antibacterial potency. Furthermore, **18a-18c** compounds proved to be more potent than vancomycin in inhibiting growth of MSSA. The compound **18a** was identified as lead compound and further studies were conducted with this compound.

2.2.2.6. ROS generation studies

We evaluated **18a** for its ability to permeate bacterial cells and generate ROS. First, DHE assay was used for the detection of intracellular $O_2^{\bullet-}$ generation.[30-31] *S. aureus* was co-incubated with DHE and with/without **18a** for 60 min. The extracellular excess reagents were removed by washing bacterial pellet with phosphate buffer and bacterial cells were lysed by vortexing in acetonitrile. The resulting cell lysate was analyzed using HPLC attached with a fluorescence detector. When, *S. aureus* was incubated with DHE, we observed peak corresponding to unreacted DHE with negligible amount of 2-OH-E^+ and E^+ (Figure 2.2.2A). However, co-incubation of *S. aureus* with **18a** and DHE produced 2-OH-E^+ suggesting the intracellular $O_2^{\bullet-}$ generation (Figure 2.2.2A). During this assay, we also observed a peak corresponding to E^+ suggesting the increased levels of other oxidative species generated in *S. aureus*, which could result in enhanced oxidative stress.

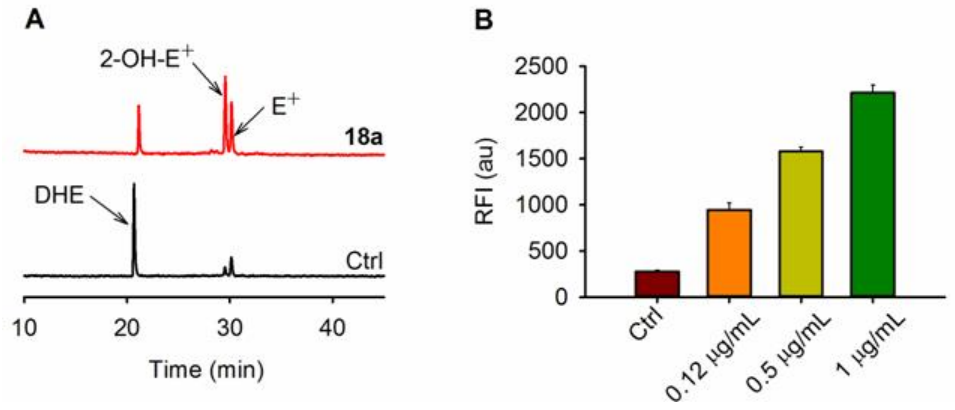

Figure 2.2.2 ROS generation by **18a** in *S. aureus* (A) $O_2^{\bullet-}$ generated during incubation of **18a** (0.5 µg/mL) with *S. aureus* was estimated using a dihydroethidium (DHE) assay. (B) Measurement of H_2O_2 generated during incubation of *S. aureus* with **18a** (0.12, 0.5, and 2 µg/mL) was estimated using an Amplex Red fluorescence assay.

Having demonstrated the $O_2^{\bullet-}$ generation in *S. aureus*, we evaluated **18a** for its ability to generate hydrogen peroxide. H_2O_2 is a freely diffusible ROS across bacterial cell wall and is

typically estimated as extracellular H_2O_2. The extracellular H_2O_2 was measured using an Amplex-Red assay.[32] When *S. aureus* was incubated with **18a** at 0.12 μg/mL (MIC concentration), an increased fluorescence was observed (Figure 2.2.2B), confirming the intermediary H_2O_2. Next, *S. aureus* was incubated with increasing concentration of **18a** and we observed a dose dependent increase in fluorescence. Together, these experiments confirmed the ability of **18a** to enhance intracellular ROS levels *S. aureus*.

2.2.2.7. Antibacterial activity against MRSA and VRSA

The increasing prevalence of pathogenic bacteria that are resistant to currently available antibiotics represents an alarming threat to public health. The most commonly encountered antibiotic-resistant bacteria, MRSA has emerged as a predominant nosocomial Gram-positive pathogen. Until recently, the treatment of infections caused by methicillin-resistant pathogens was effectively done with the vancomycin. However, overuse of this antibiotic has led to the emergence of vancomycin-intermediate and vancomycin-resistant *S. aureus* (VISA and VRSA, respectively). We investigated the potential of redox-active compound **18a** to inhibit the growth of range of MRSA and VRSA strains. First, the antibacterial activity of clinically used antibiotic, methicillin and ceftriaxon was measured against panel of 9-clinical strain of MRSA and 3-clinical strain of VRSA. As expected, these antibiotics were found to be inactive against resistant strains of *S. aureus* (Table 2.2.4). The β-lactum antibiotic meropenem displayed almost no antibacterial activity with exception being moderate activity against MRSA-10186, MRSA-10194 and VRS12 (Table 2.2.4). The glycopeptide antibiotic, vancomycin exhibited significant antibacterial activity against MRSA with MIC values ranging from 0.5–2μg/mL. However, as expected, vancomycin was found to be inactive against VRSA strains. Similarly, teicoplanin displayed high inhibitory activity against MRSA but it possessed weak inhibitory activity against VRSA. The lead compound **18a** retained its excellent inhibitory activity against 9-clinical strain of MRSA with MIC values in the range of 0.015–0.5 μg/mL. Furthermore, the lead compound also showed excellent potency against VRSA strains with MIC values of 0.01–0.03 μg/mL. This compound exhibited > 50-fold greater effectiveness than the parent compound **5f**. These results demonstrated the potential of redox-active compound to target the resistance in *S. aureus*.

Table 2.2.4. MICs of **18a** and representative antibacterial agents against MRSA and VRSA strains in μg/mL

Strain	Methicillin	Ceftriaxon	Meropenem	Vancomycin	Teicoplanin	**18a**
MSSA	2	4	0.5	0.5	1	0.12
MRSA NR129	>64	>64	64	1	0.5	0.06
MRSA NR100	>64	>64	32	1	1	0.12
MRSA 10129	>64	>64	16	2	1	0.12
MRSA 10198	>64	>64	64	1	2	0.25
MRSA 10192	>64	>64	64	2	0.5	0.06
MRSA 10191	>64	>64	64	2	2	0.5
MRSA 10193	>64	>64	>64	2	2	0.06
MRSA 10186	>64	>64	16	1	1	0.25
MRSA 10194	32	32	1	1	1	0.06
VRS1	>64	>64	64	>64	64	0.01
VRS4	>64	>64	32	>64	32	0.03
VRS12	>64	>64	8	>64	32	0.03

(Data provided by Dr. Sidharth Chopra, CDRI Lucknow, India)

2.2.2.8. Cytotoxicity assay

Having demonstrated the excellent potency of **18a** against MRSA and VRSA, we were interested in determining its cytotoxicity against mammalian cells. The cytotoxicity of **18a** was tested against Vero cells (kidney epithelial cells) using a standard cell viability assay. The growth inhibitory concentration (GI_{50}) was found to be 9.7 μg/mL. The selectivity index of **18a** was calculated (SI = GI_{50}/MIC) against MRSA NR129 and this redox-active compound displayed high SI value > 161, which was better than the parent compound **5f**. Furthermore, hemolytic activity of the lead compound was measured against red blood cells. Compound **18a** displayed no significant hemolytic activity at 100 μg/mL (>833-fold MIC). These results demonstrated the ability of mammalian cells to tolerate the lead compound at MIC concentration. Thus, cytotoxicity assays confirmed the selectivity of lead compound for bacterial cell inhibition over mammalian cells.

2.2.3. Conclusion

In this chapter, a series of compounds were designed and synthesized for understanding the structure activity relationship of benzo[*b*]phenanthridine-5,7,12-trione. First, 2-phenyl-3-amino-1,4-naphthoquinones were synthesized to check the effect of amide adjoining aromatic ring-A and quinone on antibacterial activity. The removal of amide group resulted in a loss of anti-MSSA activity. Replacing aromatic ring-A by methyl group and aromatic ring-D with bicyclic ring was tolerated but did not improve the anti-bacterial activity. Bulky group at *N*-1 position of **13** series was not tolerated. Similarly, *O*-alkyl derivatives **14c-14d** and **15a-15d** found to be inactive against MSSA suggesting that changing the amide ring to pyridine reduces biological activity. Retaining aromatic ring A and replacing aromatic ring-D with bicyclic ring was found to be the right combination. The lead compound **18a** displayed potent antibacterial activity against a wide range of antibiotic-resistant bacteria including MRSA and VRSA. This compound was minimally cytotoxic against mammalian cells and possessed essentially no hemolytic activity. Thus, together these results suggest that modification of redox-active natural product is a simple and feasible approach for developing novel antimicrobial agents with enhanced cell selectivity.

2.2.4. Experimental and Characterization Data

Compounds **6**,[16] **7**,[15] **8a**,[17] **8i**,[33] **9**,[18] **10a**,[19] **11b**,[18] and **12b**[34] have been previously reported and analytical data that we collected were consistent with the reported values.

2.2.4.1. Synthesis

General Procedure for amine addition to 2-phenyl-1,4-naphthoquinones

Procedure A: To a solution 2-phenyl-1,4-napthoquinone (1.28 mmol) dissolved in dioxane (10 mL), the amine (6.4 mmol) was added and the resulting mixture was stirred at RT until complete disappearance of the starting material (2- 24 h, TLC analysis). The resulting solution was dried under reduced pressure and resulting product was purified by column chromatography on silica gel to afford pure product. This procedure was followed for the synthesis of compounds **8a-8h** and **8l-8m**.

Procedure B: To a solution 2-phenyl-1,4-napthoquinone (0.85 mmole) in AcOH: H_2O (5 ml), aniline derivative (4.26 mmole) was added and mixture was stirred at 90 °C until the disappearance of the starting material (12- 14 h, checked by TLC). The reaction mixture extracted with ethyl acetate (10 mL), washed by saturated $NaHCO_3$ (5mL) and water. The combined extracts were dried over anhydrous Na_2SO_4 and concentrated in vacuo. The resulting product was purified by column chromatography on silica gel to afford pure product. This procedure was followed for the synthesis of compounds **8i-8k**.

2-Phenyl-3-(amino *n*-propyl)naphthalene-1,4-dione (8b)

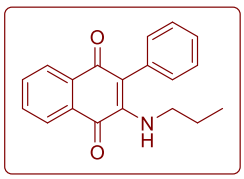

Starting from **7** (300 mg, 1.28 mmol), **8b** (240 mg, 64%) was isolated as a red solid: mp 124 – 126 °C; FT-IR (ν_{max}, cm^{-1}): 3444, 3296, 1674, 1597, 1515, 1296, 1160, 701; ^1H NMR (400 MHz, $CDCl_3$): δ 8.10 (dd, *J* = 0.9, 7.8 Hz,1H), 8.06 (dd, *J* = 0.9, 7.8 Hz,1H), 7.70 (td, *J* = 1.3, 7.3 Hz, 1H), 7.60 (td, *J* = 7.3, 1.3 Hz, 1H), 7.27-7.39 (m, 5H), 5.94 (s, 1H), 2.54 (q, *J* = 6.9 Hz, 2H), 1.35(sextet, *J* = 7.3 Hz, 2H), 0.68 (t, *J* = 7.3 Hz, 3H); ^{13}C NMR (100 MHz, $CDCl_3$): δ 183.1, 182.4, 144.5, 134.8, 134.4, 133.6, 131.9, 131.3, 130.3, 127.7, 127.5, 126.6, 126.1, 115.0, 46.5, 23.1, 11.0; HRMS (ESI): calcd. for $C_{19}H_{17}NO_2$ $[M+Na]^+$: 314.1157; Found: 314.1155.

2-Phenyl-3-(amino *n*-butyl)naphthalene-1,4-dione (8c)

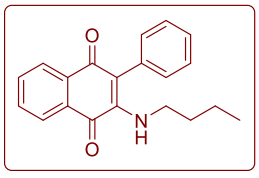

Starting from **7** (200 mg, 0.85 mmol), **8c** was isolated as a red solid (203 mg, 78%): mp 112 –116 °C; FT-IR (ν_{max}, cm^{-1}): 3466, 3262, 1675, 1604,

1513, 1297, 1071, 757; ^{1}H NMR (400 MHz, $CDCl_3$): δ 8.05-8.12 (m,2H), 7.70 (td, *J* = 1.4, 7.3 Hz, 1H), 7.60 (td, *J* = 1.4, 7.3 Hz, 1H), 7.27-7.38 (m, 5H), 5.91 (s, 1H), 2.57 (q, *J* = 6.8 Hz, 2H), 1.32 (quin, *J* = 6.8, 7.3 Hz, 2H), 1.10 (sextet, *J* = 6.8, 7.3 Hz, 2H), 0.74 (t, *J* = 7.3 Hz, 3H); ^{13}C NMR (100 MHz, $CDCl_3$): δ 183.1, 182.4, 144.5, 134.8, 134.5, 133.6, 131.9, 131.3, 130.3, 127.6, 127.5, 126.5, 126.1, 115.0, 44.6, 31.9, 19.7, 13.6; HRMS (ESI): calcd. for $C_{20}H_{19}NO_2$ $[M+Na]^+$: 328.1313; Found: 328.1313.

2-Phenyl-3-(aminoethyl-2-(*N*,*N*-dimethylamino))-3-naphthalene-1,4-dione (8d)

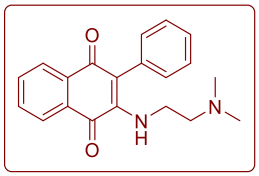

Starting from **7** (200 mg, 0.85 mmol), **8d** (198mg, 72%)was isolated as a red solid: mp 95 - 97 °C; FT-IR (ν_{max}, cm^{-1}): 3461, 2963, 1664, 1621, 1585, 1273, 1046, 860; ^{1}H NMR (400 MHz, $CDCl_3$): δ 8.11–8.04 (m, *2*H), 7.70 (td, *J* = 7.3, 1.3 Hz, 1H), 7.60 (td, *J* = 7.3, 1.3 Hz, 1H), 7.28-7.39 (m, 5H), 6.67 (s, 1H), 2.57-2.59 (m, 2H), 2.24 (t, *J* = 5.9 Hz, 2H), 2.12 (s, 6H); ^{13}C NMR (100 MHz, $CDCl_3$): δ 182.9, 182.4, 144.8, 134.7, 134.6, 133.6, 131.9, 131.4, 130.4, 127.6, 127.5, 126.5, 126.1, 115, 57.7, 44.9, 42.0; HRMS (ESI): calcd. for $C_{20}H_{20}N_2O_2$ $[M+Na]^+$: 321.1603; Found: 321.1604.

2-Phenyl-3-(amino-prop-2-enyl)naphthalene-1,4-dione (8e)

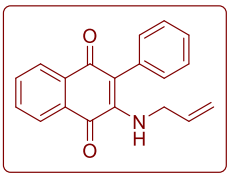

Starting from **7** (300 mg, 1.28 mmol), **8e** (224mg, 60%) was isolated as a red solid: mp 116 - 118 °C; FT-IR (ν_{max}, cm^{-1}): 3285, 1675, 1603, 1564, 1512, 1327, 898; ^{1}H NMR (400 MHz, $CDCl_3$): δ 8.06–8.12 (m, *2*H), 7.71 (td, *J* = 1.3, 7.3 Hz, 1H), 7.61 (td, *J* = 1.3,7.3 Hz, 1H), 7.27-7.40 (m, 5H), 5.98 (s, 1H), 5.54-5.64 (m, 1H), 4.99-5.08 (m, 2H), 3.25 (t, *J* = 5.9 Hz, 2H); ^{13}C NMR (100 MHz, $CDCl_3$): δ 182.9, 182.5, 144.2, 134.8, 134.1, 133.6, 133.4, 132.1, 131.2, 130.3, 127.8, 127.7, 126.6, 126.1, 117.1, 115.7, 47.0; HRMS (ESI): calcd. for $C_{19}H_{15}NO_2$ $[M+Na]^+$: 312.1000; Found: 312.1002.

2-Phenyl-3-(benzylamino)naphthalene-1,4-dione(8f)

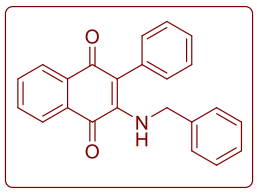

Starting from **7** (300 mg, 1.28 mmol), **8f** (348mg, 80%) was isolated as a red solid: mp 130 – 132 °C; FT-IR (ν_{max}, cm^{-1}): 3418, 2926, 1674, 1606, 1568, 1510, 1333, 1122, 727; ^{1}H NMR (400 MHz, $CDCl_3$): δ 8.06–8.12 (m,2H), 7.72 (td, *J* = 0.9, 7.3 Hz, 1H), 7.62 (td, *J* = 0.9, 7.3 Hz, 1H), 7.25-7.38 (m, 8H), 6.99–7.01 (m, 2H), 6.15 (s, 1H), 3.78 (d, J = 5.4 Hz, 2H); ^{13}C NMR (100 MHz,

$CDCl_3$): δ 182.9, 182.6, 144.2, 137.6, 134.9, 134.0, 133.4, 132.1, 131.3, 130.3, 128.8, 127.8, 127.7, 127.6, 126.6, 126.2, 115.9, 49.2; HRMS (ESI): calcd. for $C_{23}H_{17}NO_2$ $[M+Na]^+$: 362.1157; Found: 362.1157.

2-Phenyl-3-(4-methoxybenzylamino)naphthalene-1,4-dione (8g)

Starting from **7** (300 mg, 1.28 mmol), **8g** (383mg, 81%) was isolated as a red solid: mp 112 – 114 °C; FT-IR (ν_{max}, cm^{-1}): 3437, 2925, 1675, 1569, 1509, 1415, 1120, 809; ^1H NMR (400 MHz, $CDCl_3$): δ 8.04-8.12 (m, 2H), *7*.71 (td, *J* = 1.4, 7.3 Hz, 1H), 7.61 (td, *J* = 1.4, 7.3 Hz, 1H), 7.29-7.39 (m, 5H), 6.94 (d, *J* = 7.8 Hz, 2H), 6.78 (d, *J* = 7.8 Hz, 2H), 6.05 (s, 1H), 3.76 (s, 3H), 3.69 (d, *J* = 5.5 Hz, 2H); ^{13}C NMR (100 MHz, $CDCl_3$): δ 182.9, 182.5, 159.2, 144.2, 134.8, 134.2, 133.5, 132.1, 131.4, 130.3, 129.6, 129.0, 127.7, 126.6, 126.1, 115.7, 114.1, 55.3, 48.9; HRMS (ESI): calcd. for $C_{24}H_{19}NO_3$ $[M+Na]^+$: 369.1365; Found: 369.1315.

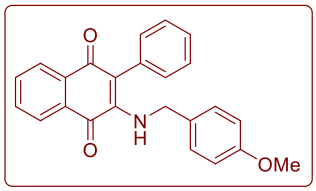

2-Phenyl-3-(4-chlorobenzylamino)naphthalene-1,4-dione (8h)

Starting from **7** (300 mg, 1.28 mmol), **8h** (304mg, 63%) was isolated as a red solid: mp 158 - 160 °C; FT-IR (ν_{max}, cm^{-1}): 3299, 2924, 1673, 1603, 1568, 1508, 1331, 1017, 728; ^1H NMR (400 MHz, $CDCl_3$): δ 8.06–8.11 (m, *2*H), 7.70-7.73 (t, *J* = 7.4 Hz, 1H), 7.60-7.64 (t, *J* = 7.4 Hz, 1H), 7.31-7.36 (m, 3H), 7.19-7.24 (m, 4H), 6.90 (d, *J* = 8.2 Hz, 2H), 6.13 (s, 1H), 3.79 (d, J = 5.9 Hz, 2H); ^{13}C NMR (100 MHz, $CDCl_3$): δ 182.8, 183.6, 144.0, 136.2, 134.9, 133.8, 133.6, 133.3, 132.2, 131.3, 130.2, 128.9, 128.7, 127.8, 126.7, 126.2, 116.2, 48.3; HRMS (ESI): calcd. for $C_{23}H_{16}ClNO_2$ $[M+Na]^+$: 412.0507; Found: 412.2647.

2-Phenyl-4-(4-methoxyphenylamino)naphthalene-1,4-dione (8j)

Starting from **7** (200 mg, 0.85 mmol), **8j** (178mg, 58%) was isolated as a red solid: mp 143 - 145 °C; FT-IR (ν_{max}, cm^{-1}): 3303, 1662, 1632, 1561, 1514, 1333, 1030, 758; ^1H NMR (400 MHz, $CDCl_3$): δ 8.15 (td, *J* = 1.3, 8.2 Hz, *2*H), 7.64-7.77 (m, 3H), 6.94-6.99 (m, 5H), 6.52 (d, *J* = 8.7 Hz, 2H), 6.39 (d, *J* = 8.7 Hz, 2H), 3.64 (s, 3H); ^{13}C NMR (100 MHz, $CDCl_3$): δ 183.3, 182.5, 156.5, 141.3, 134.9, 133.5, 132.6, 132.3, 130.6, 130.5, 130.3, 127.1, 127.0, 126.8, 126.2, 124.3, 116.2, 113.2, 55.5; HRMS (ESI): calcd. for $C_{23}H_{17}NO_3$ $[M+Na]^+$: 378.1106; Found: 378.1106.

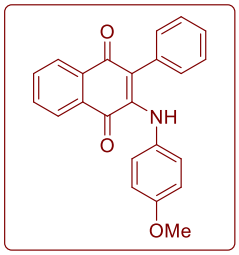

2-Phenyl-3-(4-nitrophenylamino)naphthalene-1,4-dione (8k)

Starting from **7** (300 mg, 1.28 mmol), **8k** was isolated as a red solid (120mg, 25%): mp 209 - 211°C; FT-IR (ν_{max}, cm^{-1}): 3461, 2963, 1664, 1621, 1585, 1273, 1046, 860; ^{1}H NMR (400 MHz, $CDCl_3$): δ 8.17 (m, 2H), 7.70-7.82 (m, 5H), 7.04-7.12 (m, 5H), 6.64 (d, *J* = 9.1 Hz, 2H); ^{13}C NMR (100 MHz, $CDCl_3$): δ182.8, 182.6, 143.5, 142.7, 139.7, 135.2, 133.1, 132.9, 132.2, 130.1, 128.3, 127.1, 126.4, 123.7, 121.0, 120.5; HRMS (ESI): calcd. for $C_{22}H_{14}N_2O_4$ $[M+Na]^+$:393.0851; Found: 393.0852.

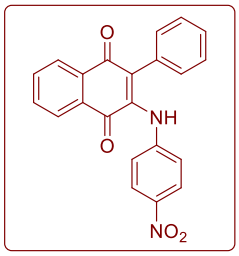

2-Phenyl-3-(pyrrolidin-1-yl)naphthalene-1,4-dione (8l)

Starting from **7** (300 mg, 1.28 mmol), **8l** (300 mg, 77%) was isolated as a red solid: mp 98 – 100 °C; FT-IR (ν_{max}, cm^{-1}): 3461, 2963, 1664, 1621, 1585, 1273, 1046, 860; ^{1}H NMR (400 MHz, $CDCl_3$): δ 8.06 (d, *J* = 7.3 Hz, 1H), 7.93 (d, *J* = 7.3 Hz, 1H), 7.66 (t, *J* = 7.3 Hz, 1H), 7.57 (t, *J* = 7.3 Hz, 1H), 7.23-7.32 (m, 5H), 3.28 - 3.31 (m, 4H), 1.67–1.71 (m, 4H); ^{13}C NMR (100 MHz, $CDCl_3$): δ 185.7, 181.4, 150.6, 136.5, 133.9, 133.3, 131.9, 131.8, 131.6, 127.5, 126.8, 125.9, 125.5, 117.3, 53.9, 25.5; HRMS (ESI): calcd. for $C_{20}H_{17}NO_2$ $[M+Na]^+$: 326.1157; Found: 326.1155.

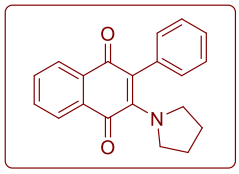

2-Phenyl-3-(piperidin-1-yl)naphthalene-1,4-dione (8m)

Starting from **7** (300 mg, 1.28 mmol), **8m** (351 mg, 86%) was isolated as a dark red solid: mp 184 – 186 °C; FT-IR (ν_{max}, cm^{-1}): 3454, 2933, 1663, 1629, 1586, 1281, 714; ^{1}H NMR (400 MHz, $CDCl_3$): δ 8.02–8.08 (m, 2H), 7.61–7.69 (m, 2H), 7.38–7.45 (m, 2H), 7.23-7.31 (m, 3H), 2.88–2.90 (m, 4H), 1.50–1.59 (m, 6H); ^{13}C NMR (100 MHz, $CDCl_3$): δ 184.3, 183.5, 151.8, 135.4, 133.7, 132.6, 132.5, 132.3, 130.8, 127.9, 127.4, 126.7, 126.1, 53.6, 26.5, 24.1; HRMS (ESI): calcd. for $C_{21}H_{19}NO_2$ $[M+Na]^+$: 340.1313; Found: 340.1315.

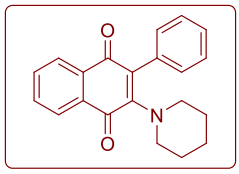

General procedure for synthesis of 11b-11e and 12b-12e

To a solution of **10a** (9.12 mmol) in DMF (20 mL), NaH (18.24 mmol, 60% dispersion in mineral oil) was added and the reaction mixture was stirred at 40 °C for 1 h. The resulting mixture was cooled to RT, and then alkyl halide (13.68 mmol) was added. The mixture was stirred at 80 °C until the completion of reaction, as monitored by TLC (12-18h). After completion, the reaction was quenched with ice cold water and extracted with CH_2Cl_2 (20 mL x 3). The combined organic layer was washed with brine, dried over Na_2SO_4, and concentrated *in*

vacuo to give the residue. 1-alkyl-5,8-dimethoxy-4-methylquinolin-2(1H)-one and 2-alkoxy-5,8-dimethoxy-4-methylquinoline isomers were separated by column chromatography eluting with hexanes/EtOAc (9:1). Using this procedure compounds **11b-11e** and **12b-12e** were prepared.

1-Ethyl-5,8-dimethoxy-4-methylquinolin-2(1H)-one (11c) and 2-Ethoxy-5,8-dimethoxy-4-methylquinoline (12c)

Starting from **10a** (1 g, 4.56 mmol), **11c** (550 mg, 49%) and **12c** (280 mg, 25%) were obtained as

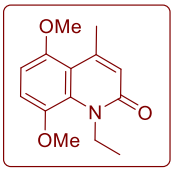

white solid. **11c**: mp: 108-109 °C; FT-IR (ν_{max}, cm^{-1}): 2928, 1655, 1594, 1142, 1476, 1423, 1383, 1363, 1321, 801; ^{1}H NMR (400 MHz, $CDCl_3$): δ 6.99 (d, *J* = 8.9 Hz, 1H), 6.60 (d, *J* = 9.0 Hz, 1H), 6.42 (d, *J* = 0.9 Hz, 1H), 4.46 (q, *J* = 6.8 Hz, 2H), 3.84 (s, 3H), 3.81 (s, 3H), 2.57 (d, *J* = 1.2 Hz, 2H), 1.36 (t, *J* = 6.9 Hz, 3H); 13C NMR (100 MHz, $CDCl_3$) δ 163.3, 153.0, 147.4, 142.9, 133.0, 122.4, 114.9, 114.3, 104.0, 57.3, 55.9, 43.2, 25.4, 15.2; HRMS (ESI): calcd. For $C_{14}H_{17}NO_3$ $[M+H]^+$: 248.1287; Found: 248.1290.

12c: mp: 77-78 °C; FT-IR (ν_{max}, cm^{-1}):2971, 2828, 1615, 1523, 1451, 1382, 1109; ^{1}H NMR (400

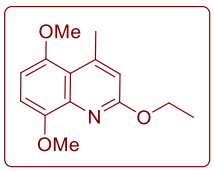

MHz, $CDCl_3$): δ 6.93 (d, *J* = 8.6 Hz, 1H), 6.66 (s, 1H), 6.62 (d, *J* = 8.6 Hz, 1H), 4.55 (q, *J* = 7.0 Hz, 2H), 3.99 (s, 3H), 3.86 (s, 2H), 2.78 (s, 3H), 1.43 (t, *J* = 7.1 Hz, 3H); ^{13}C NMR (100 MHz, $CDCl_3$): δ 161.7, 152.1, 148.7, 148.7, 140.2, 118.4, 114.2, 109.2, 102.9, 61.4, 57.0, 55.7, 24.7, 14.8; HRMS (ESI): calcd. For $C_{14}H_{17}NO_3$ $[M+H]^+$: 248.1287; Found: 248.1290.

1-Allyl-5,8-dimethoxy-4-methylquinolin-2(1H)-one (11d) and 2-(Allyloxy)-5,8-dimethoxy-4-methylquinoline (12d)

Starting from **10a** (2 g, 9.12 mmol), **11d** (558 mg, 27%) and **12d** (684 mg, 33%) were obtained

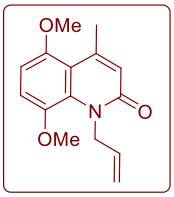

as white solid. **11d**: mp: 74-76 °C; FT-IR (ν_{max}, cm^{-1}): 2928, 1664, 1591, 1474, 1462, 1435, 1368,993, 742; ^{1}H NMR (400 MHz, $CDCl_3$): δ 6.99 (d, *J* = 8.9 Hz, 1H), 6.62 (d, *J* = 9.0 Hz, 1H), 6.46 (s, 1H), 6.04–5.92 (m, 1H), 5.18–5.12 (m, 2H), 5.09–4.97 (m, 2H), 3.82 (s, 3H), 3.79 (s, 3H), 2.59 (s, 3H); ^{13}C NMR (100 MHz, $CDCl_3$): δ 163.1, 153.0, 147.9, 143.0, 135.2, 132.8, 122.1, 114.9, 104.4, 57.6, 55.9, 49.2, 25.4; HRMS (ESI): calcd. For $C_{15}H_{17}NO_3$ $[M+H]^+$: 260.1287; Found: 260.1288.

12d: mp 76-78 °C; FT-IR (ν_{max}, cm^{-1}): 2980, 1609, 1591, 1523, 1431, 1449, 1385, 915; ^1H NMR

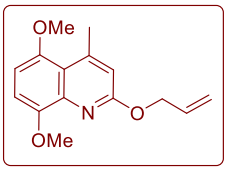

(400 MHz, $CDCl_3$): δ 6.93 (d, *J* = 8.6 Hz, 1H), 6.70 (s, 1H), 6.63 (d, *J* = 8.6 Hz, 1H), 6.21–6.08 (m, 1H), 5.46 (dd, *J* = 17.2, 1.6 Hz, 1H), 5.27 (dd, *J* = 10.4, 1.4 Hz, 1H), 5.03 (dt, *J* = 5.5, 1.2 Hz, 2H), 3.99 (s, 1H), 3.86 (s, 1H), 2.79 (s, 1H); ^{13}C NMR (100 MHz, $CDCl_3$): δ 161.2, 152.1, 148.9, 148.7, 140.0, 133.8, 118.5, 117.7, 114.1, 109.4, 103.1, 66.4, 57.0, 55.7, 24.7; HRMS (ESI): calcd. For $C_{15}H_{17}NO_3$ $[M+H]^+$: 260.1287; Found: 260.1287.

1-Benzyl-5,8-dimethoxy-4-methylquinolin-2(1H)-one (11e) and 2-(Benzyloxy)-5,8-dimethoxy-4-methylquinoline (12e):

Starting from **10a** (2 g, 9.12 mmol), **11e** (670 mg, 24%), and **12f** (1.3 g, 46%) were obtained as

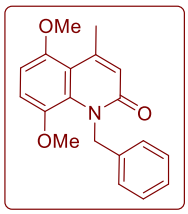

white solid. **11e**: mp 176-178 °C; FT-IR (ν_{max}, cm^{-1}): 2934, 1660, 1593, 1496, 1473, 1370, 1320, 1266; ^1H NMR (400 MHz, $CDCl_3$): δ 7.26-7.21 (m, 2H), 7.15 (d, *J* = 7.1 Hz, 1H), 7.07 (d, *J* = 7.5 Hz, 2H), 6.90 (d, *J* = 9.0 Hz, 1H), 6.60 (d, *J* = 8.9 Hz, 1H), 6.55 (s, 1H), 5.78 (s, 2H), 3.83 (s, 3H), 3.42 (s, 3H), 2.65 (s, 3H); ^{13}C NMR (100 MHz, $CDCl_3$): δ 163.5, 153.0, 148.2, 139.7, 133.0, 128.1, 126.0, 125.8, 122.1, 115.1, 114.9, 104.5, 57.5, 55.9, 50.6, 25.6; HRMS (ESI): calcd. For $C_{19}H_{19}NO_3$ $[M+H]^+$: 310.1443; Found: 310.1454.

12e: mp 118-120 °C; FT-IR (ν_{max}, cm^{-1}): 2991, 1707, 1726, 1697, 1612, 1522, 1495, 1479, 1265, 1171, 804; ^1H NMR (400 MHz, $CDCl_3$): δ 7.56-7.54 (m, 2H), 7.41–7.31 (m, 3H), 6.96 (d, *J* = 8.6 Hz, 1H), 6.75 (s, 1H), 6.65 (d, *J* = 8.6 Hz, 1H), 5.57 (s, 2H), 4.02 (s, 3H), 3.87 (s, 3H), 2.80 (s, 3H); ^{13}C NMR (100 MHz, $CDCl_3$): δ 161.4, 152.1, 148.9, 148.7, 140.0, 137.5, 128.5, 127.9, 118.6, 114.2, 109.3, 103.1, 67.5, 57.0, 55.7, 24.7; HRMS (ESI): calcd. For $C_{19}H_{19}NO_3$ $[M+H]^+$: 310.1443; Found: 310.1468.

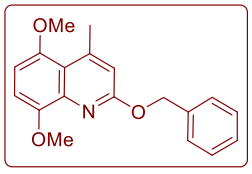

General procedure for oxidation and Diels-Alder reaction with 1, 3-cyclohaxadiene

To a solution of 1-alkyl-5,8-dimethoxy-4-methylquinolin-2(1H)-one or 2-alkoxy-5,8-dimethoxy-4-methylquinoline (1.01 mmol) in water (5 mL) and MeCN (5 mL), ceric ammonium nitrate (3.03 mmol) was added. The resulting mixture was stirred at RT for 10 min. The resulting mixture was diluted with water (20 ml) and extracted with CH_2Cl_2 (3 ×10 ml). The combined organic layer was dried over sodium sulfate, filtered and filtrate was concentrated *in vacuo*. The

crude compound was then dissolved in toluene (10 ml) and freshly distilled 1,3-cyclohexadiene (1.01 mmol) was added to the reaction mixture. The resulting mixture was stirred at 90 °C (10-12 h). The reaction progress was monitored by TLC. After completion of the reaction, volatiles were evaporated under reduced pressure to obtain crude product, which was purified by column chromatography to afford pure material.

General procedure of oxidation and Diels-Alder reaction with 1,3-cyclopentanone

To a solution of 2-alkoxy-5,8-dimethoxy-4-methylquinoline (1.01 mmol) in water (5 mL) and MeCN (5 mL), ceric ammonium nitrate (3.03 mmol) was added. The resulting mixture was stirred at RT for 10 min and then diluted with water (20 ml) and extracted with CH_2Cl_2 (3 ×10 ml). The combined organic layer was dried over sodium sulfate, filtered and filtrate was evaporated under reduced pressure. The crude compound was dissolved in CH_2Cl_2 (10 ml) and cooled to 0 °C. 1,3-cyclopentadiene (1.03 mmol) was added to mixture and the resulting mixture was stirred at 0 °C (10-12 h). The reaction progress was monitored by TLC and after completion of the reaction the volatiles were evaporated under reduced pressure to obtain crude product, which was purified using silica gel column chromatography.

4-Methyl-6,9-dihydro-6,9-ethanobenzo[*g*]quinoline-2,5,10(1*H*)-trione (13a)

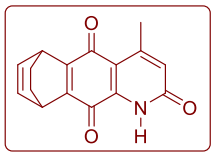

Starting from **10a** (200 mg, 0.91 mmol), **13a** (70 mg, 29%) was isolated as a red solid; mp: at 171 °C decomposes; FT-IR (ν_{max}, cm^{-1}) 2937, 1658, 1591, 1528, 1467, 1375, 1312, 1151, 1037, 980, 876, 819; ^{1}H NMR (400 MHz, $CDCl_3$): δ 10.58 (bs, 1H), 6.59 (s, 1H), 6.43–6.38 (m, 2H), 4.50–4.41 (m, 2H), 2.57 (s, 3H), 1.57–1.49 (m, 2H), 1.38-1.36 (m, 2H); ^{13}C NMR (100 MHz, $CDCl_3$): δ 180.7, 175.9, 161.5, 152.4, 152.0, 145.7, 138.9, 133.8, 126.3, 113.7, 34.5, 33.7, 24.7, 22.4; HRMS (ESI): calcd. For $C_{16}H_{13}NO_3$ $[M+H]^+$: 268.0974; Found: 268.0972.

1,4-Dimethyl-6,9-dihydro-6,9-ethanobenzo[*g*]quinoline-2,5,10(1*H*)-trione (13b)

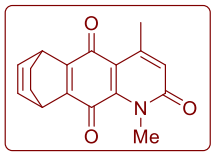

Starting from **11b** (250 mg,1.07 mmol), **13b** (79 mg, 26%) was isolated as a orange solid: mp 193-195°C; FT-IR (ν_{max}, cm^{-1}) 2961, 1654, 1633, 1592, 1578, 1503, 1472, 1433, 1403, 1355, 1381, 1294, 1265, 1155, 1179, 1144, 1134, 1101, 1032, 967, 891, 868, 832, 816, 745, 709, 693, 666, 537;^{1}H NMR (400 MHz, $CDCl_3$): δ 6.60 (d, *J* = 1.12 Hz, 1H), 6.44-6.40 (m, 2H), 4.42-4.39 (m, 2H), 3.84 (s, 3H), 2.56 (d, *J*=0.9 Hz, 3H), 1.53-1.48 (m, 2H), 1.39-1.36 (m, 2H); ^{13}C NMR (100 MHz, $CDCl_3$): δ 181.2,

179.3, 162.3, 149.7, 149.6, 147.4, 142.3, 134.0, 133.9, 125.1, 116.8, 34.6, 34.5, 34.3, 25.1, 25.0, 23.1; HRMS (ESI): calcd. For $C_{17}H_{15}NO_3$ $[M+H]^+$: 282.1130; Found: 282.1138.

1-Benzyl-4-methyl-6,9-dihydro-6,9-ethanobenzo[*g*]quinoline-2,5,10(1*H*)-trione (13e)

Starting from **11e** (270 mg, 0.87mmol), **13e** (146 mg, 47%) was isolated as a orange solid: mp

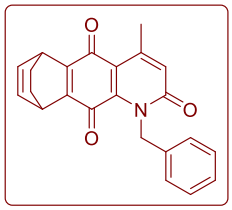

136-137 °C; FT-IR (ν_{max}, cm^{-1}) 2958, 1662, 1634, 1696, 1595, 1496, 1452, 1434, 1414, 1368, 1347, 1327, 1296, 1272, 1180, 1141, 1030, 940, 929, 883, 834, 745, 710; ^{1}H NMR (400 MHz, $CDCl_3$): δ 7.30-7.15 (m, 5H), 6.70 (d, *J* =0.8 Hz, 1H), 6.40-6.33 (m, 2H), 5.88-5.76 (m, 2H), 4.40-4.37 (m, 1H), 4.30-4.27 (m, 1H), 2.60 (d, *J* = 0.8 Hz, 3H), 1.53-1.42 (m, 2H), 1.37-1.28 (m, 2H); ^{13}C NMR (100 MHz, $CDCl_3$): δ 181.3, 178.8, 162.1, 150.0, 149.3, 147.5, 141.8, 137.4, 133.8, 133.7, 128.6, 127.1, 126.7, 125.6, 117.4, 48.5, 34.4, 34.2, 24.9, 23.3; HRMS (ESI): calcd. For $C_{23}H_{19}NO_3$ $[M+H]^+$: 358.1443; Found: 358.1463.

2-Methoxy-4-methyl-6,9-dihydro-6,9-methanobenzo[*g*]quinoline-5,10-dione (14b)

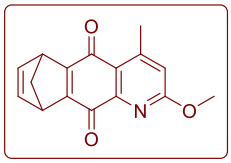

Starting from **12b** (200 mg, 0.85mmol), **14b** (89 mg, 39%) was isolated as a yellow solid; mp170-171°C; FT-IR (ν_{max}, cm^{-1}) 2994, 1664, 1647, 1612, 1589, 1560, 1535, 1475, 1436, 1366, 1328, 1308, 1287, 1187, 1150, 1124, 1115, 1052, 1018, 836, 799, 759, 702; ^{1}H NMR (400 MHz, $CDCl_3$): δ 6.90-6.85 (m, 2H), 6.73 (s, 1H), 4.24(bs, 1H), 4.18 (bs, 1H), 4.07 (s, 3H), 2.66 (s, 3H), 2.36-2.33 (m, 1H), 2.30-2.27 (m, 1H); ^{13}C NMR (100 MHz, $CDCl_3$): δ 183.4, 180.1, 165.7, 163.8, 160.6, 152.7, 149.5, 142.8, 142.6, 123.1, 117.1, 73.1, 54.3, 48.9, 48.7, 22.5; HRMS (ESI): calcd. For $C_{16}H_{13}NO_3$ $[M+H]^+$: 268.0974; Found: 268.0976.

2-Ethoxy-4-methyl-6,9-dihydro-6,9-methanobenzo[*g*]quinoline-5,10-dione (14c)

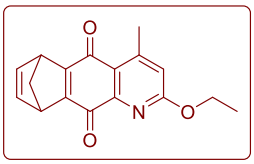

Starting from **12c** (250 mg, 1.01 mmol), **14c** (60 mg, 21%) was isolated as a yellow solid: mp 180-182°C; FT-IR (ν_{max}, cm^{-1}) 2988, 1668, 1645, 1616, 1586, 1534, 1452, 1347, 1378, 1327, 1306, 1290, 1183, 1154, 1122, 1049, 861, 797, 759, 705;^{1}H NMR (400 MHz, $CDCl_3$): δ 6.90-6.86 (m, 2H), 6.71 (d, *J* = 0.68 Hz, 1H), 4.53 (q, *J* = 7.04Hz, 2H) ,4.23 (bs, 1H), 4.19 (bs, 1H), 2.68 (s, 3H), 2.36-2.34 (m, 1H), 2.30-2.28 (m, 1H), 1.40 (t, *J* = 7.04 Hz, 3H);^{13}C NMR (100 MHz, $CDCl_3$): δ 183.4, 180.1, 165.5, 163.8, 160.6, 152.6, 149.5, 142.8, 142.6, 123.0, 117.1, 73.1, 62.9, 48.9, 48.7, 22.5, 14.6; HRMS (ESI): calcd. For $C_{17}H_{15}NO_3$ $[M+H]^+$: 282.1130; Found: 282.1135.

2-(Allyloxy)-4-methyl-6,9-dihydro-6,9-methanobenzo[*g*]quinoline-5,10-dione (14d)

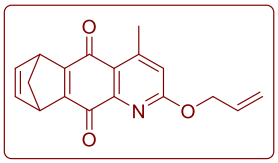

Starting from **12d** (200 mg, 0.77 mmol), **14d** (80 mg, 35%) was isolated as a pale yellow solid: mp 165-167 °C; FT-IR (ν_{max}, cm^{-1}): 2995, 1668, 1644, 1613, 1587, 1534, 1451, 1391, 1326, 1306, 1288, 1138, 1153, 1123, 1047, 985, 862, 769, 760, 709; ^{1}H NMR (400 MHz, $CDCl_3$): δ 6.91-6.87 (m, 2H), 6.79 (s, 1H), 6.14-6.04 (m, 1H), 5.48-5.42 (m, 1H), 5.30-5.27 (m, 1H), 5.04-4.02 (m, 2H), 4.25 (s, 1H), 4.20 (s, 1H), .2.71 (s, 3H), 2.38-2.35 (m, 1H), 2.32-2.30 (m, 1H); ^{13}C NMR (100 MHz, $CDCl_3$): δ 183.3, 180.0, 165.0, 163.8, 160.6, 152.8, 149.4, 142.8, 142.6, 132.8, 123.2, 118.5, 117.2, 73.1, 67.6, 48.9, 48.7, 22.5; HRMS (ESI): calcd. For $C_{18}H_{15}NO_3$ $[M+H]^+$:294.1130; Found: 294.1137.

2-(Benzyloxy)-4-methyl-6,9-dihydro-6,9-methanobenzo[*g*]quinoline-5,10-dione (14e)

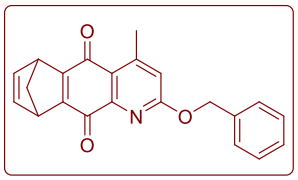

Starting from **12e** (300 mg,0. 96 mmol), **14e** (mg, 83%) was isolated as a yellow solid: mp 188-190°C; FT-IR (ν_{max}, cm^{-1})1666, 1644, 1587, 1529, 1452, 1349, 1325, 1306, 1151, 1122, 1045, 979, 915, 858, 797, 761, 750, 711; ^{1}H NMR (400 MHz, $CDCl_3$): δ 7.52 (d, *J* = 7.98 Hz, 2H), 7.39-7.30 (m, 3H), 6.97-6.87.(m, 2H), 6.80 (s, 1H), 5.55 (s, 2H), 4.26 (s, 1H), 4.20 (s,1H), 2.69 (s, 3H), 2.36 (d, *J* = 7.08 Hz, 1H), 2.31 (d, *J* = 7.12 Hz, 1H); ^{13}C NMR (100 MHz, $CDCl_3$): δ 183.3, 180.0, 165.1, 163.9, 160.6, 152.9, 149.3, 142.8, 142.6, 136.5, 128.8, 128.6, 128.3, 123.3, 117.4, 73.2, 68.7, 48.9, 48.7, 22.5; HRMS (ESI): calcd. For $C_{22}H_{17}NO_3$ $[M+H]^+$:344.1287; Found: 344.1295.

2-Methoxy-4-methyl-6,9-dihydro-6,9-ethanobenzo[*g*]quinoline-5,10-dione (15b)

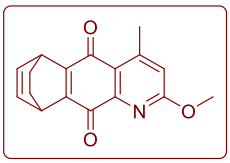

Starting from **12b** (200mg, 0.85mmol), **15b** (61 mg, 26 %) was isolated as a pale yellow solid: mp 182-184°C; FT-IR (ν_{max}, cm^{-1}) 3057, 2935, 1650, 1670, 1632, 1588, 1540, 1476, 1434, 1340, 1310, 1260, 1221, 1190, 1183, 1138, 1104, 1052, 1037, 1017, 991, 868, 812, 756, 696; ^{1}H NMR (400 MHz, $CDCl_3$): δ 6.76 (d, *J* = 0.7 Hz, 1H), 6.46-6.40 (m, 2H), 4.53 (bs, 1H), 4.49 (bs, 1H), 4.09 (d, *J* = 0.6 Hz, 3H), 2.70 (s, 3H), 1.55-1.50 (m, 2H), 1.41-1.38 (m, 2H); ^{13}C NMR (100 MHz, $CDCl_3$): δ 182.9, 180.1, 165.8, 152.8, 151.0, 148.8, 134.0, 133.9, 123.0, 117.4, 54.3, 34.3, 34.1, 24.9, 24.8, 22.6; HRMS (ESI): calcd. For $C_{17}H_{15}NO_3$ $[M+H]^+$: 282.1130; Found: 282.1132.

2-Ethoxy-4-methyl-6,9-dihydro-6,9-ethanobenzo[*g*]quinoline-5,10-dione (15c)

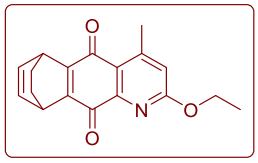

Starting from **12c** (250 mg, 1.01 mmol), **15c** (50 mg,14%) was isolated as a yellow solid: mp 161-162°C; FT-IR (ν_{max}, cm^{-1}) 2989, 1669, 1649, 1588, 1536, 1455, 1375, 1338, 1309, 1181, 1142, 1051, 864, 820, 754, 703; ^{1}H NMR (400 MHz, $CDCl_3$): δ 6.73 (s, 1H), 6.44-6.40 (m, 2H), 4.55 (q, *J* = 7.1 Hz, 2H), 4.50-4.47 (m, 2H), 2.69 (s, 3H), 1.52-1.50 (m, 2H), 1.41-1.37 (m, 5H); ^{13}C NMR (100 MHz, $CDCl_3$): δ 182.9, 180.2, 165.5, 152.7, 151.0, 148.8, 148.7, 134.1, 133.9, 122.8, 117.4, 62.9, 34.3, 34.1, 24.9, 24.8, 22.6, 14.6; HRMS (ESI): calcd. For $C_{18}H_{17}NO_3$ $[M+H]^+$: 295.1208; Found: 295.1214.

2-(Allyloxy)-4-methyl-6,9-dihydro-6,9-ethanobenzo[*g*]quinoline-5,10-dione (15d)

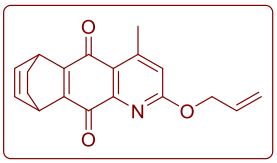

Starting from **12d** (300 mg, 1.15mmol), **15d** (75 mg, 31%) was isolated as a pale yellow solid: mp 155-157 °C; FT-IR (ν_{max}, cm^{-1}): 2978, 2931, 1669, 1650, 1632, 1588, 1535, 1455, 1428, 1376, 1338, 1308, 1258, 1181; ^{1}H NMR (400 MHz, $CDCl_3$): δ 6.79 (s, 1H), 6.45-6.40 (m, 2H), 6.13-6.04 (m, 1H), 5.46-5.41 (m, 1H), 5.29-5.26 (m, 1H), 5.02 (dt, *J* = 5.64, 1.28 Hz, 2H), 4.52-4.48 (m, 2H), 2.70 (s, 3H), 1.5-1.51 (m, 2H), 1.40-1.38 (m, 2H); ^{13}C NMR (100 MHz, $CDCl_3$): δ 182.9, 180.1, 165.1, 152.9, 151.0, 148.7, 134.1, 133.9, 132.8, 123.1, 118.5, 117.5, 67.6, 34.3, 34.1, 24.9, 24.8, 22.6; HRMS (ESI): calcd. For $C_{19}H_{17}NO_3$ $[M+H]^+$: 308.1287; Found: 308.1293.

2-(Benzyloxy)-4-methyl-6,9-dihydro-6,9-ethanobenzo[*g*]quinoline-5,10-dione (15e)

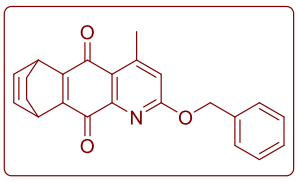

Starting from **12e** (500 mg, 1.61mmol), **15e** (250mg, 43%) was isolated as a pale yellow solid: mp 159-161°C; FT-IR (ν_{max}, cm^{-1})2973, 2929, 1666, 1649, 1630, 1588, 1531, 1455, 1379, 1340, 1307, 1256, 1183, 1138, 1046, 921, 867, 823, 766, 756, 710; ^{1}H NMR (400 MHz, $CDCl_3$): δ 7.53-7.51 (m, 2H), 7.39-7.32 (m, 3H), 6.81 (s, 1H), 6.45-6.41 (m, 2H), 5.56 (s, 2H), 4.55-4.50 (m, 2H), 2.70 (s, 3H), 1.56-1.52(m, 2H), 1.42-1-39(m, 2H);^{13}C NMR (100 MHz, $CDCl_3$): δ 182.9, 180.1, 165.2, 153.0, 151.0, 148.8, 148.7, 136.6, 134.1, 133.9, 128.8, 128.6, 128.3, 123.2, 117.6, 68.7, 34.3, 34.1, 24.9, 24.8, 22.6; HRMS (ESI): calcd. For $C_{23}H_{19}NO_3$ $[M+H]^+$ 358.1443; Found: 358.1451.

Synthesis of 1,4-dimethoxyphenanthridin-6(5*H*)-one(17a)

N-(2,5-dimethoxyphenyl)-2-iodobenzamide (1 g, 2.61 mmol), potassium t-butoxide (1.46 g, 13.05 mmol) and 1,10-phenanthroline (118 mg, 0.65 mmol) were added in benzene (15 mL) in a sealed tube. White colored reaction mixture was heated at 110 °C for 16 h. After completion, mixture poured over water (50 mL), extracted with ethyl acetate (20 mL x 3), dried over Na_2SO_4, and evaporated under reduced pressure on rotary evaporator. The crude product was purified on silica gel by column chromatography using hexane/EtOAc (5: 1) to afford **17a** (485 mg, 73%) as a white solid; mp: 209-211 °C; FT-IR (ν_{max}, cm^{-1}) 2917, 1791, 1647, 1601, 1507, 1450, 1370, 1251, 971, 854; ^{1}H NMR (400 MHz, $CDCl_3$): 9.24 (d, *J* = 8.5 Hz, 1H), 9.15 (bs, 1H), 8.57 (dd, *J* = 7.9, 1.3 Hz, 1H), 7.78-7.74 (m, 1H), 7.56-7.56 (m, 1H), 6.91 (d, *J* = 8.9 Hz, 1H), 6.70 (d, *J* = 8.9 Hz, 1H), 4.01 (s, 3H), 3.95 (s, 3H); ^{13}C NMR (100 MHz, $CDCl_3$): δ 161.3, 152.7, 140.2, 134.9, 132.8, 128.2, 128.1, 127.5, 127.4, 126.1, 109.4, 103.8, 56.5, 56.1; HRMS (ESI): calcd. For $C_{16}H_{15}NO_3$ $[M+H]^+$: 256.0974; Found: 256.0977.

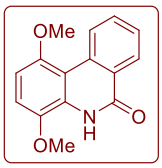

General procedure for synthesis of 17b and 17c

To a solution of **17a** (1 mmol) in DMF (20 mL), NaH (1.5 mmol, 60% dispersion in mineral oil) was added and the reaction mixture was stirred at 40 °C for 1 h. The resulting mixture was cooled to RT, and then alkyl halide (1.2 mmol) was added. The reaction mixture was stirred at 60 °C until the completion of reaction, as monitored by TLC (12-18h). After completion, the reaction was quenched with ice cold water and extracted with CH_2Cl_2 (20 mL x 3). The combined organic layer was washed with brine, dried over Na_2SO_4, and concentrated *in vacuo* to give the residue. The crude compound was purified using silica gel column chromatography eluting with hexanes/EtOAc (9:1). Using this procedure compound **17b** and **17c** were prepared.

1,4-Dimethoxy-5-methylphenanthridin-6(5*H*)-one (17b)

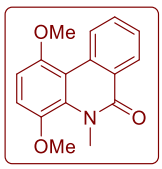

Starting from **17a** (400 mg, 1.57 mmol), **17b** (360 mg, 85%) was obtained as a white solid. mp: 135-137 °C; FT-IR (ν_{max}, cm^{-1}) 1634, 1589, 1497, 1446, 1418, 1387, 1335, 1275, 1235, 1185, 1115, 923, 787; ^{1}H NMR (400 MHz, $CDCl_3$): δ 9.19 (d, *J* = 8.4 Hz, 1H), 8.56 (dd, *J* = 7.9, 1.5 Hz, 1H), 7.72–7.68 (m, 1H),7.57-7.53 (m, 1H), 7.05 (d, *J* = 9.0 Hz, 1H), 6.82 (d, *J* = 9.0 Hz, 1H), 4.00 (s, 3H), 3.86 (s, 3H), 3.85 (s, 3H); ^{13}C NMR (100 MHz, $CDCl_3$): δ 163.7, 153.2, 143.8, 133.3, 132.1, 131.6, 128.2, 127.8,

127.5, 126.0, 114.6, 112.5, 106.1, 57.8, 56.3, 38.0; HRMS (ESI): calcd. For $C_{16}H_{15}NO_3$ $[M+H]^+$: 270.1130; Found: 270.1133.

5-Allyl-1,4-dimethoxyphenanthridin-6(5*H*)-one (17c)

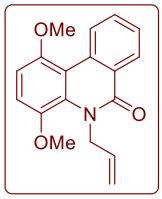

Starting from **17a** (600 mg, 2.35 mmol), **17c** (490 mg, 71%) was obtained as a white solid. mp: 77-49 °C; FT-IR (ν_{max}, cm^{-1}) 2913, 1737, 1635, 1591, 1494, 1452, 1422, 1393, 1355, 1317, 1283, 1012, 964;^{1}H NMR (400 MHz, $CDCl_3$): δ 9.20 (d, *J* = 8.5 Hz, 1H), 8.56 (dd, *J* = 7.9, 1.7 Hz, 1H), 7.71–7.67 (m, 1H), 7.56–7.52 (m, 1H), 7.01 (d, *J* = 9.1 Hz, 1H), 6.81 (d, *J* = 9.1 Hz, 1H), 6.11–6.01 (m, 1H), 5.18-5.11 (m, 4H), 3.98 (s, 3H), 3.82 (s, 3H); ^{13}C NMR (100 MHz, $CDCl_3$): δ 163.5, 153.1, 143.4, 135.6, 133.4, 132.2, 130.3, 128.3, 127.8, 127.5, 125.9, 115.3, 113.6, 112.6, 106.1, 57.3, 56.2, 51.3; HRMS (ESI): calcd. For $C_{18}H_{17}NO_3$ $[M+H]^+$: 296.1287; Found: 296.1286.

General procedure for oxidation and Diels-Alder reaction with 1, 3-cyclohaxadiene

To a solution 5-alkyl-1,4-dimethoxyphenanthridin-6(5H)-one **17** (0.78 mmol)in water (5 mL) and MeCN (5 mL), ceric ammonium nitrate (2.34 mmol) was added. The resulting mixture was stirred at RT for 10 min. After completion of reaction, the mixture was diluted with water (20 ml) and extracted with CH_2Cl_2 (3 ×10 ml). The combined organic layer was dried over sodium sulfate, filtered and filtrate was concentrated *in vacuo*. The crude compound was then dissolved in toluene (10 ml) and freshly distilled 1,3-cyclohexadiene (0.78 mmol) was added to the reaction mixture. The resulting mixture was stirred at 90 °C (10-12 h). The reaction progress was monitored by TLC. After completion of the reaction, volatiles were evaporated under reduced pressure to obtain crude product. The crude compound was then dissolved in THF (10 mL) and treated with K_2CO_3 (1.56 mmol)and stirred at RT for 2 h. The volatile from the reaction mixture was evaporated and residue was diluted in water (10 mL) and extracted with EtOAc (10 mL x 3). The combined organic layers dried over sodium sulfate, filtered and filtrate was evaporated to obtain crude compound. The crude compound was purified by column chromatography to afford pure material.

8,11-Dihydro-8,11-ethanobenzo[*b*]phenanthridine-5,7,12(6*H*)-trione (18a)

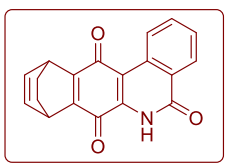

Starting from **17a** (200 mg,0.78 mmol), **18a** (145mg, 61%) was isolated as a red solid: mp >248°C; FT-IR (ν_{max}, cm^{-1}) 1635, 1488, 1432, 1327, 1297, 1136, 1030, 875, 816; ^{1}H NMR (400 MHz, $CDCl_3$): δ 9.37 (bs, 1H), 9.26(d,

J =8.4 Hz, 1H), 8.46 (d, *J* = 7.9 Hz, 1H), 7.84-7.80 (m, 1H), 7.65-7.61 (m, 1H), 6.46-6.44 (m, 2H), 4.54 (bs, 1H), 4.44 (bs, 1H), 1.55-1.52 (m, 2H), 1.46-1.42 (m, 2H); ^{13}C NMR (100 MHz, $CDCl_3$): δ 182.1, 176.6, 161.1, 152.4, 144.9, 135.0, 134.3, 133.9, 133.8, 133.5, 129.4, 128.1, 128.0, 127.9, 110.8, 34.6, 33.7, 24.8; HRMS (ESI): calcd. For $C_{19}H_{13}NO_3$ $[M+H]^+$: 304.0973; Found: 304.0972.

6-Methyl-8,11-dihydro-8,11-ethanobenzo[*b*]phenanthridine-5,7,12(6*H*)-trione (18b)

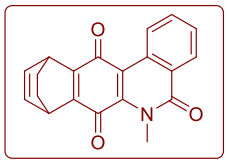

Starting from **17b** (50 mg, 0.18 mmol), **18b** (37mg, 63%) was isolated as a red solid: mp: 150-152 °C; FT-IR (ν_{max}, cm^{-1}) 1646, 1478, 1439, 1315, 1236, 1141, 991; ^{1}H NMR (400 MHz, $CDCl_3$): δ 9.22 (d, *J* = 8.6 Hz, 1H), 8.47 (dd, *J* = 8.1, 1.3 Hz, 1H), 7.84–7.74 (m, 1H), 7.68–7.57 (m, 1H), 6.48-6.44 (m, 2H), 4.54–4.37 (m, 2H), 3.90 (s, 3H), 1.56-1.54 (m, 2H), 1.47–1.37 (m, 2H); ^{13}C NMR (100 MHz, $CDCl_3$): δ 182.6, 180.1, 163.1, 149.8, 146.9, 139.7, 134.1, 133.9, 133.8, 132.2, 129.5, 128.3, 128.0, 176.0, 114.5, 35.4, 34.5, 34.4, 29.8, 25.2; HRMS (ESI): calcd. For $C_{20}H_{15}NO_3$ $[M+H]^+$: 318.1130; Found:318.1128.

6-Allyl-8,11-dihydro-8,11-ethanobenzo[*b*]phenanthridine-5,7,12(6*H*)-trione (18c)

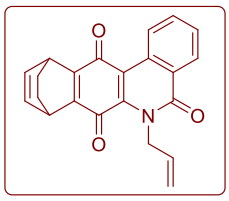

Starting from **17c** (50 mg, 0.16 mmol), **18c** (34mg, 58%) was isolated as a red solid: mp: 159-161 °C; FT-IR (ν_{max}, cm^{-1}) 1664, 1435, 1385, 1304, 1196, 1140, 995, 924, 819, 768; ^{1}H NMR (400 MHz, $CDCl_3$): δ 9.21 (d, *J* = 8.5 Hz, 1H), 8.49 – 8.46 (m, 1H), 7.81-7.77 (m, 1H), 7.64-7.62 (m, 1H), 6.53–6.45 (m, 2H), 6.08 (ddt, *J* = 17.4, 10.4, 5.3 Hz, 1H), 5.27–5.12 (m, 4H), 4.49-4.47 (m, 1H), 4.41-4.39 (m, 1H), 1.55-1.53 (m, 2H), 1.43–1.41 (m, 2H); ^{13}C NMR (100 MHz, $CDCl_3$): δ 182.7, 179.9, 162.7, 1.49.6, 147.1, 139.1, 134.0, 133.9, 132.2, 129.5, 128.4, 128.0, 127.1, 117.2, 114.9, 48.4, 36.4, 34.4, 25.1; HRMS (ESI): calcd. For $C_{22}H_{17}NO_3$ $[M+H]^+$: 344.1286; Found: 344.1284.

4.2.4.2. Cyclic voltammetry analysis

Cyclic voltammetric analysis was performed using a CHI900B electrochemical analyzer. A three-electrode setup was used: Pt wire auxiliary electrode, glassy carbonas a working electrode and Ag/Ag^+ as a reference electrode. The working electrode was polished with 0.05 µM alumina (Basi polishing solution) on a felt pad and washed with de-ionized water and rinsed using acetonitrile. All electrochemical samples were purged with argon for 5 min and were measured under argon atmosphere. The supporting electrolyte of 0.1 M tetrabutyl ammonium

hexafluorophosphate ($TBAPF_6$) and a 1 mM stock solution of the compound in DMSO were used and the analysis was carried out in acetonitrile.

4.2.4.3. Minimum Inhibitory Concentration Determination

The Minimum Inhibitory Concentration (MIC) assay is used to determine the inhibitory potential of a compound against bacterial pathogens. To determine the MIC, the microbroth dilution technique is commonly used as recommended by National Committee for Clinical Laboratory Standards. For this, a fixed bacterial inoculum (5×10^5 CFU/mL) is added into a series of test wells in a microtitre plate that contain various concentrations of compound under test. Following a period of incubation (37 °C, 18-20 hours), the wells are examined for growth. The lowest concentration of antibiotic that inhibits growth of the organism, as detected visually is designated as the MIC.

4.2.4.4. ROS generation by 18a in *S. aureus*

4.2.4.4.A. Intracellular superoxide detection using DHE assay

Staphylococcus aureus was cultured in 5 mL of Cation Adjusted Mueller-Hinton Broth (CAMHB) medium at 37 ºC to obtain O.D. of 0.5. This bacterial solution was incubated with dihydroethidium (50 μM) and **18a** (0.5 μg/mL) at 37 ºC for 1 h under dark conditions. The suspension was centrifuged to aspirate out excess of compound and dihydroethidium in the medium. The bacterial pellet was washed with PB pH 7.4.[31,35] The resulting pellet was resuspended with acetonitrile and bacterial cells were lysed by vortexing for 1 min. The cell lysate was then removed by centrifugation and the supernatant acetonitrile was separated and stored at -20 ºC before injecting in HPLC. The HPLC method used was as described previously (Chapter 2.1.4.6).

4.2.4.4. B. Extracellular H_2O_2 estimation

S. aureus was cultured in 5 mL of CAMHB medium at 37 ºC for ~2 hrs to obtain O.D. of 0.1. This bacterial solution (50 μL) was treated with **18a** in DMSO (1%) so that the final concentration was 0.12, 0.5 and 1μg/mL and incubated at 37 ºC for 60 min. 50 μL of a premixed solution of 10-acetyl-3,7-dihydroxyphenoxazine or Amplex Red® (prepared by following manufacturer's protocol from Invitrogen) was added and incubated at RT for 25 min before measuring the fluorescence using a microtiter plate reader (λ_{ex}- 550 nm and λ_{em}-590 nm).[32]

4.2.4.5. Cytotoxicity Assay

To test the effect of compound on the growth of mammalian cells, a cytotoxicity assay was performed as per published protocols. In brief, 5000 Vero cells (African green monkey kidney cell line) were seeded in a 96-well plate and grown for 24 hours at 37 °C in a humidified atmosphere of 5% CO_2 and 95% air in DMEM medium supplemented with 10% fetal bovine serum, 1.5 g Sodium bicarbonate/L, 100 µg/mL of Penicillin and 10 µg/mL of Streptomycin. The next day different concentrations of compounds were added in media in triplicate. Following 72 hours of incubation, MTT (3-(4,5-Dimethyl-2-thiazolyl)-2,5-diphenyl-2H-tetrazolium bromide) was added to a final concentration of 1 mg/mL for 2 h. At the end of the incubation period, the media were removed by gently inverting the plate. DMSO was added to the wells to solubilize the formazan crystals and absorbance was read at 595 nm in a plate reader. The absorbance of treated vs. untreated cells was compared. % survival vs. concentration of compound was plotted to determine the IC_{50} concentration.

2.2. 5.Spectral Charts

^{1}H NMR Spectrum (400 MHz, $CDCl_3$) of **8b**

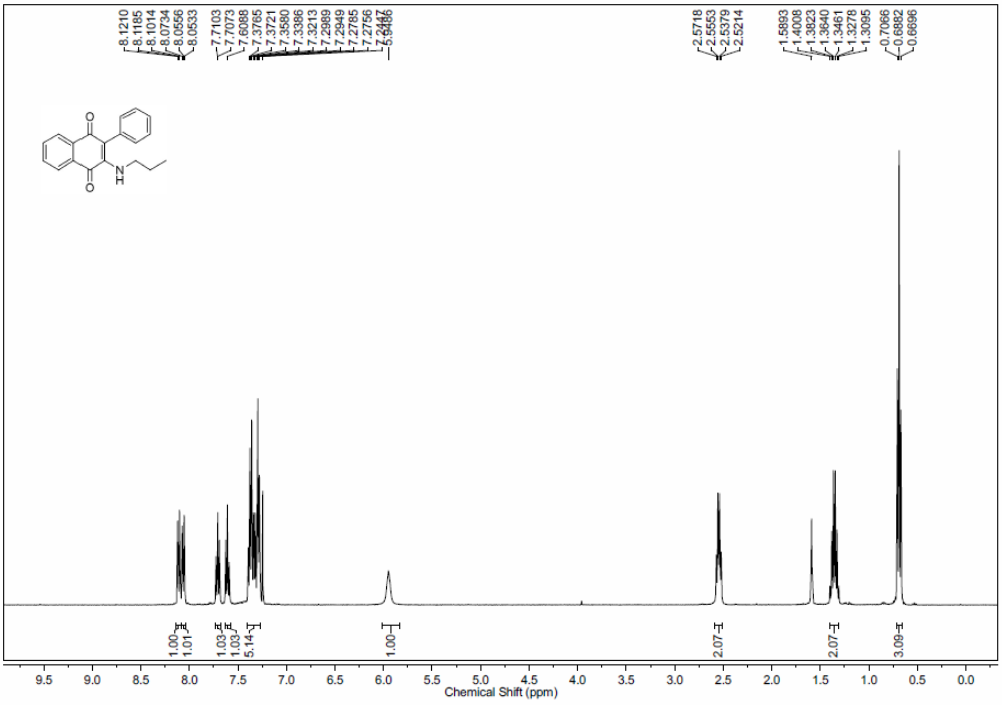

^{13}C NMR Spectrum (100 MHz, $CDCl_3$) of **8b**

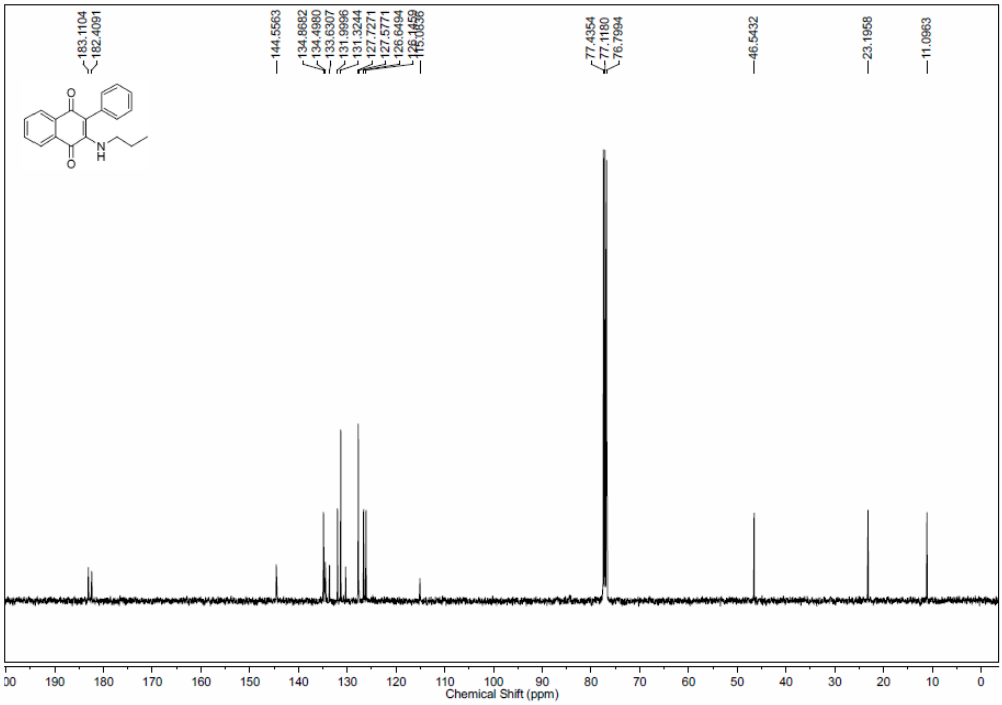

^{1}H NMR Spectrum (400 MHz, $CDCl_3$) of **8c**

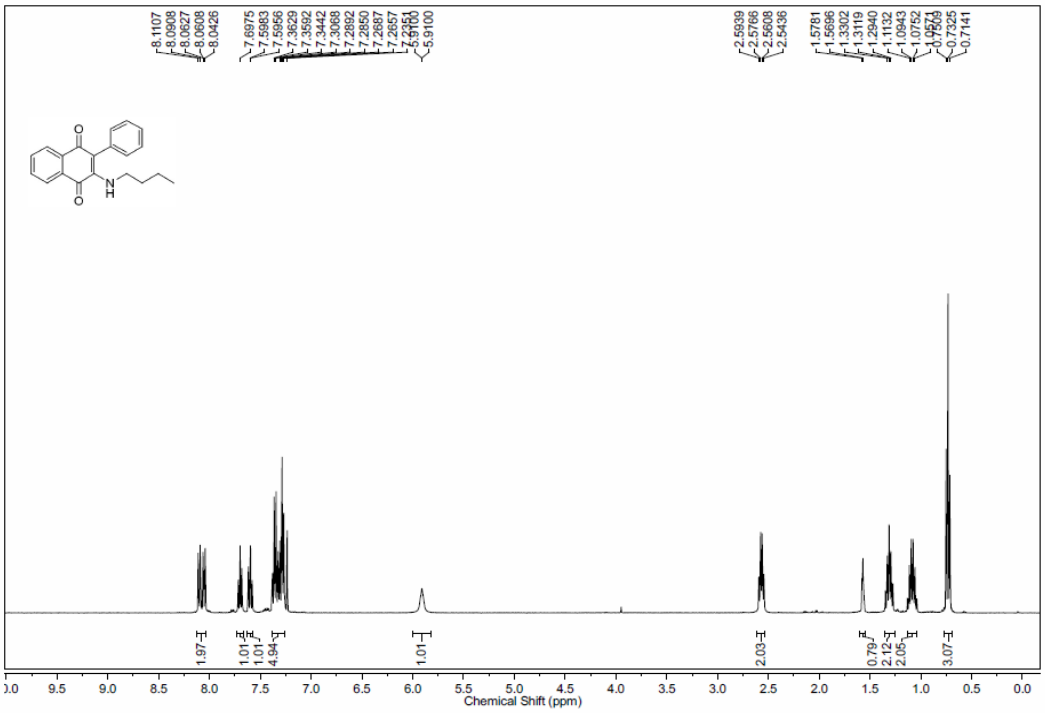

^{13}C NMR Spectrum (100 MHz, $CDCl_3$) of **8c**

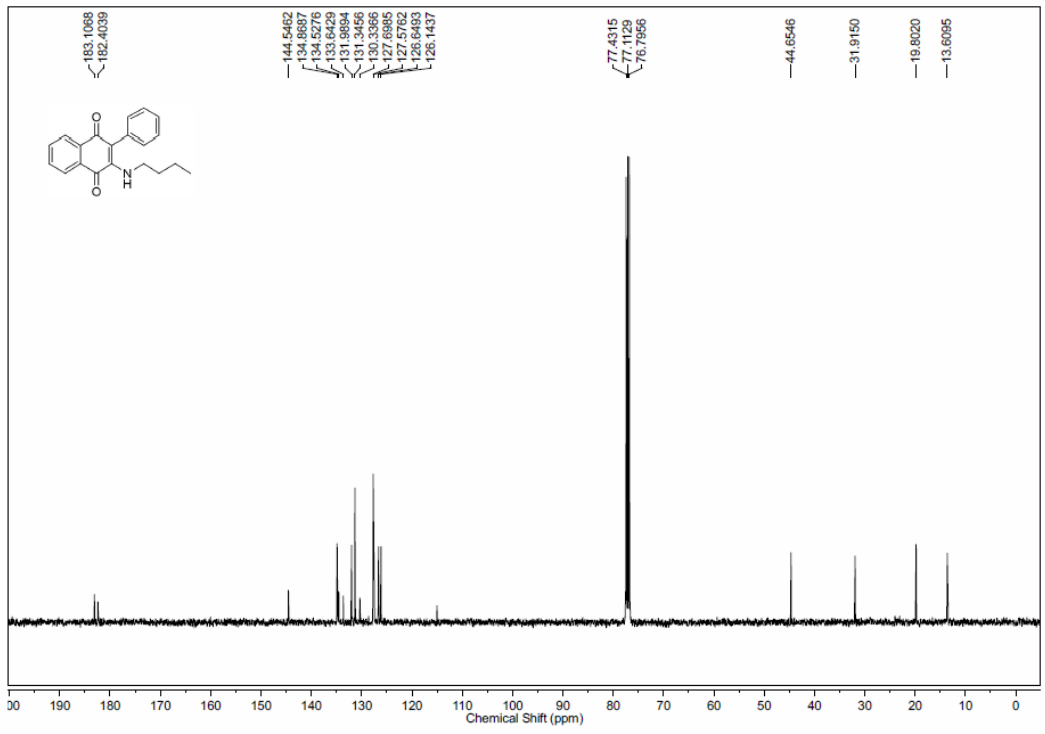

^{1}H NMR Spectrum (400 MHz, $CDCl_3$) of **8d**

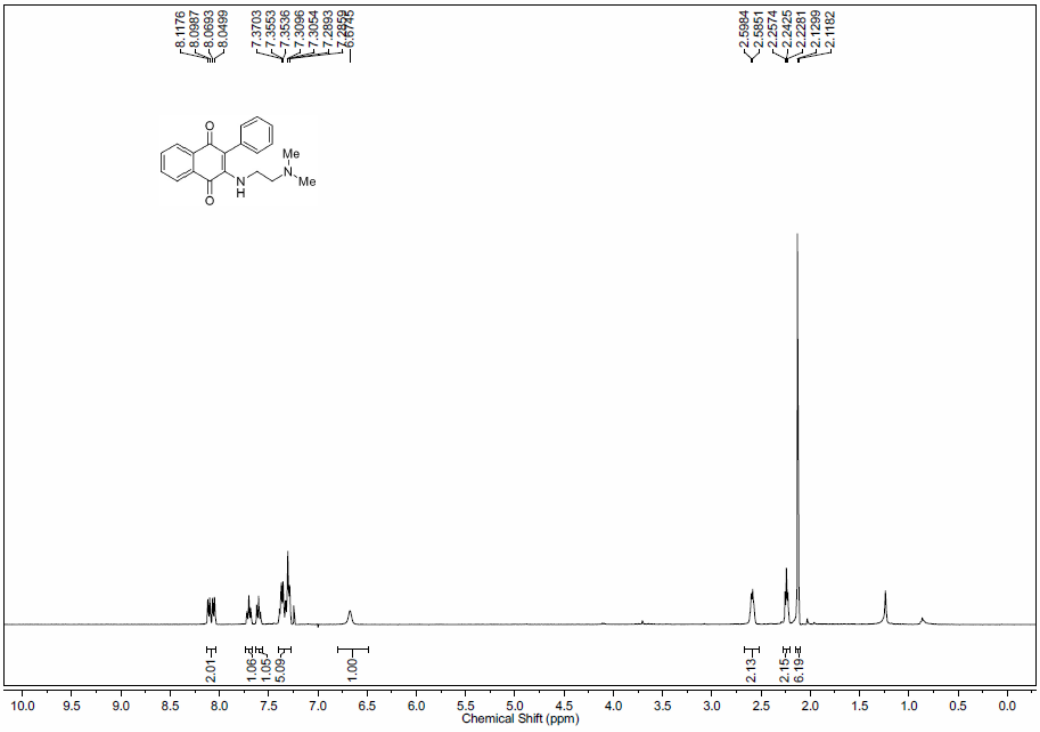

^{13}C NMR Spectrum (100 MHz, $CDCl_3$) of **8d**

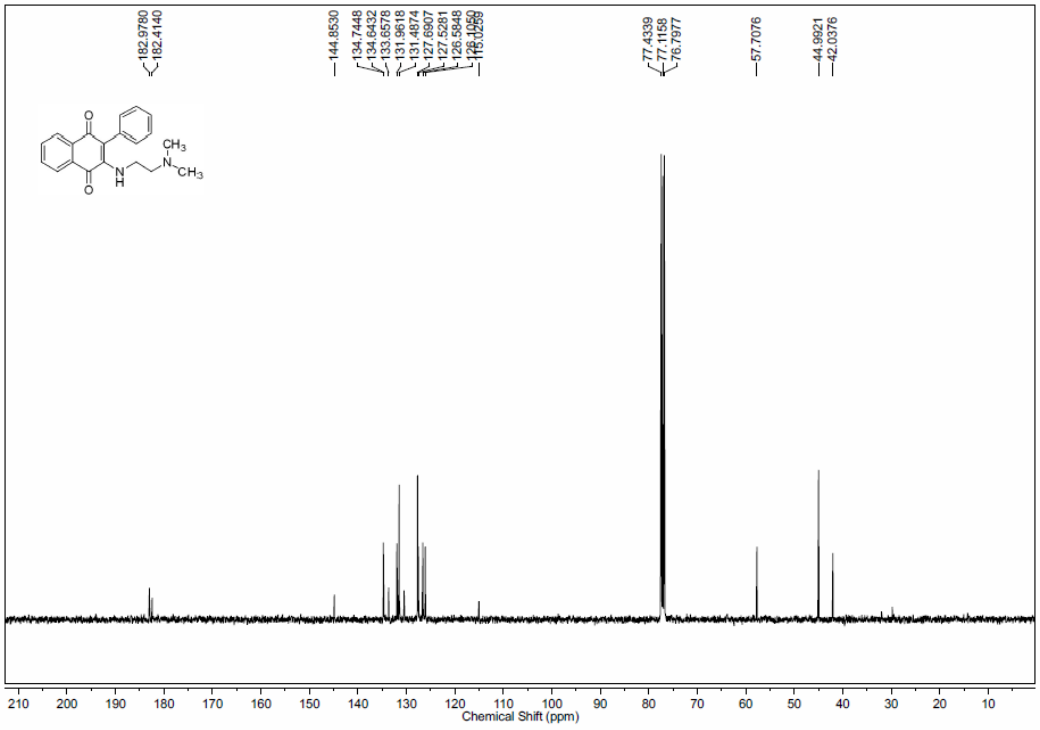

^{1}H NMR Spectrum (400 MHz, $CDCl_3$) of **8e**

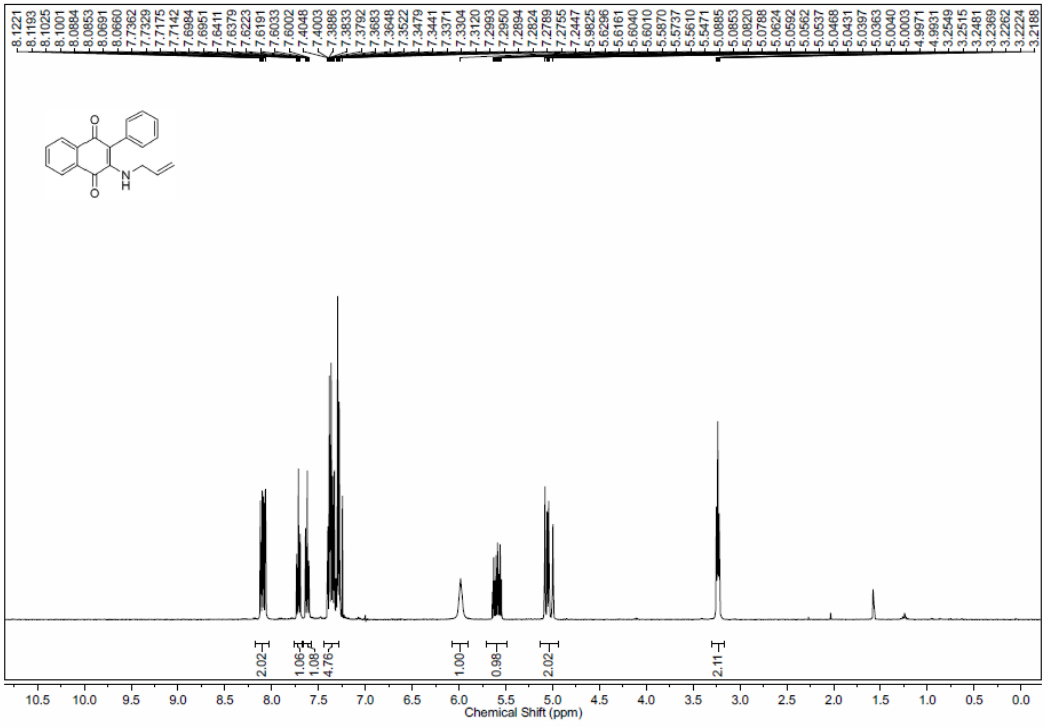

^{13}C NMR Spectrum (100 MHz, $CDCl_3$) of **8e**

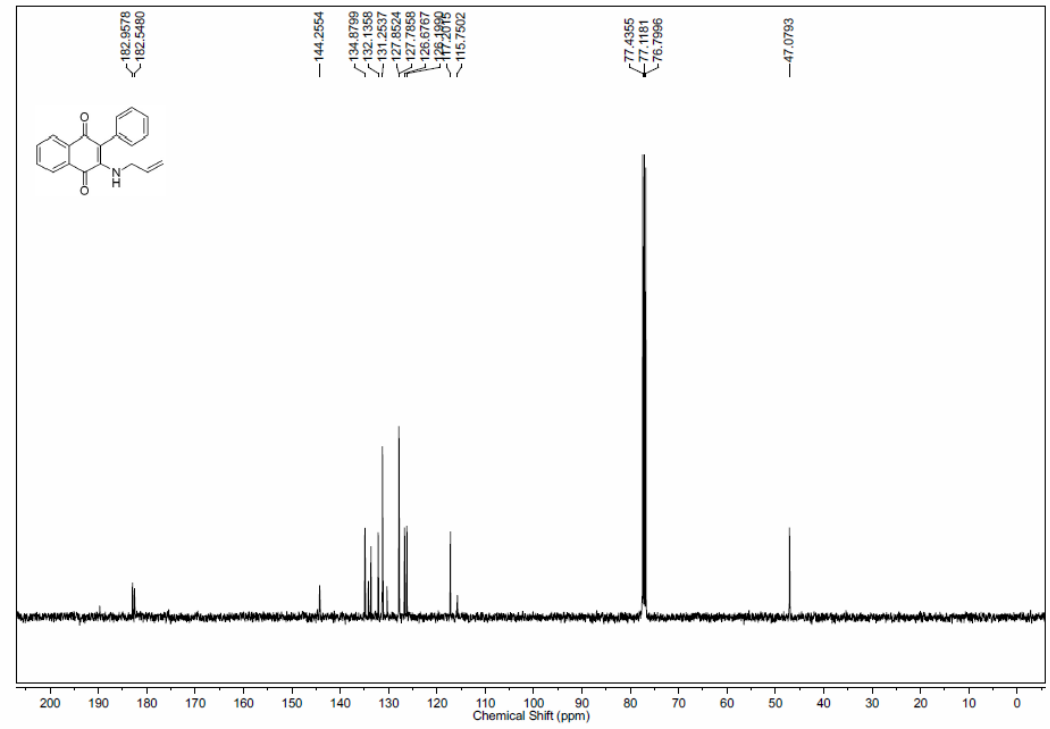

^{1}H NMR Spectrum (400 MHz, $CDCl_3$) of **8f**

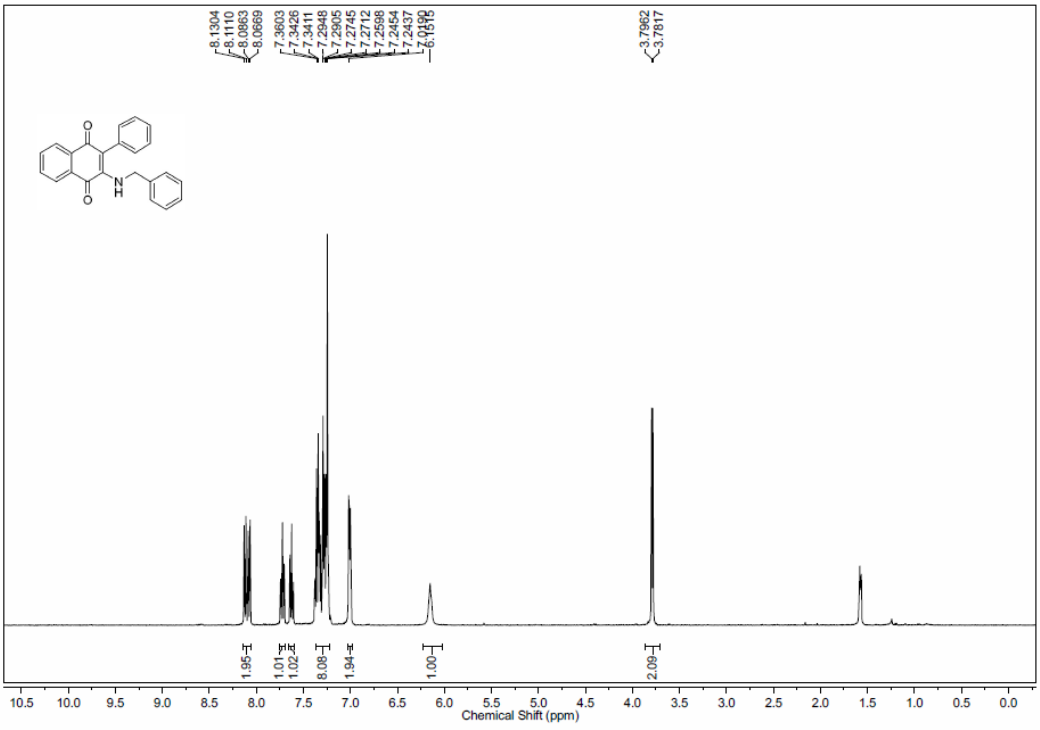

^{13}C NMR Spectrum (100 MHz, $CDCl_3$) of **8f**

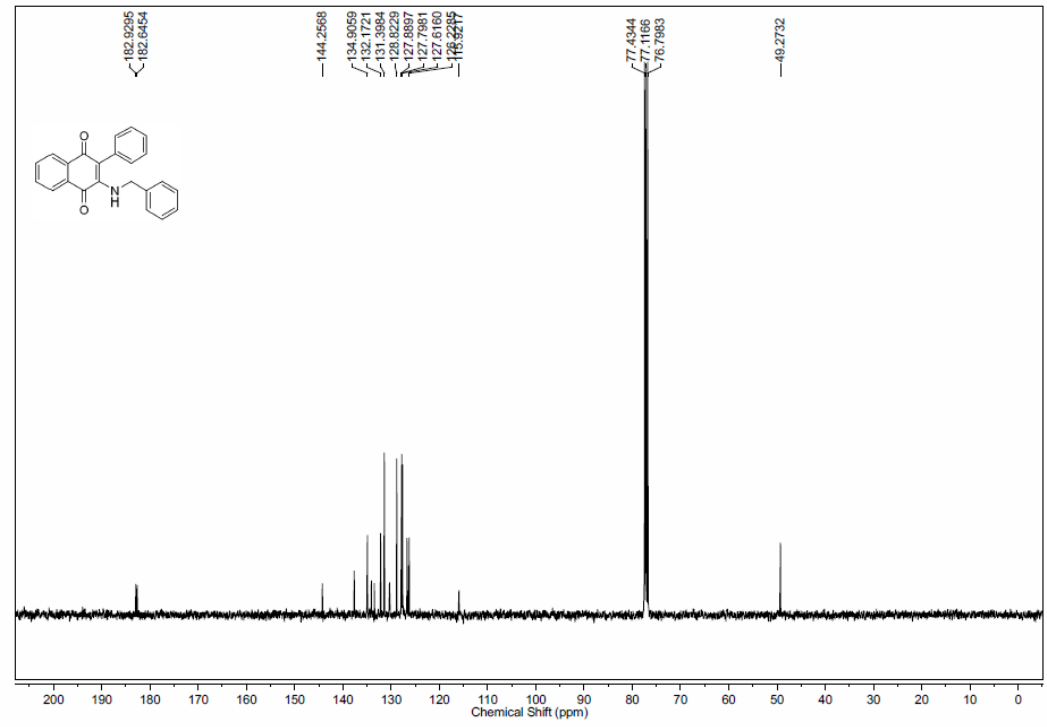

^{1}H NMR Spectrum (400 MHz, $CDCl_3$) of **8g**

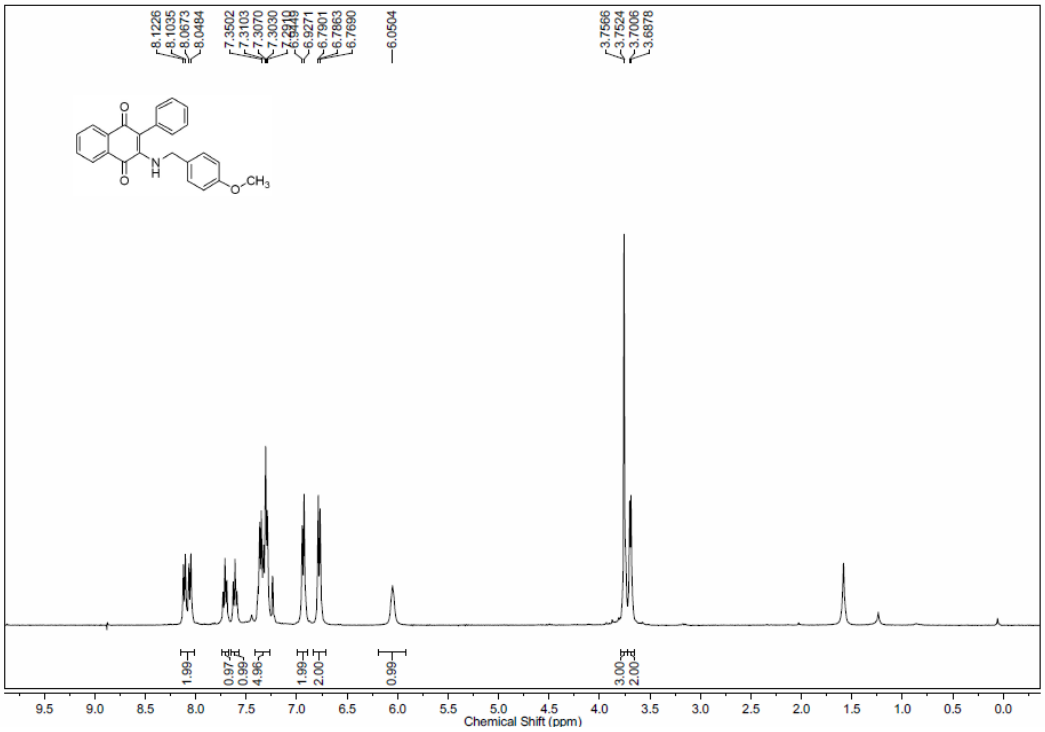

^{13}C NMR Spectrum (100 MHz, $CDCl_3$) of **8g**

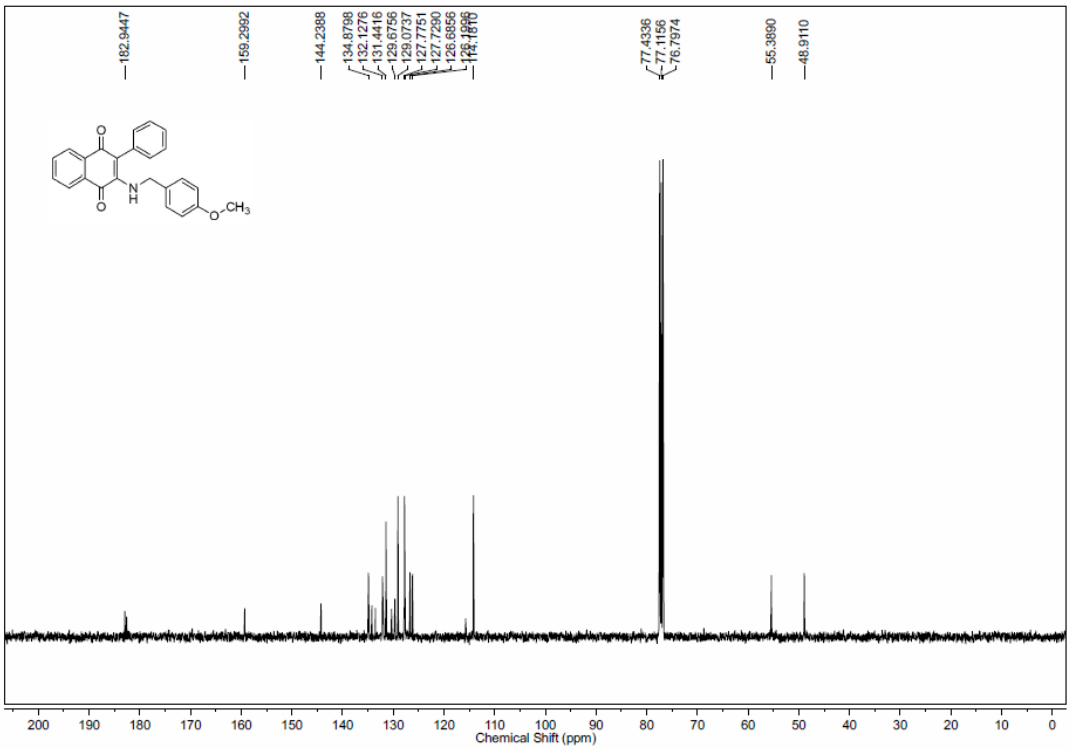

^{1}H NMR Spectrum (400 MHz, $CDCl_3$) of **8h**

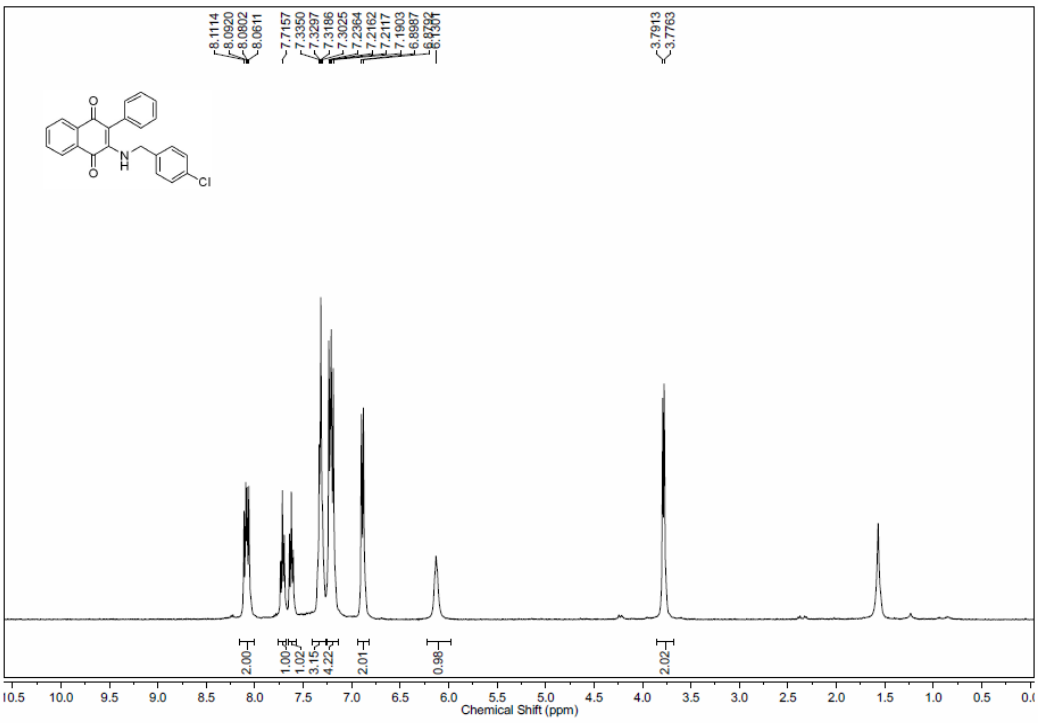

^{13}C NMR Spectrum (100 MHz, $CDCl_3$) of **8h**

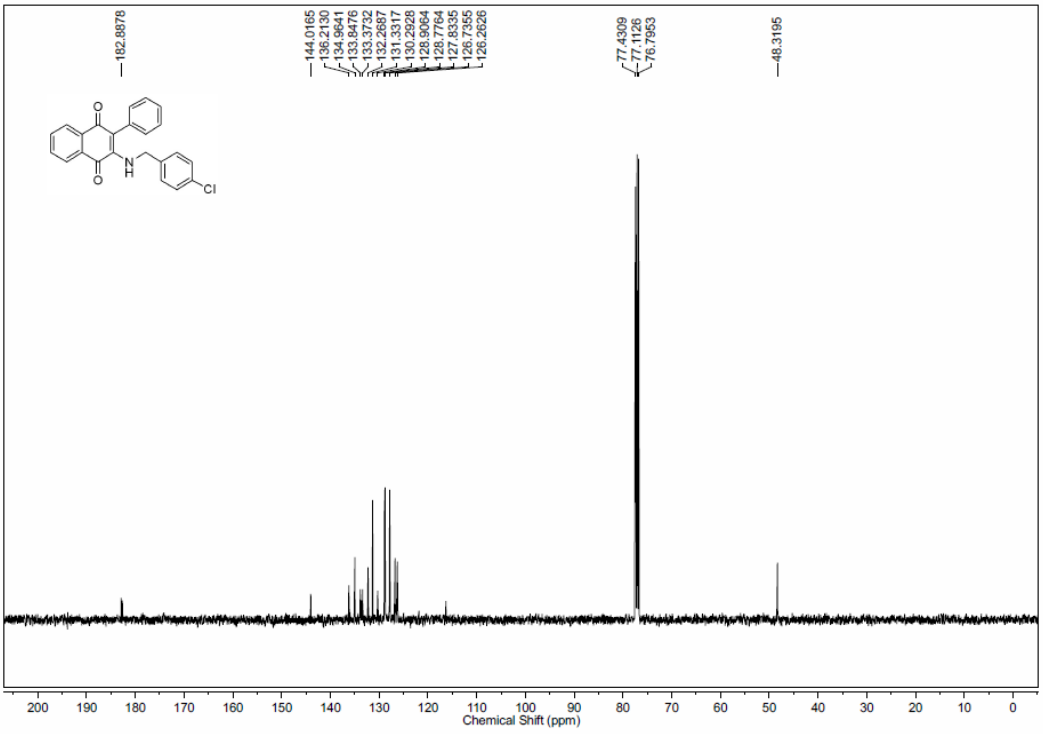

^{1}H NMR Spectrum (400 MHz, $CDCl_3$) of **8j**

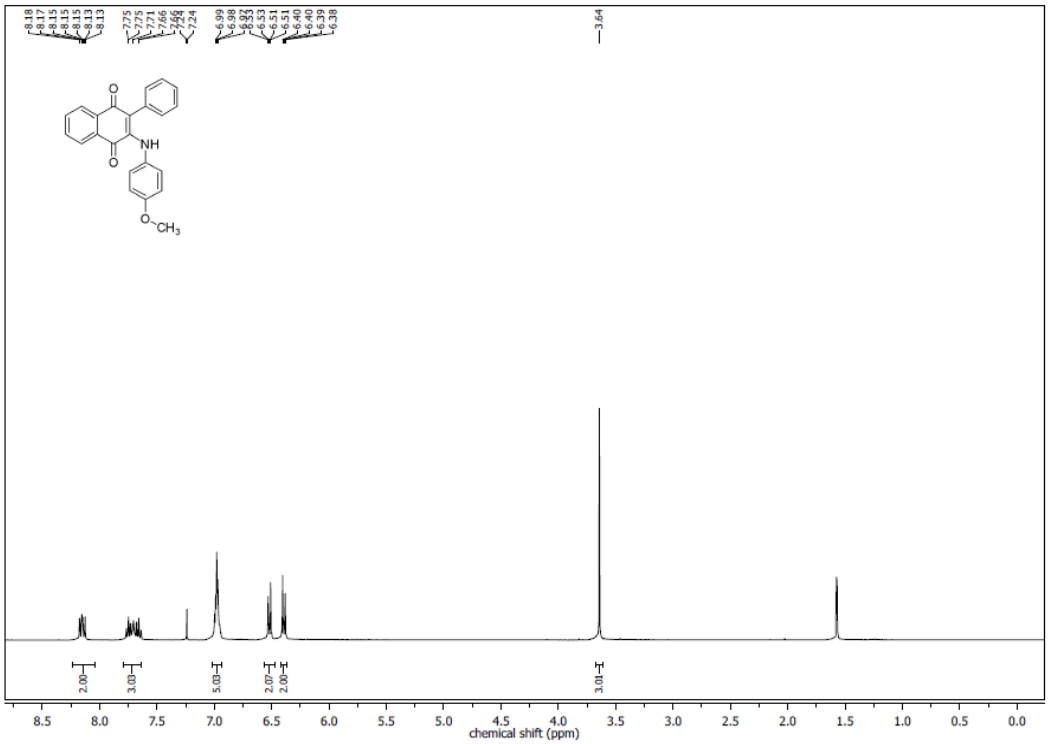

^{13}C NMR Spectrum (100 MHz, $CDCl_3$) of **8j**

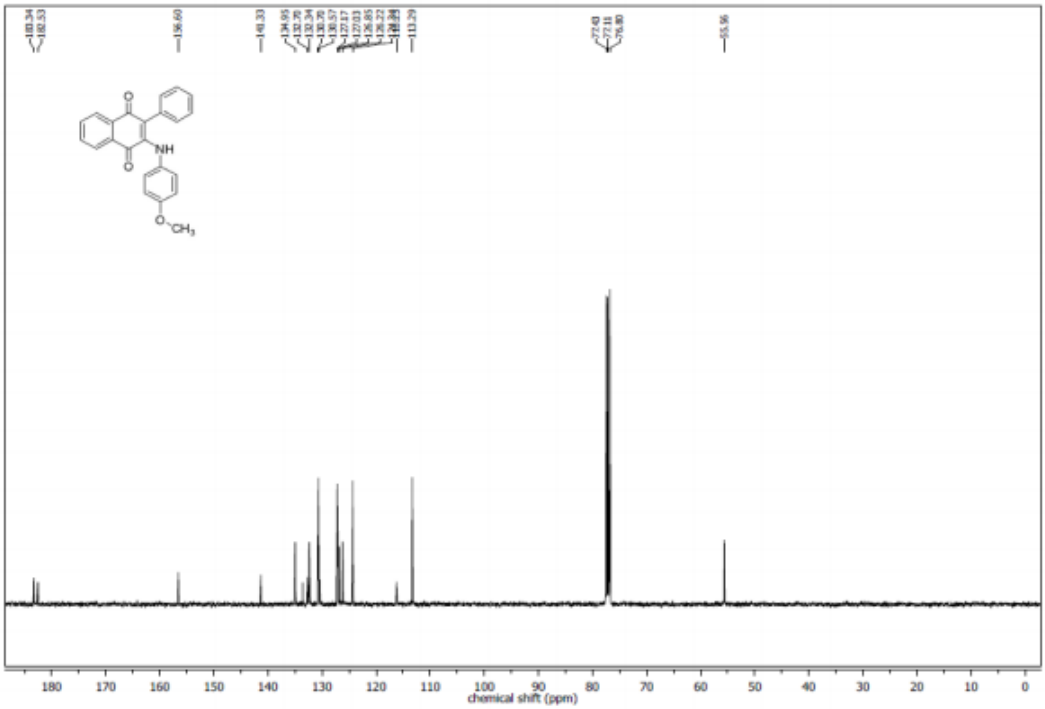

^{1}H NMR Spectrum (400 MHz, $CDCl_3$) of **8k**

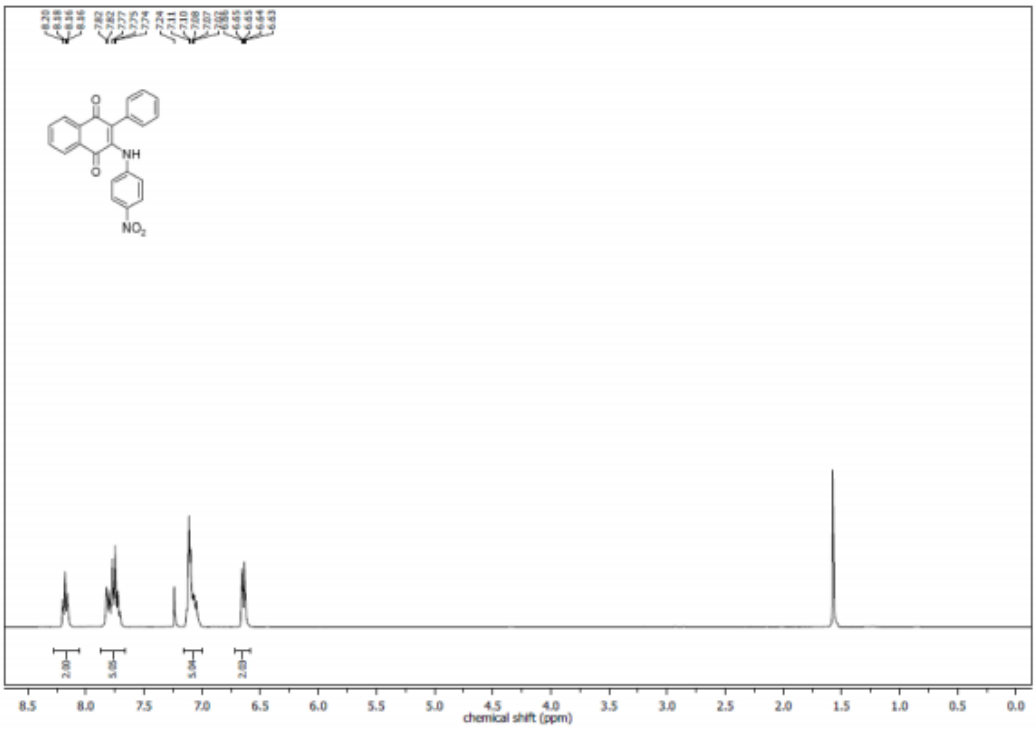

^{13}C NMR Spectrum (100 MHz, $CDCl_3$) of **8k**

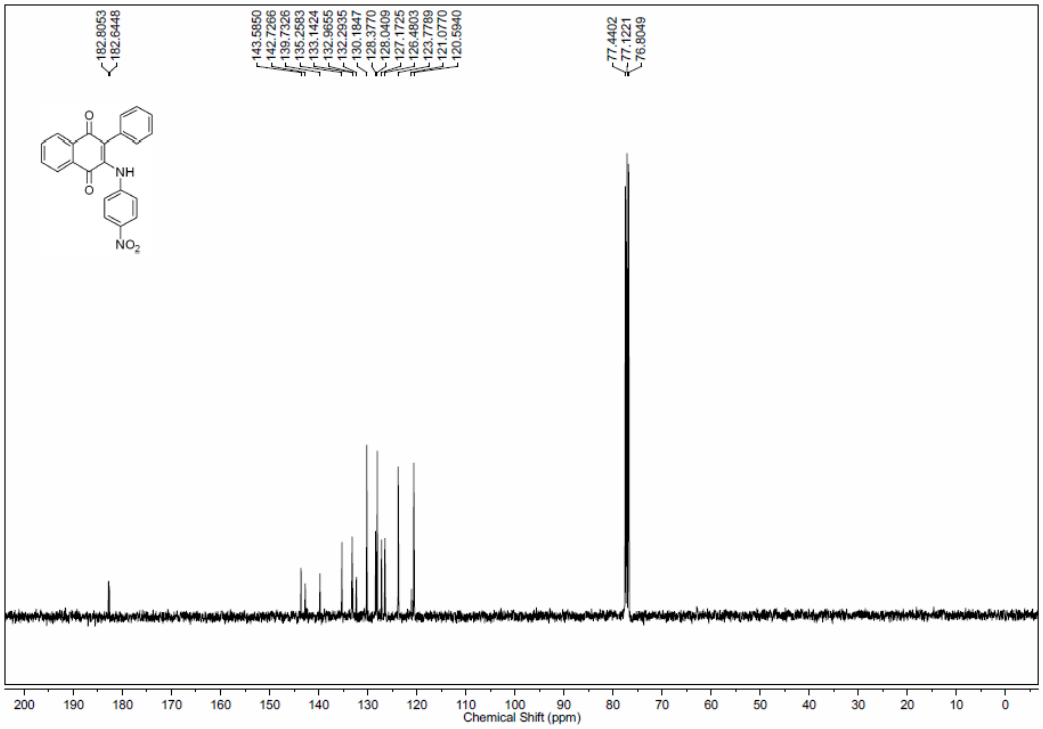

^{1}H NMR Spectrum (400 MHz, $CDCl_3$) of **8l**

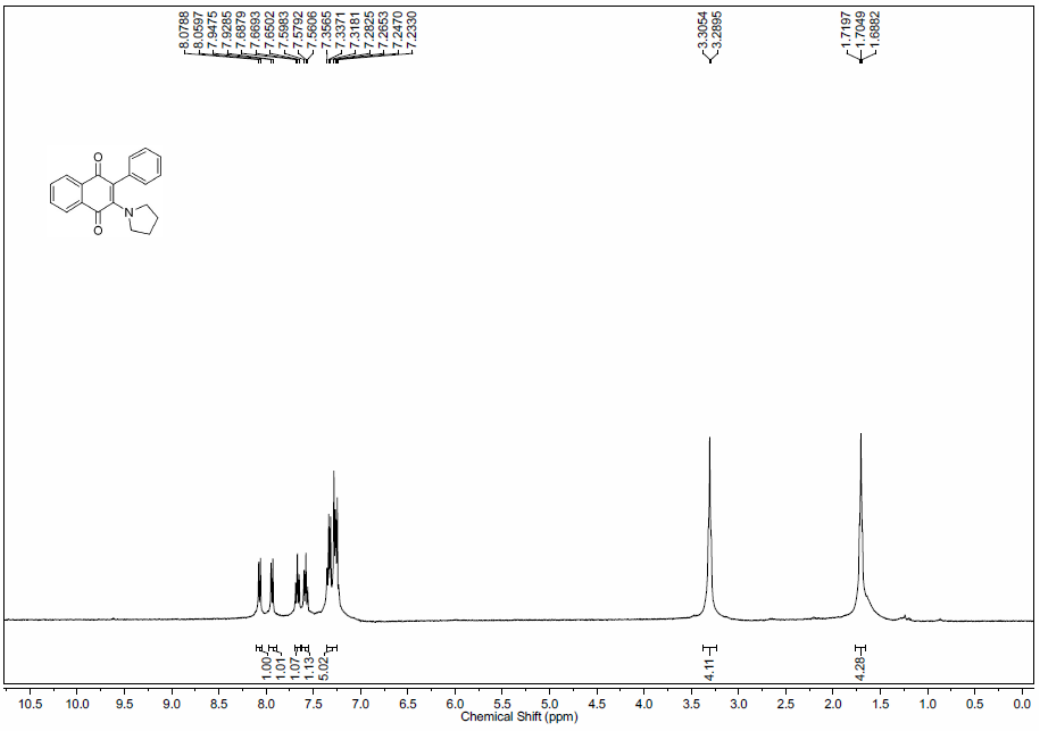

^{13}C NMR Spectrum (100 MHz, $CDCl_3$) of **8l**

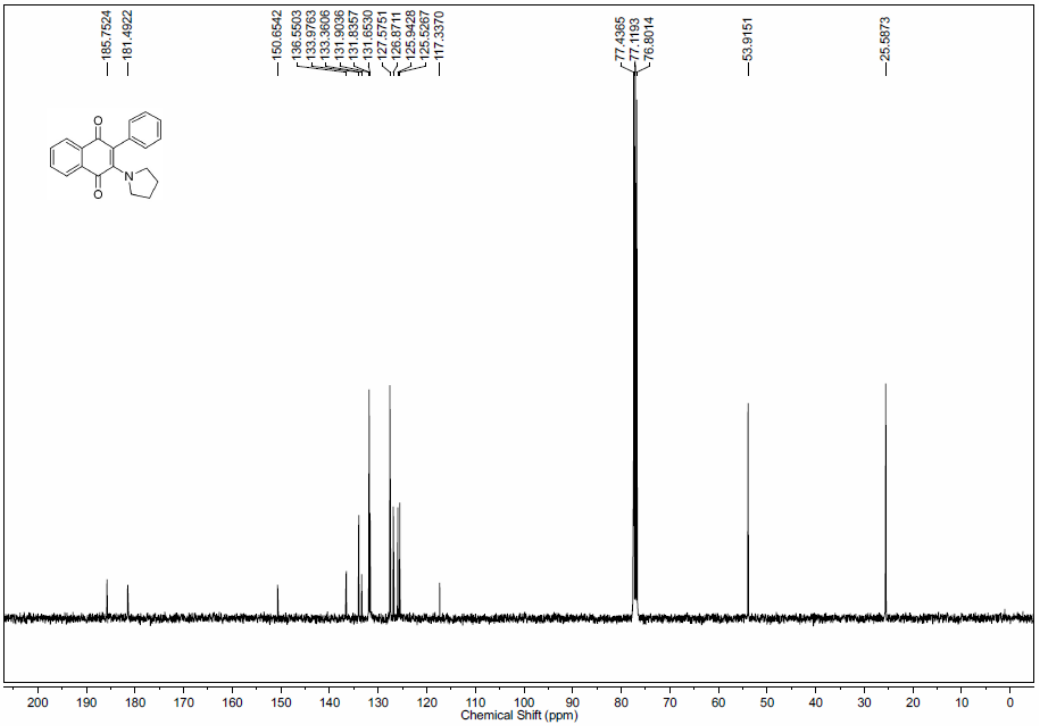

^{1}H NMR Spectrum (400 MHz, $CDCl_3$) of **8m**

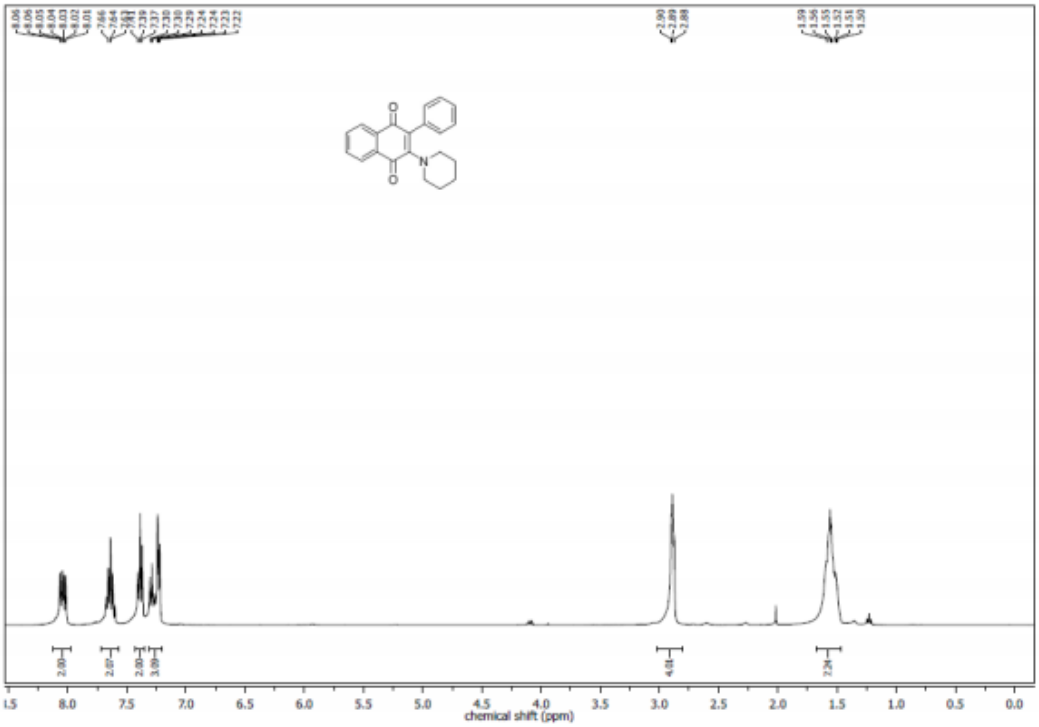

^{13}C NMR Spectrum (100 MHz, $CDCl_3$) of **8m**

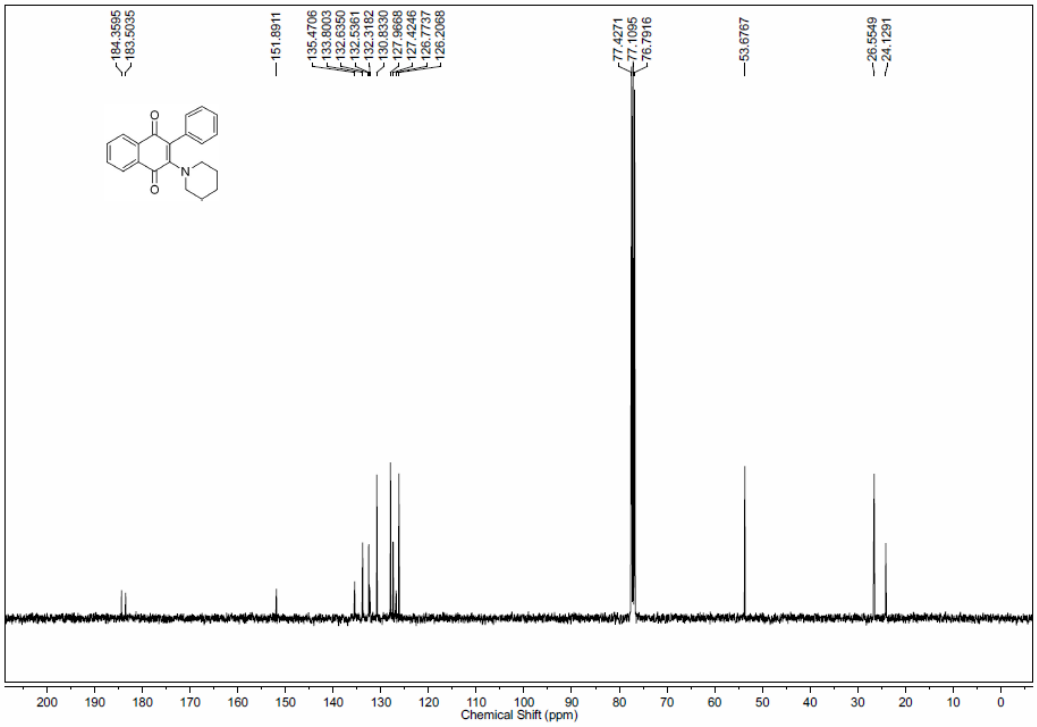

^{1}H NMR Spectrum (400 MHz, $CDCl_3$) of **11c**

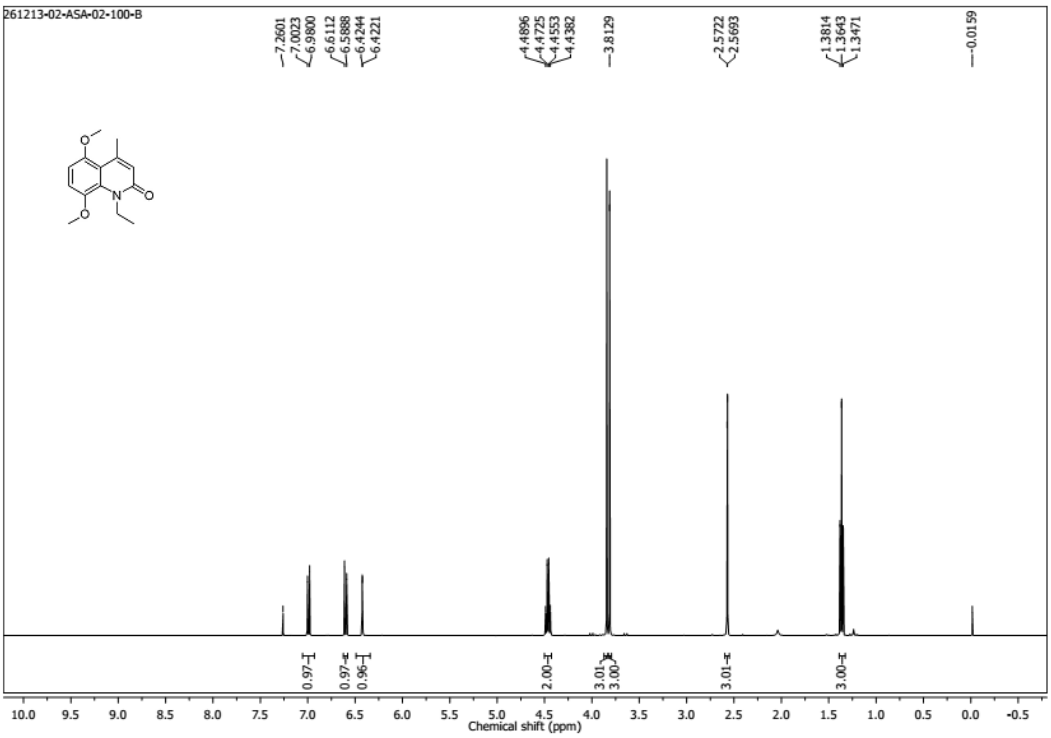

^{13}C NMR Spectrum (100 MHz, $CDCl_3$) of **11c**

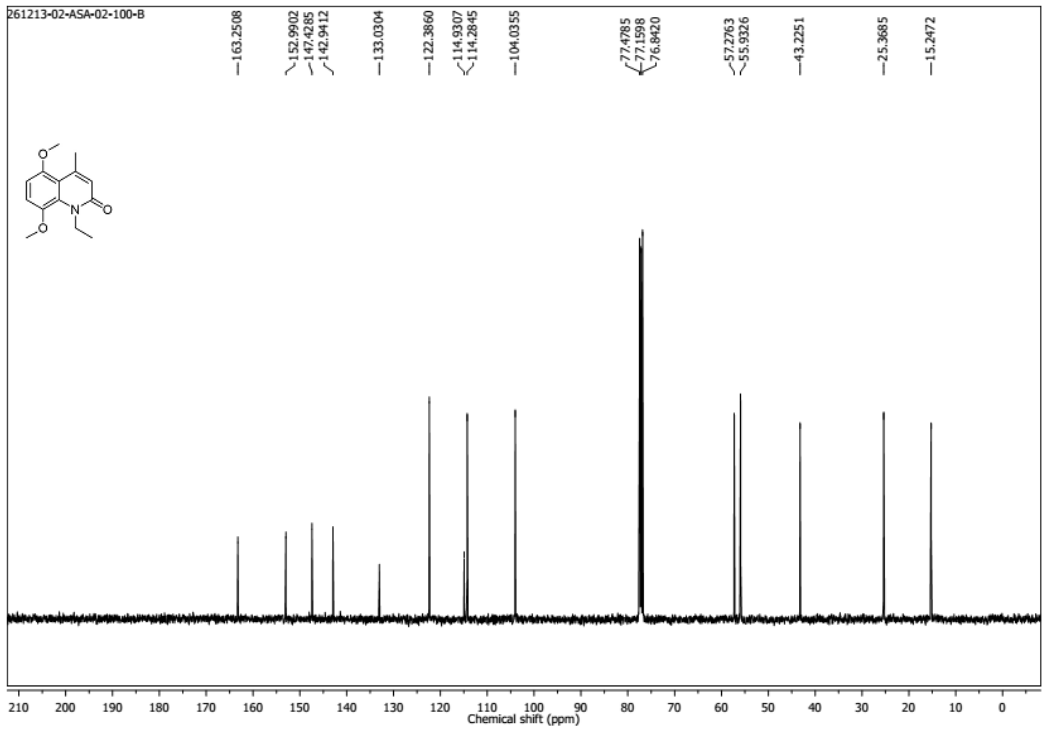

^{1}H NMR Spectrum (400 MHz, $CDCl_3$) of **12c**

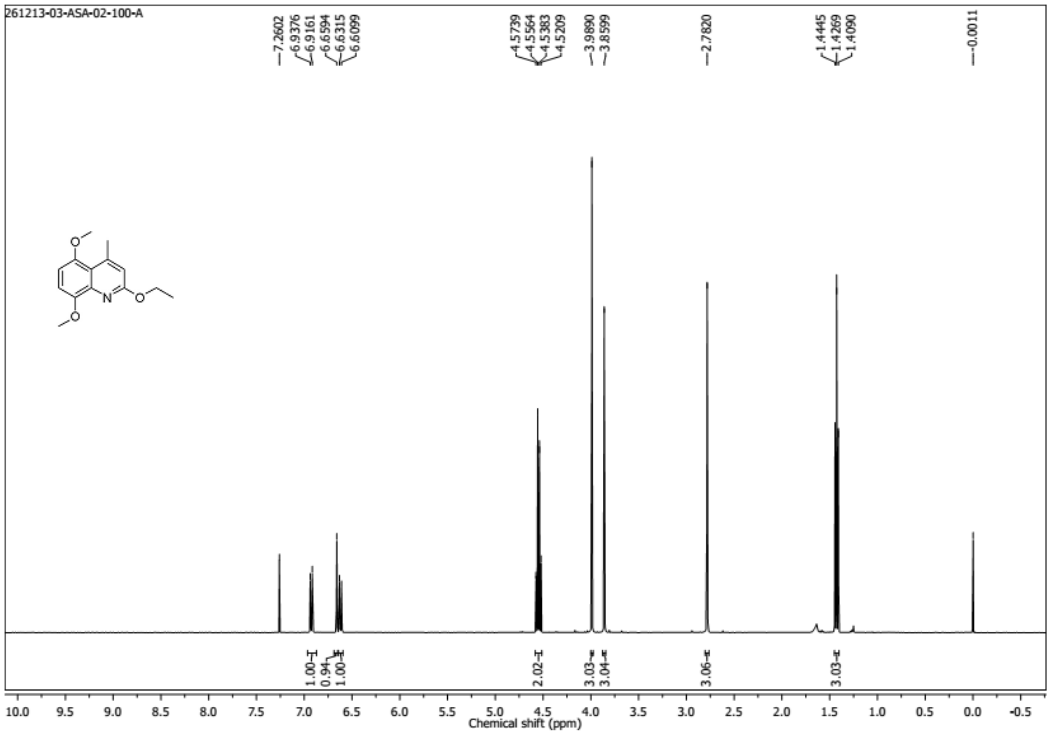

^{13}C NMR Spectrum (100 MHz, $CDCl_3$) of **12c**

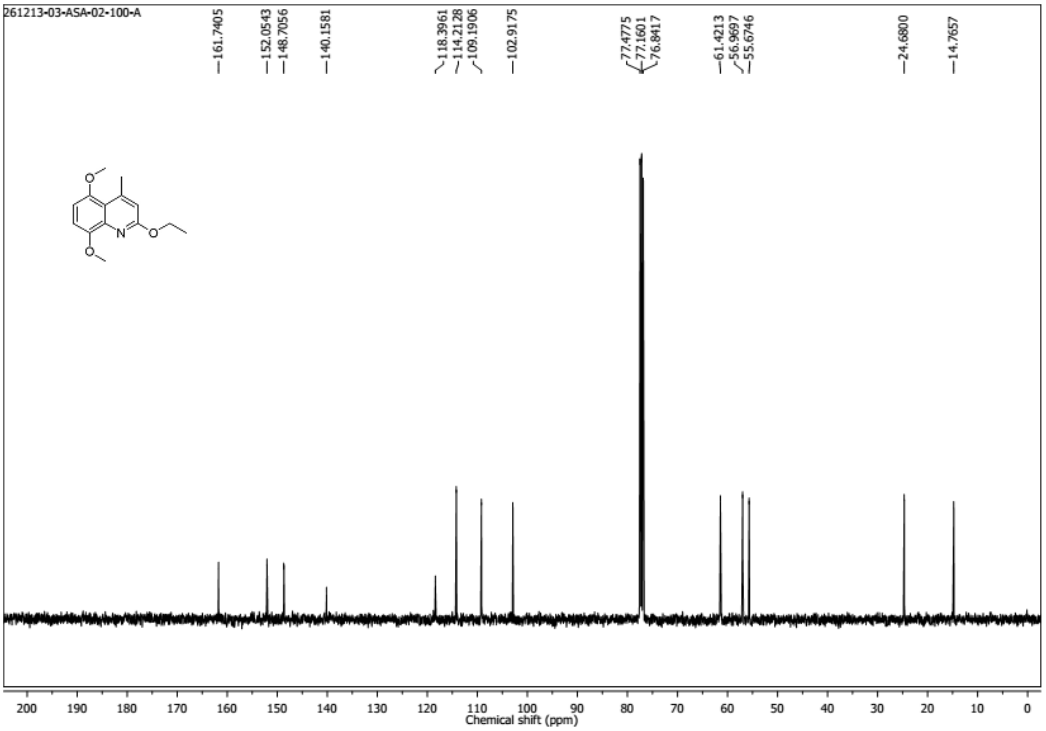

^{1}H NMR Spectrum (400 MHz, $CDCl_3$) of **11d**

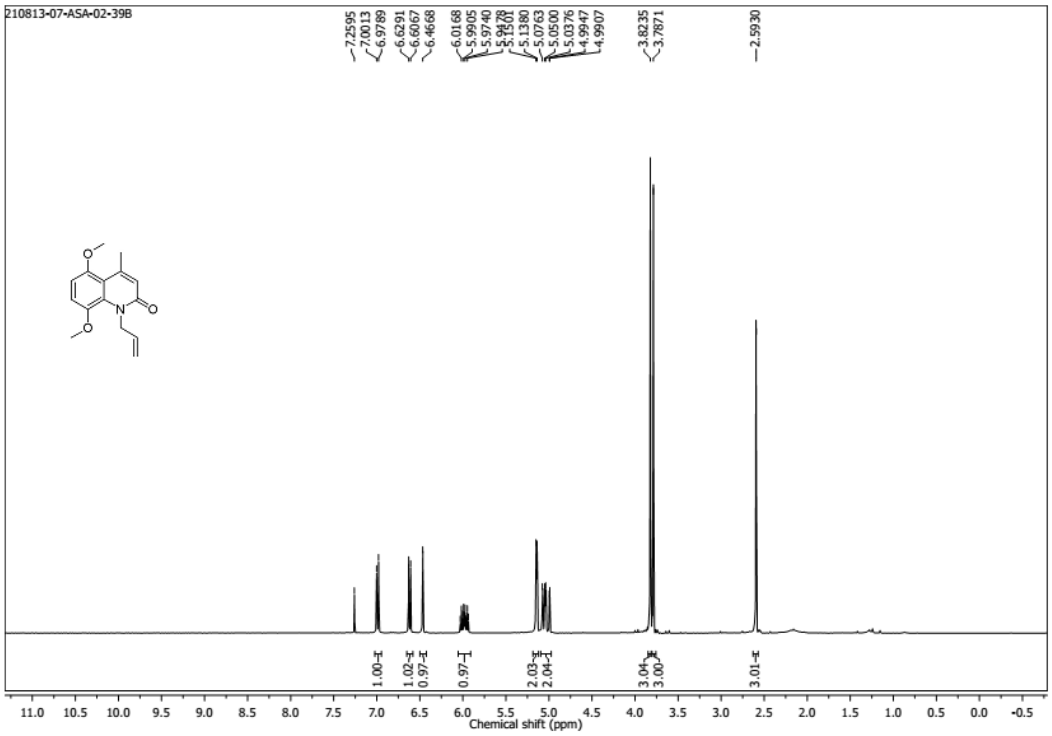

^{13}C NMR Spectrum (100 MHz, $CDCl_3$) of **11d**

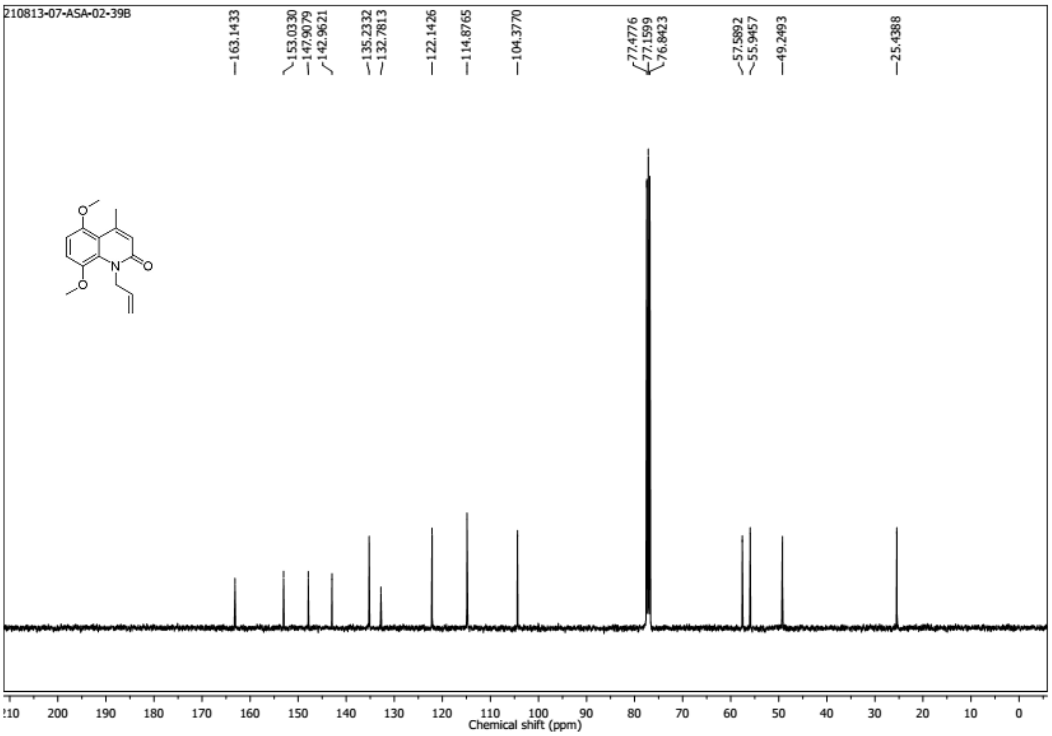

^{1}H NMR Spectrum (400 MHz, $CDCl_3$) of **12d**

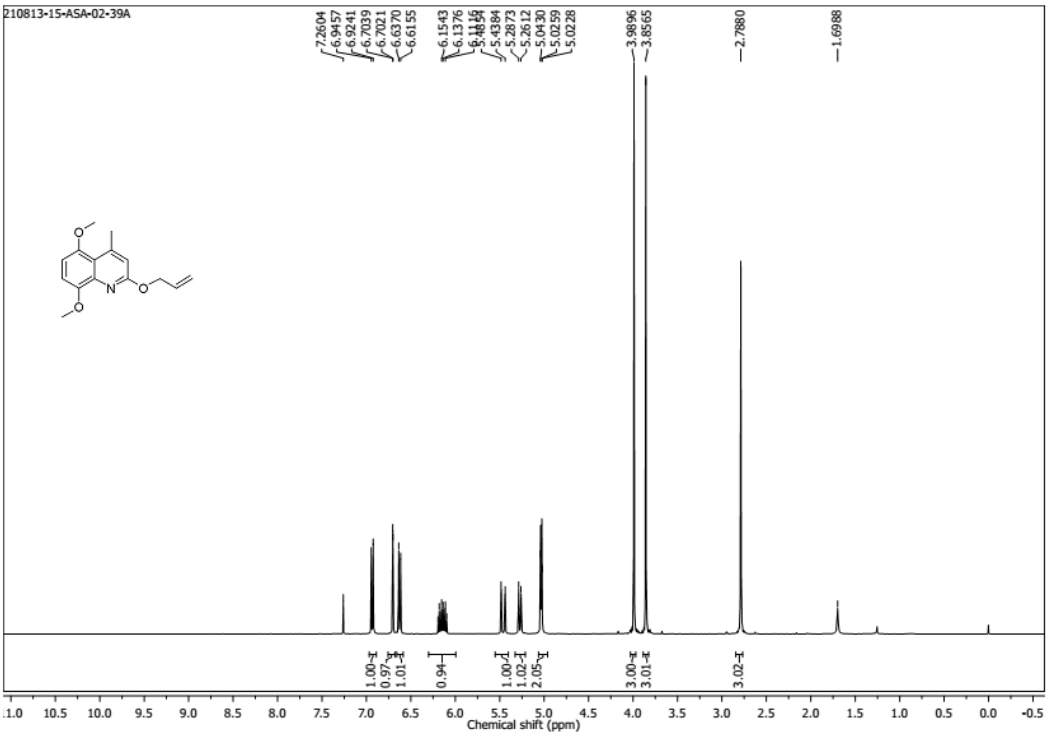

^{13}C NMR Spectrum (100 MHz, $CDCl_3$) of **12d**

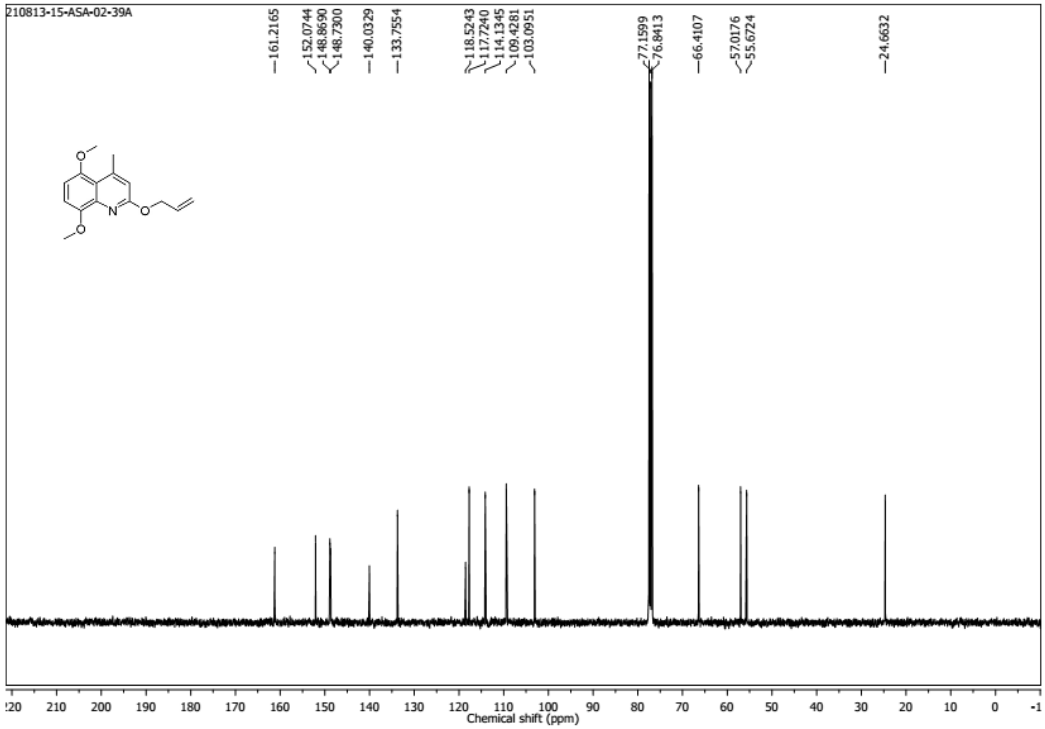

^{1}H NMR Spectrum (400 MHz, $CDCl_3$) of **11e**

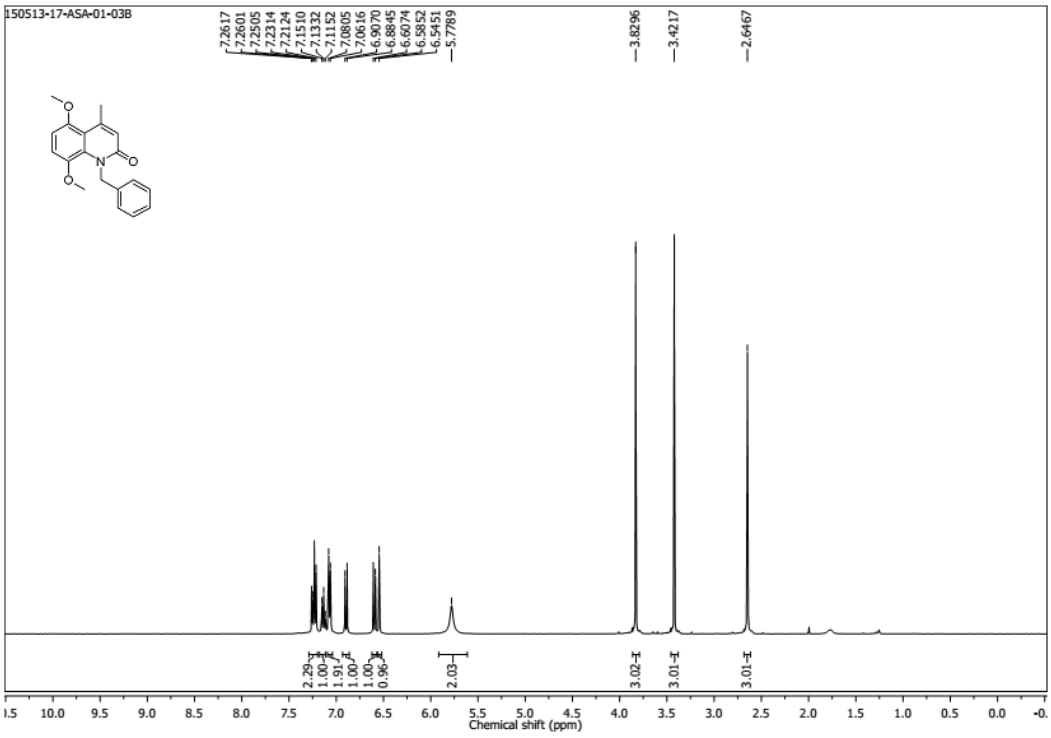

^{13}C NMR Spectrum (100 MHz, $CDCl_3$) of **11e**

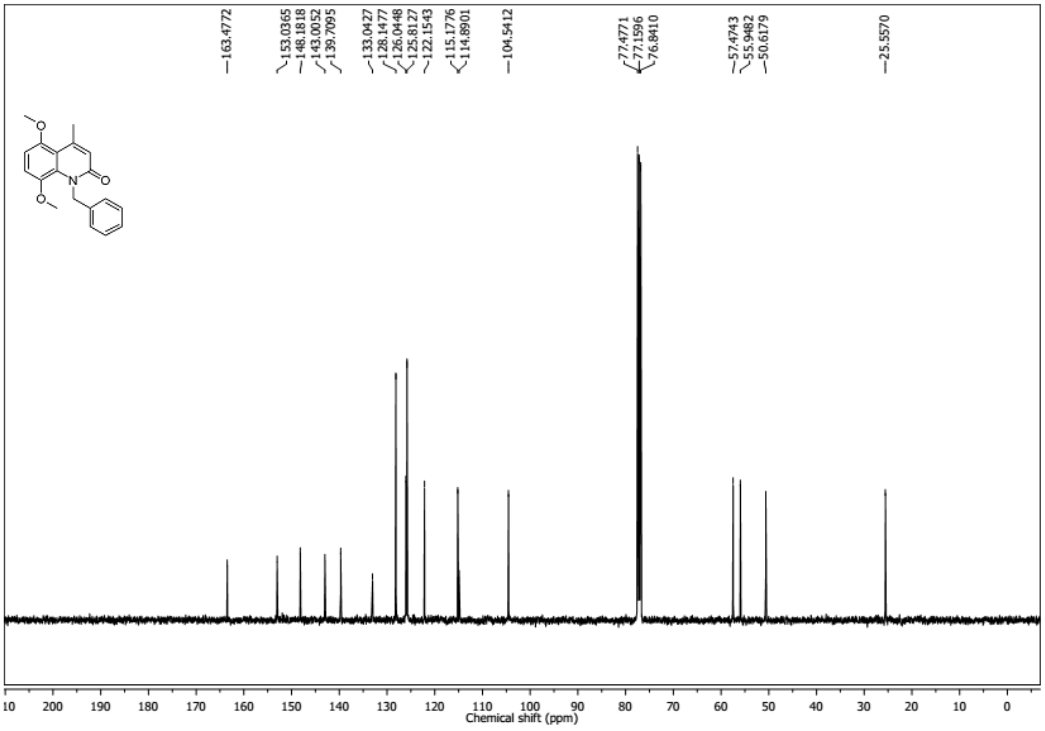

^{1}H NMR Spectrum (400 MHz, $CDCl_3$) of **12e**

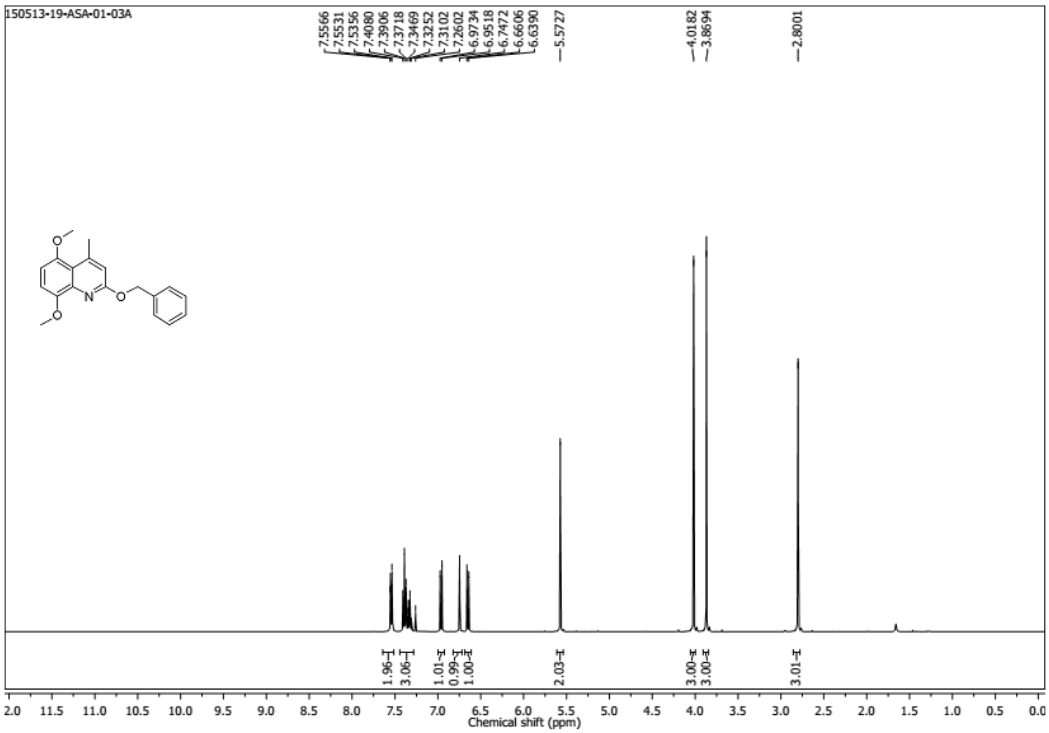

^{13}C NMR Spectrum (100 MHz, $CDCl_3$) of **12e**

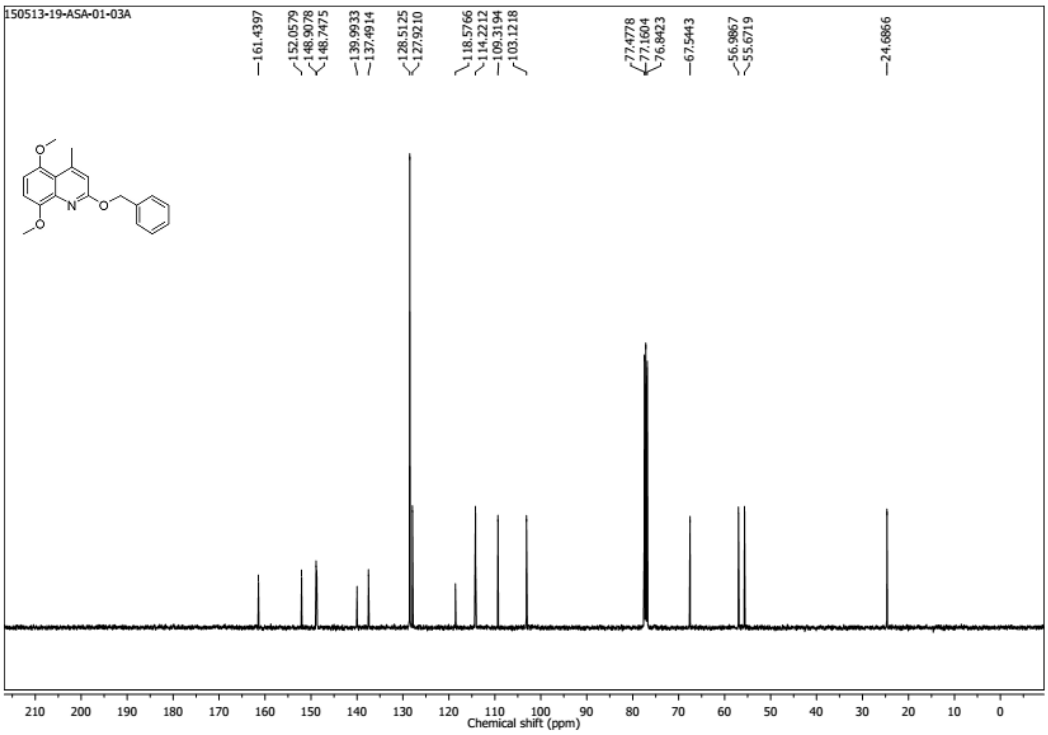

^{1}H NMR Spectrum (400 MHz, $CDCl_3$) of **13a**

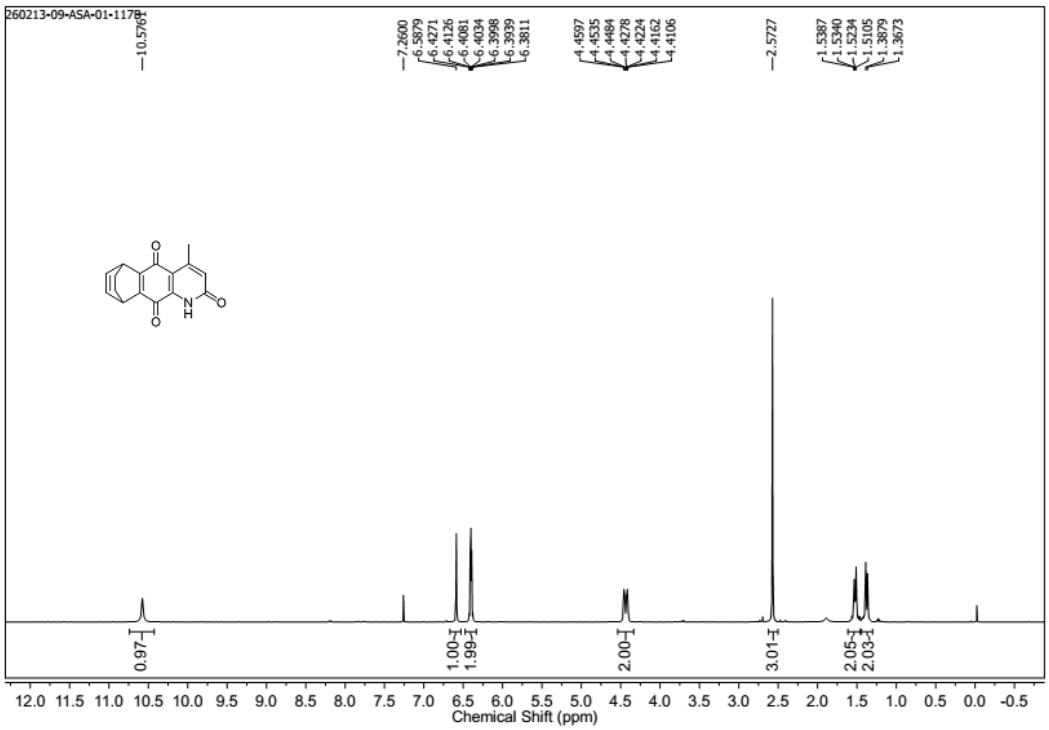

^{13}C NMR Spectrum (100 MHz, $CDCl_3$) of **13a**

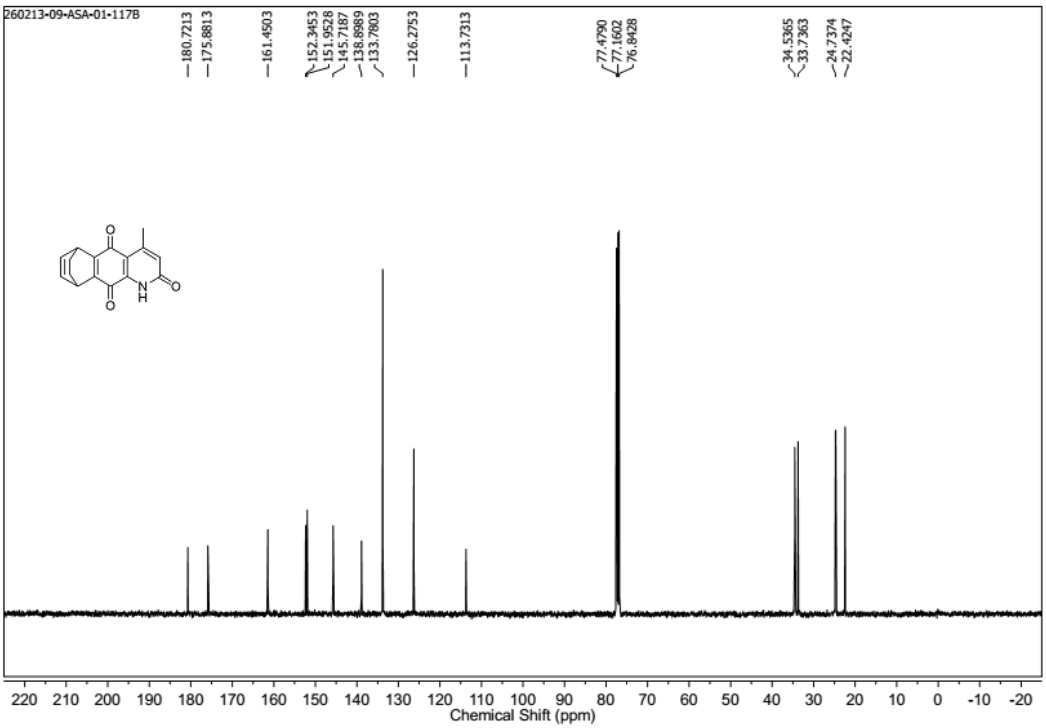

^{1}H NMR Spectrum (400 MHz, $CDCl_3$) of **13b**

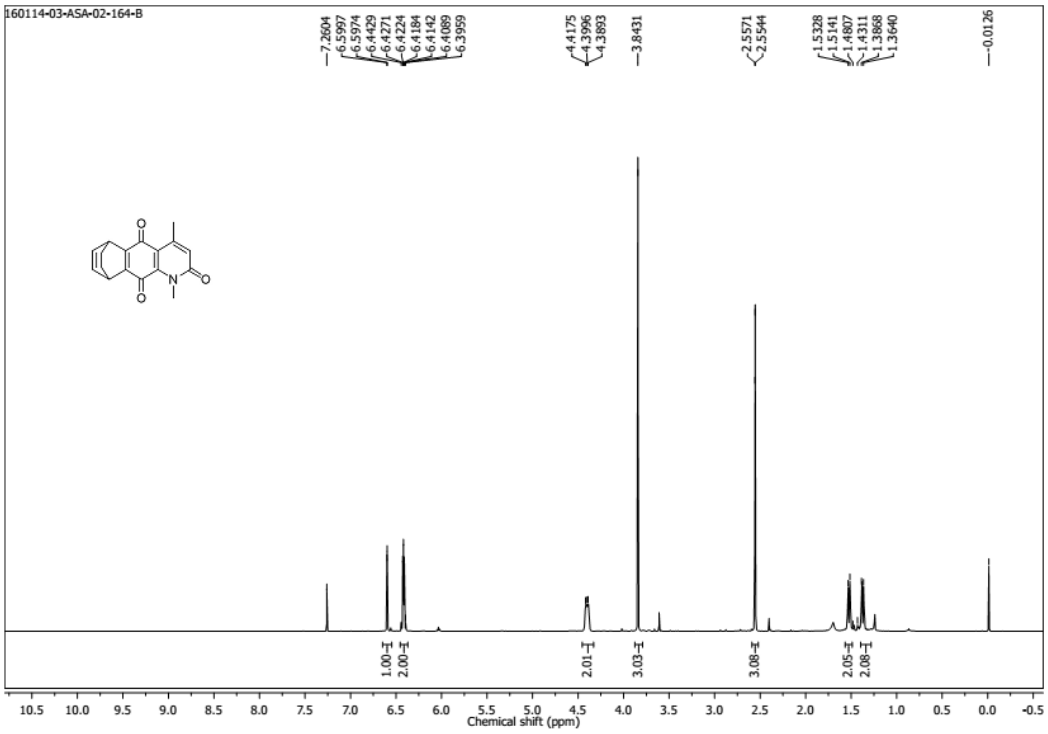

^{13}C NMR Spectrum (100 MHz, $CDCl_3$) of **13b**

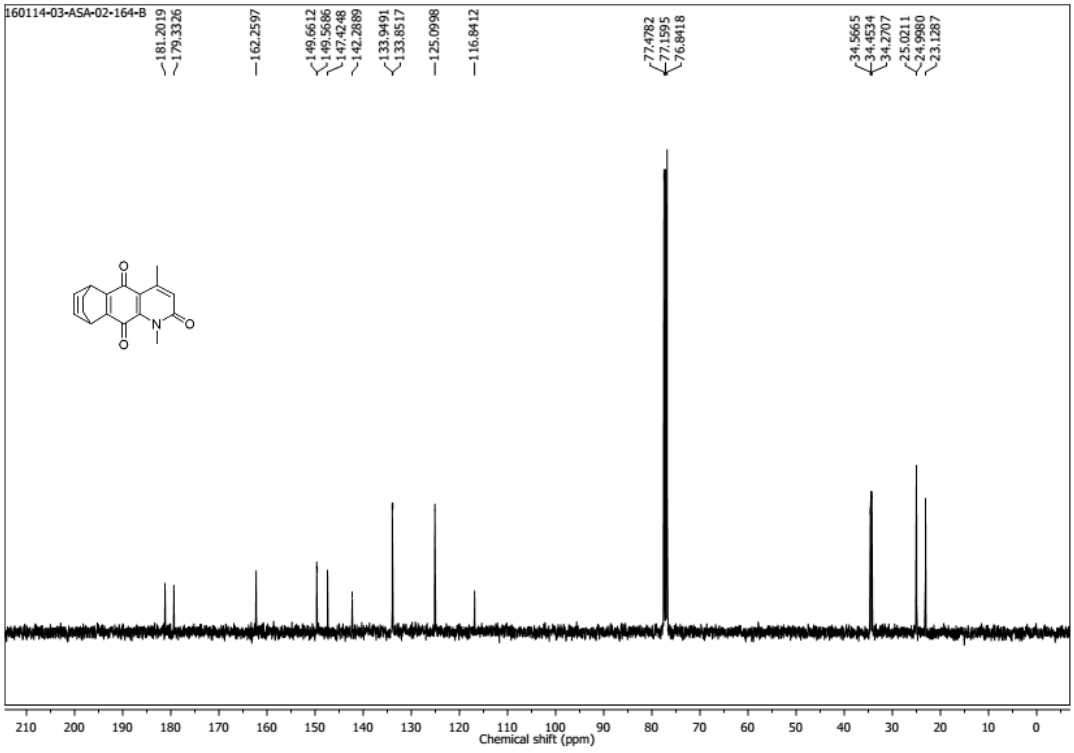

^{1}H NMR Spectrum (400 MHz, $CDCl_3$) of **13e**

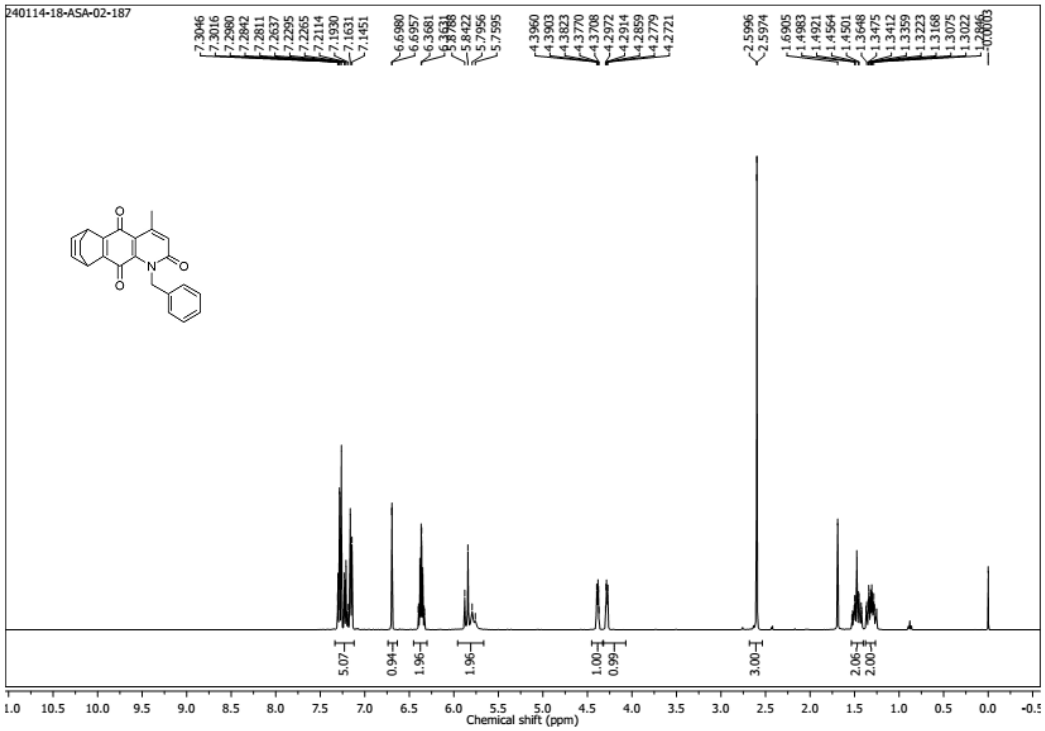

^{13}C NMR Spectrum (100 MHz, $CDCl_3$) of **13e**

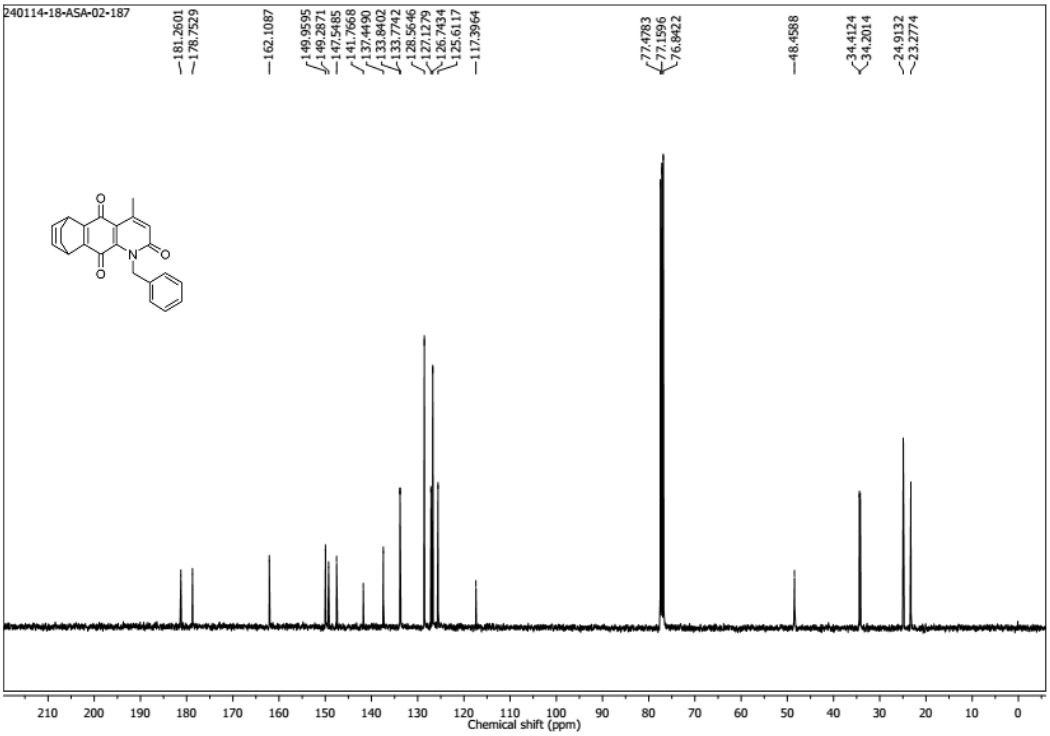

^{1}H NMR Spectrum (400 MHz, $CDCl_3$) of **14b**

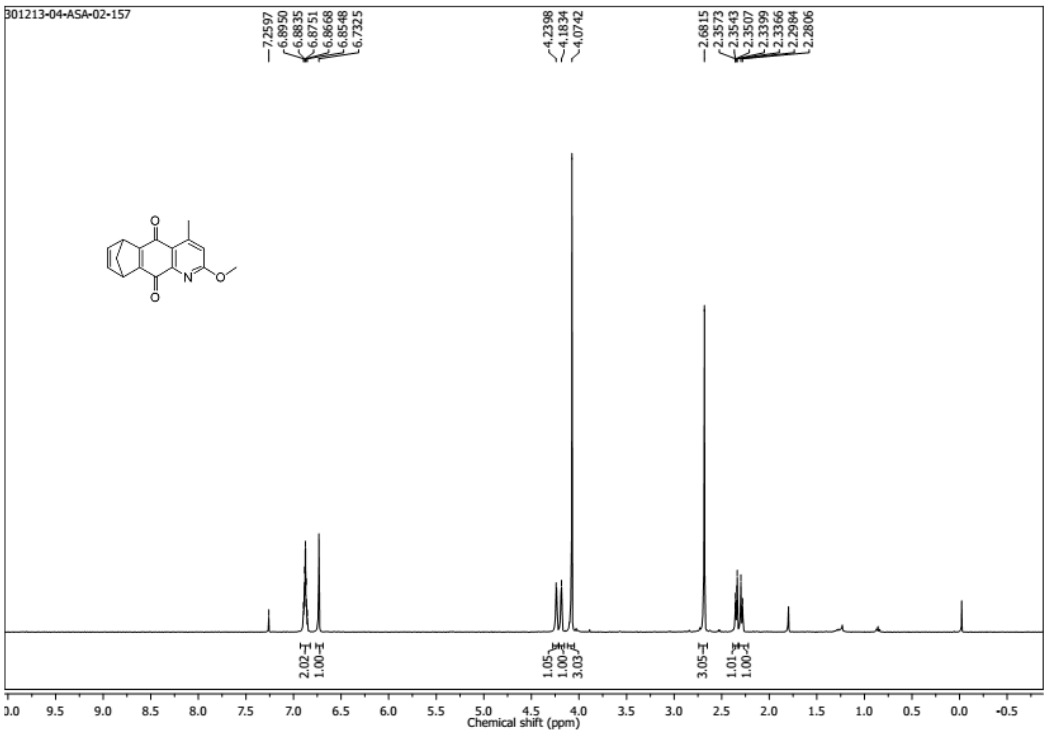

^{13}C NMR Spectrum (100 MHz, $CDCl_3$) of **14b**

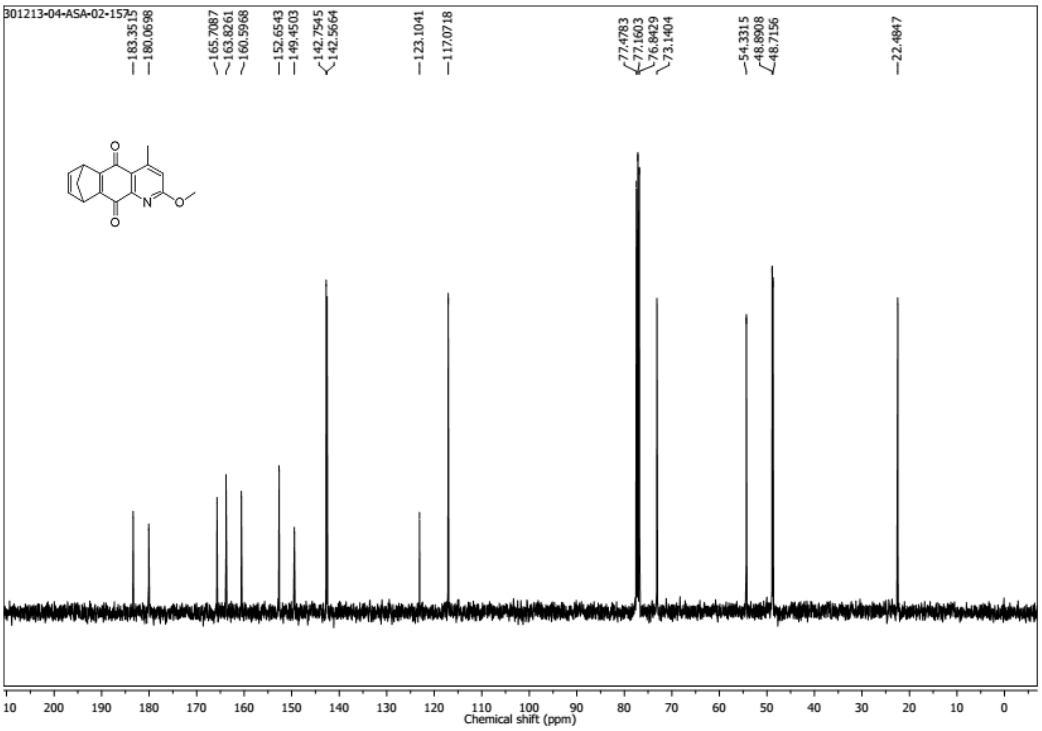

^{1}H NMR Spectrum (400 MHz, $CDCl_3$) of **14c**

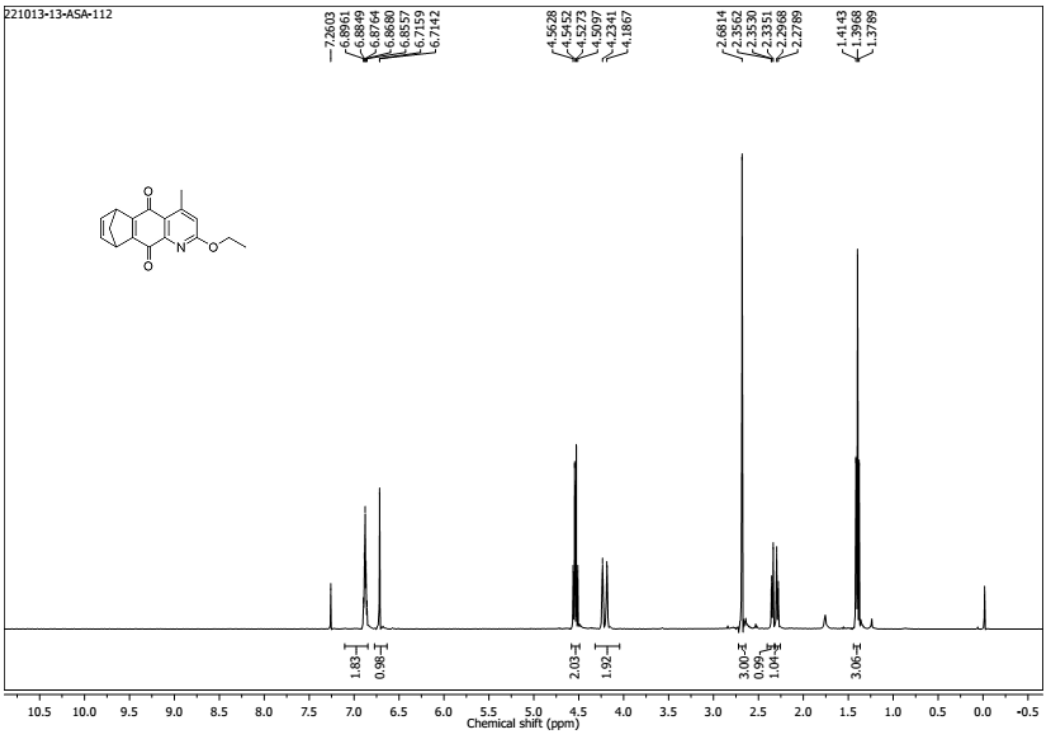

^{13}C NMR Spectrum (100 MHz, $CDCl_3$) of **14c**

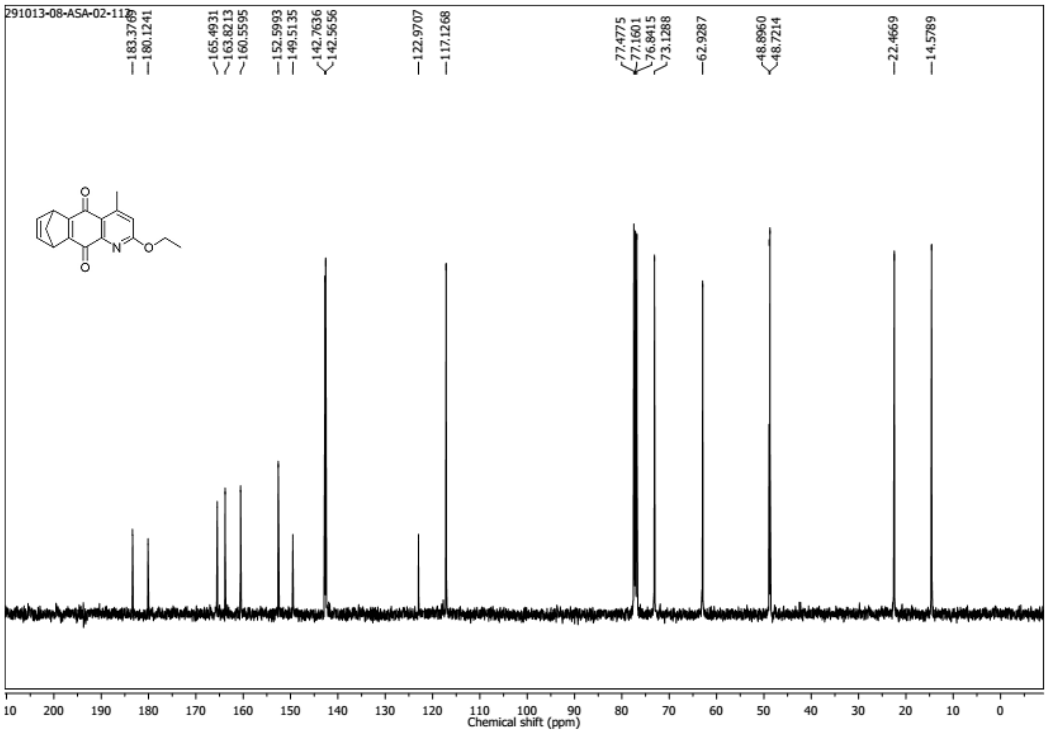

^{1}H NMR Spectrum (400 MHz, $CDCl_3$) of **14d**

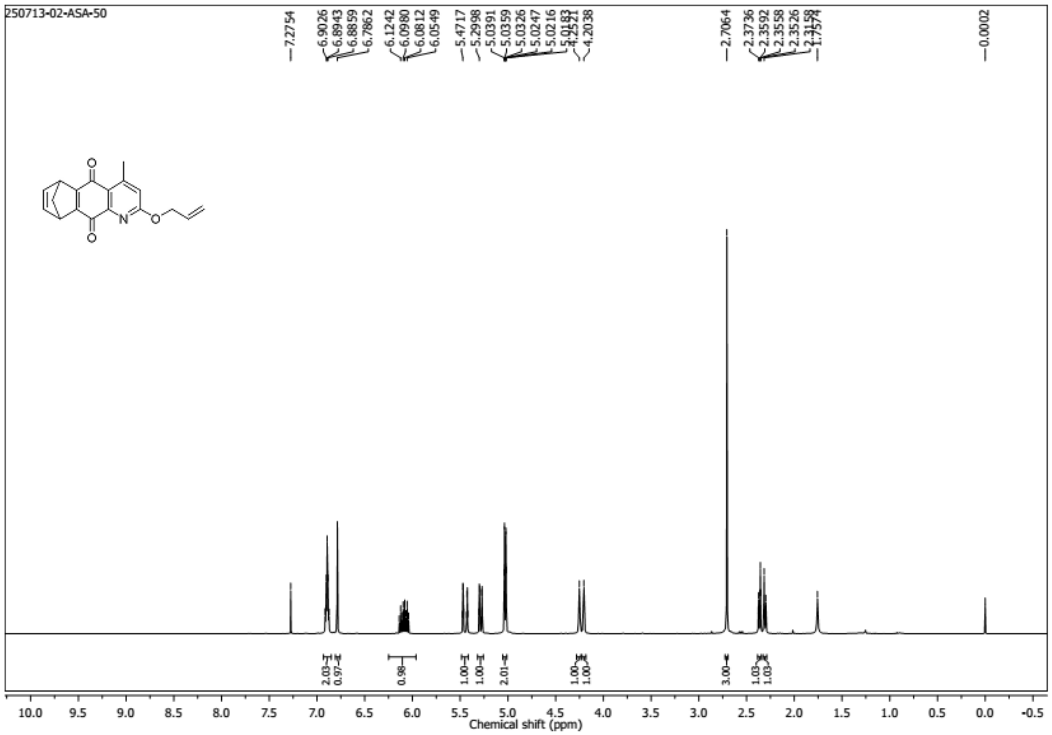

^{13}C NMR Spectrum (100 MHz, $CDCl_3$) of **14d**

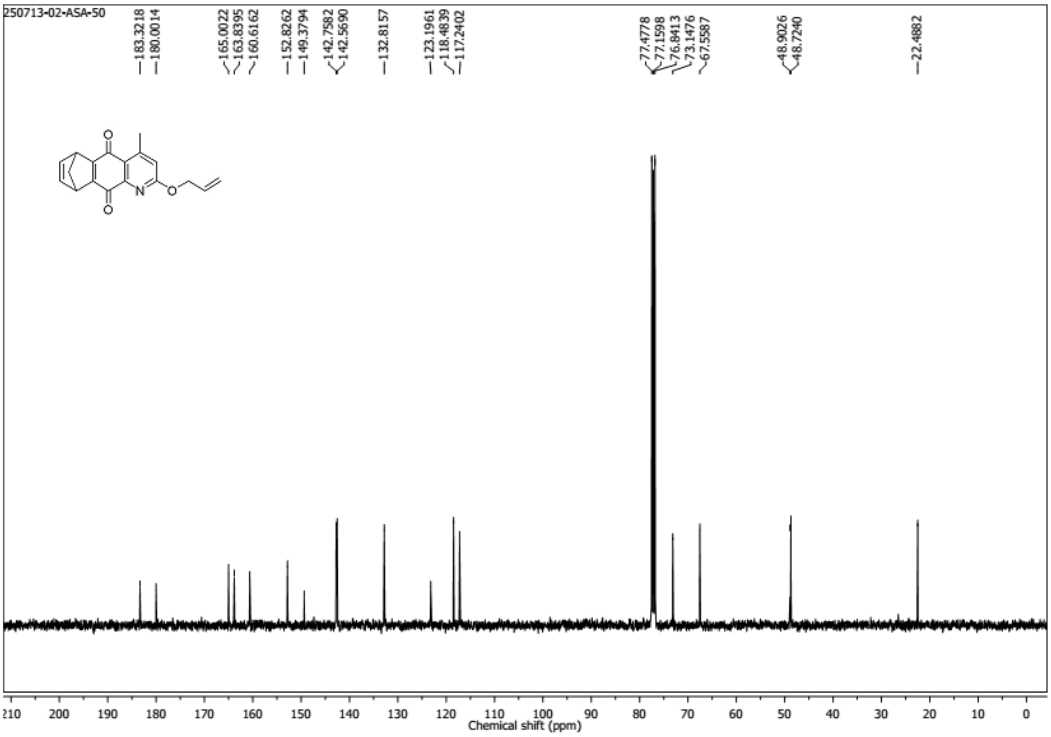

^{1}H NMR Spectrum (400 MHz, $CDCl_3$) of **14e**

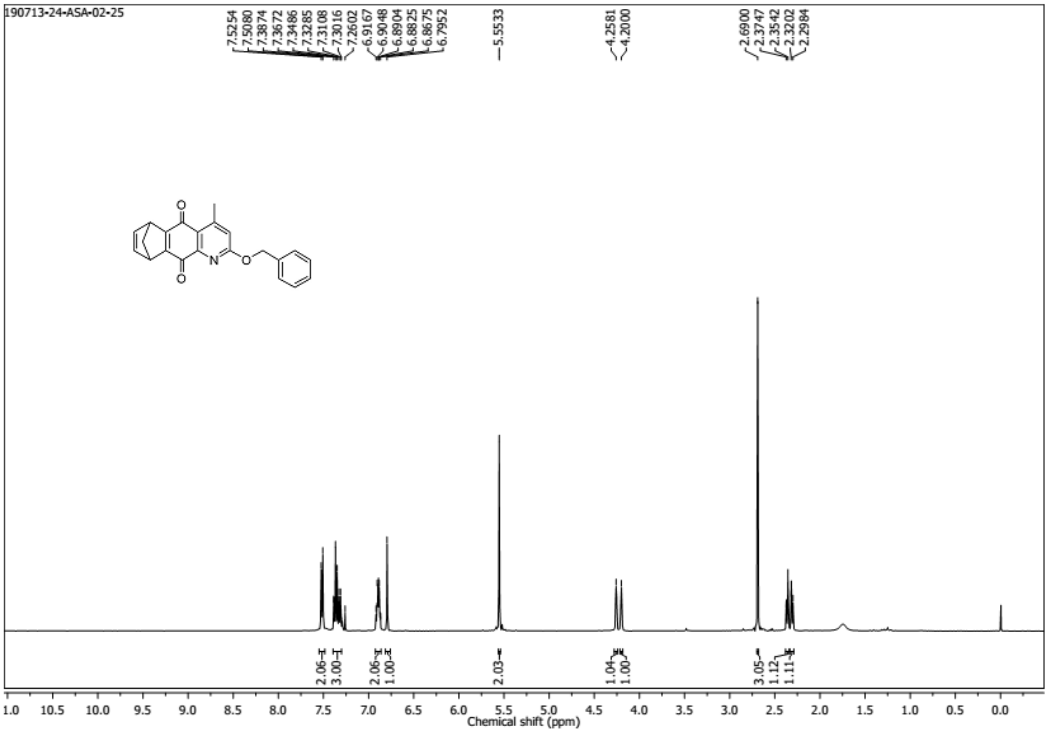

^{13}C NMR Spectrum (100 MHz, $CDCl_3$) of **14e**

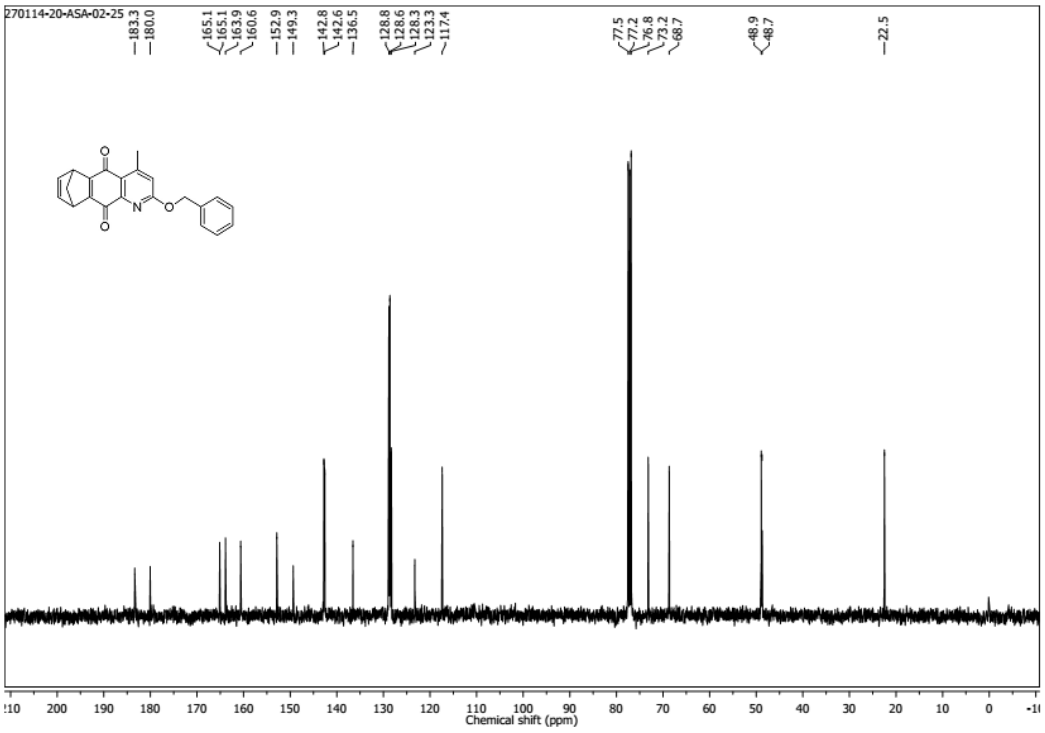

^{1}H NMR Spectrum (400 MHz, $CDCl_3$) of **15b**

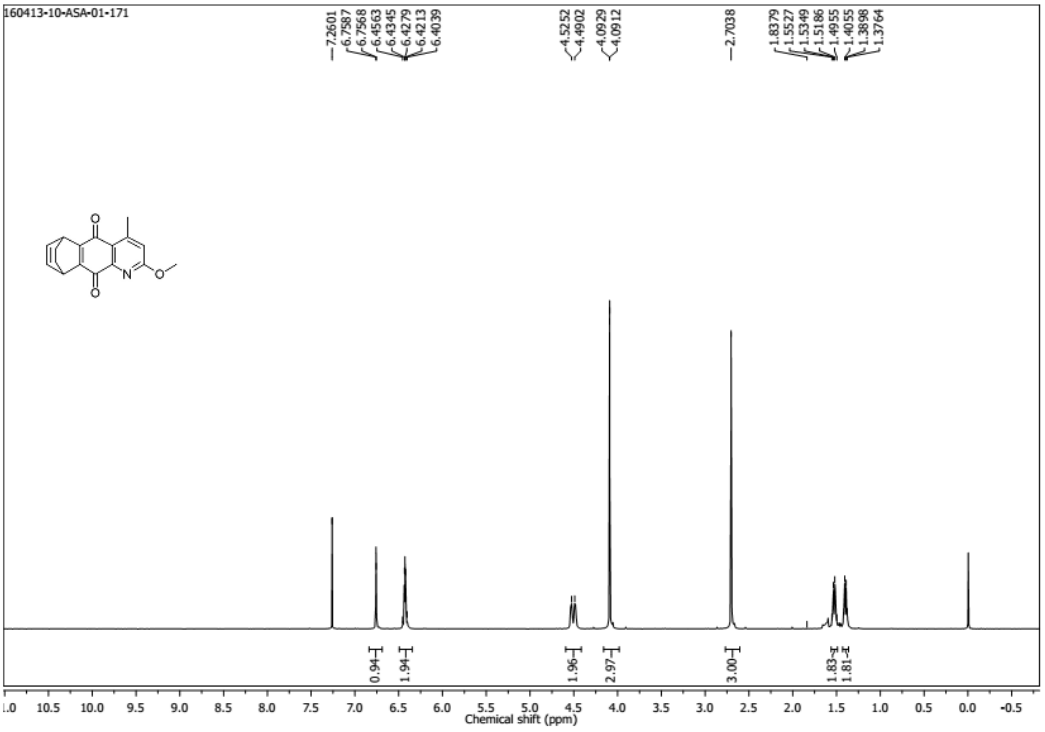

^{13}C NMR Spectrum (100 MHz, $CDCl_3$) of **15b**

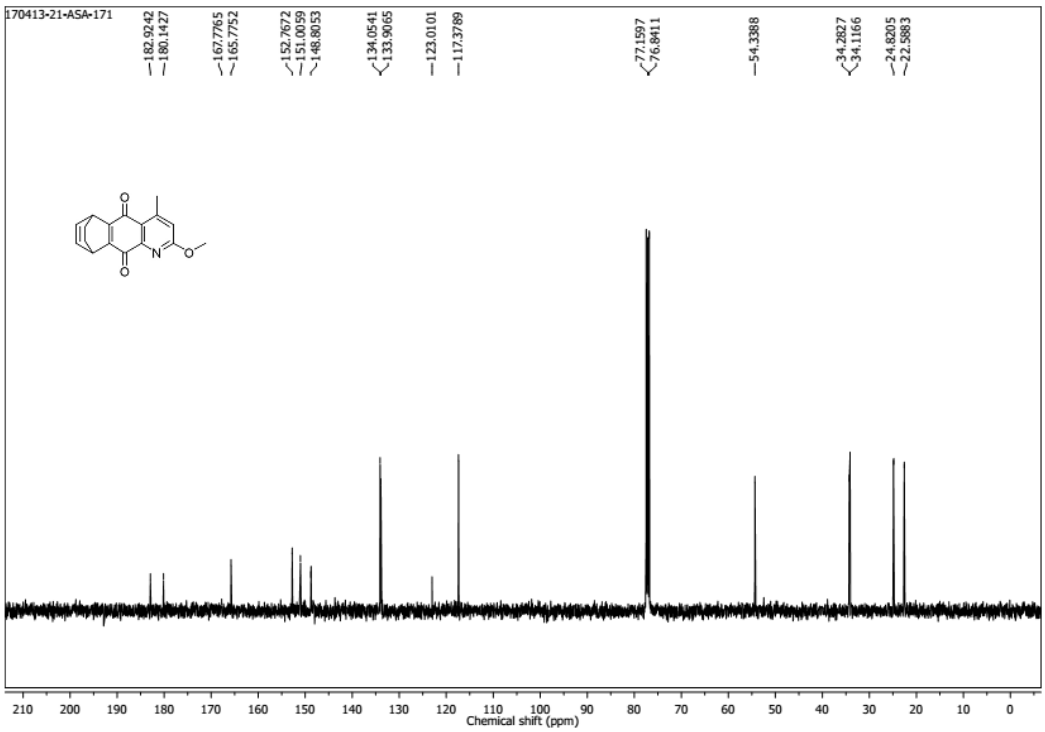

^{1}H NMR Spectrum (400 MHz, $CDCl_3$) of **15c**

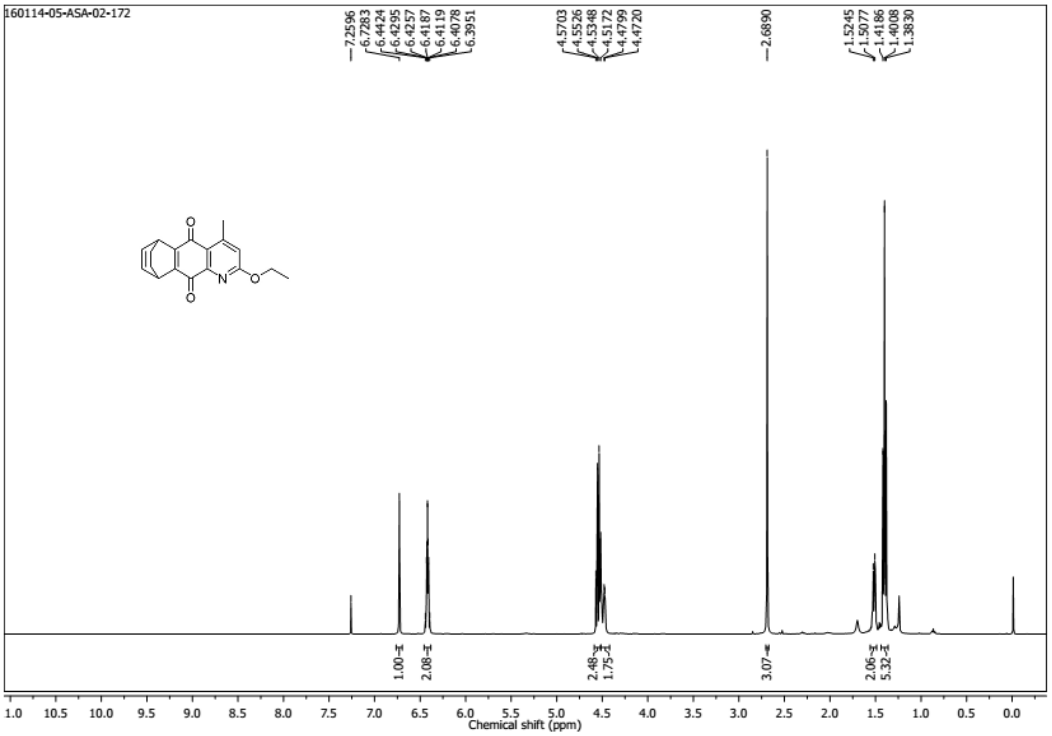

^{13}C NMR Spectrum (100 MHz, $CDCl_3$) of **15c**

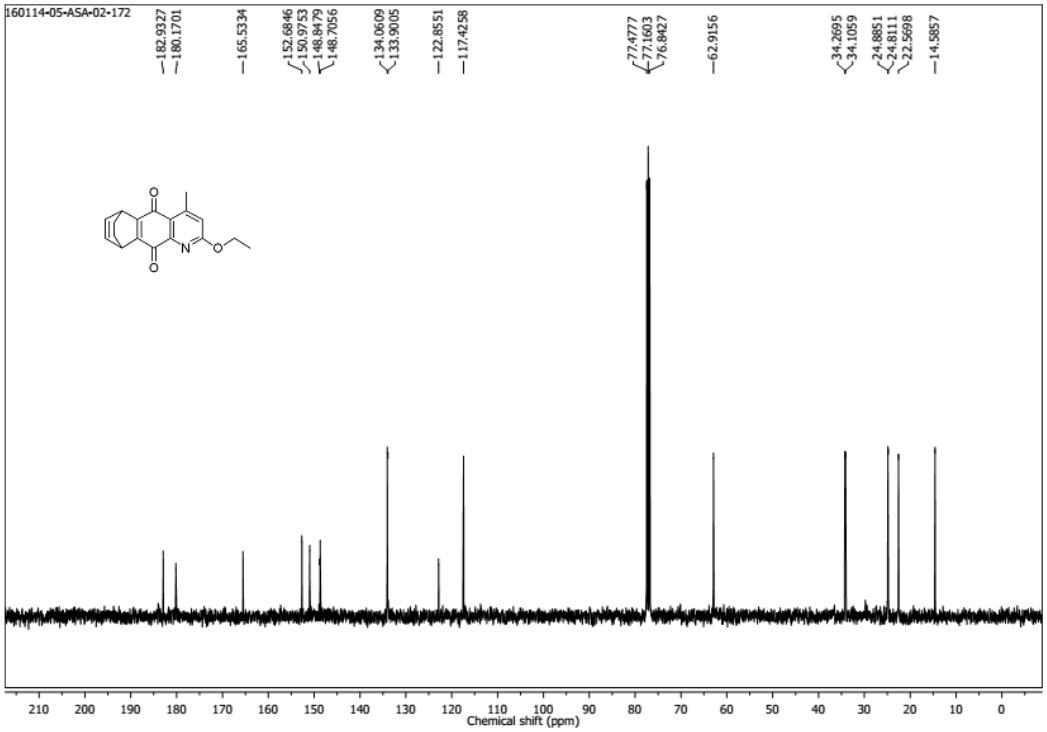

^{1}H NMR Spectrum (400 MHz, $CDCl_3$) of **15d**

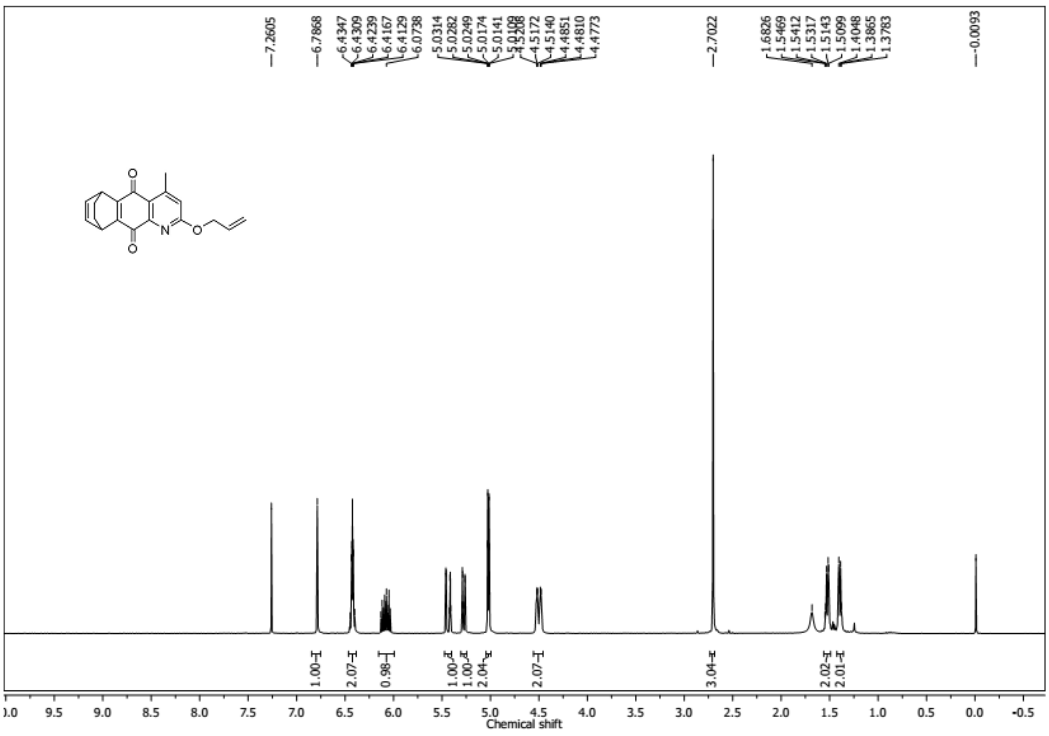

^{13}C NMR Spectrum (100 MHz, $CDCl_3$) of **15d**

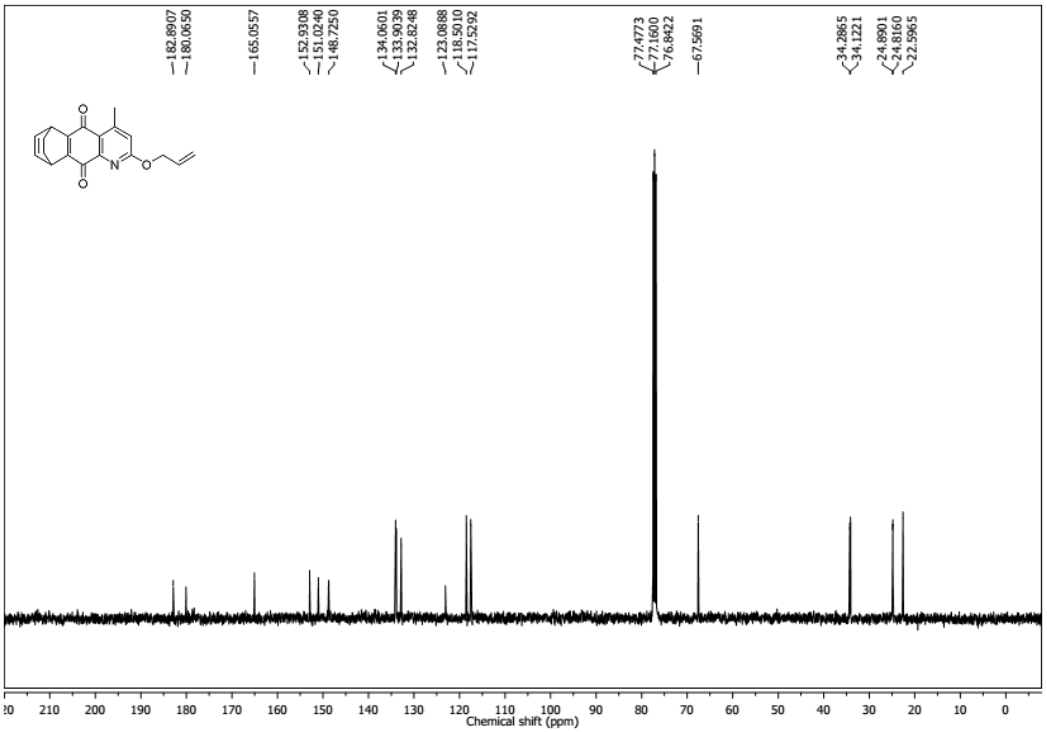

^{1}H NMR Spectrum (400 MHz, $CDCl_3$) of **15e**

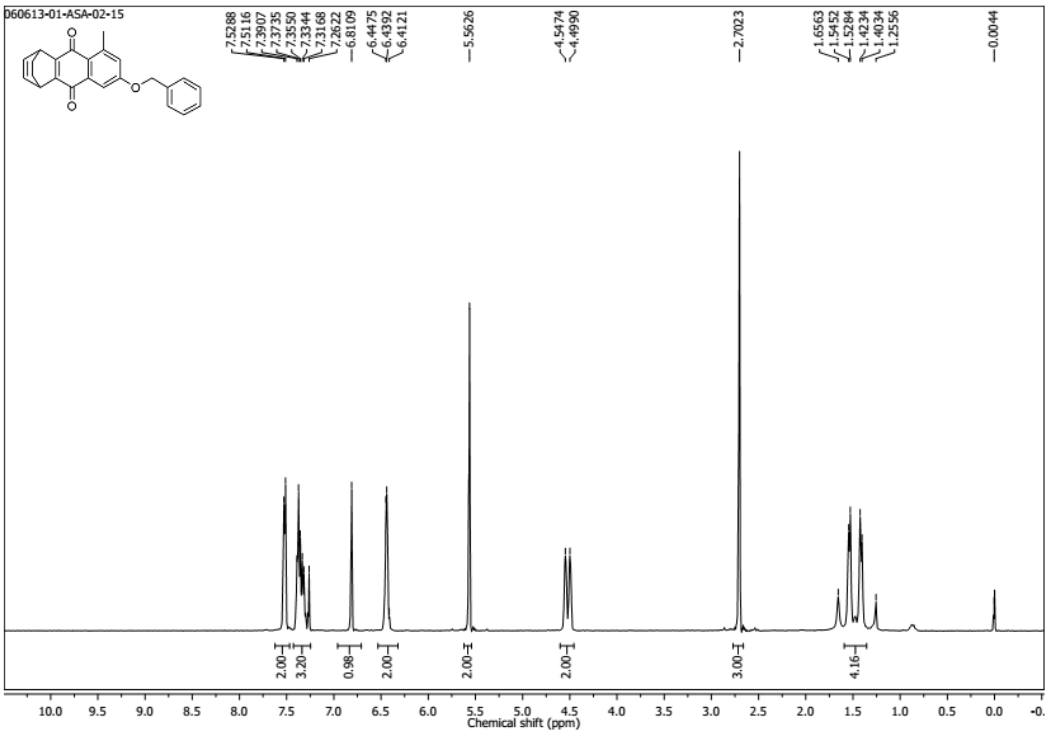

^{13}C NMR Spectrum (100 MHz, $CDCl_3$) of **15e**

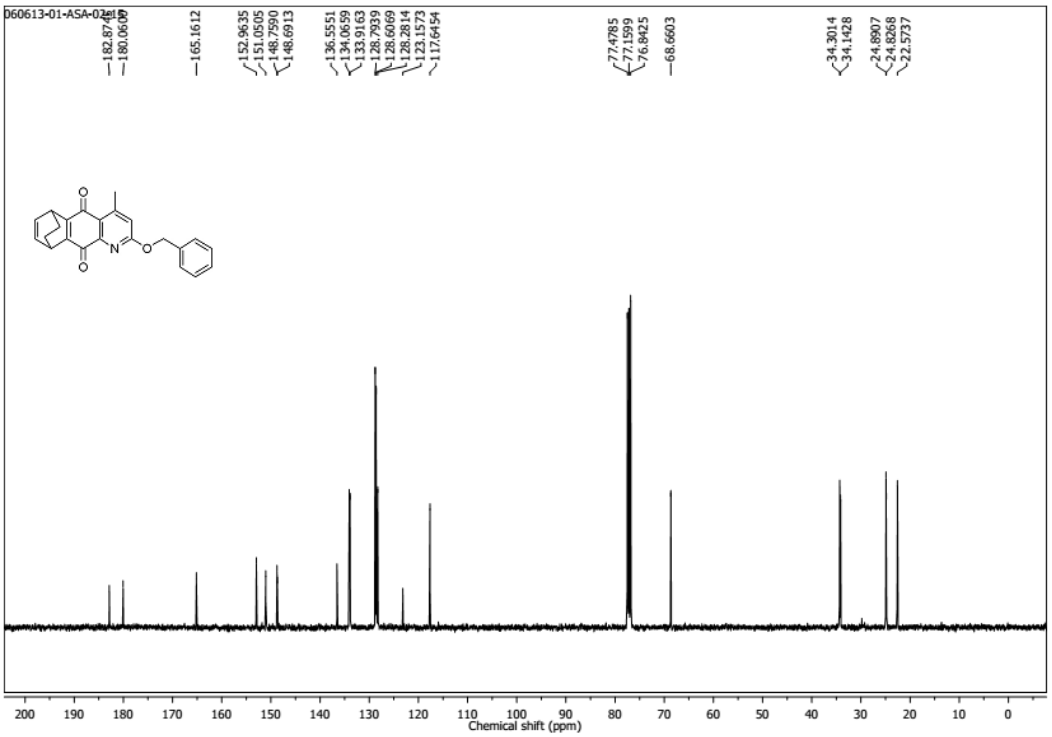

^{1}H NMR Spectrum (400 MHz, $CDCl_3$) of **17a**

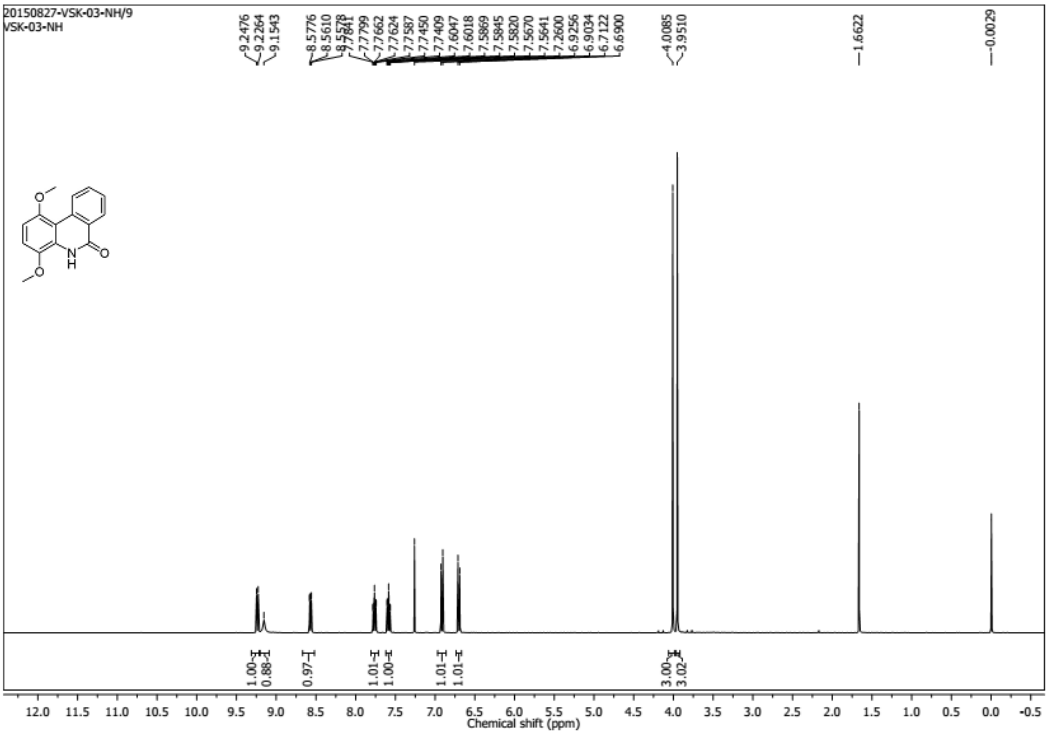

^{13}C NMR Spectrum (100 MHz, $CDCl_3$) of **17a**

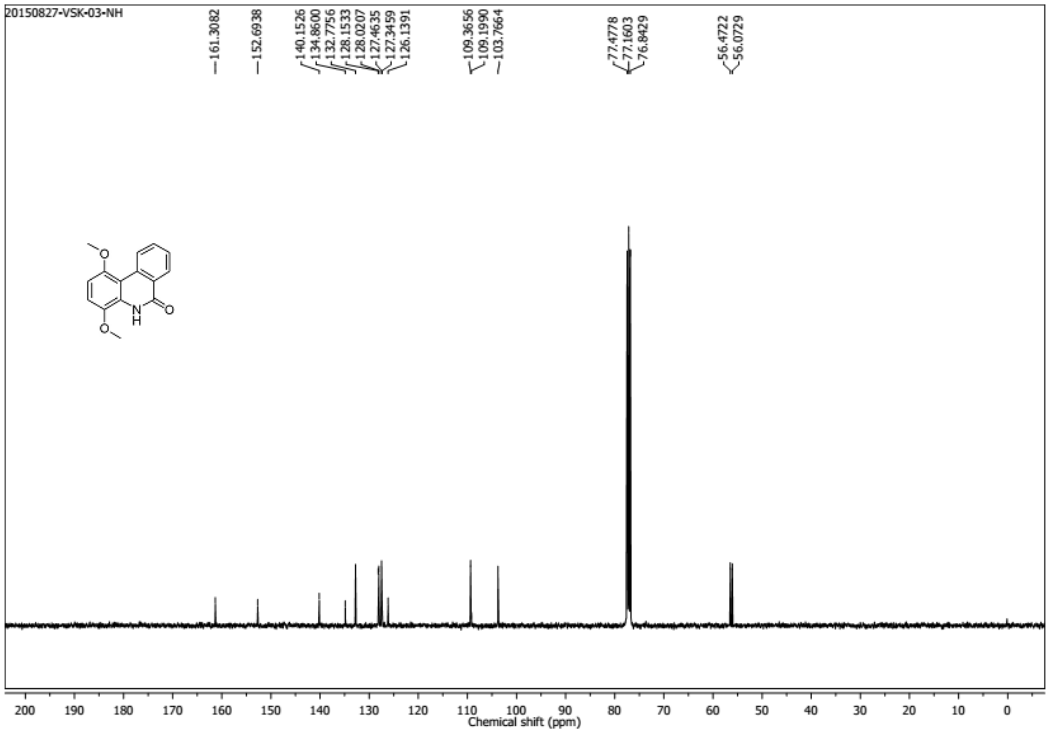

^{1}H NMR Spectrum (400 MHz, $CDCl_3$) of **17b**

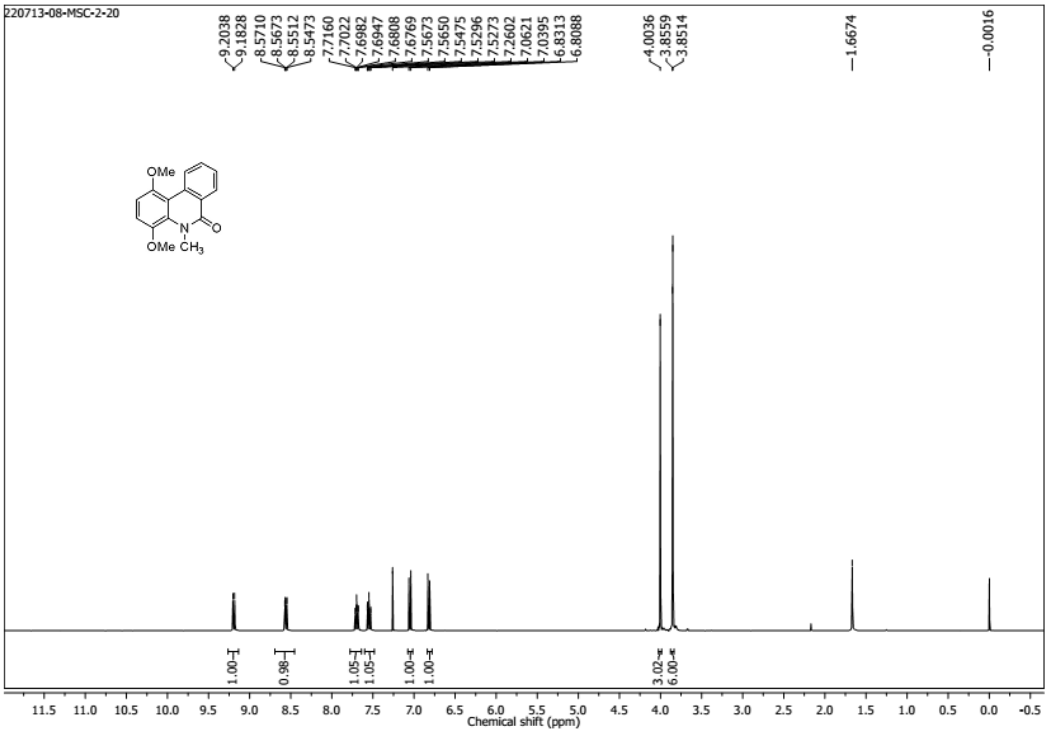

^{13}C NMR Spectrum (100 MHz, $CDCl_3$) of **17b**

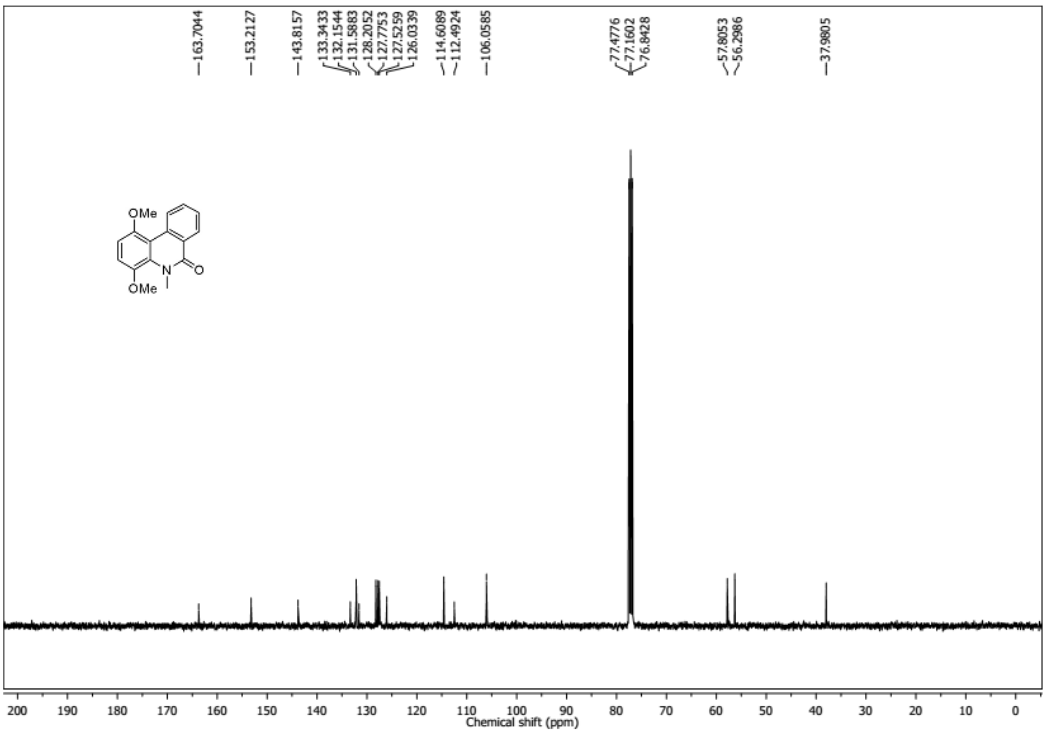

^{1}H NMR Spectrum (400 MHz, $CDCl_3$) of **17c**

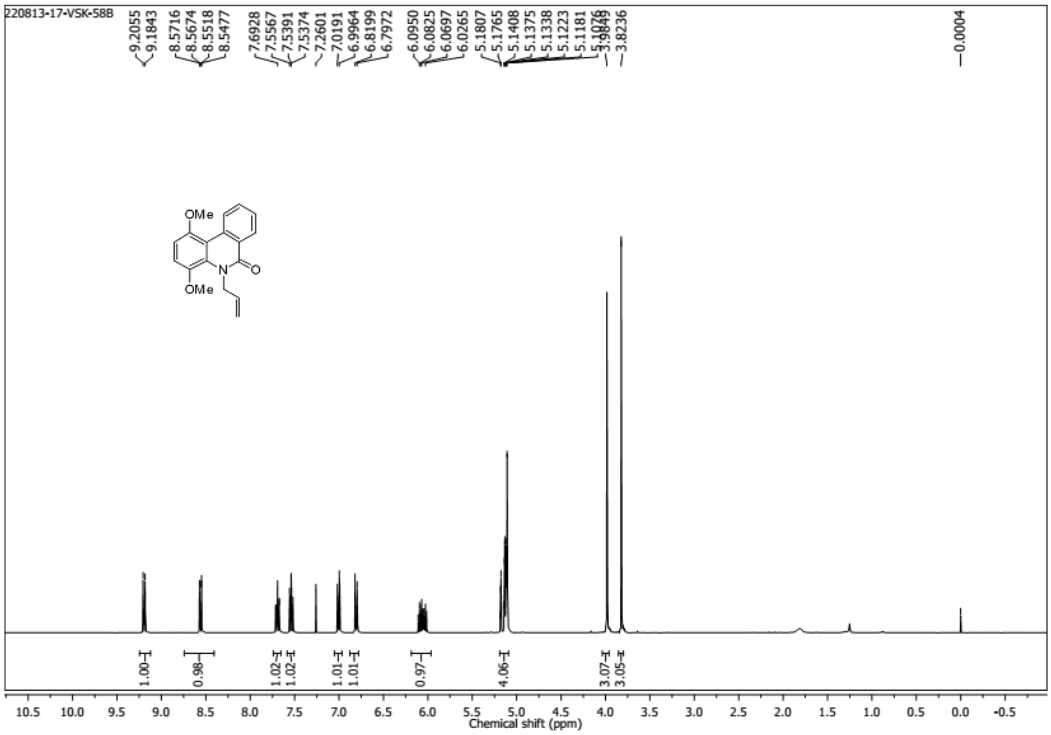

^{13}C NMR Spectrum (100 MHz, $CDCl_3$) of **17c**

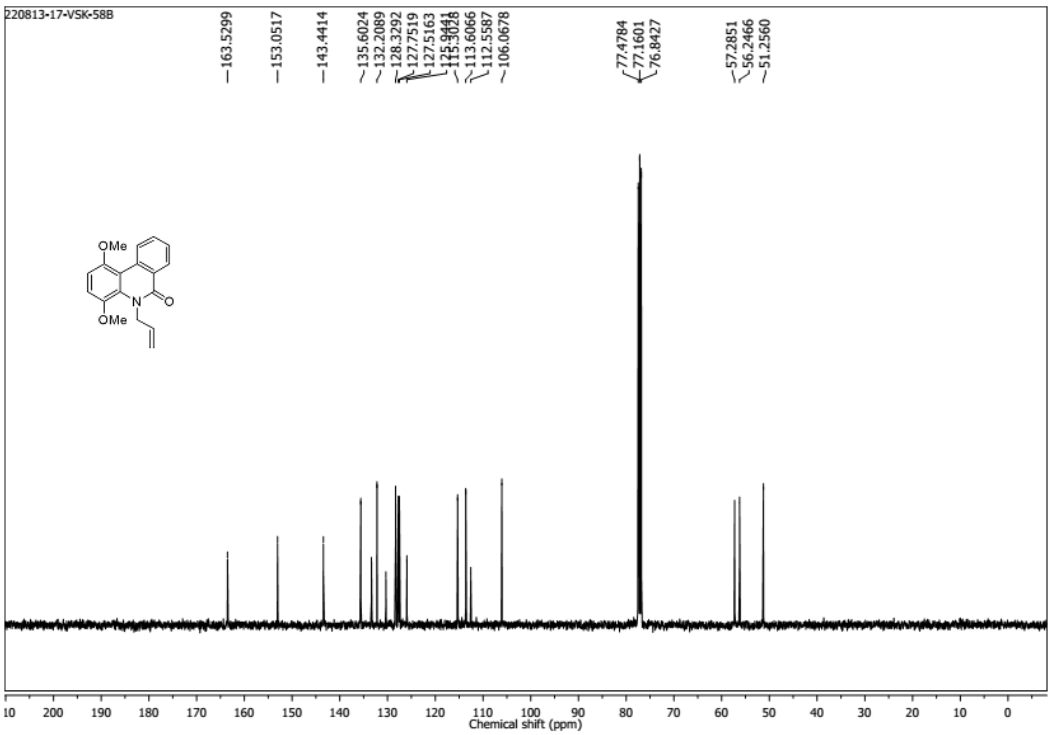

^{1}H NMR Spectrum (400 MHz, $CDCl_3$) of **18a**

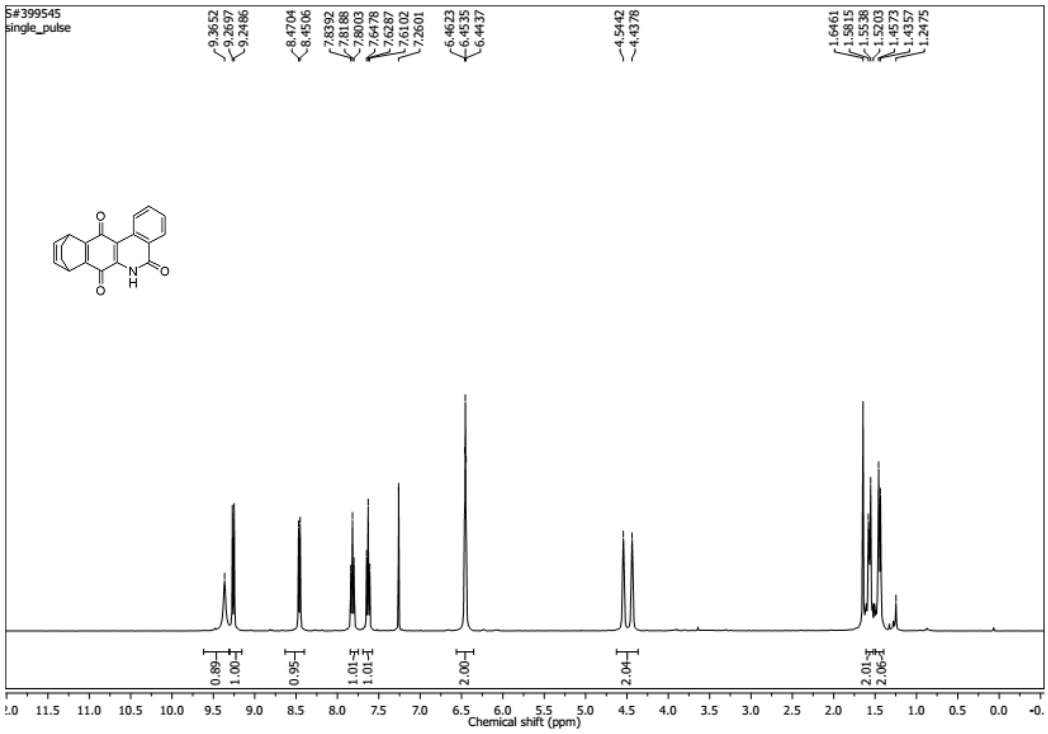

^{13}C NMR Spectrum (100 MHz, $CDCl_3$) of **18a**

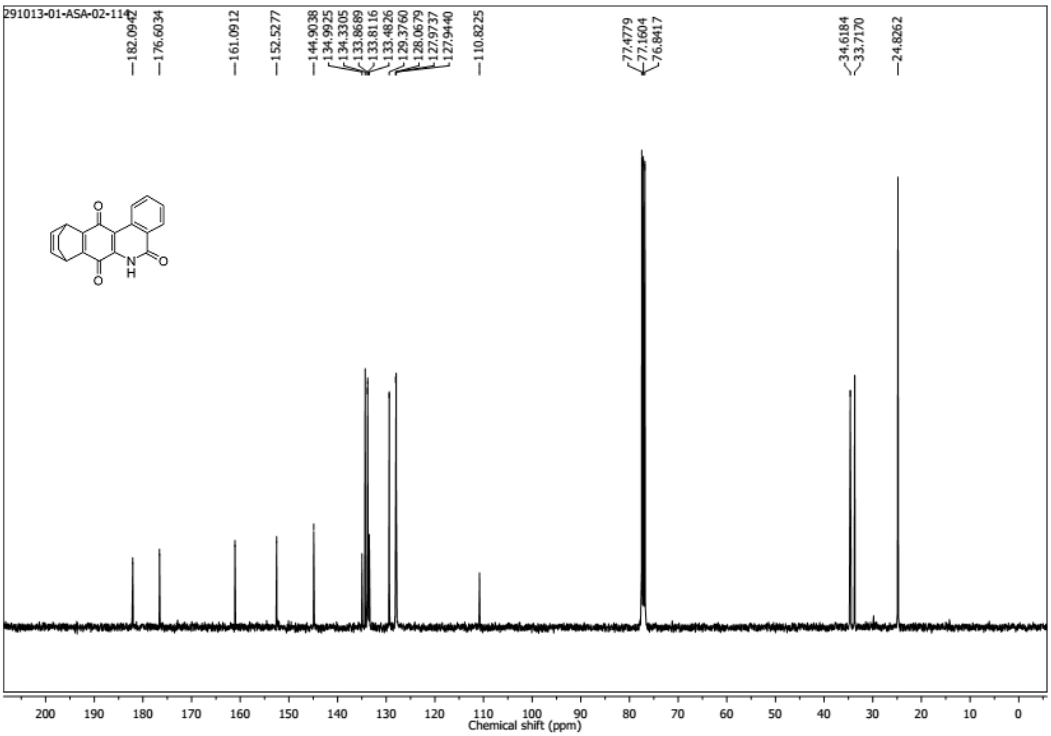

^{1}H NMR Spectrum (400 MHz, $CDCl_3$) of **18b**

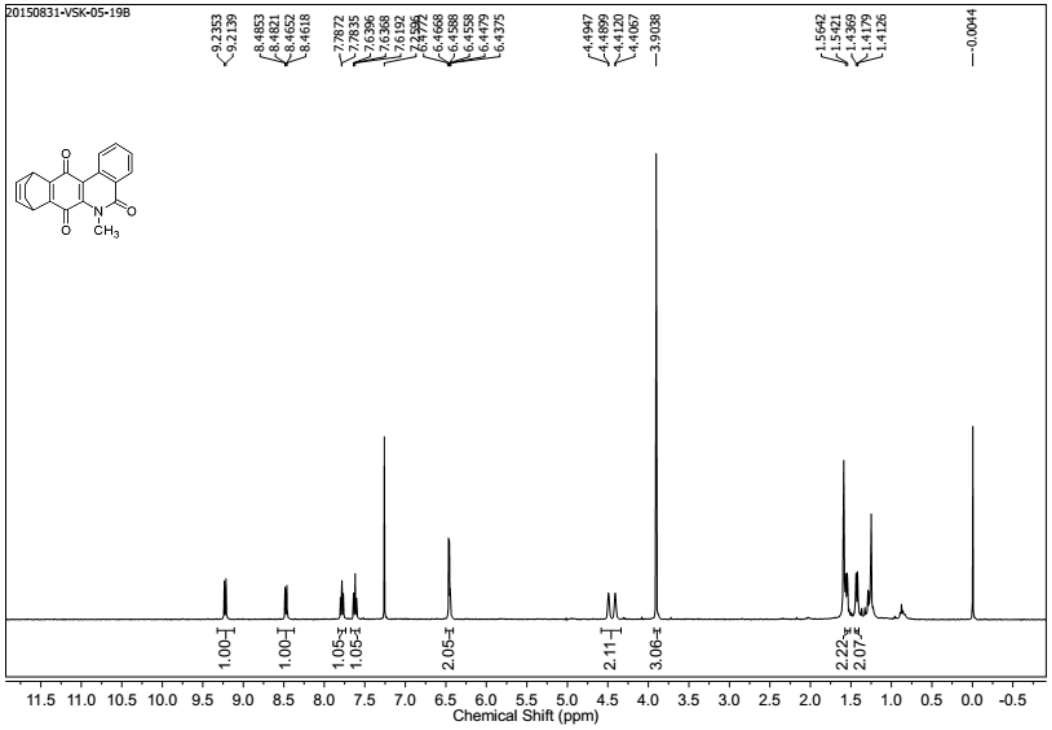

^{13}C NMR Spectrum (100 MHz, $CDCl_3$) of **18b**

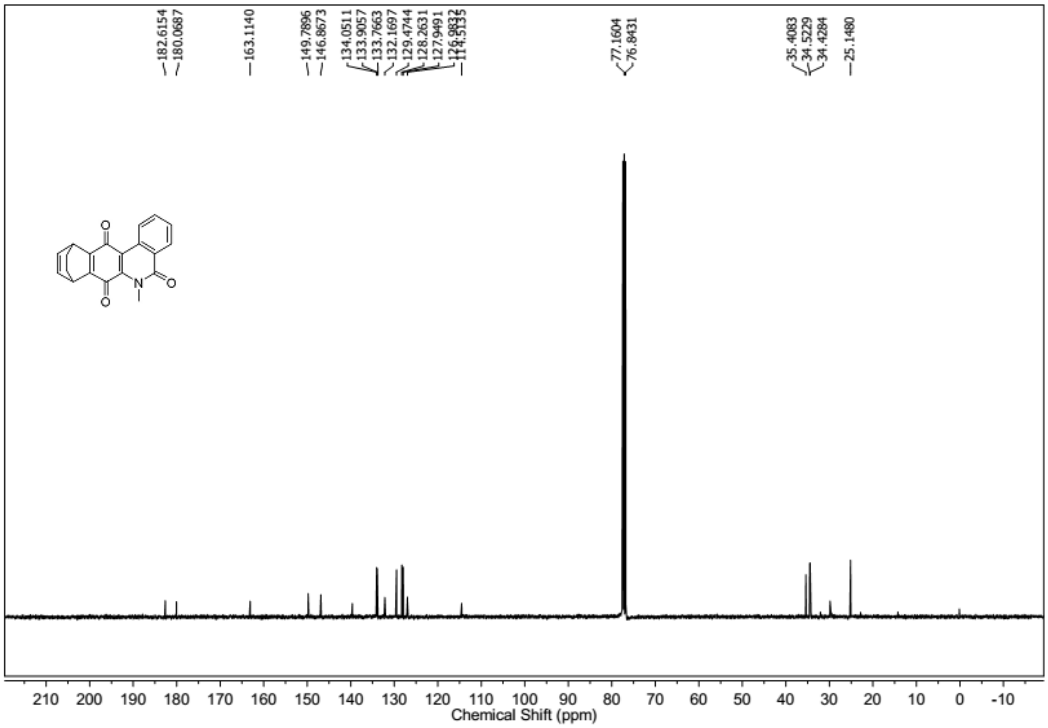

^{1}H NMR Spectrum (400 MHz, $CDCl_3$) of **18c**

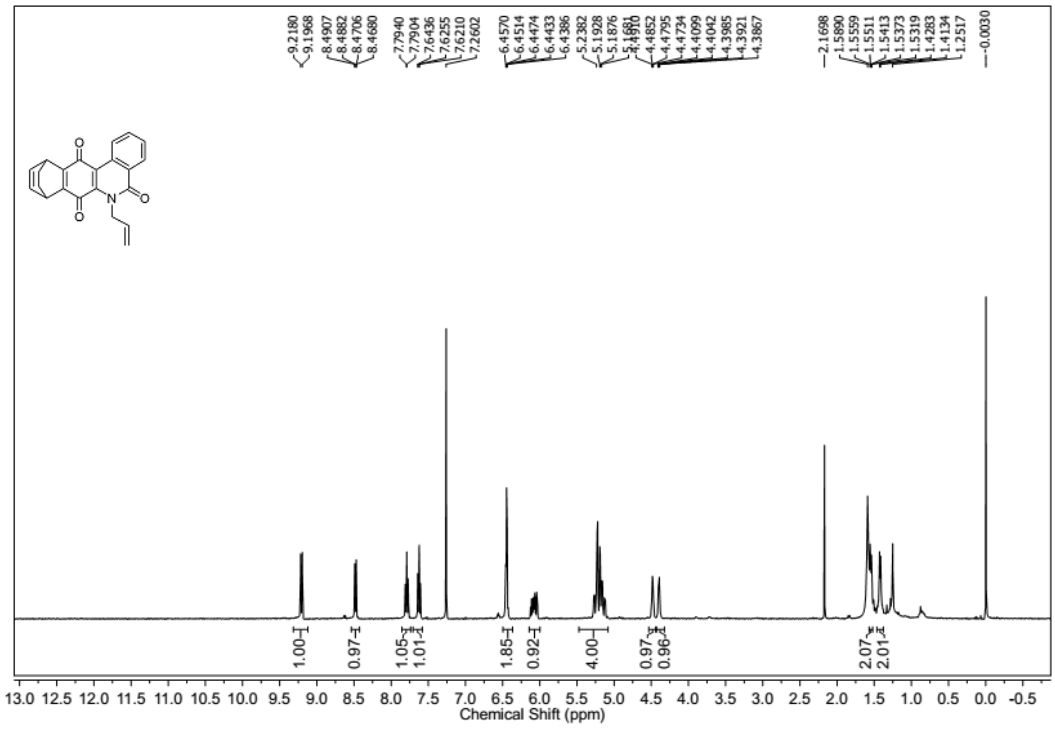

^{13}C NMR Spectrum (100 MHz, $CDCl_3$) of **18c**

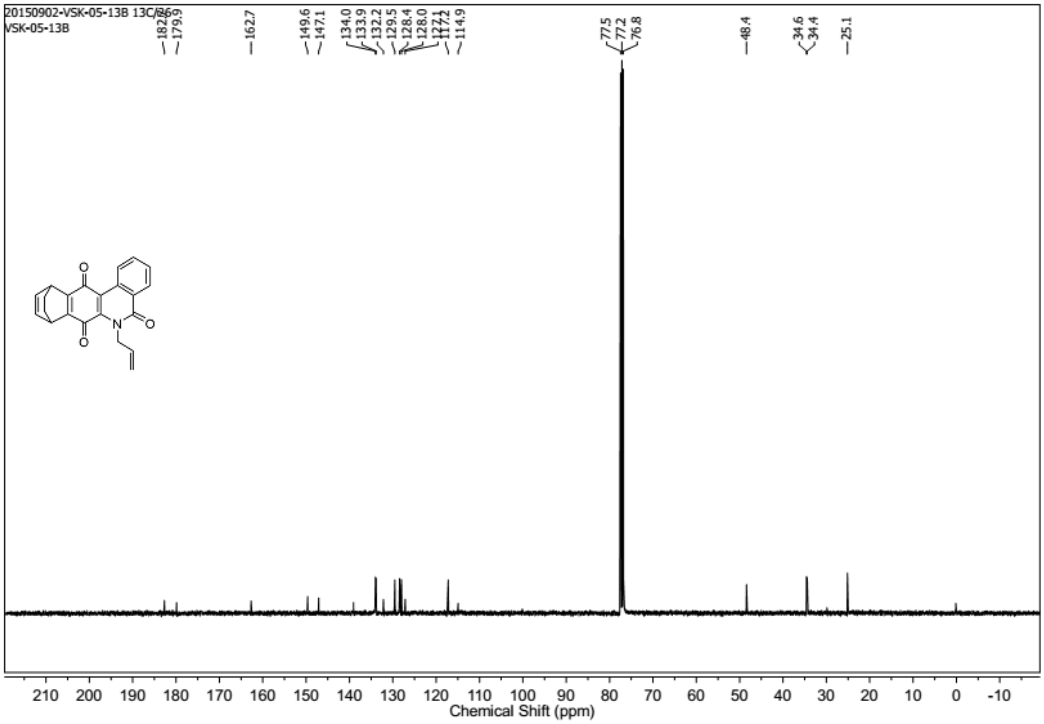

2.2.6. References

(1) Smith , T. L.; Pearson , M. L.; Wilcox , K. R.; Cruz , C.; Lancaster , M. V.; Robinson-Dunn , B.; Tenover , F. C.; Zervos , M. J.; Band , J. D.; White , E.; Jarvis , W. R. *N. Eng. J. Med.* **1999**, *340*, 493.

(2) Hiramatsu, K.; Hanaki, H.; Ino, T.; Yabuta, K.; Oguri, T.; Tenover, F. C. *J. Antimicrob. Chemother*. **1997**, *40*, 135.

(3) Bragginton, E. C.; Piddock, L. J. V. *Lancet Infect. Dis.* **2014**, *14*, 857.

(4) Arias , C. A.; Murray , B. E. *N. Engl. J. Med.* **2009**, *360*, 439.

(5) Kohanski, M. A.; Dwyer, D. J.; Hayete, B.; Lawrence, C. A.; Collins, J. J. *Cell* **2007**, *130*, 797.

(6) Foti, J. J.; Devadoss, B.; Winkler, J. A.; Collins, J. J.; Walker, G. C. *Science* **2012**, *336*, 315.

(7) Liu, Y.; Imlay, J. A. *Science* **2013**, *339*, 1210.

(8) Keren, I.; Wu, Y.; Inocencio, J.; Mulcahy, L. R.; Lewis, K. *Science* **2013**, *339*, 1213.

(9) Dwyer, D. J.; Belenky, P. A.; Yang, J. H.; MacDonald, I. C.; Martell, J. D.; Takahashi, N.; Chan, C. T. Y.; Lobritz, M. A.; Braff, D.; Schwarz, E. G.; Ye, J. D.; Pati, M.; Vercruysse, M.; Ralifo, P. S.; Allison, K. R.; Khalil, A. S.; Ting, A. Y.; Walker, G. C.; Collins, J. J. *Proc. Natl. Acad. Sci. U.S.A* .**2014**, *111*, E2100.

(10) Shen, F.; Tang, X.; Cheng, W.; Wang, Y.; Wang, C.; Shi, X.; An, Y.; Zhang, Q.; Liu, M.; Liu, B.; Yu, L. *Sci. Rep.* **2016**, *6*, 19262.

(11) Dai, T.; Huang, Y.-Y.; Hamblin, M. R. *Photodiagn. Photodyn. Ther.* **2009**, *6*, 170.

(12) Khodade, V. S.; Sharath Chandra, M.; Banerjee, A.; Lahiri, S.; Pulipeta, M.; Rangarajan, R.; Chakrapani, H. *ACS Med. Chem. Lett.* **2014**, *5*, 777.

(13) Van, T. N.; Kimpe, N. D. *Tetrahedron* **2003**, *59*, 5941.

(14) Bachu, P.; Sperry, J.; Brimble, M. A. *Tetrahedron* **2008**, *64*, 4827.

(15) Dharmaraja, A. T.; Dash, T. K.; Konkimalla, V. B.; Chakrapani, H. *Med. Chem. Comm.* **2012**, *3*, 219.

(16) Brimble, M. A.; Bachu, P.; Sperry, J. *Synthesis* **2007**, *2007*, 2887.

(17) Hadden, M. K.; Hill, S. A.; Davenport, J.; Matts, R. L.; Blagg, B. S. J. *Bioorg. Med. Chem.* **2009**, *17*, 634.

(18) Wang, M.; Gao, M.; Miller, K. D.; Sledge, G. W.; Hutchins, G. D.; Zheng, Q.-H. *Steroids* **2010**, *75*, 967.

(19) Maiti, A.; Reddy, P. V. N.; Sturdy, M.; Marler, L.; Pegan, S. D.; Mesecar, A. D.; Pezzuto, J. M.; Cushman, M. *J. Med. Chem.* **2009**, *52*, 1873.

(20) Sánchez, J. D.; Egris, R.; Perumal, S.; Villacampa, M.; Menéndez, J. C. *Eur. J. Org. Chem.* **2012**, *2012*, 2375.

(21) Alonso, M. Á.; López-Alvarado, P.; Avendaño, C.; Menéndez, J. C. *Tetrahedron* **2003**, *59*, 2821.

(22) Jacob, P.; Callery, P. S.; Shulgin, A. T.; Castagnoli, N. *J. Org. Chem.* **1976**, *41*, 3627.

(23) Bhakuni, B. S.; Kumar, A.; Balkrishna, S. J.; Sheikh, J. A.; Konar, S.; Kumar, S. *Org. Lett.* **2012**, *14*, 2838.

(24) Dharmaraja, A. T.; Alvala, M.; Sriram, D.; Yogeeswari, P.; Chakrapani, H. *Chem. Commun.* **2012**, *48*, 10325.

(25) Criddle, D. N.; Gillies, S.; Baumgartner-Wilson, H. K.; Jaffar, M.; Chinje, E. C.; Passmore, S.; Chvanov, M.; Barrow, S.; Gerasimenko, O. V.; Tepikin, A. V.; Sutton, R.; Petersen, O. H. *J. Biol. Chem.* **2006**, *281*, 40485.

(26) Parkinson, E. I.; Hergenrother, P. J. *Acc. Chem. Res.* **2015**, *48*, 2715.

(27) Jacobs, N.; Lang, S.; Panisch, R.; Wittstock, G.; Groth, U.; Nasiri, H. R. *RSC Adv.* **2015**, *5*, 58561.

(28) Cui, S.-F.; Addla, D.; Zhou, C.-H. *J. Med. Chem.* **2016**, *59*, 4488.

(29) Zhang, L.; Chang, J.-J.; Zhang, S.-L.; Damu, G. L. V.; Geng, R.-X.; Zhou, C.-H. *Bioorg. Med. Chem.* **2013**, *21*, 4158.

(30) Georgiou, C. D.; Papapostolou, I.; Grintzalis, K. *Nat. Protoc.* **2008**, *3*, 1679.

(31) Zielonka, J.; Vasquez-Vivar, J.; Kalyanaraman, B. *Nat. Protoc.* **2008**, *3*, 8.

(32) Zhou, M.; Diwu, Z.; Panchuk-Voloshina, N.; Haugland, R. P. *Anal. Biochem.* **1997**, *253*, 162.

(33) Forrester, A. R.; Ingram, A. S.; John, I. L.; Thomson, R. H. *J. Chem. Soc. Perkin Trans.* **1975**, 1115.

(34) Lang, S.; Groth, U. *Angew. Chem. Int. Ed.* **2009**, *48*, 911.

(35) Zhao, H.; Joseph, J.; Fales, H. M.; Sokoloski, E. A.; Levine, R. L.; Vasquez-Vivar, J.; Kalyanaraman, B. *Proc. Natl. Acad. Sci. U.S.A.* **2005**, *102*, 5727.

Chapter 3: Design, Synthesis and Evaluation of Small Molecule for Controlled Generation of Peroxynitrite

3.1. Introduction

In chapter 2, we have described the design and synthesis of natural product-inspired bioreductively activated reactive oxygen species (ROS) generators. A mechanism for ROS generation from these compounds involved reduction of 1,4-benzoquinone scaffold by bioreductive enzymes to produce an aromatic 1,4-diol intermediate, which then reacts with molecular oxygen to produce superoxide radical ($O_2^{\bullet-}$). This radical species is short-lived and it can undergo spontaneous or enzymatic dismutation to hydrogen peroxide (H_2O_2). In addition, $O_2^{\bullet-}$ can react with nitric oxide (NO) at diffusion controlled-rate to produce peroxynitrite ($ONOO^-$), a reactive nitrogen species. Peroxynitrite is a highly reactive species than its precursors $O_2^{\bullet-}$ and NO. Being a strong oxidant and a nitrating agent, elevated levels of $ONOO^-$ can cause oxidative bimolecular damage and redox imbalance possibly leading to irreversible cellular dysfunction, impaired growth and cell death. Therefore, mammalian immune system deploys this reactive species along with other ROS while combating infectious pathogens. The immune cells such as macrophages upon engulfing pathogens produce fluxes of both NO as well as $O_2^{\bullet-}$, which presumably combine to produce peroxynitrite.[1] Although a number of *in vitro* studies have demonstrated the microbicidal role of $ONOO^-$, assessing its cellular effects *in vivo* is challenging due to its transient nature. In addition, a number of recent studies have demonstrated the importance of peroxynitrite-mediated cell signaling, which occurs at sub-lethal concentrations.[2-4] However, this transition of $ONOO^-$ from nontoxic, to signaling, to toxic peroxynitrite levels is poorly characterized. This is in part, due to the difficulty associated with controlled generation of this reactive species. A number of methodologies have been developed to deliver $ONOO^-$ in cells, but they are often associated with various limitations. The currently available methods for $ONOO^-$ generation and their limitations are summarized below.

3.1.1. Peroxynitrite sources

3.1.1.A. Peroxynitrite solution

A highly alkaline solution of peroxynitrite synthesized by the reaction of hydrogen peroxide with nitrite has been commonly used as $ONOO^-$ source.[5-6] However, this method does not mimic the

physiological generation of this reactive species. This solution rapidly undergoes decomposition under physiological conditions. Hence millmolar concentrations (0.2 mM – 1 mM) of $ONOO^-$ are required for cellular studies.[7] However, such concentrated solution results in rapid generation of other radical species, which can complicate the interpretation of results. Furthermore, this method is not suited for cellular studies as peroxynitrite has poor cell-permeability and bioavailability.

3.1.1. B. 3-Morpholinosydnonimine

The heterocyclic aromatic compound, 3-Morpholinosydnonimine (SIN-1) is commonly used as $ONOO^-$ donor. A mechanism of peroxynitrite generation from SIN-1 begins with a base-catalyzed ring-opening to generate the reactive metabolite of SIN-1 (A) (Scheme 3.1). This intermediate reduces oxygen to produce $O_2^{\bullet-}$ and unstable hydrazinium radical intermediate (B) that rapidly releases NO (Scheme 3.1).[8] The *in situ* generated NO and $O_2^{\bullet-}$ reacts with each other at diffusion controlled rate and forms peroxynitrite.

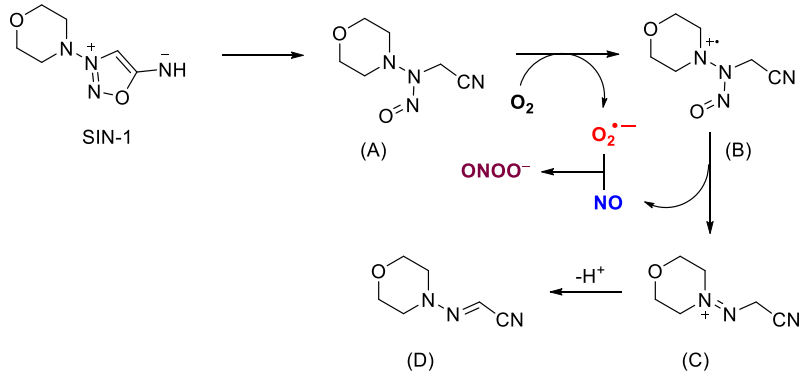

Scheme 3.1. Mechanism of peroxynitrite generation from SIN-1

Peroxynitrite generation from SIN-1 is depends on concentration of molecular oxygen present within solution. Although SIN-1 has been commonly used for biochemical assays, however its solution preparation requires optimal condition to maximize the peroxynitrite formation. For example, SIN-1 solution is prepared in acidic media to inhibit its activation to release $O_2^{\bullet-}$ and NO. In addition, it cannot be used in cellular media as it releases only NO in the presence of electron acceptors.[9] It has been reported that intermediates produced after decomposition of SIN-1 are potentially cytotoxic. Furthermore, this compound does not provide spatiotemporal control over peroxynitrite generation and it is typically used at elevated concentrations during cellular

studeis.[10] However, despite these limitations, SIN-1 is used as a peroxynitrite donor because it is convenient to store as a solid and can be used before any experiment.

3.1.1.C. Two-component system

Another approach that has been commonly used for $ONOO^-$ generation is by combining separate sources of $O_2^{\bullet-}$ and NO. A number of organic compounds such as diazeniumdiolates and S-nitrosothiols have been used for NO generation, whereas $O_2^{\bullet-}$ is produced from the enzymatic oxidation of hypoxanthine by xanthine oxidase.[11] However, due to variation in releasing rate of NO and $O_2^{\bullet-}$ from their sources, peroxynitrite generation rate is difficult to control. Recently, Mascharak and coworker have developed two-component system capable of generating peroxynitrite in a controlled manner.[12] In this method photocontrollable Mn(NO) complex encapsulated within biologically inert silicate sol–gel matrix was used as NO source and $O_2^{\bullet-}$ was generated by enzymatic oxidation of hypoxanthine using xanthine oxidase (XO/HX). Catalase was also incorporated into the sol–gel matrix to minimize the hydrogen peroxide generation from the XO/HX. This biomimetic peroxynitrite-generating platform was prepared by addition of Mn(NO) and XO/catalase sol-gel material into a multiwell plate. This platform generates $ONOO^-$ upon simultaneous addition of hypoxanthine and illumination with low-power visible light. Aryl boronic acid-based probe, coumarin-7-boronic acid was used to quantify the $ONOO^-$ generation. This method gives opportunity to maintain physiological concentrations of $ONOO^-$ (sub-micromolar concentrations) in biochemical assays, however very little evidence is available for its utility in cellular studies.[13]

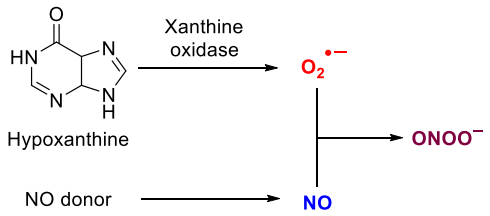

Scheme 3.2. Schematic representation of peroxynitrite generation by two component system

3.1.1.D. Light-activated peroxynitrite donor

Recently, Ieda and coworker have reported photochemically activated $ONOO^-$ generators.[14-16] They have synthesized N-methyl-N-nitrosoaminophenol based small molecule, P-NAP as

photocontrollable peroxynitrite generator. This compound upon activation with UV light releases NO and produces semiquinoneimine intermediate, which then reacts with oxygen to produce $O_2^{\bullet-}$ (Scheme 3.3). NO generation from P-NAP was demonstrated using ESR spin trapping method. $ONOO^-$ generation form this compound was shown using peroxynitrite-specific probe, HK Green-3. P-NAP upon activation with UV light efficiently generates peroxynitrite under ambient aerobic conditions. The suitability of this compound to enhance $ONOO^-$ levels in mammalian cells was demonstrated using confocal microscopy. Furthermore, this compound can be used for cellular assay because byproduct (duroquinone) formed after photodecomposition of P-NAP is also less toxic. Although spatiotemporal control over $ONOO^-$ generation is achieved using this method, the use of an external light source may not always be convenient for cell-based studies.

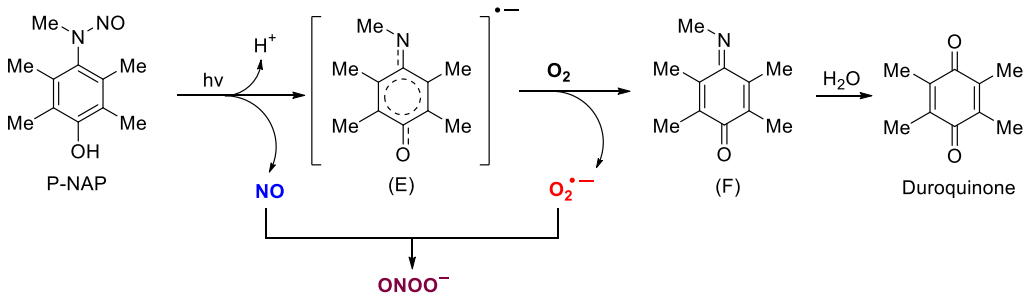

Scheme3.3. Mechanism of NO and $O_2^{\bullet-}$ generation from P-NAP upon activation with UV light

3.1.1.E. Immunomodulatory reagents

Exogenous immunomodulatory reagents such as lipopolysaccharide (LPS), a stimulator of inducible nitric oxide synthase (iNOS, NO biosynthesis enzyme), and phorbol 12-myristate 13-acetate (PMA), a stimulant of superoxide generation are frequently used for inducing intracellular peroxynitrite generation.[3] However, these stimulants can be used only in certain cells such as macrophages and they can activate a large number of cellular pathways that complicate the interpretation of the results. In addition, the inhibitor of iNOS and NADPH oxidase has been used for modulating $ONOO^-$ generation. However, due to lack of their specific inhibitors, this method cannot be used for studying the effects of $ONOO^-$ during host-pathogen interaction.

Thus, taken together, there is no uniform and convenient methodology available to reliably enhance peroxynitrite within cells. We proposed to develop a small molecule peroxynitrite generator with following properties (a) it should be a stable solid; (b) it should co-generate $O_2^{\bullet-}$ and NO upon reaction with cellular trigger.

3.1.2. Design of peroxynitrite generator

In order to maximize the yield of peroxynitrite, the simultaneous generation of $O_2^{\bullet-}$ and NO is essential. In Chapter 2, an efficient $O_2^{\bullet-}$ generation from aromatic hydroquinone intermediate was demonstrated. These hydroquinones can be produced *in situ* by reduction of 1,4-benzoquinone scaffold by bioreductive enzymes such as DT-diaphorase.[17] In order to generate NO, diazeniumdiolates have been used.[18] Diazeniumdiolates undergo hydrolysis to release up to two moles of NO in neutral and acidic solutions. Therefore, diazeniumdiolates are derivatized into stable form by protecting terminal oxygen with different protecting groups.[19] The protected diazeniumdiolates can be metabolized into an active NO-donor by specific enzymes/biological triggers present within cells for intracellular NO release. The choice of protecting group gives opportunity to selectively deliver NO in certain cell type.[20]

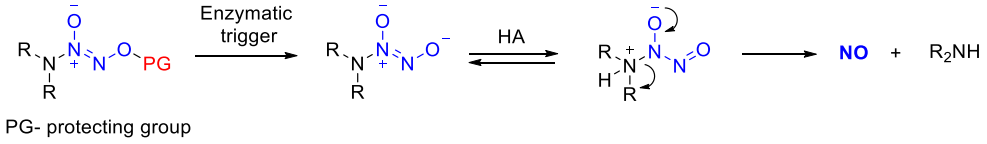

Scheme 3.4. Enzymatic activation of protected diazeniumdiolate to release NO in aqueous medium

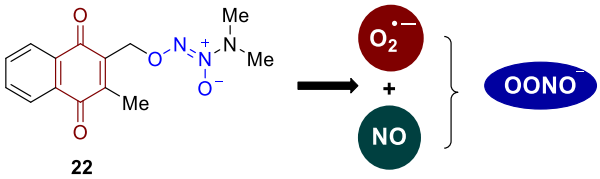

Scheme 3.5. Peroxynitrite donor **22**, where a NO generating diazeniumdiolate is linked to a $O_2^{\bullet-}$ generating 1,4-naphthoquinone group.

We proposed to link 1,4-benzoquione scaffold ($O_2^{\bullet-}$ generator) to diazeniumdiolates (NO donor) in a such way that upon reaction with cellular enzyme it should co-generate $O_2^{\bullet-}$ and NO. Based on this design principle, compound **22** was proposed as a potential candidate for peroxynitrite generation. We predicted that this compound upon bioreduction would produce a hydroquinone

intermediate, which is known to react with O_2 to produce $O_2^{\bullet-}$ and subsequently regenerate parent quinone compound. Alternatively, the hydroquinone intermediate can trigger the electronic rearrangements that lead to expulsion of the DMA/NO, which is known to hydrolyze in buffer to produce NO.[21-22] Together, these two processes can produce proximal fluxes of $O_2^{\bullet-}$ as well as NO, increasing the likelihood of $ONOO^-$ formation.

3.2. Results and Discussion

3.2.1. Synthesis and characterization

In order to test the hypothesis, compound **22** was synthesized in three steps (Scheme 3.6). First, 1,4-dimethoxy-2-methylnaphthalene was reacted with paraformaldehyde and HBr in the presence of acetic acid to give bromomethyl derivative **20** in 43 % yield.[23] Reaction of **20** with sodium *N,N*-(dimethylamino)diazen-1-ium-1,2-diolate (DMA/NO) afforded **21** in 47% yield. Oxidation of **21** by ceric ammonium nitrate gave **22** in a 48% yield.

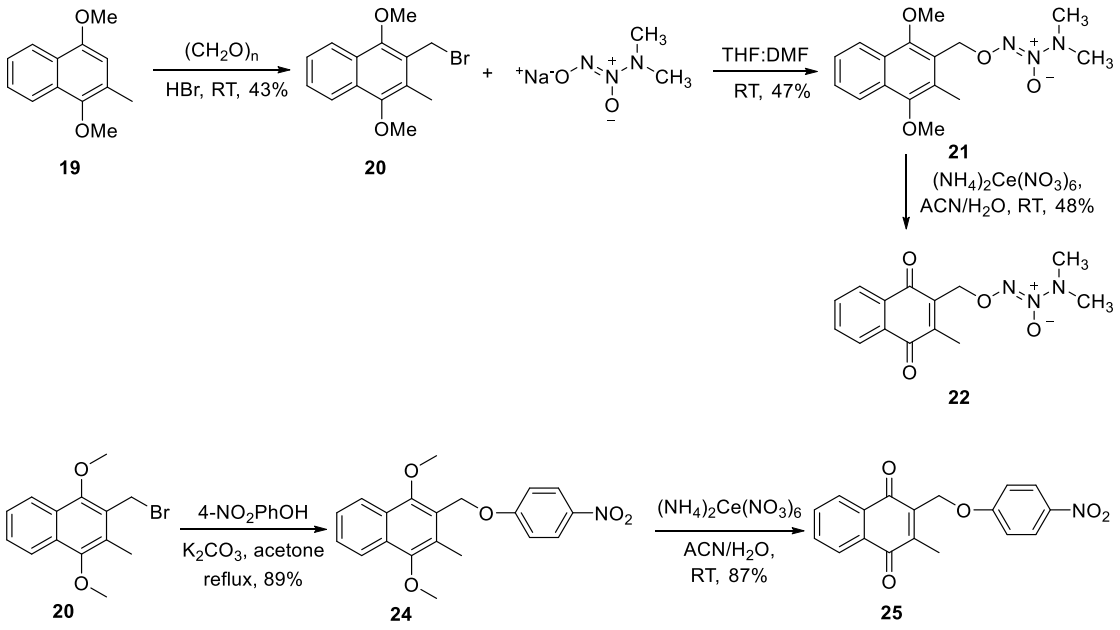

Scheme 3.6. Synthesis of peroxynitrite generator **22** and superoxide generator **25**

In addition, compound **25** was designed and synthesized as a negative control. This compound upon bioreduction would produce a hydroquinone intermediate, which then can trigger the release of 4-nitrophenolate as a byproduct and generate superoxide radical. On the other hand, compound **22** upon bioreduction would release DMA/NO and superoxide radical. The reaction

of 4-nitrophenol with the bromide derivative **20** afforded **24** in excellent yield. Oxidation of **24** carried out using ceric ammonium nitrate to afford **25** in 87% yield (Scheme 3.6). The final compounds **22** and **25** were purified using silica gel column chromatography using hexane and ethyl acetate as eluent. The purity of **22** and **25** was recorded using HPLC and was found to be > 95 %.

3.2.2. Superoxide generation from 22

In order to evaluate the ability of **22** to generate $O_2^{\bullet-}$ in the presence of a bioreductive enzyme, dihydroethidine (DHE) assay was used.[24-25] In this assay, the reaction of DHE with superoxide produces 2-hydroxyethidium (2-OH-E^+) as a specific oxidized product, whereas the non-specific oxidation of DHE with other ROS produces ethidium (E^+) dye. The formation of these oxidized fluorescent products can be monitored using HPLC attached with fluorescent detector.

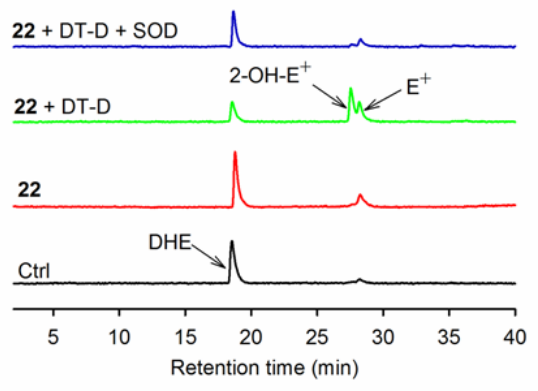

Figure 3.1. Superoxide generated during incubation of **22** (25 μM) with DT-D was estimated using a dihydroethidium (DHE) assay. Ctrl is DHE (25 μM) in pH 7.4 buffer; + DT-D implies DT-diaphorase and NADPH; + SOD implies co-incubation with superoxide dismutase.

DT-diaphorase (DT-D) was used as a model bioreductive enzyme in the presence of cofactor NADH in pH 7.4 buffer. The authentic sample of DHE was injected into HPLC and we observed a peak at 18.7 min corresponding to DHE in the fluorescence channel (λ_{ex}-510 nm and λ_{em}- 595 nm). Next, **22** was incubated in pH 7.4 buffer and injected into a HPLC, but we did not found the evidence of $O_2^{\bullet-}$ generation in the absence of a bioreductive enzyme suggesting the stability of compound in buffer (Figure 3.1). However, incubation of **22** with DT-D gave a peak corresponding to 2-OH-E^+, which confirms the intermediacy of $O_2^{\bullet-}$. When **22** + DT-D was co-incubated with superoxide dismutase (SOD), an enzyme that quenches any $O_2^{\bullet-}$ that is produced,

we found nearly complete disappearance of the peak attributable to 2-OH-E^+ (Figure 3.1). The xanthine and xanthine oxidase (X + XO) were used to generate authentic $O_2^{\bullet-}$ and as expected, under the assay conditions used, a peak for 2-OH-E^+ was seen. Together, these data confirmed the $O_2^{\bullet-}$ generation from **22** upon bioreduction with DT-D.

3.2.3. Nitric oxide generation from 22

The ability of **22** to produce NO was tested using a chemiluminescence based Nitric Oxide Analyzer (NOA).[26] In this assay, NO reacts with O_3 to form NO_2^* which then emits photons to come to ground state. The emitted photons are measured by chemiluminescence detector. The compound **22** was incubated in pH 7.4 buffer and NO release was analyzed using NOA. In the absence of DT-D, compound was found to be stable with no evidence for NO generation. Whereas, in the presence of DT-D, NO generation was seen confirming the ability of **22** to produce NO (Figure 3.2). Under similar conditions, when **22** + DT-D was co-incubated with 2-(4-carboxyphenyl)-4,4,5,5-tetramethylimidazoline-1-oxyl-3-oxide potassium salt (c-PTIO), NO quencher,[27-28] nearly complete disappearance of NO signal (Figure 3.2) was observed. These experiments confirmed the NO generation from **22** upon reaction with DT-D.

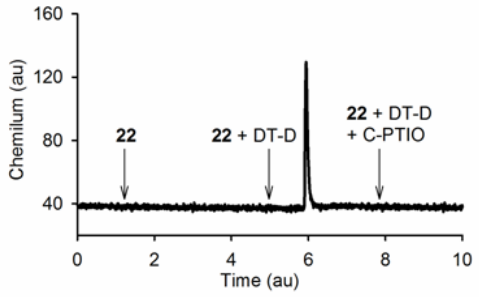

Figure 3.2. NO analysis using a chemiluminescence detector during incubation of **22** (100 μM). + DT-D implies DT-diaphorase and NADPH; + c-PTIO implies co-incubation with c-PTIO. Arrows indicate approximate points of injections of the analyte after 1 h incubation.

3.2.4. Peroxynitrite generation from 22

3.2.4.1. Detection of peroxynitrite using boronate ester probe 23a

Having established the generation of $O_2^{\bullet-}$ and NO from **22**, next we tested if $ONOO^-$ was being produced. Due to its short half-life under physiological conditions, the direct detection and quantification of $ONOO^-$ is challenging. Most existing methods for $ONOO^-$ detection are based

on reaction of its secondary radical species ($^{\bullet}OH$ and $^{\bullet}NO_2$) with small organic molecules such as tyrosine, tryptophan and dihydrorhodamine. Recently, a number of fluorescent probes have been developed for the direct detection of $ONOO^-$. We chose two turn-on fluorescent probes with distinct chemistry to infer the $ONOO^-$ generation. Arylboronic acids are known to rapidly react with peroxynitrite ($\sim 10^6$ $M^{-1}s^{-1}$) and this property has been used for development of peroxynitrite probes. Recently, Kalyanaraman and coworker have developed boronate-containing fluorogenic compounds for peroxynitrite detection. We synthesized peroxynitrite probe **23a** by Pd(II) catalyzed borylation of 3-methyl-2-oxo-*2H*-chromen-7-yl trifluoromethanesulfonate, which in turn was synthesized from 7-hydroxy-3-methylcoumarin and trifluromethanesulfonic anhydride in 65 % yield (Scheme 3.7). The boronate ester of **23a** rapidly undergoes hydrolysis in buffer to produce the boronic acid **23b**. This boronic acid is weakly fluorescent and upon reaction with peroxynitrite produces 3-methyl-7-hydroxycoumarin **23c**, which has a strong fluorescence emission at 460 nm (Scheme 3.8).

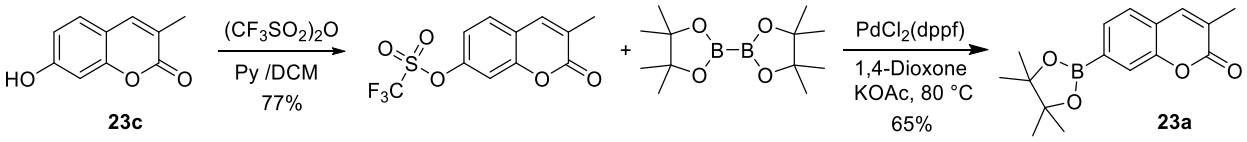

Scheme 3.7. Synthesis of peroxynitrite probe **23a**

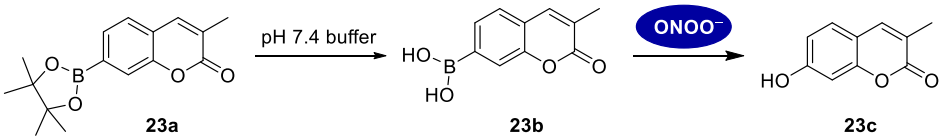

Scheme 3.8. Hydrolysis of peroxynitrite probe **23a** in pH 7.4 buffer to **23b**, which reacts with peroxynitrite to produce fluorescent compound **23c**.

We next measured the peroxynitrite generation from **22** upon reaction with DT-D. When compound **22** was incubated with **23a** in pH 7.4 buffer, no evidence of $ONOO^-$ generation was observed. On the other hand, when **22** incubated with **23a** were exposed to an enzyme DT-D, a distinct increase in fluorescence emission at 460 nm was observed (Figure 3.3A). As arylboronic acids are known to react with hydrogen peroxide as well (with lower rate than peroxynitrite $\sim$ 2-3 $M^{-1}s^{-1}$), the mixture of **22** + DT-D and **23a** was co-incubated with catalase, an enzyme that quenches H_2O_2 by converting it into H_2O and O_2. The emission profiles were recorded and we

observed no major difference in the fluorescence emission profile in presence of catalase (Figure 3.3A). This experiment suggested the peroxynitrite was a major species formed during this reaction. In order to confirm the fluorescence signal obtained during incubation with **22** + DT-D was mainly because of $ONOO^-$ and not due to other ROS such as superoxide and hydrogen peroxide; a similar experiment was conducted with a control compound **25**. We predicted that this compound would undergo bioreduction to generate $O_2^{\bullet-}$ and 4-nitrophenolate, which should not react with peroxynitrite probe to give fluorescence signal. Indeed, when **25** + DT-D was incubated with probe **23a**, negligible increase in fluorescence was observed (Figure 3.3B). The yield of **23c** formed during this assay was estimated as 2.5 % confirming the slow reaction of hydrogen peroxide with boronic acid. Under similar conditions, when H_2O_2 was incubated with peroxynitrite probe **23a**, a small increase in the fluorescence was observed (Figure 3.3B) again confirming the slow reaction of hydrogen peroxide with boronate ester compared with peroxynitrite. Together, these results demonstrated the $ONOO^-$ was the major species generated during incubation of **22** with DT-D.

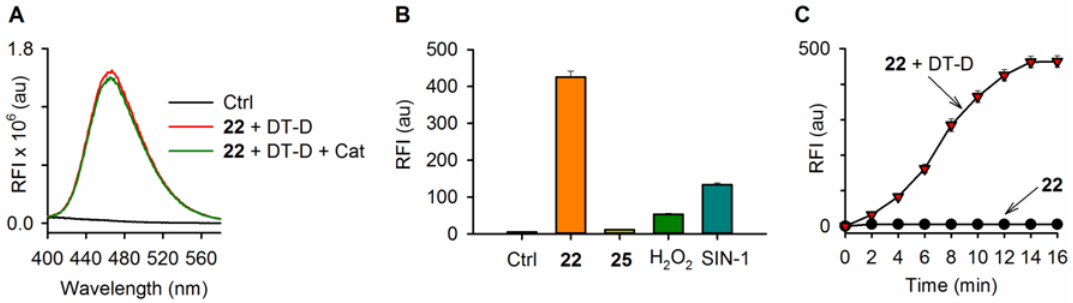

Figure 3.3. Analysis of peroxynitrite generation from **22** (A) Fluorescence emission spectra during incubation of **23a** (100 μM) with **22** (100 μM) + DT-D in PB pH 7.4, (λ_{ex} = 315 nm); In case of an H_2O_2 scavenger, **22** + DT-D was co-incubated with catalase (100 U/mL); Ctrl is **23a** incubated with **22**. (B) Fluorescence intensity of **23a** during incubation with **22** (25 μM) + DT-D and with catalase (100 U/mL); **25** (25 μM) + DT-D and with catalase, H_2O_2 (25 μM) and SIN-1 (25 μM) for 15 min in pH 7.4 buffer. (C) Time course of peroxynitrite generation during the incubation of **22** (50 μM) in the presence of DT-D estimated by a fluorescence based assay.

Unlike other fluorescent dyes, **23a** stoichiometrically reacts with $ONOO^-$ to form fluorescent compound, 3-methyl-7-hydroxycoumarin. Hence, this probe was used for the quantification of $ONOO^-$ generated during incubation of **22** with bioreductive enzyme. First, a calibration curve

was generated using known concentrations of 3-methyl-7-hydroxycoumarin using a 96-well plate reader (Figure S2). The yield of peroxynitrite generated during incubation of **22** with DT-D in pH 7.4 buffer was calculated using standard calibration curve. The compound **22** (25 μM) produced 8.9 μM of peroxynitrite, however, under similar conditions, SIN-1 (25 μM) produced 2.4 μM of peroxynitrite suggesting the superiority of **22** over commercially available source of $ONOO^-$. Next, the real time monitoring of $ONOO^-$ generation from **22** was studied using probe **23a**. The peroxynitrite generator **22** was incubated with DT-D along with probe **23a** and fluorescence was measured using 96 well plate reader. A gradual increase in fluorescence was observed during 15 min (Figure 3.3C). Together, these results confirmed the $ONOO^-$ generation from **22** upon reaction with bioreductive enzyme DT-D.

3.2.4.2. HPLC studies for peroxynitrite detection

Peroxynitrite mediated conversion of **23a** to **23c** in the aforementioned assay was also studied using HPLC based assay. Peroxynitrite probe **23a** rapidly undergoes hydrolysis in buffer to produce boronic acid **23b**, which then reacts with peroxynitrite to form 3-methyl-7-hydroxycoumarin **23c**. This conversion was monitored using HPLC attached with U.V. as well as fluorescence detector.

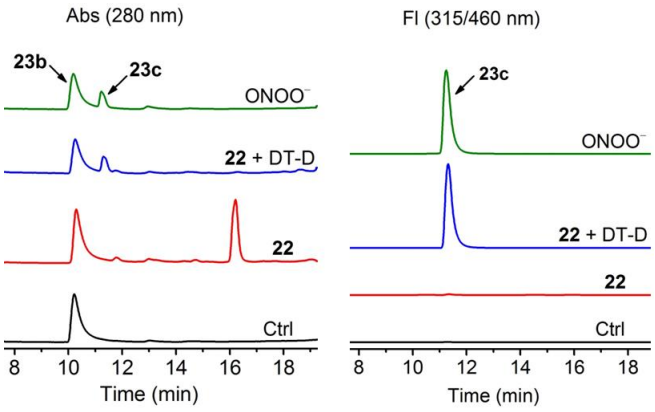

Figure 3.4. HPLC based estimation of $ONOO^-$ generation during incubation of **22** (100 μM) with DT-D in pH 7.4 buffer. Ctrl is **23a** (100 μM) in pH 7.4 buffer; + DT-D implies DT-diaphorase and NADPH; Authentic $ONOO^-$ (100 μM) was used as a positive control. The left panel represents the signal detected using the absorption (Abs) detector set at 280 nm; the right panel represents the signal detected using the fluorescence detector with the excitation set at 315 nm and emission at 460 nm.

When peroxynitrite probe **23a** was incubated in pH 7.4 buffer, the HPLC analysis revealed the formation of new peak at 10.2 min corresponding to **23b** confirming the hydrolysis of boronate ester to boronic acid (Figure 3.4). Next, compound **22** was incubated with probe **23a** and injected into a HPLC. The HPLC analysis revealed no significant change in the peak attributable to **23b** during 1h incubation, suggesting the stability of peroxynitrite generator under physiological conditions. However, when **22** was exposed to DT-D in the presence of peroxynitrite probe **23a**, we observed a new peak at 11.3 min corresponding to **23c** (Figure, 3.4, left panel). Furthermore, when fluorescence detector was used in this HPLC analysis, we found a distinct peak corresponding to **23c** at the same retention time of 11.3 min (Figure 3.4, right panel). A similar experiment was conducted with an authentic $ONOO^-$ solution and the formation of **23c** was independently verified. Thus, the HPLC based experiment confirmed the peroxynitrite generation from **22** upon activation with bioreductive enzyme.

3.2.4.3. Peroxynitrite detection using Ds-DAB

The ability of **22** to generate $ONOO^-$ was independently verified using *N*-(2-aminophenyl)-5-(dimethylamino)-1-naphthalene sulfonic amide (Ds-DAB), a probe that is reported to be sensitive to $ONOO^-$. The peroxynitrite probe Ds-DAB was synthesized using a reported procedure.[29] The reaction of dansylcholride with o-phenylenediamine afforded Ds-DAB in 90% yield (Scheme 3.9). This probe is highly specific and sensitive for peroxynitrite and it avoids interference from other ROS and RNS. The reaction of $ONOO^-$ with Ds-DAB produces dansylsulfonic acid, which has a strong fluorescence emission at 505 nm.

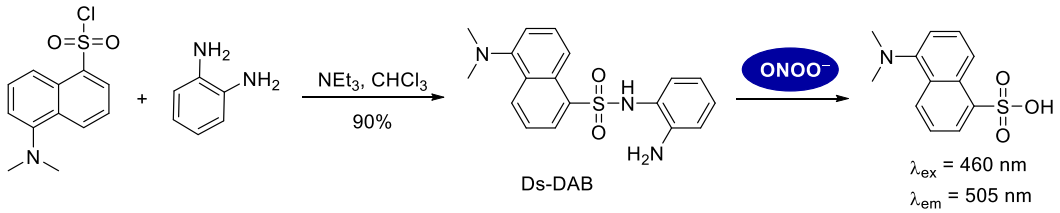

Scheme 3.9. Synthesis of Ds-DAB and its reaction with $ONOO^-$ to produce dansylsulfonic acid.

The peroxynitrite generated during incubation of **22** with DT-D was measured using Ds-DAB. When Ds-DAB was incubated with authentic $ONOO^-$, a characteristic fluorescence emission at 505 nm was observed (Figure 3.5). Similarly, when Ds-DAB was incubated with **22** in the

presence of DT-D, we found a similar increase in fluorescence (Figure 3.5) confirming the generation of $ONOO^-$. The fluorescence intensity obtained from **22** + DT-D was found to be comparatively less than authentic peroxynitrite, because this compound produces 36% of peroxynitrite (8.9 μM of $ONOO^-$ from 25 μM of **22**), whereas authentic $ONOO^-$ was used at 100 μM during this assay.

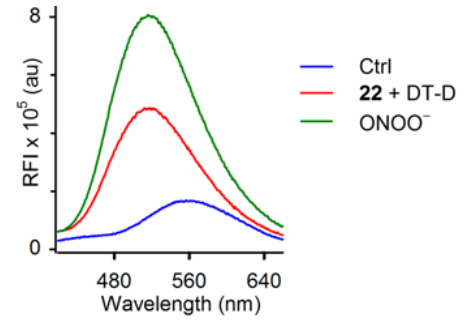

Figure 3.5. Fluorescence emission spectra of Ds-DAB (10 μM) during incubation with **22** (100 μM) + DT-D in pH 7.4 buffer (λ_{ex} = 350 nm); Authentic peroxynitrite (100 μM) was reacted with Ds-DAB and served as a positive control; Ctrl is Ds-DAB (10 μM) in pH 7.4 buffer.

3.2.5. Peroxynitrite mediated tyrosine nitration

At elevated concentrations, peroxynitrite induces nitration of the amino acid tyrosine to produce 3-nitrotyrosine.[30-32] Under physiological conditions, $ONOO^-$ reacts rapidly with CO_2 to yield nitrosoperoxocarbonate intermediate ($ONOOCO_2^-$). This intermediate undergoes homolysis to yield a carbonate ($CO_3^{\bullet-}$) and nitrogen dioxide ($^{\bullet}NO_2$) radicals,[33-35] both of which participate in the tyrosine nitration.[36] The product 3-nitrotyrosine has been identified as the hallmark footprint of peroxynitrite. Tyrosine nitration is known to trigger an aberrant protein function and elevated levels of nitrotyrosine are associated with numerous disease states.[30-32]

Next, peroxynitrite generation from **22** was independently assessed using tyrosine nitration assay. The formation of 3-nitrotyrosine was measured using HPLC based assay. When tyrosine was incubated with **22** + DT-D, we found a distinct peak for 3-nitrotyrosine (Figure 3.6A). In addition, the formation of 3-nitrotyrosine during this assay was also confirmed by mass spectrometry m/z 226.19. Under similar conditions, when tyrosine was incubated with authentic $ONOO^-$, we observed a similar peak attributable to 3-nitrotyrosine (Figure 3.6B). Peroxynitrite at low concentration has been reported to dimerize tyrosine to dityrosine,[11] a fluorescent

molecule. The formation of dityrosine was assessed using HPLC attached with a fluorescence detector. When tyrosine was incubated with **22** + DT-D, we found enhanced levels of dityrosineas determined by a characteristic fluorescent signal for this dimer (Figure S3). The formation of dityrosine was also confirmed by mass spectrometry m/z 361.16 (Figure S12). Thus, formation of 3-nitrotyrosine during incubation of tyrosine with **22** + DT-D confirmed $ONOO^-$ generation.

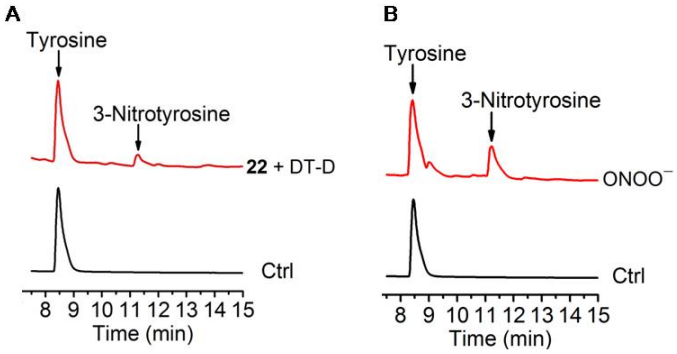

Figure 3.6. (A) HPLC traces for peroxynitrite mediated tyrosine nitration during incubation of tyrosine (500 μM) with **22** (300 μM) + DT-D; Control is tyrosine incubated with **22** in the absence of DT-D (B) 3-nitrotyrosine formation during incubation of authentic $ONOO^-$ (100 μM) with tyrosine in pH 7.4 buffer.

3.2.6. Mechanisms of peroxynitrite generation

A mechanism for $ONOO^-$ generation from **22** involving enzyme triggered generation of $O_2^{\bullet-}$ and NO was proposed (Scheme 3.10). Quinones are substrates of $1e^-$ reductases, such as cytochrome P450s, cytochrome b5, xanthine oxidase, and glutathione reductase.[37-38] Reduction of **22** by these enzymes can generate a highly reactive semiquinone intermediate **I**, that can either undergo oxidation with molecular oxygen resulting in the formation of superoxide radical and the parent quinone or it can further undergo $1e^-$ reduction to form intermediate **II**. Alternatively, intermediate **II** can be directly formed by reduction with $2e^-$ reductases, which can trigger the rearrangement of electrons that result in departure of leaving group. DT-diaphorase (2-electron reductase) was used as a model bioreductive enzyme during mechanistic studies. We predicted that, **22** upon bioreduction with DT-D would produce hydroquinone intermediate **II**, which then can trigger the rearrangement of electrons that results in the departure of leaving group either the DMA/NO in the case of **22** or 4-nitrophenolate in the case of **25**. Indeed, when **22** was incubated

with DT-D, instant burst release of NO was observed suggesting departure of DMA/NO from the hydroquinone intermediate.

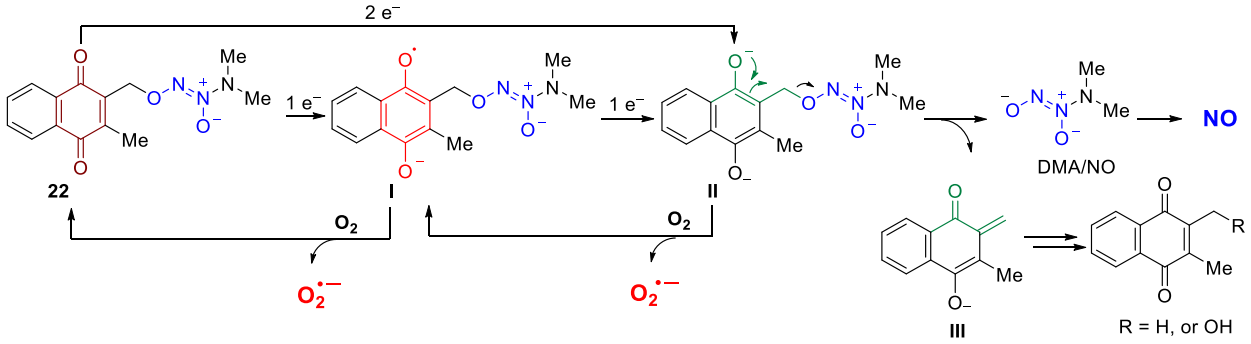

Scheme 3.10. Proposed mechanism for $O_2^{\bullet-}$ and NO generation during incubation of **22** with a bioreductive enzyme

HPLC decomposition study was conducted with **22** in the presence of DT-D and nearly complete disappearance of **22** was observed within 10 minutes of incubation. Similarly, when **25** was incubated with DT-D, a HPLC analysis revealed the formation of new peak at 7.5 min. corresponding to 4-nitrophenol (Figure 3.7). Interestingly, similar byproducts were obtained from **22** and **25**, which suggest that both of these compounds follow similar decomposition mechanism (Figure 3.7).

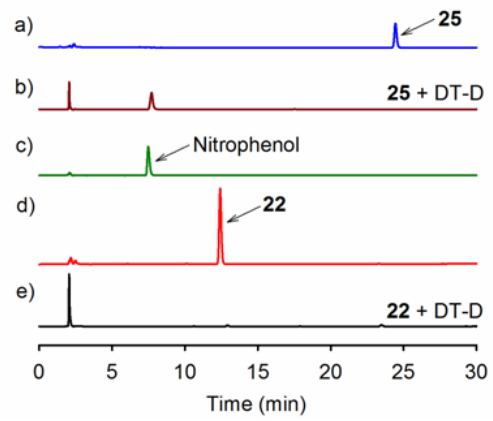

Figure 3.7. HPLC traces for decomposition of **22** and **25** in the presence and absence of DT-D. (a) A solution of **25** (25 µM) in pH 7.4 buffer; (b) A solution of **25** + DT-D after incubation for 10 min; (c) A solution of authentic 4-nitrophenol (25 µM); (d) A solution of **22** (25 µM); (e) A solution of **22** + DT-D after incubation for 10 min.

Lastly, the likely byproduct formed after departure of the DMA/NO is **III**, which can either react with water to produce 2-hydroxymethyl-3-methyl-1,4-naphthoquinone or rearrange to give 2,3-dimethyl-1,4-naphthoquinone (Scheme 3.10). Our TLC analysis revealed the formation of 2-hydroxymethyl-3-methyl-1,4-naphthoquinone during this reaction. After verifying the proposed mechanism of NO generation, we proceeded to validate the superoxide generation from **22**. The bioreduction of **22** by DT-D would generate a highly reactive hydroquinone intermediate **II**, which can transfer an electron to molecular oxygen to produce superoxide. Indeed, when **22** was incubated with DT-D, the superoxide generation was observed as detected by DHE assay. In addition, superoxide generation was inferred indirectly by measuring NO in the presence of superoxide dismutase, a quencher of superoxide. We expected that the yield of NO should increase in the presence of superoxide dismutase, due to a decrease in the availability of $O_2^{\bullet-}$ to react with NO to form peroxynitrite. Indeed, when NO was measured in the presence SOD, a higher NO production was observed confirming the intermediacy of superoxide (Figure 3.8A).

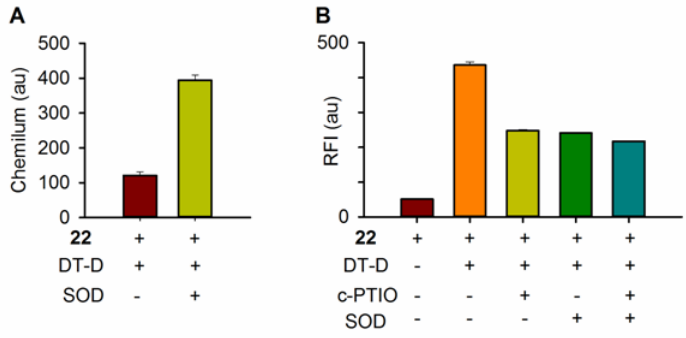

Figure 3.8. (A) NO generation from **22** + DT-D with and without superoxide dismutase (SOD) in pH 7.4 buffer. (B) Fluorescence intensity of **23a** during incubation of **22** + DT-D and in the presence of c-PTIO, SOD and both in pH 7.4 buffer.

The peroxynitrite generation was also confirmed by measuring the yield of peroxynitrite in the presence of scavengers of NO and $O_2^{\bullet-}$. The yield of $ONOO^-$ from **22** is expected to decrease if either NO or $O_2^{\bullet-}$ is partially quenched. Indeed, when **22** + DT-D was co-incubated with c-PTIO, the yield $ONOO^-$ reduced as expected (Figure 3.8B). A similar experiment was conducted in the presence of SOD and we found diminished yields of $ONOO^-$. Further when both c-PTIO as well as SOD were added to **22** + DT-D, the yield of $ONOO^-$ reduced further (Figure 3.8B). These

studies support the proposed mechanism outlined in scheme 3.10. One potential limitation with this compound could be more superoxide generation from quinone byproduct formed during this reaction; however head-to-head comparisons with SIN-1 demonstrates the superiority of **22** as a peroxynitrite donor in cell-free system.

3.2.7. Intracellular peroxynitrite generation

Having established $ONOO^-$ generation in buffer, the ability of **22** to permeate mammalian cells and enhance $ONOO^-$ level was tested using Ds-DAB. Human adenocarcinoma DLD-1 cells pre-incubated with Ds-DAB were treated with **22** and a fluorescence signal at 505 nm was measured using confocal microscopy. An increase in fluorescence in cells treated with **22** was observed (Figure 3.9). Under similar conditions, when DLD-1 cells were treated with authentic $ONOO^-$, a diminished fluorescence signal was observed compared to **22** possibly due to poor cell permeability of authentic peroxynitrite solution (Figure 3.9).

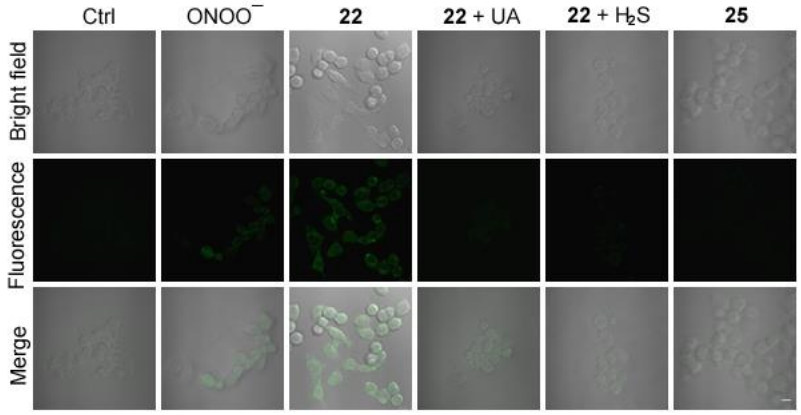

Figure 3.9. $ONOO^-$ generation in DLD-1 cells by **22**. DLD-1 cells were preincubated with Ds-DAB (10 μM) for 30 min and then incubated with $ONOO^-$ solution (25 μM) or **22** (25 μM) for 1h; Also, cells were pre-incubated with uric acid (100 μM) for 1 h or sodium sulphide (100 μM) for 10 min and then co-incubated with Ds-DAB and **22**; Cells were treated with $O_2^{\bullet-}$ generator **25** (25 μM) which served as negative control; bright field (top lane); fluorescence (middle lane); merge (bottom lane).Scale bar: 10 μm.

The ability of **22** to generate peroxynitrite in cells was studied in the presence of its scavenger. We expected that in the presence of peroxynitrite scavenger, the fluorescence signal attributed to

peroxynitrite would diminish. Indeed, when DLD-1 cells pretreated with uric acid (UA), a quencher of peroxynitrite[39-41], were co-incubated with **22** and Ds-DAB, we found nearly complete abrogation of signal attributable to $ONOO^-$. Next, cells pre-treated with hydrogen sulfide, a reported antioxidant that directly interacts with $ONOO^-$,[42-43] were exposed to **22** + Ds-DAB (Figure 3.9). Again, we found diminished fluorescence possibly due to decomposition of $ONOO^-$ induced by hydrogen sulfide. In order to confirm the fluorescence signal obtained during incubation of **22** is due to peroxynitrite and not due to reactive oxygen species, a similar experiment was conducted with a control compound **25**. DLD-1 cells pre-incubated with Ds-DAB were treated with the $O_2^{\bullet-}$ generator **25** and fluorescence was measured using confocal microscopy. As expected, no fluorescence signal was seen) confirming the peroxynitrite generation from **22** (Figure 3.9.)

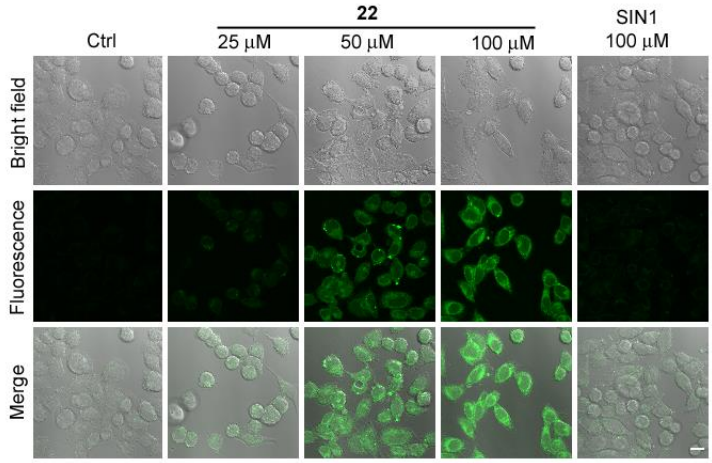

Figure 3.10. Peroxynitrite generation in DLD-1 cells treated with **22** at 25, 50, 100 μM and SIN-1 (100 μM) for 1 h using Ds-DAB; Ctrl is untreated DLD-1 cells; scale bar: 10 μm.

Next, DLD-1 cells were treated with increasing concentrations of **22** and a dose-dependent increase in the fluorescence was seen supporting the reliability of this donor in enhancing intracellular $ONOO^-$ (Figure 3.10). We also measured the peroxynitrite generation from commercially available peroxynitrite donor SIN-1 in DLD-1 cells. However, SIN-1 had diminished capacity to enhance $ONOO^-$ in DLD-1 cells under similar conditions and an elevated concentration of 100 μM was necessary for a significant signal to be recorded (Figure 3.10). The suitability of **22** to enhance $ONOO^-$ in a variety of cell lines including SW480 colon cancer

cells, A549 lung cancer cells and primary corneal fibroblast cells was demonstrated by confocal microscopy (Figures 3.11). The levels of peroxynitrite produced during incubation of cells with **22** will depend on the cellular expression of bioreductive enzymes as well as oxygen concentrations. However, our data shows that **22** uniformly generated $ONOO^-$ in a dose-dependent manner as well as in a variety of cell types.

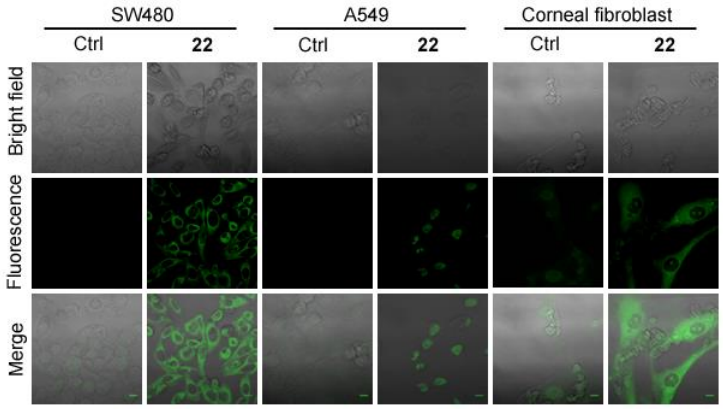

Figure 3.11. Fluorescence images of SW480, A549 and corneal fibroblast cells treated with Ds-DAB (10 μM) for 30 min and then incubated with **22** (25 μM) for 1h; Scale bar: 10 μm

3.2.8. Peroxynitrite generation in bacteria

In response to infections, the immune cells like macrophages produce fluxes of superoxide and nitric oxide, which presumably combines to produce peroxynitrite. Being a strong oxidant and nitrating agent, peroxynitrite can react with different biomolecules, including nucleic acids, proteins, lipids and transition-metal containing enzyme centers through direct oxidation, which can possibly lead to cell death. In contrast, bacteria counter oxidative and nitrosative stresses induced by peroxynitrite by producing antioxidants and expressing $ONOO^-$ detoxifying enzymes such as alkylhydroperoxide reductase (AhpCF) and catalase-hydroperoxidase (KatG).[44-45] The interaction of peroxynitrite with antioxidants and peroxynitrite detoxifying enzymes plays critical role during survival of bacteria from the arsenal of host-derived reactive species. However, studying this interaction is challenging due to lack of reliable method available for generation of this reactive species. The most common strategies used for studying the role of $ONOO^-$ during host-pathogen interactions involve the use of inhibitors of iNOS or NADPH oxidase. However, there is no effective and specific NADPH oxidase inhibitor and iNOS

inhibitor. Furthermore, the knockout of one of these proteins in mice has been used for modulating $ONOO^-$ generation, but mice lacking some of the subunits of NADPH oxidase or iNOS deficiency are more prone to infections.[46] Although a strong argument has been made in the literature regarding the importance of reactive nitrogen species in controlling invasion of microorganisms but assessing their cellular effects *in vivo* are challenging.

The small molecule peroxynitrite generator developed by us might give opportunity to study the role of this reactive species during host-pathogen interaction. For proof of concept, we have studied the cytotoxicity of peroxynitrite generator against different bacteria. First, the inhibitory potential of **22** was tested against methicillin sensitive *Staphylococcus aureus* (MSSA). Compound **22** showed potent inhibitory activity against MSSA with MIC of 2 μg/mL. Similarly, the inhibitory activity of this compound was tested against methicillin resistant *S. aureus* (MRSA) and this compound showed potent inhibitory activity with MIC 2μg/mL. The inhibitory potential of peroxynitrite generator was also tested against gram negative bacteria: *Escherichia coli and Pseudomonas aeruginosa.* However, compound **22** was found to be inactive against these two gram-negative bacteria. These results suggested that gram-positive bacterium *S. aureus* appears sensitive to peroxynitrite.

3.3. Conclusion and outlook

In this chapter, we presented the design and synthesis of novel small molecule **22** as a controlled $ONOO^-$ generator. This compound produces temporally concurrent fluxes of superoxide and nitric oxide in the presence of DT-D. The $ONOO^-$ generation from **22** was demonstrated using several independent assays. In particular, an arylboronic acid-based probe **23a** was used to demonstrate the controlled generation of $ONOO^-$. Similarly, peroxynitrite generation was also inferred using tyrosine nitration assay and we observed 3-nitrotyrosine formation during incubation of tyrosine with **22** + DT-D. The yield of $ONOO^-$ generated from **22** was quantified in cell-free system and we found $ONOO^-$ yields superior than SIN-1. The ability of this small molecule to permeate mammalian cells and enhance intracellular peroxynitrite level was demonstrated in variety of cancer cell lines. Furthermore, this compound also showed superior peroxynitrite generation within cells when compared with SIN-1 and authentic peroxynitrite. The spatiotemporal control over $ONOO^-$ generation offered by this tool allowed us to study the effects of this reactive species in bacteria as well. The $ONOO^-$ generator exhibited potent inhibitory activity against gram positive bacterium *S. aureus,* but gram-negative bacteria *E. coli* tolerated this compound, suggesting sensitivity of *S. aureus* toward peroxynitrite. In summary, we have developed a novel small molecule that reliably enhances peroxynitrite level in cells and we believe that **22** will be a useful tool for controllable $ONOO^-$ generation in biological research.

The $ONOO^-$ generator that we have developed here can favor $O_2^{\bullet-}$ than NO because the byproduct formed after release of $ONOO^-$ can further undergo bioreduction to generate $O_2^{\bullet-}$. However, the use of control compounds such as $O_2^{\bullet-}$ generator **25** would be useful for differentiating peroxynitrite effects from ROS. Further, peroxynitrite generation efficiency can be improved by altering the kinetics of NO and $O_2^{\bullet-}$ generation. Since diazeniumdiolates have variable half-lives, the rate of NO generation can be altered by changing the diazeniumdiolate. Similarly, rate of $O_2^{\bullet-}$ generation can be varied by the structural modification on quinone scaffold. Thus, further future work warrant for the improving the yield and specificity of peroxynitrite generation.

3.4. Experimental Section

3.4.1. Synthesis and characterization

Compounds **20**[23], **23c**[47] and Ds-DAB[29] have been previously reported and analytical data that we collected were consistent with the reported values.

(1,4-Dimethoxy-3-methylnaphthalen-2-yl)methyl-1-[1-(*N*,*N*-dimethylamino) diazen-1-ium-1,2-diol-2-ate] (21)

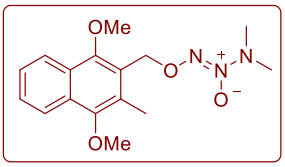

To an ice cold solution of sodium *N*,*N*-(dimethylamino)diazen-1-ium-1,2-diolate (0.32 g, 2.54 mmol) in THF (10 mL) and DMF (5 mL), 15-crown-5 (0.05 mL) was added and stirred at 0 °C for 15 min under a nitrogen atmosphere. Compound **20** (0.50 g, 1.69 mmol) was added to the reaction mixture at 0 °C. The resulting mixture was allowed to warm up to room temperature (RT) and stirred for 12 h at RT. The mixture was diluted with water (25 mL) and extracted with ethyl acetate (15 mL × 3). The combined organic layer was washed with brine, dried over sodium sulfate, filtered and the filtrate was concentrated to give crude compound, which was purified using silica gel column chromatography using 10% EtOAc/hexane as eluent to afford **21** as a colorless semi-solid (0.25 g, 47%): FT-IR (ν_{max}, cm^{-1}): 1592, 1497, 1353, 1269, 1190, 1085, 773; ^{1}H NMR (400 MHz, $CDCl_3$): δ 8.10–8.06 (m, 2H), 7.54-7.45 (m, 2H), 5.50 (s, 2H), 3.99 (s, 3H), 3.86 (s, 3H), 2.98 (s, 6H), 2.51 (s, 3H); ^{13}C NMR (100 MHz, $CDCl_3$): δ 152.7, 150.1, 129.4, 127.2, 127.0, 126.9, 125.6, 123.9, 122.9, 122.2, 68.0, 63.8, 61.4, 42.8, 12.4; HRMS (ESI): calcd. for $C_{16}H_{21}N_3O_4$ $[M+Na]^+$: Calcd. 342.1430, Found 342.1429.

2-Methyl-3-[1-(*N*,*N*-Dimethylamino)diazen-1-ium-1,2-diol-2-ato-methyl]-naphthalene-1,4-dione (22)

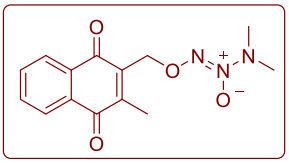

To a solution of **21** (88 mg, 0.28 mmol) in acetonitrile (6 mL) and water (3 mL), ceric ammonium nitrate (450 mg, 0.83 mmol) was added, and the mixture was stirred at RT for 20 min. The resulting mixture was diluted with water (10 mL) and extracted with chloroform (10 mL × 3). The combined organic layer was dried over sodium sulfate, filtered and the filtrate was concentrated to give crude compound, which was purified using silica gel column chromatography using 12% EtOAc/Pet ether as eluent to afford **22** as a yellow solid (38 mg, 48%): mp 125-127 ºC; FT-IR (ν_{max}, cm^{-}

[1]):1663, 1594, 1493, 1380, 1295, 1188, 1001, 791; ^{1}H NMR (400 MHz, $CDCl_3$): δ 8.11-8.08 (m, 2H), 7.73–7.71 (m, 2H), 5.30 (s, 2H), 2.98 (s, 6H), 2.33 (s, 3H); ^{13}C NMR (100 MHz, $CDCl_3$): δ 185.2, 183.3, 148.8, 138.8, 134.0, 133.8, 132.2, 131.9, 126.7, 126.6, 65.7, 42.7, 13.3; HRMS (ESI): calcd. For $C_{14}H_{15}N_3O_4$ $[M+Na]^+$: 312.0960; Found: 312.0956.

3-Methyl-2-oxo-*2H*-chromen-7-yl trifluoromethanesulfonate

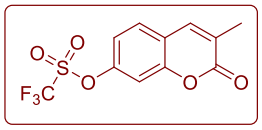

To a solution of 3-methyl-7-hydroxycoumarin(1 g, 5.68 mmol) in anhydrous CH_2Cl_2 (20 mL), pyridine (0.46 mL, 5.68 mmol) was added at 0 ºC and stirred for 30 min. To this mixture, trifluoromethanesulfonic anhydride (1.15 mL, 6.81 mmol) was added drop wise at 0 ºC under N_2 atmosphere. The resulting mixture was allowed to warm up to RT and stirred for 24 h. The mixture was diluted with water (25 mL) and aqueous solution was extracted with CH_2Cl_2 (15 mL × 3). The combined organic layer was washed with brine, dried over sodium sulfate, filtered and the filtrate was concentrated to give crude compound, which was purified using silica gel column chromatography using 10 % EtOAc/Pet ether as eluent to afford 3-methyl-2-oxo-*2H*-chromen-7-yl trifluoromethanesulfonate as a white solid (1.35 g, 77%): mp 75-77 ºC; FT-IR (ν_{max}, cm^{-1}): 3054, 2930, 1727, 1647, 1606, 1541, 1419, 1368, 1200, 1123; ^{1}H NMR (400 MHz, $CDCl_3$): δ 7.53 (d, *J* = 1.3 Hz, 1H), 7.51 (d, *J* = 8.6 Hz, 1H), 7.25 (d, *J* = 2.4 Hz, 1H), 7.19 (dd, *J* = 8.6, 2.4 Hz, 1H), 2.23 (d, *J* = 1.3 Hz, 3H); ^{13}C NMR (100 MHz, $CDCl_3$): δ 161.1, 153.7, 149.9, 137.9, 128.5, 127.4, 120.4, 119.7, 117.7, 110.2, 17.4; HRMS (ESI): calcd. for $C_{11}H_7F_3O_5S[M+H]^+$: Calcd. 309.0045, Found 309.0045.

3-Methyl-7-(4,4,5,5-tetramethyl-1,3,2-dioxaborolan-2-yl)-*2H*-chromen-2-one (23a)

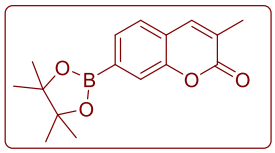

To a suspension of 3-methyl-2-oxo-*2H*-chromen-7-yl trifluoromethanesulfonate (0.5 g, 1.62 mmol), bis(pinacolato)diboron (0.49 g, 1.95 mmol) and potassium acetate (0.48 g, 4.86 mmol) in dioxane (10 mL), $[PdCl_2(dppf)]CH_2Cl_2$ (40 mg, 0.04 mmol) was added. The resulting mixture was refluxed for 12 h. Then, the reaction mixture was filtered (celite) and the filtrate was diluted with water and extracted in ethyl acetate (10 mL ×3). The combined organic layer was washed with brine, dried over sodium sulfate and solvent was separated and evaporated under reduced pressure. The crude compound was purified using silica gel chromatography using 15 %

EtOAc/pet ether as eluent to afford **23a** (0.30 g, 65%) as a white solid: mp 168-170 ºC; FT-IR (ν_{max}, cm^{-1}): 3743, 2969, 2361, 2318, 1708, 1646, 1532, 1484, 1391, 1141; ^{1}H NMR (400 MHz, $CDCl_3$): δ 7.71 (s, 1H), 7.64 (d, *J* = 7.5 Hz, 1H), 7.50 (s, 1H), 7.39 (d, *J* = 7.6 Hz, 1H), 2.22 (d, *J* = 1.1 Hz, 3H), 1.35 (s, 12H); ^{13}C NMR (100 MHz, $CDCl_3$): δ 162.4, 152.8, 139.1, 130.3, 127.1, 126.3, 122.5, 121.8, 84.5, 25.0, 17.5; HRMS (ESI): calcd. for $C_{16}H_{19}BO_4$ $[M+H]^+$: Calcd. 287.1455, Found 287.1456.

1,4-Dimethoxy-2-methyl-3-((4-nitrophenoxy)methyl)naphthalene (24)

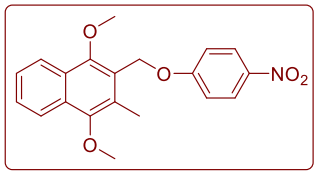

To a solution of **20** (200 mg, 0.67 mmol) in acetone (10 mL), 4-nitrophenol (95 mg, 0.67 mmol) and potassium carbonate (94 mg, 0.67 mmol) was added and the mixture was refluxed for 3 h. This mixture was filtered and the filtrate was concentrated under reduced pressure. The crude compound thus obtained, was purified using silica gel column chromatography using 10% EtOAc/Pet ether as eluent to afford **24** as a colorless solid (213 mg, 89%): mp 177-179 ºC; FT-IR (ν_{max}, cm^{-1}): 1586, 1501, 1451, 1377, 1331, 1330, 1244, 1178; ^{1}H NMR (400 MHz, $CDCl_3$): δ 8.24 (d, *J* = 9.2 Hz, 2H), 8.25-8.10 (m, 2H), 7.62 – 7.47 (m, 2H), 7.14 (d, *J* = 9.2 Hz, 2H), 5.38 (s, 2H), 3.95 (s, 3H), 3.90 (s, 3H), 2.48 (s, 3H).^{13}C NMR (100 MHz, $CDCl_3$): δ 164.0, 152.3, 150.7, 141.9, 129.6, 127.2, 127.2, 126.9, 126.2, 126.1, 124.0, 123.0, 122.5, 114.9, 64.1, 63.7, 61.6, 12.3;MALDI (TOF-TOF):calcd. for $C_{20}H_{19}NO_5$ $[M+H]^+$: Calcd. 354.12, Found 354.10

2-Methyl-3-((4-nitrophenoxy)methyl)naphthalene-1,4-dione (25)

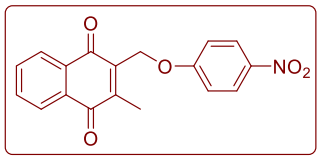

To a solution of **24** (200 mg, 0.56 mmol) in acetonitrile (10 mL) and water (5 mL), ceric ammonium nitrate (931 mg, 1.70 mmol) was added, and the mixture was stirred at RT for 20 min. The resulting mixture was diluted with water (10 mL) and extracted with chloroform (10 mL × 3). The combined organic layer was dried over sodium sulfate, filtered and the filtrate was concentrated to give crude compound, which was purified using silica gel column chromatography using 10% EtOAc/Pet ether as eluent to afford **25** as a yellow solid (159 mg, 87%): mp 145-147 ºC; FT-IR (ν_{max}, cm^{-1}):1659, 1586, 1499, 1457, 1383, 1333, 1291, 1169; ^{1}H NMR (400 MHz, $CDCl_3$): δ 8.22 (d, *J* = 9.1 Hz, 2H), 8.18–8.07 (m, 2H), 7.82–7.72 (m, 2H), 7.06 (d, *J* = 9.1 Hz, 2H), 5.24 (s, 2H), 2.34 (s, 3H); ^{13}C NMR (100 MHz, $CDCl_3$): δ 185.0, 183.6, 163.4, 148.9, 142.1, 138.8,

134.2, 134.1, 132.1, 131.7, 126.8, 126.7, 126.1, 114.8, 61.5, 13.4; HRMS (ESI): calcd. For $C_{18}H_{13}NO_5$ $[M+H]^+$: 324.0872; Found: 324.0867.

3.4.2. Synthesis of peroxynitrite solution

The authentic peroxynitrite solution was prepared using a reported procedure.[48] A solution of 30 % H_2O_2 (5.7 mL) was diluted to 50 mL with water and cooled to 4 ºC. To this cooled solution, 5N NaOH (30 mL) and 0.04M DTPA (5 mL) were added and the mixture was diluted to 100 mL with water. The resulting mixture was stirred vigorously with an equimolar amount of isoamyl nitrite (6.7 mL) for 3–4 h at RT. The progress of reaction was monitored by withdrawing aliquots at an interval of 15 or 30 min, and assaying for peroxynitrite at 302 nm by UV/Vis spectrophotometer. After the absorption at 302 nm reached saturation, the aqueous phase was washed with dichloromethane, chloroform, and hexane (100 mL x 3) to remove the isoamyl alcohol and the remaining isoamyl nitrite. The aqueous phase was passed through granular MnO_2 (25 g) to remove unreacted H_2O_2. The concentration of the stock solution of peroxynitrite was measured after 500 times dilution with 0.1 N NaOH solution and then assaying for peroxynitrite at 302 nm (ε =1670 M^{-1} cm^{-1}) was done by UV/Vis spectrophotometric method.

3.4.3. Dihydroethidium (DHE) assay for detection of superoxide

A stock solution of DT-diaphorase was prepared by dissolving 1.5 mg of the lyophilized human DT-Diaphorase (DT-D, Sigma, ≥100 units (U); wherein 1 U is 1.0 μmol cytochrome c reduced per min/mg) in phosphate buffer (PB) pH 7.4 (1 mL). 20 μL of this enzyme solution was further diluted to 100 μL PB and was used in the following experiments. A stock solution of NADH (10 mM) was prepared in PB pH 7.4.A stock solution of dihydroethidium (0.8 mg, 10 mM) was prepared in DMSO (253 μL) and stored in the dark at –20 °C. The reaction mixture was prepared by dissolving of **22** (5 μL, 2.5 mM), NADH solution (50 μL, 1 mM), dihydroethidium (2.5 μL, 10 mM) and 5 μL of DT-D enzyme solution in pH 7.4 HEPES buffer (437.5 μL). The reaction mixture denoted as **22** + DT-D was incubated at 37 ºC for 1 h. The resulting mixture was filtered (0.22 μm) and injected (50 μL) in a HPLC (Agilent Technologies 1260 Infinity). The mobile phase was H_2O/CH_3CN containing 0.1 % trifluroacetic acid. The stationary phase was a C-18 reverse-phase column (5 μm, 4.6 × 250 mm). DHE, ethidium (E^+) and 2-hydroxyethidium (2-OH-E^+) were separated by a linear increase in CH_3CN concentration from 10% to 70% in 46 min at a flow rate of 0.5 mL/ min. The elution was monitored by a UV-visible detector at 210 nm and

350 nm as well as a fluorescence detector with excitation at 510 and emission at 595 nm, respectively. Hypoxanthine (5 µL, 2.5 mM) and xanthine oxidase (5 µL of 0.02 U/mL) were reacted with DHE (2.5 µL, 10 mM) in HEPES buffer (pH 7.4, 487.5 µL) for 15 min and served as a positive control. For the experiment with superoxide dismutase (SOD from bovine erythrocytes 5 µL, 200 U/mL) was mixed with the reaction mixture of **22** + DT-D. The peak attributable to 2-OH-E^+ was seen to disappeared when **22** + DT-D was co-incubated with SOD.

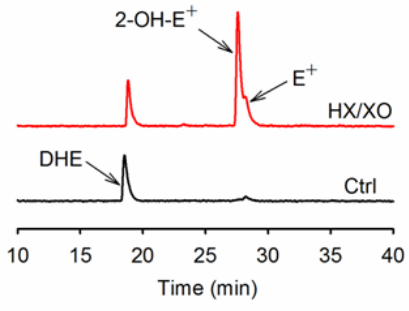

Figure S1. Superoxide generated during incubation of hypoxanthine in the presence of xanthine oxidase was estimated using a dihydroethidium (DHE) assay. Superoxide specifically react with DHE to produce 2-hydroxyethidium (2-OH-E^+); Ethidium (E^+) is formed by non-specific oxidation of DHE and is indicative of a general increase in oxidative species.

3.4.4. NO generation from 22

3.4.4.1. NO detection

Relevant stock solutions were prepared as described earlier. The reaction mixture was prepared by dissolving of **22** (5 µL, 10 mM), NADH solution (20 µL, 10 mM), and 20 µL of the DT-D enzyme solution in 455 µL HEPES buffer pH 7.4 at 37 ºC. The resulting solution was incubated for 5 min and an aliquot of reaction mixture (10 µL) was injected into a Sievers Nitric Oxide Analyzer (NOA 280i). For the experiment with NO scavenger 2-(4-carboxyphenyl)-4,4,5,5-tetramethylimidazoline-1-oxyl-3-oxide potassium salt (50 µL, 10 mM, 10 eq., c-PTIO) was added to the above reaction mixture and the 10 µL aliquot was injected into the NOA chamber.

3.4.4.2. Real time monitoring of NO generation from 22

To the vessel of NOA analyzer, **22** (12.5 µL, 10 mM), NADH (50 µL, 10 mM) and DTPA (10 µL, 10 mM) were added in PB (4927.5 µL). The reaction mixture was purged with argon for 5 min. DT-D enzyme (5 µL) was added to the mixture and NO generation was monitored using a

NOA at low sensitivity mode. For the experiment with the NO scavenger, 2-(4-carboxyphenyl)-4,4,5,5-tetramethylimidazoline-1-oxyl-3-oxide potassium salt (c-PTIO, 25 μL, 25 mM, 5 eq.) was added to the reaction mixture and NO generation was monitored.

3.4.4.3. NO generation from 22 in the presence of SOD

The reaction mixture was prepared by dissolving **22** (2 μL, 2.5 mM), NADH (2 μL, 10 mM), DTPA (2 μL, 1 mM) and DT-D enzyme (2 μL) in PB pH 7.4 (192 μL). The reaction mixture was incubated under ambient aerobic conditions for 5 min and an aliquot (10 μL) was injected into a NOA. For the experiment of NO measurement in the presence of superoxide scavenger, SOD (2 μL, 200 U/mL) was added to **22** + DT-D and the resulting mixture was incubated for 5 min. An aliquot (10 μL) from the reaction vial was injected into a NOAand NO generation was measured at high sensitivity mode.

3.4.5. Peroxynitrite detection using the boronate ester probe 23a

3.4.5.1. Fluorescence-based method

The stock solutions of **22** (25 mM) and **23a** (10 mM) were prepared in DMSO. The reaction mixture was prepared (total 1 mL volume) by dissolving **22**(4 μL, 25 mM), NADH solution (40 μL, 10 mM), DTPA (10 μL, 1 mM), **23a** (10 μL, 10 mM) and 20 μL of DT-D enzyme solution in PB pH 7.4 (916 μL). The reaction mixture was incubated at 37 °C for 10 min under dark conditions and fluorescence spectra was recorded at λ_{ex} = 315 nm using a Fluoromax 4 instrument (Horiba JobinYvon). The slit width was set to 4 nm for both excitation and emission. In case of the H_2O_2 scavenging experiment, 100 units/mL catalase was added to the mixture of **22** + DT-D. The resulting mixture was incubated at 37 °C for 10 min under dark conditions and fluorescence spectra was was recorded at λ_{ex} = 315 nm.

3.4.5.2. Control experiments to validate the peroxynitrite generation from 22

To a 96 -microwell plate, the reaction mixture was prepared by dissolving **23a** (2 μL, 2.5 mM), **22** (2 μL, 2.5 mM), NADH solution (2 μL, 10 mM), DTPA (2 μL, 1 mM), and 2 μL of DT-D enzyme solution in pH 7.4 PB (190 μL). The resulting mixture was incubated at 37 ºC for 15 min and the fluorescence of the reaction mixture was measured using a microtiter plate reader (excitation 315 nm; emission 460 nm). The peroxynitrite probe **23a** is also known to react with

H_2O_2. Therefore, **23a** was incubated with H_2O_2 (25 μM) for 15 min. In order to validate that the fluorescence emission from **23a** during incubation with **22** + DT-D is because of peroxynitrite generation and not because of H_2O_2, we co-incubated the reaction mixture of **22** + DT-D with catalase (100 U/mL). Also, **23a** (25 μM) was incubated with superoxide generator **25** (25 μM) + DT-D and with catalase (100 U/mL). SIN-1 (25 μM) was incubated with **23a** for 15 min and fluorescence was measured.

3.4.5.3. Time course of peroxynitrite generation from 22

To a 96-microwell plate, the reaction mixture was prepared in quadruplicate by dissolving **23a** (2 μL, 2.5 mM), **22** (2 μL, 2.5 mM), NADH solution (2 μL, 10 mM), DTPA (2 μL, 1 mM), catalase (100 units/mL) and 2 μL of DT-D enzyme solution in pH 7.4 PB (188 μL). The resulting mixture was incubated at 37 °C and the fluorescence from reaction mixture was measured using microtiter plate reader (λ_{ex} - 315 nm; λ_{em}- 460 nm) at 2 min interval for 16 minutes.

Standard calibration curve for 23c

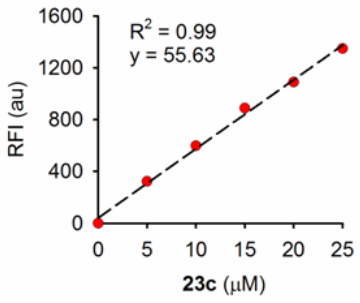

Figure S2. Relative fluorescence intensity of known concentration of **23c** measured using 96 well plate reader with excitation 315 nm and emission 460 nm.

3.4.5.4. Peroxynitrite detection in the presence of NO and superoxide scavenger

To a 96-microwell plate, the reaction mixture was prepared by dissolving **22** (1 μL, 5 mM), NADH solution (2 μL, 10 mM), DTPA (2 μL, 1 mM), **23a** (1 μL, 5 mM) and 2 μL of DT-D enzyme solution in 192 μL phosphate buffer pH 7.4. The resulting mixture was incubated at 37 ºC for 15 min. The increase in fluorescence of reaction mixture was measured using a microtiter plate reader (excitation 315 nm; emission 460 nm). For the experiment with superoxide dismutase (SOD from bovine erythrocytes), SOD (2 μL, 200 U/mL) was added to the reaction

mixture (**22** + DT-D) and increase influorescence was measured. For the experiment with NO scavenger, 2-(4-carboxyphenyl)-4,4,5,5-tetramethylimidazoline-1-oxyl-3-oxide potassium salt (c-PTIO) (4 μL, 10 mM) was added to the reaction mixture (**22** + DT-D) and fluorescence was measured (excitation 315 nm; emission 460 nm).

3.4.5.5. HPLC-based method

A stock solution of **22** (10 mM) and **23a** (10 mM) were prepared in DMSO. The reaction mixture was prepared by dissolving **22** (10 μL, 10 mM), NADH solution (40 μL, 10 mM), DTPA (10 μL, 1 mM), **23a** (10 μL, 10 mM), catalase (10 μL, 10000 units/mL) and 20 μL of DT-D enzyme solution in 900 μL PB pH 7.4 and incubated at 37 ºC for 20 min. The resulting mixture was filtered (0.22 μm) and injected (5 μL) in a HPLC(Agilent Technologies 1260 Infinity). The mobile phase was H_2O/CH_3CN containing 0.1 % trifluroacetic acid. The stationary phase was a C-18 reverse-phase column (5 μm, 4.6 × 250 mm). **23b**and**23c** were separated by a linear increase in CH_3CN concentration from 10% to 65% over 15 min and then keeping 65% up to 20 min at a flow rate of 1 mL/min. The elution was monitored by UV detector at 280 nm and a fluorescence detector with excitation at 315 and emission at 460 nm. Authentic peroxynitrite solution (100 μM) was reacted with **23a** (100 μM) in PB pH 7.4 and used as a positive control. Under these conditions, **23b** eluted at 10.2 min and **23c** eluted at 11.3 min.

3.4.6. Peroxynitrite detection using the sulfonamide-based probe Ds-DAB

A stock solution of Ds-DAB (1 mM) was prepared in DMSO. The reaction mixture was prepared (total 1 mL volume) by dissolving Ds-DAB (10 μL, 1 mM), **22** (10 μL, 10 mM), NADH solution (40 μL, 10 mM), DTPA (1 mM, 10 μL), catalase (100 U/mL) and 10 μL of DT-D enzyme solution in HEPES buffer pH 7.4 (910 μL, 10 mM). The reaction mixture was incubated at 37 °C under dark conditions for 15 min. The fluorescence spectra was recorded at λ_{ex} = 350 nm using a Fluoromax 4 instrument (Horiba JobinYvon). The slit width was set to 3 nm for excitation and 5 nm for emission. Authentic peroxynitrite solution (100 μM) was reacted with Ds-DAB (10 μM) in HEPES buffer pH 7.4 at 37 °C for 15 min and served as positive control.

3.4.7. Tyrosine nitration assay

A stock solution of L-tyrosine (10 mM) in 1M HCl and **22** (25 mM) in DMSO was prepared. NADH (10 mM) and DT-diphorase solution was prepared as mentioned earlier. The reaction

mixture was prepared by dissolving of **22** (300 μM), NADH (300 μM), L-tyrosine (500 μM) and DT-D enzyme (10 μL) in HEPES buffer (total volume 500 μL). The reaction mixture was incubated at 37 °C for 30 min. The resulting mixture was filtered (0.22 μm) and injected (25 μL) in a HPLC (Agilent Technologies 1260 Infinity with a Zorbax SB C-18 reverse phase column 250 × 4.5 mm). The mobile phase was H_2O/CH_3CN containing 0.1 % trifluroacetic acid. Tyrosine, 3-nitrotyrosine and dityrosine were separated by a linear increase in acetonitrile concentration from 0% to 40% in 16 min at a flow rate 1 mL/min. The formation of 3-nitrotyrosine was monitored at 275 nm wavelength. The formation of dityrosine was monitored using fluorescence detector with excitation and emission at 285 and 410 nm, respectively. Authentic peroxynitrite (100 μM) was reacted with L-tyrosine (500 μM) in HEPES buffer pH 7.4 as positive control. As expected, at lower concentration of authentic peroxynitrite (10 μM), we observed exclusively dityrosine formation.

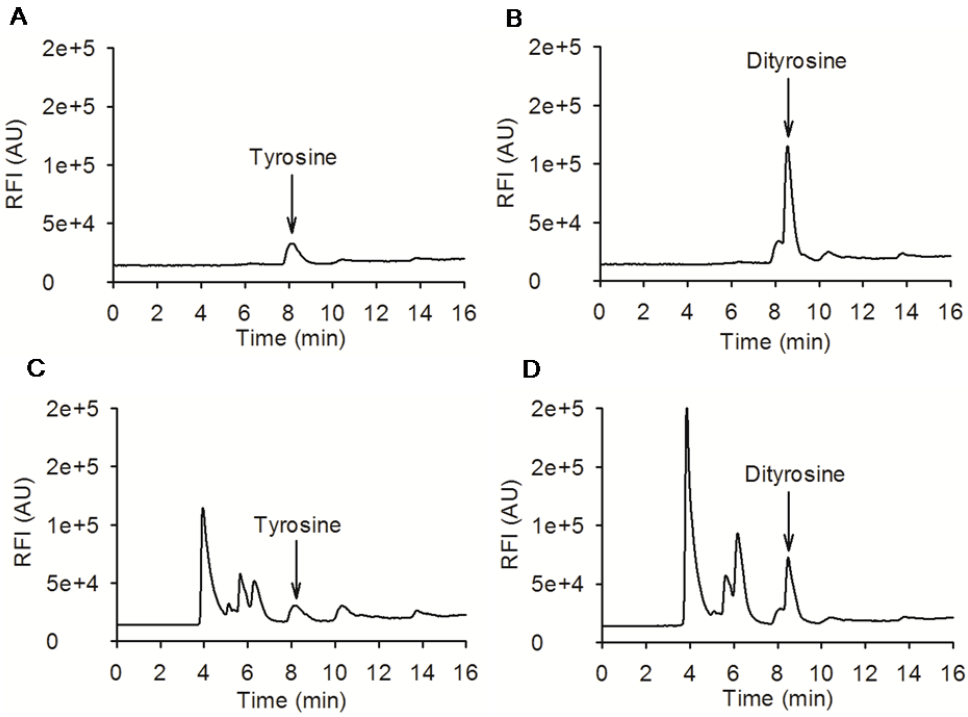

Figure S3.HPLC traces for dityrosine formation (a) Tyrosine (500 μM); (b) Tyrosine (500 μM) was incubated with peroxynitrite (10 μM) at 37 °C for 10 min and analyzed using HPLC attached with fluorescence detector with excitation and emission at 285 and 410 nm,

respectively; (c) Tyrosine (500 μM) was incubated with **22** (300 μM) in pH 7.4 buffer at 37 °C; (d) Tyrosine (500 μM) was incubated with **22** + DT-D in pH 7.4 buffer at 37 °C for 30 min.

3.4.8. Decomposition study of 22 using HPLC

The stock solutions of **22** and **25** (2.5 mM) were prepared in DMSO and other relevant stock solutions were prepared as described earlier. The reaction mixture was prepared by dissolving **22** or **25** (2 μL, 2.5 mM), NADH (2 μL, 10 mM), DT-D enzyme (2 μL) and DTPA (2 μL, 1 mM) in PB (192 μL) and incubated under ambient aerobic conditions at 37 °C for 10 min. The reaction mixture was filtered (0.22 μm) and injected (50 μL) in an HPLC attached with a diode-array detector (detection wavelength was 254 nm) and a Phenomenex Luna C-18 reversed phase column (250 mm × 4.6 mm × 5 μm). A mobile phase of water: acetonitrile was used with a run time of 30 min with a linear increase in CH_3CN concentration from 40% to 80% in 30 min at a flow rate of 1 mL/ min. Authentic compound, 4-nitrophenol (25 μM) was injected to identify the peak position of the reaction product.

3.4.9. Confocal assay for intracellular peroxynitrite detection

DLD-1, SW480, A549 and primary corneal fibroblast cells (1.0×10^6/well) were seeded on glass cover slips in a 6 well plate and grown in complete RPMI 1640 medium at 37 °C overnight in a humidified 5 % CO_2 atmosphere. Cells were treated with Ds-DAB (10 μM) for 30 min and then incubated with **1** (25 μM) for 1 h. In case of peroxynitrite scavengers experiment, cells were pre-treated with uric acid (100 μM) for 1h or sodium sulphide (100 μM) for 10 min prior to Ds-DAB and **22** treatments. Authentic peroxynitrite solution (25 μM) and SIN-1 (100 μM) were used as positive control. Also cells were treated with superoxide generator, **25** (25 μM). Prior to imaging, cells were washed three times with PBS and fixed with 4% paraformaldehyde for 10 min at room temperature followed by a PBS wash. Cover slips were mounted on the slide. Cells were imaged on a Zeiss LSM710 confocal microscope with 405 nm laser lines at 4.5% power using a 63X oil immersion objective, NA 1.4 at 1X digital zoom. X-Y resolution was 512 pixels X 512 pixels (1 pixel = 0.11 μm). Confocal z-stacks were collected at an interval of 0.35 μm. Fluorescence intensity in each cell was quantified using Image J software by applying threshold to mark the fluorescence region and then integrated density was calculated.

3.4.10. Determination of minimum inhibitory concentration

The Minimum Inhibitory Concentration (MIC) assay was used to determine the inhibitory potential of the compound against bacterial pathogens. To determine the MIC, the microbroth dilution technique is commonly used as recommended by National Committee for Clinical Laboratory Standards. For this, a fixed bacterial inoculum (5×10^5 CFU/mL) is added into a series of test wells in a microtitre plate that contain various concentrations of compound under test. Following a period of incubation (37 ºC, 18-20 h), the wells are examined for growth. The lowest concentration of antibiotic that inhibits growth of the organism, as detected visually is designated as the MIC.

3.5. Spectra Charts

^{1}H NMR Spectrum (400 MHz, $CDCl_3$) of **21**

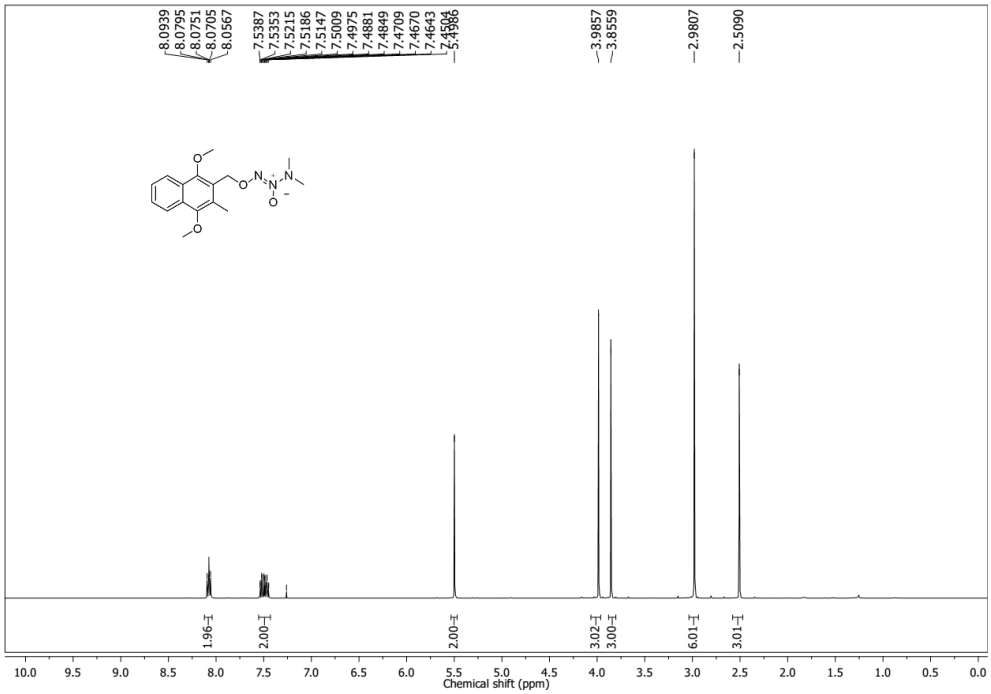

^{13}C NMR Spectrum (100 MHz, $CDCl_3$) of **21**

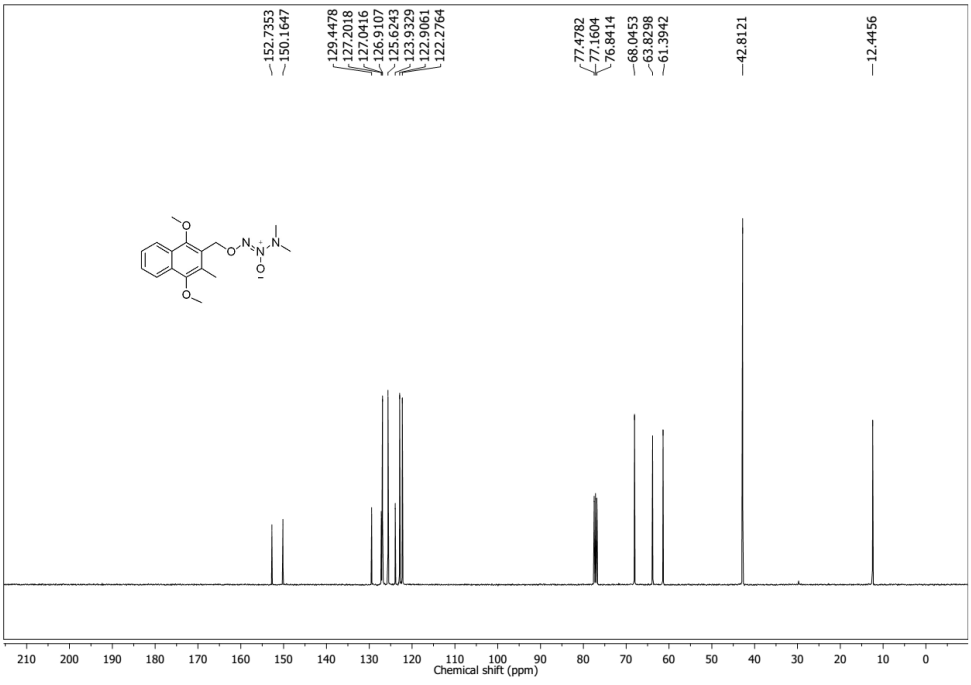

^{1}H NMR Spectrum (400 MHz, $CDCl_3$) of **22**

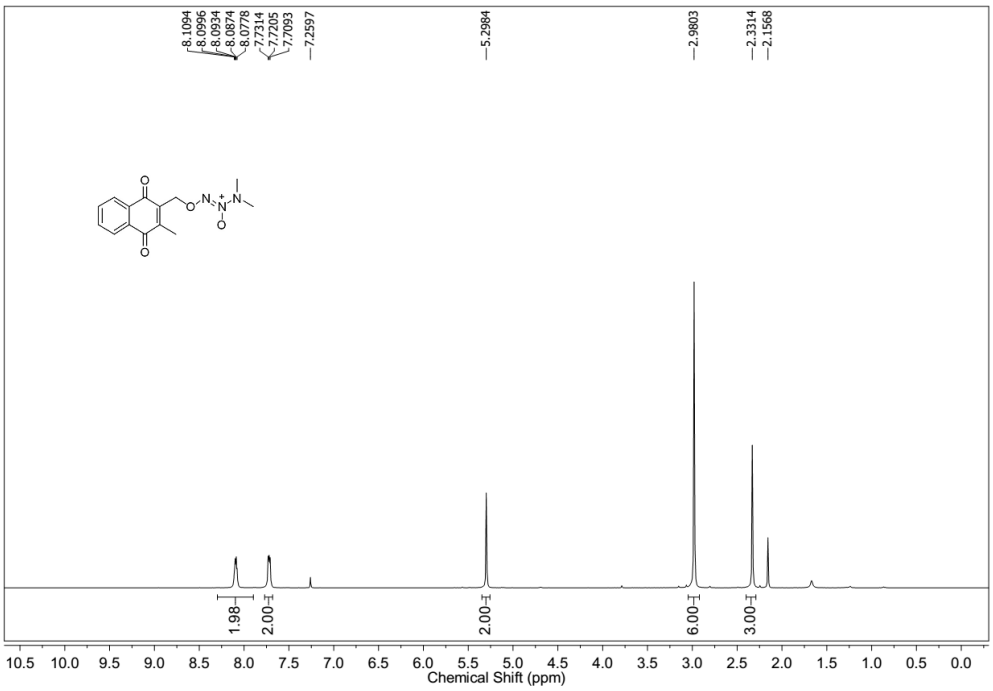

^{13}C NMR Spectrum (100 MHz, $CDCl_3$) of **22**

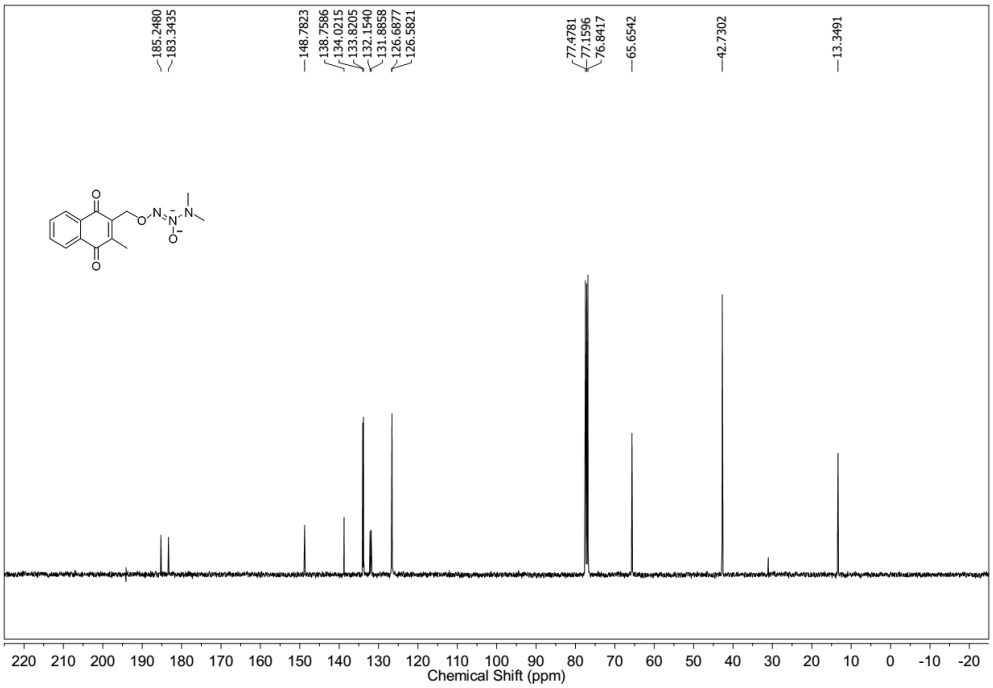

^{1}H NMR Spectrum of 3-methyl-2-oxo-2H-chromen-7-yl trifluoromethanesulfonate

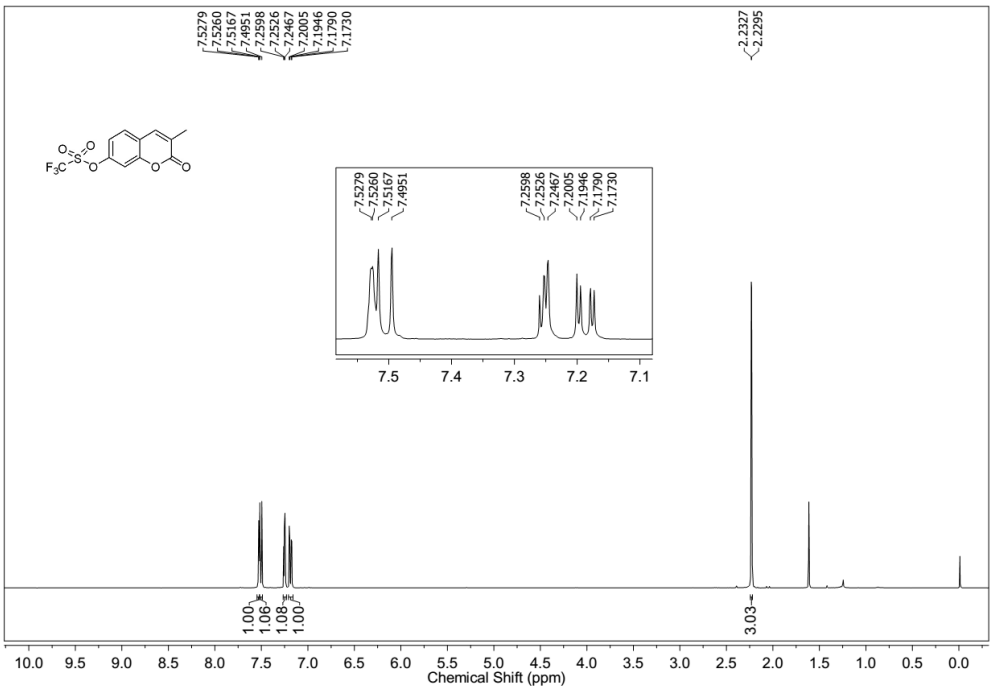

^{13}C NMR Spectrum of 3-methyl-2-oxo-2H-chromen-7-yl trifluoromethanesulfonate

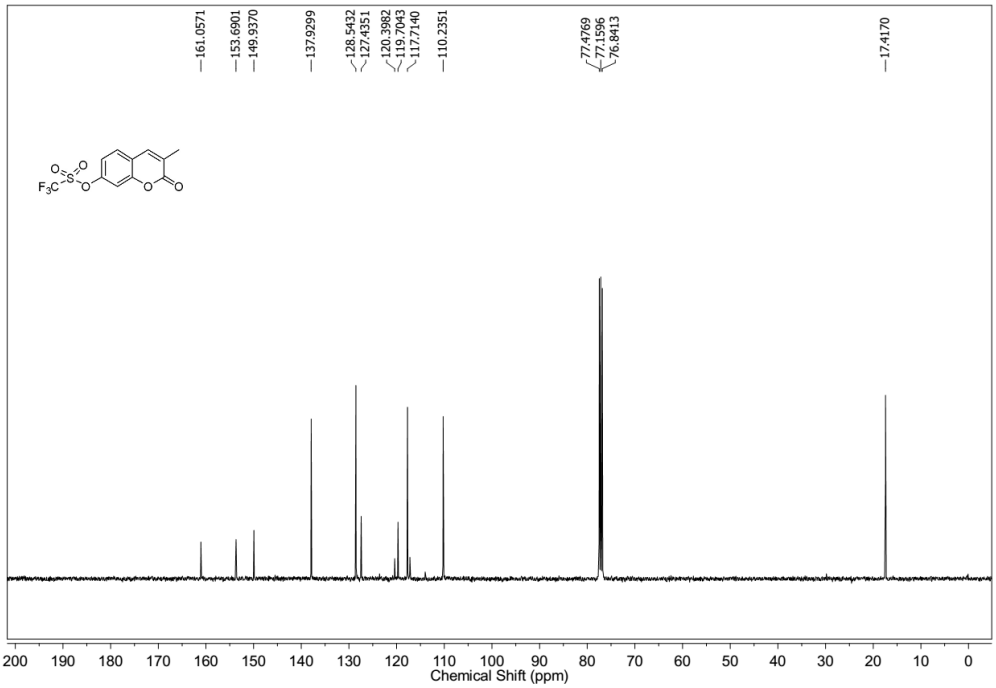

^{1}H NMR Spectrum (400 MHz, $CDCl_3$) of **23a**

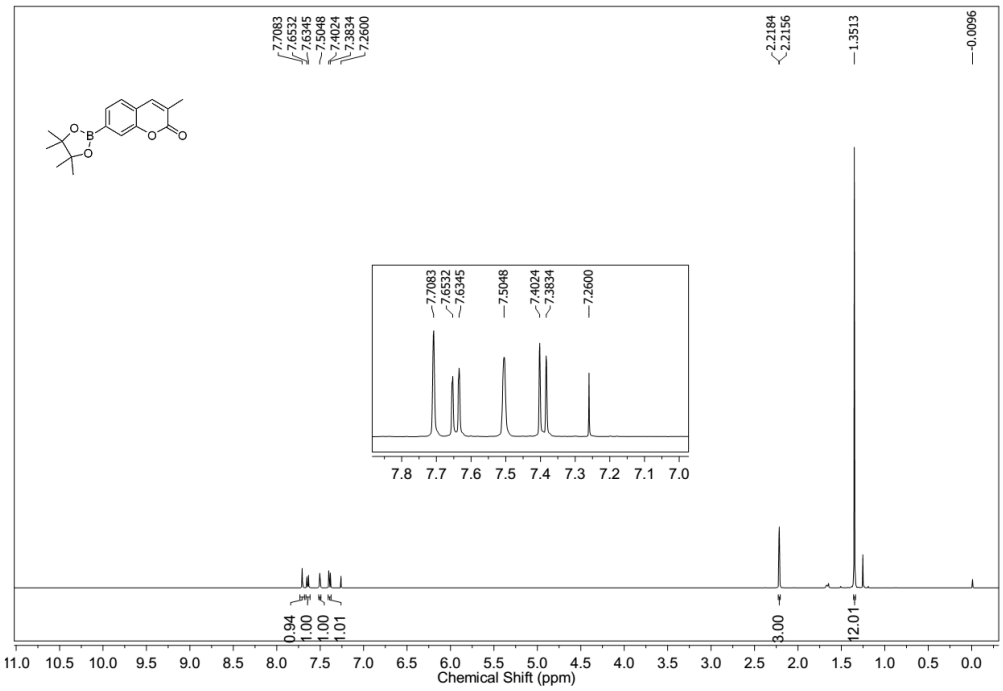

^{13}C NMR Spectrum (100 MHz, $CDCl_3$) of **23a**

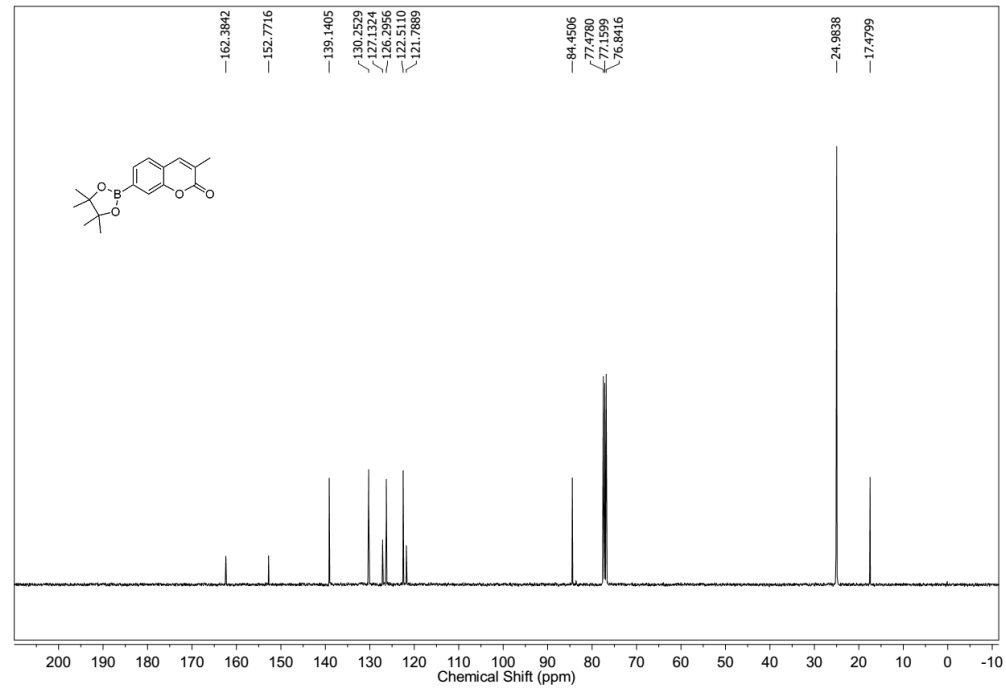

^{1}H NMR Spectrum (400 MHz, $CDCl_3$) of **24**

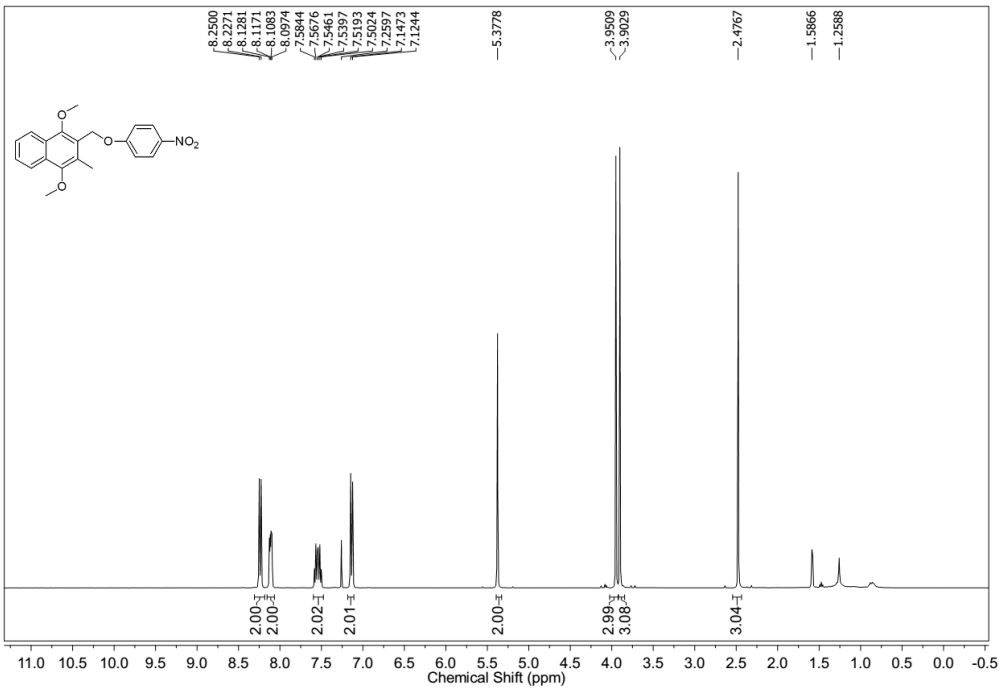

^{13}C NMR Spectrum (100 MHz, $CDCl_3$) of **24**

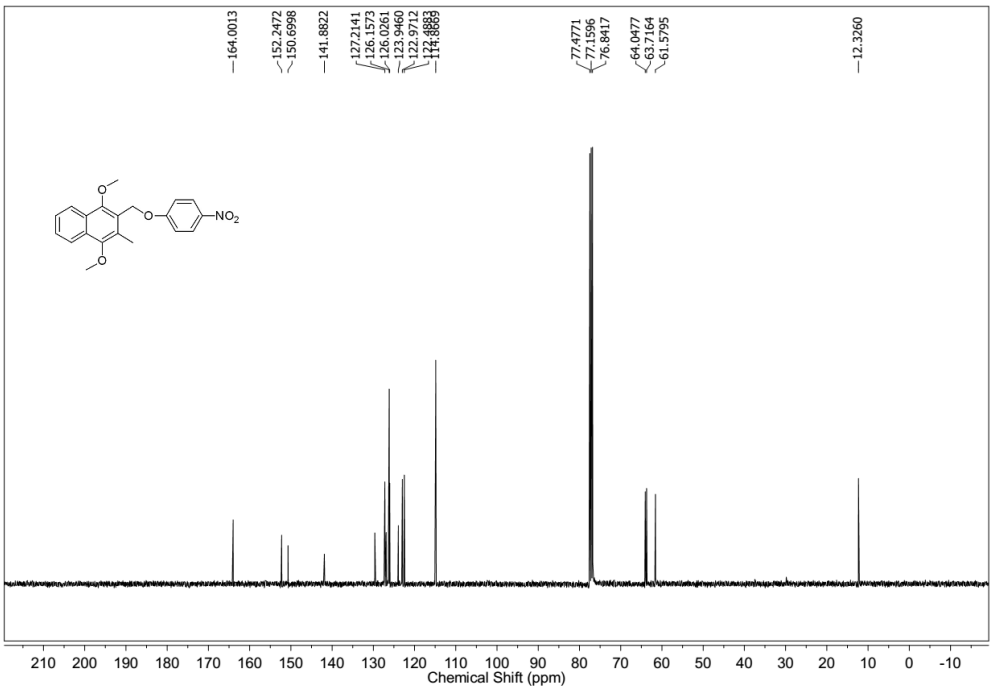

^{1}H NMR Spectrum (400 MHz, $CDCl_3$) of **25**

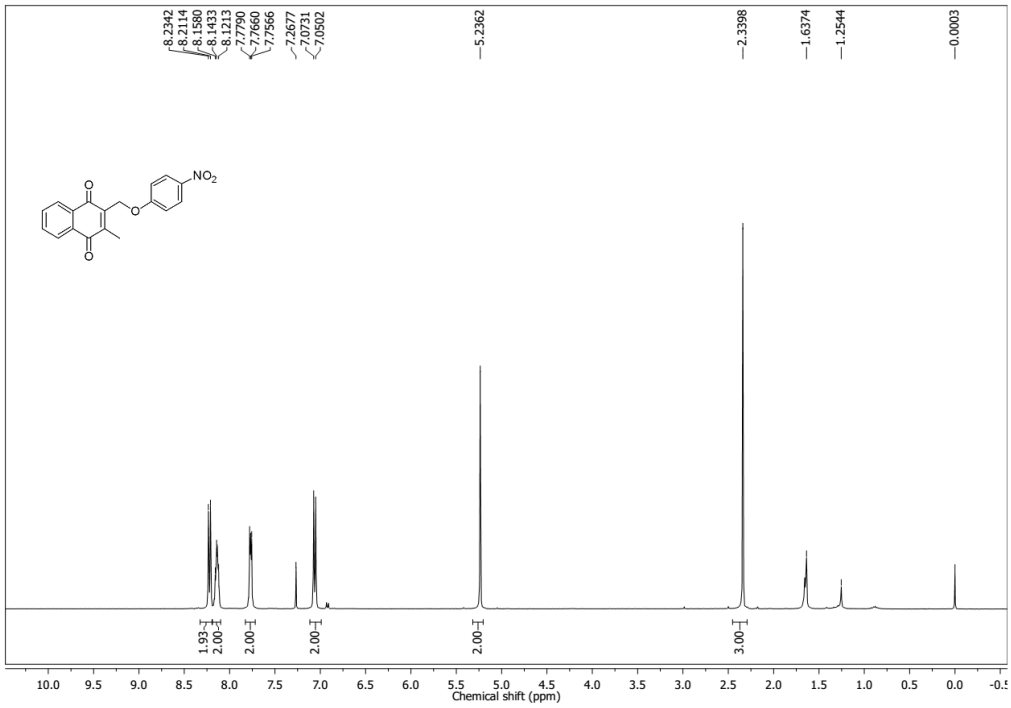

^{13}C NMR Spectrum (100 MHz, $CDCl_3$) of **25**

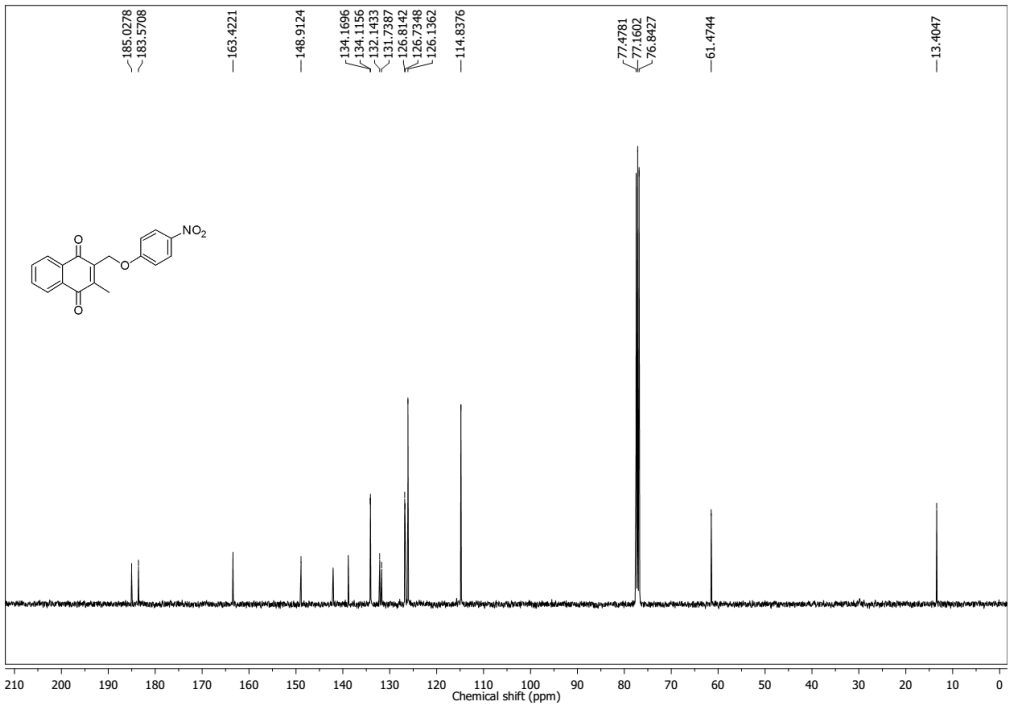

^{1}H NMR Spectrum (400 MHz, $CDCl_3$) of Ds-DAB

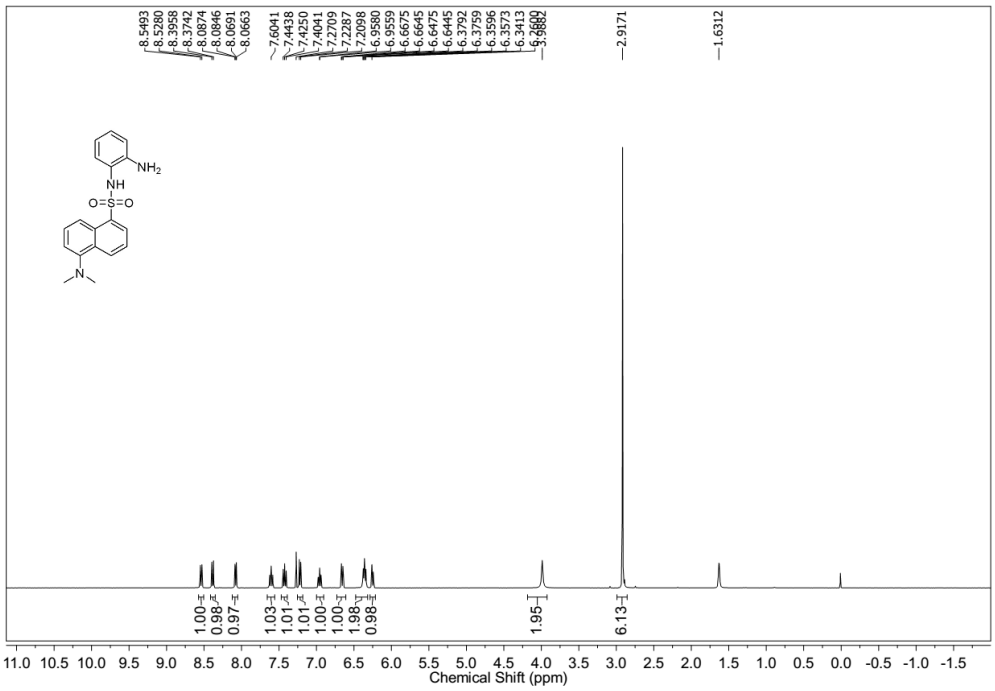

^{13}C NMR Spectrum (100 MHz, $CDCl_3$) of Ds-DAB

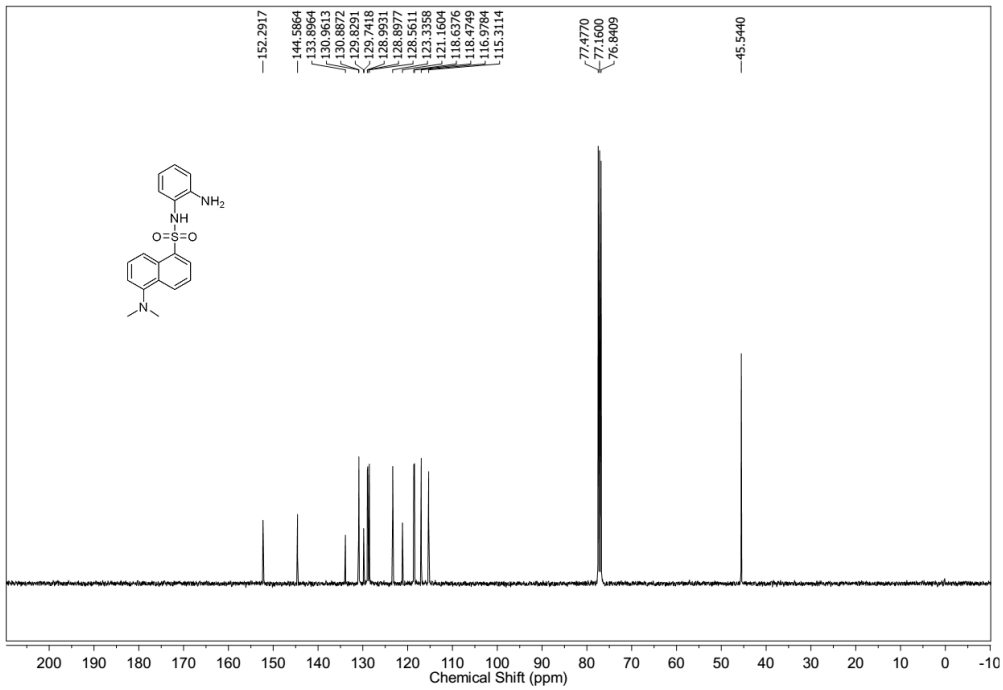

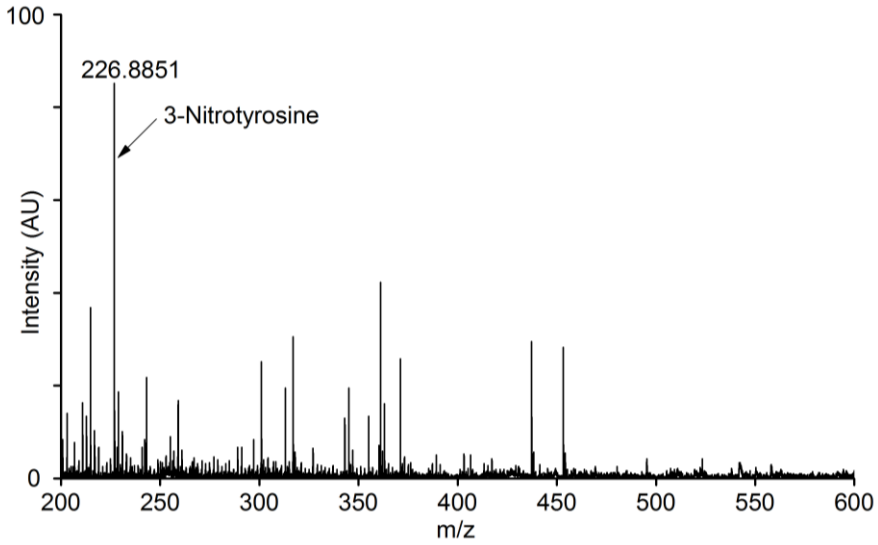

Mass spectra for 3-nitrotyrosine formation during incubation of tyrosine with **22** + DTD in phosphate buffer pH 7.4. The HPLC eluent (~11.2 min peak) was analyzed using MALDI (TOF-TOF), $C_9H_{10}N_2O_5$ $[M]^+$Calcd. 226.1861, Found 226.8851.

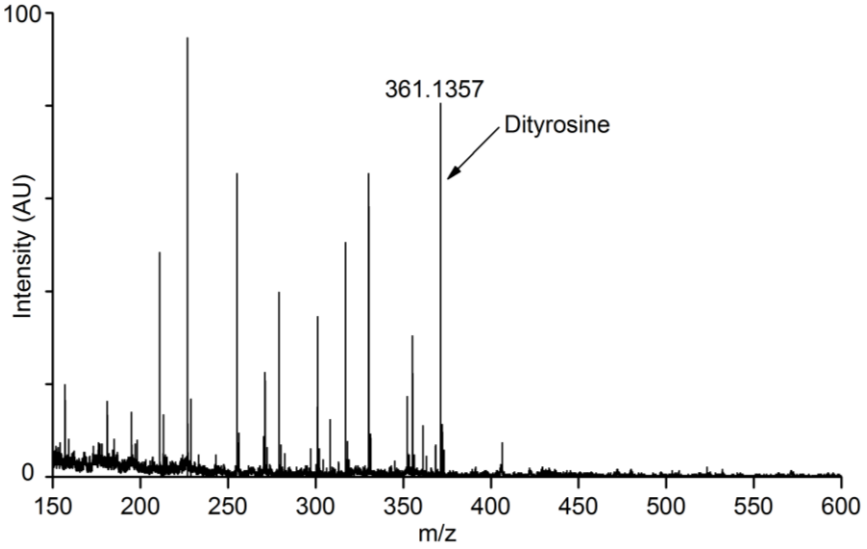

Mass spectra for dityrosine formation during incubation of tyrosine with **22** + DT-D in pH 7.4 buffer; MALDI (TOF-TOF), $C_{18}H_{20}N_2O_6$ $[M+H]^+$: Calcd. 361.3691, Found 361.1357.

3.6. References

(1) Fang, F. C. *Nat. Rev. Micro.* **2004**, *2*, 820.

(2) Sawa, T.; Zaki, M. H.; Okamoto, T.; Akuta, T.; Tokutomi, Y.; Kim-Mitsuyama, S.; Ihara, H.; Kobayashi, A.; Yamamoto, M.; Fujii, S.; Arimoto, H.; Akaike, T. *Nat. Chem. Biol.* **2007**, *3*, 727.

(3) Ito, C.; Saito, Y.; Nozawa, T.; Fujii, S.; Sawa, T.; Inoue, H.; Matsunaga, T.; Khan, S.; Akashi, S.; Hashimoto, R.; Aikawa, C.; Takahashi, E.; Sagara, H.; Komatsu, M.; Tanaka, K.; Akaike, T.; Nakagawa, I.; Arimoto, H. *Mol. Cell* **2013**, *52*, 794.

(4) Akaike, T.; Nishida, M.; Fujii, S. *J. Biochem.* **2013**, *153*, 131.

(5) Pfeiffer, S.; Mayer, B. *J. Biol. Chem.* **1998**, *273*, 27280.

(6) Kuhn, D. M.; Aretha, C. W.; Geddes, T. J. *J. Neurosci.* **1999**, *19*, 10289.

(7) Wang, C.; Deen, W. M. *Chem. Res. Toxicol.* **2004**, *17*, 32.

(8) Estévez, A. G.; Spear, N.; Pelluffo, H.; Kamaid, A.; Barbetto, L.; Beckman, J. S. In *Methods enzymol.*; Academic Press: 1999; Vol. Volume 301, p 393.

(9) Li, C.-Q.; Trudel, L. J.; Wogan, G. N. *Chem. Res. Toxicol.* **2002**, *15*, 527.

(10) Hogg, N.; Darley-Usmar, V. M.; Wilson, M. T.; Moncada, S. *FEBS Lett.* **1993**, *326*, 199.

(11) Pfeiffer, S.; Schmidt, K.; Mayer, B. *J. Biol. Chem.* **2000**, *275*, 6346.

(12) de Boer-Maggard, T. R.; Resendez, A.; Mascharak, P. K. *Chem. Bio. Chem.* **2013**, *14*, 2106.

(13) Korshunov, S. S.; Imlay, J. A. *Mol. Microbiol.* **2002**, *43*, 95.

(14) Ieda, N.; Nakagawa, H.; Horinouchi, T.; Peng, T.; Yang, D.; Tsumoto, H.; Suzuki, T.; Fukuhara, K.; Miyata, N. *Chem. Commun.* **2011**, *47*, 6449.

(15) Ieda, N.; Nakagawa, H.; Peng, T.; Yang, D.; Suzuki, T.; Miyata, N. *J. Am. Chem. Soc.* **2012**, *134*, 2563.

(16) deBoer, T. R.; Palomino, R. I.; Idiga, S. O.; Millhauser, G. L.; Mascharak, P. K. *J. Inorg. Biochem.* **2014**, *138*, 24.

(17) Parkinson, E. I.; Hergenrother, P. J. *Acc. Chem. Res.* **2015**, *48*, 2715.

(18) Keefer, L. K.; Flippen-Anderson, J. L.; George, C.; Shanklin, A. P.; Dunams, T. M.; Christodoulou, D.; Saavedra, J. E.; Sagan, E. S.; Bohle, D. S. *Nitric Oxide* **2001**, *5*, 377.

(19) Sharma, K.; Chakrapani, H. *Nitric Oxide* **2014**, *43*, 8.

(20) Sharma, K.; Iyer, A.; Sengupta, K.; Chakrapani, H. *Org. Lett.* **2013**, *15*, 2636.

(21) Davies, K. M.; Wink, D. A.; Saavedra, J. E.; Keefer, L. K. *J. Am. Chem. Soc.* **2001**, *123*, 5473.

(22) Keefer, L. K. *ACS Chem. Biol.* **2011**, *6*, 1147.

(23) Syper, L.; Młochowski, J.; Kloc, K. *Tetrahedron* **1983**, *39*, 781.

(24) Georgiou, C. D.; Papapostolou, I.; Grintzalis, K. *Nat. Protocols* **2008**, *3*, 1679.

(25) Zhao, H.; Joseph, J.; Fales, H. M.; Sokoloski, E. A.; Levine, R. L.; Vasquez-Vivar, J.; Kalyanaraman, B. *Proc. Natl. Acad. Sci. U. S. A.* **2005**, *102*, 5727.

(26) Dharmaraja, A. T.; Ravikumar, G.; Chakrapani, H. *Org. Lett.* **2014**, *16*, 2610.

(27) Woldman, Y. Y.; Khramtsov, V. V.; Grigorev, I. A.; Kiriljuk, I. A.; Utepbergenov, D. I. *Biochem. Biophys. Res. Commun.* **1994**, *202*, 195.

(28) Akaike, T.; Yoshida, M.; Miyamoto, Y.; Sato, K.; Kohno, M.; Sasamoto, K.; Miyazaki, K.; Ueda, S.; Maeda, H. *Biochemistry* **1993**, *32*, 827.

(29) Lin, K.-K.; Wu, S.-C.; Hsu, K.-M.; Hung, C.-H.; Liaw, W.-F.; Wang, Y.-M. *Org. Lett.* **2013**, *15*, 4242.

(30) Sawa, T.; Akaike, T.; Maeda, H. *J. Biol. Chem.* **2000**, *275*, 32467.

(31) Radi, R. *Proc. Natl. Acad. Sci. U. S. A.* **2004**, *101*, 4003.

(32) Gunaydin, H.; Houk, K. N. *Chem. Res. Toxicol.* **2009**, *22*, 894.

(33) Goldstein, S.; Czapski, G. *J. Am. Chem. Soc.* **1998**, *120*, 3458.

(34) Bonini, M. G.; Radi, R.; Ferrer-Sueta, G.; Ferreira, A. M. D. C.; Augusto, O. *J. Biol. Chem.* **1999**, *274*, 10802.

(35) Augusto, O.; Bonini, M. G.; Amanso, A. M.; Linares, E.; Santos, C. C. X.; De Menezes, S. l. L. *Free Radic. Biol. Med.* **2002**, *32*, 841.

(36) Radi, R. *Proc. Natl Acad. Sci. USA* **2004**, *101*, 4003.

(37) Iyanagi, T.; Yamazaki, I. *Biochim. Biophys. Acta* **1969**, *172*, 370.

(38) Iyanagi, T.; Yamazaki, I. *Biochim. Biophys. Acta* **1970**, *216*, 282.

(39) Li, X.; Tao, R.-R.; Hong, L.-J.; Cheng, J.; Jiang, Q.; Lu, Y.-M.; Liao, M.-H.; Ye, W.-F.; Lu, N.-N.; Han, F.; Hu, Y.-Z.; Hu, Y.-H. *J. Am. Chem. Soc.* **2015**, *137*, 12296.

(40) Kuzkaya, N.; Weissmann, N.; Harrison, D. G.; Dikalov, S. *Biochem. Pharmacol.* **2005**, *70*, 343.

(41) Sautin, Y. Y.; Johnson, R. J. *Nucleosides, Nucleotides Nucleic Acids* **2008**, *27*, 608.

(42) Carballal, S.; Trujillo, M.; Cuevasanta, E.; Bartesaghi, S.; Möller, M. N.; Folkes, L. K.; García-Bereguiaín, M. A.; Gutiérrez-Merino, C.; Wardman, P.; Denicola, A.; Radi, R.; Alvarez, B. *Free Radic. Biol. Med.* **2011**, *50*, 196.

(43) Li, Q.; Lancaster Jr, J. R. *Nitric Oxide* **2013**, *35*, 21.

(44) Bryk, R.; Griffin, P.; Nathan, C. *Nature* **2000**, *407*, 211.

(45) Master, S. S.; Springer, B.; Sander, P.; Boettger, E. C.; Deretic, V.; Timmins, G. S. *Microbiology* **2002**, *148*, 3139.

(46) Prolo, C.; Álvarez, M. N.; Radi, R. *BioFactors* **2014**, *40*, 215.

(47) Catto, M.; Nicolotti, O.; Leonetti, F.; Carotti, A.; Favia, A. D.; Soto-Otero, R.; Méndez-Álvarez, E.; Carotti, A. *J. Med. Chem.* **2006**, *49*, 4912.

(48) Bhabak, K. P.; Mugesh, G. *Chem. Eur. J.* **2010**, *16*, 1175.

Chapter 4: Design, Synthesis and Evaluation of Nitroreductase Activated Hydrogen Sulfide Donors

4.1. Introduction

In order to understand and address antibiotic-resistance, several approaches including synthesis of new classes of antibiotics, identification of novel targets and use of different antibiotic combinations have been considered. In chapter 2, we had described the design and synthesis of natural product-inspired ROS generators as MRSA inhibitors. These redox-active small molecules have shown potent inhibitory activity against multi-drug resistant strain of *S. aureus* presumably through ROS generation. In chapter 3, we described the design and synthesis of a small molecule peroxynitrite generator. The peroxynitrite generator also showed potent inhibitory activity against MRSA. Having demonstrated the potential of ROS and RNS generators to target antibiotic-resistance in some bacteria, we proceeded to study the role of reactive sulfur species (RSS) in antibiotic-resistance. Hydrogen sulfide (H_2S) is a prototypical example of RSS and recently this reactive species has been identified as a third gaseous signaling molecule along with nitric oxide (NO) and carbon monoxide (CO).[1-3] H_2S generation in bacteria has been known from centuries but it was only considered as a by-product of sulfur metabolism.[4-6] In the bacterial genome, mammalian orthologs of H_2S producing enzymes such as cystathionine-β-synthase (CBS), cystathionine-γ-lyase (CSE), and 3-mercaptopyruvate sulfurtransferase (3MST) are evolutionarily conserved, suggesting the significant role of H_2S in basic cellular processes. Bacteria deploy this gaseous molecule to counter the oxidative stress induced by mammalian immune system through antioxidant mechanism.[7-8] Recently, Shatalin and coworkers have reported that H_2S plays a critical protective role during exposure of bacteria to antibiotics suggesting a role of this gaseous molecule in antibiotic resistance.[9] Furthermore, several recent studies have demonstrated that bacterial hydrogen sulfide is integral to virulence.[10] The precise mechanisms by which this RSS acts remain to be completely understood. Thus, understanding the mechanism of cytoprotective role of H_2S is important for the development of new antibiotics that can overcome the resistance problem.[11] A common strategy used for studying the role of H_2S involves the use of H_2S biosynthesis inhibitors. However, due to the lack of specific inhibitors of these enzymes, this method is not well suited for studying the role of H_2S in bacteria.[12] In order to understand the mechanism of H_2S-mediated protection of bacteria from antibiotics, hydrogen sulphide generation in bacteria would be useful. However,

producing this gaseous molecule in a controlled manner is challenging. A number of H_2S donors have been developed but they are associated with certain limitations. We have summarized in the following section the currently available methods for H_2S generation and their limitations.

4.1.1 H_2S donors

4.1.1.A. Inorganic salts

Inorganic salts such as NaHS and Na_2S have been extensively used in studying the biological effects of H_2S, but they are associated with certain limitations such as uncontrolled H_2S generation, poor bioavailability and a lack of site-specificity.[13] In addition, these inorganic salts produce a burst H_2S in aqueous solution and cannot mimic the slow and continuous H_2S production in biological systems. Furthermore, due to its susceptibility to auto-oxidation, unless carefully prepared, H_2S solutions typically contain other higher oxidation state species such as thiosulfate, sulfite and sulfate.[14-15] Hence use of inorganic salts for H_2S generation is not suitable for cellular studies.

4.1.1.B. Lawesson's reagent and GYY4137

2,4-Bis(4-methoxyphenyl)-1,3,2,4-dithiadiphosphetane 2,4-disulfide (Lawesson's reagent) has been used for H_2S generation (Figure 4.1).[16] This compound releases H_2S upon hydrolysis in aqueous solution. The half-life of this compound is comparatively more than the inorganic salts (Na_2S and NaHS). Therefore, it generates H_2S over a longer period of time. However, poor solubility of Lawesson's reagent in aqueous solutions limits its applications. Morpholin-4-ium(4-methoxyphenyl)(morpholino)phosphinodithioate (GYY4137) has been developed as water soluble derivative of Lawesson's reagent (Figure 4.1).[17] H_2S generation from this compound depends on temperature and pH of the medium. However, due to lack of structural handle over H_2S release makes it difficult to mimic endogenous H_2S formation.

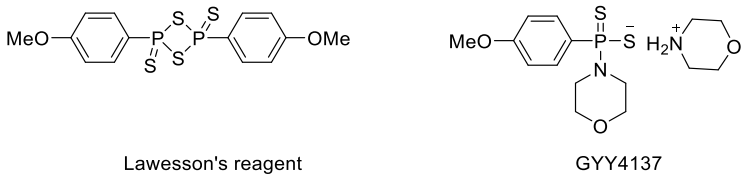

Figure 4.1. Structures of Lawesson's reagent and GYY4137

4.1.1.C. 1,2-Dithiole-3-thiones and derivatives

1,2-Dithiole-3-thiones (DTT) have been used as a H_2S donor (Figure 4.2). Although the detail mechanism of H_2S-release is still not clear, it is widely accepted that hydrolysis is part of the underlying mechanism for the generation of H_2S from DTT.[18] The hybrid analogues of DTT with non-steroidal anti-inflammatory drugs (NSAIDs) have been developed for reducing the side-effects associated with these drugs. Recently, Whiteman and coworkers have reported mitochondria targeted dithiolethione that played a key role in protecting cells from oxidative stress.[19] However, due to lack of trigger to release H_2S, controlled generation of H_2S cannot be achieved using these donors.

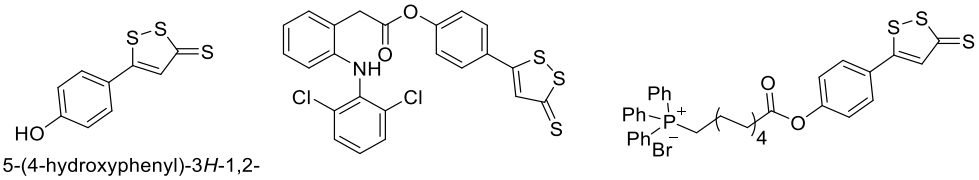

Figure 4.2. Structures of representative dithiolethione derivatives

4.1.1.D. Thiol activated H_2S donors

In the recent years, Ming Xian and coworkers have developed a number of thiol-activated controllable H_2S donors, which mainly includes N-SH-based donors, S-SH-based donors, dithioperoxyanhydrides and arylthioamides (Figure 4.3).[20-23] These compounds react with cysteine and/or glutathione to produce H_2S under physiological conditions. H_2S release rates from these compounds can be tuned by structural modifications. These derivatives have shown important biological activities of H_2S such as anti-inflammatory, vasodilation and cytoprotective effects.[24] However, these donors are not capable of selectively generate H_2S in bacteria, as thiols are present both in bacteria as well as mammalian cells. Furthermore, due to fundamental role of thiols as a general antioxidant within cells, using thiol as a trigger may complicate mechanistic interpretations.

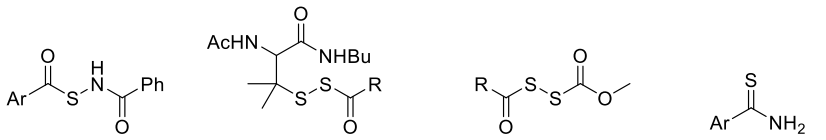

Figure 4.3. Structures of representative thiol-activated H_2S donors

4.1.1.E. Light activated H_2S donors

Ming Xian *et al.* have developed light-activated H_2S donors. They have used gem-dithiol as a template for H_2S generation (Figure 4.4). The gem-dithiol group was protected with light sensitive protecting group, 2-nitrobenzyl, which can be deprotected by irradiation of UV-light. Gem-dithiols are unstable in aqueous solution and therefore it undergoes hydrolysis to produce H_2S.[25] Recently, Nakagawa and coworkers have developed ketoprofenate based photolabile H_2S donor (Figure 4.4).[26] This ketoprofenate-caged donor can release H_2S by eliminating 2-propenylbenzophenone and CO_2 upon irradiation of UV-light at 300–350 nm. Although site-specificity have been achieved using these donors, the use of UV-light as a trigger for H_2S generation is not always convenient under cell culture conditions. In addition, this UV-radiation is known to be cytotoxic to bacteria and may not be appropriate to study the role of H_2S in antibiotic resistance.

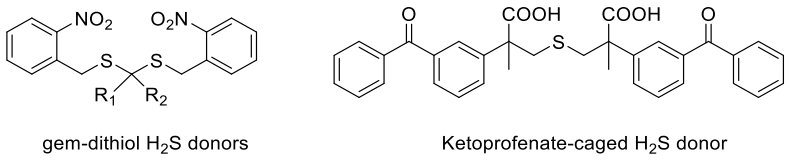

Figure 4.4. Structures of light activated H_2S donors

4.1.1.F. Esterase-activated H_2S donors

Recently, esterase activated H_2S donors have been developed for controlled H_2S generation.[27] Esterase reacts with these prodrugs and cleaves ester group to produce hydroxy compound, which then spontaneously undergoes lactonization to release H_2S (Scheme 4.1). The rate of H_2S generation from these prodrugs was tuned by modifying the ester group and changing the substituent on the aromatic ring. These compounds gives opportunity to tune the H_2S generation, however due to ubiquitous nature of esterase in biological system, species-specificity cannot be achieved.

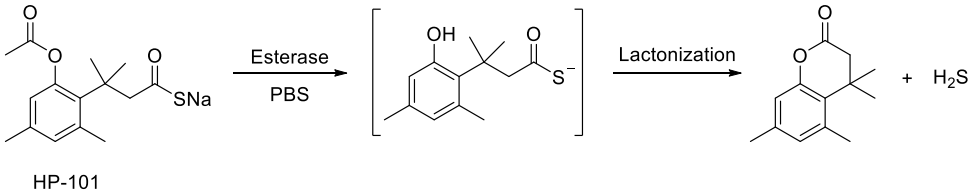

Scheme4.1. Structures of H_2S prodrug HP-101 and the mechanism of esterase-triggered H_2S release.

4.1.1.G. pH-Controlled H_2S donors

Recently, Jianming Kang and coworkers have developed phosphonamidothioate-based pH-controlled H_2S donors.[28] These compounds undergo pH-dependent intramolecular cyclisation to release H_2S (Scheme 4.2). H_2S release from these donors was tuned by the structural modifications of the side-chain residue (R_1). Similar to GYY4137, these phosphorodithioate-based donors showed slow H_2S release under acidic conditions. These donors also exhibited potent cardioprotective effects in an *in vivo* murine model of myocardial ischemia-reperfusion injury. However, using these donors species-specific H_2S generation cannot be achieved. These compounds can release H_2S both in bacteria as well as mammalian cells.

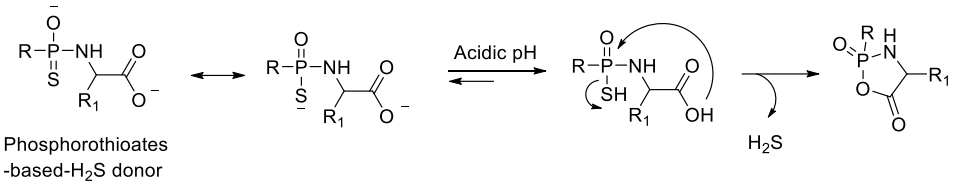

Scheme4.2. Mechanism H_2S release from phosphonamidothioate-based H_2S donors

Thus, in order to study the effect of H_2S in bacterial system there is need for new H_2S donors, which can selectively release H_2S in bacterial cells without affecting the redox-balance of the cellular environment.

4.1.2. Design of H_2S donors

In order to selectively generate H_2S in bacteria, we proposed to synthesize H_2S donors that can be activated by enzyme which is specifically found in bacteria. Enzymatic activation of donor molecule provides unique opportunity for localized delivery of a gaseous molecule. Upon entry into cells, bacterial enzyme can react with its substrate and release the gas molecule. The choice of enzyme and its expression levels can be used to modulate the site-specific delivery of H_2S. Nitroreductase (NTR) is a bacterial enzyme that reduces a broad range of aromatic nitro compounds to amines using nicotinamide adenine dinucleotide phosphate (NADPH) as a reducing cofactor.[29-31] NTR has been used as metabolic trigger for activation of several prodrugs and releases bioactive moleceuls.[32] Typical NTR-activated prodrugs contain 4-nitrobenzyl group which forms a substrate for NTR.[33-35] For example, recently 4-nitrobenzyl protected diazeniumdiolates have been developed as NTR-activated NO donors. Upon activation with

NTR, these compounds releases free diazeniumdiolate, which then undergoes hydrolysis in aqueous solution to produce NO (Scheme 4.3).[36]

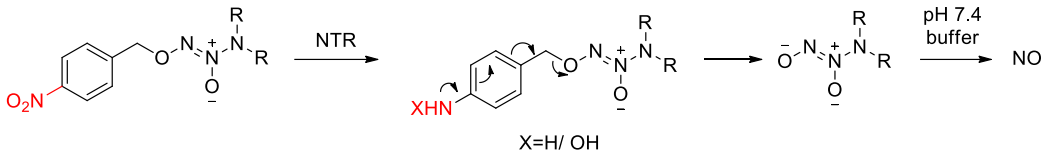

Scheme 4.3. Mechanism of NTR activation of O^2-(4-nitrobenzyl) diazeniumdiolates to release NO

Furthermore, it has been reported that gem-dithiols are unstable species in aqueous environments and they undergo hydrolysis to release H_2S.[37-38] Therefore, we proposed to protect gem-dithiol with a self-immolative linker attached with a substrate for an enzyme that is expressed in bacterial cells. As NTR is not usually found in human cells, this enzyme can facilitate selective generation of H_2S in bacteria. The bis(4-nitrobenzyl)sulfane **29** was proposed as a potential candidate of NTR activated H_2S donors. The 4-nitrobenzyl group of **29** can be used as a functional group for metabolism by the enzyme NTR. The proposed mechanism of activation of bis(4-nitrobenzyl)sulfanes to release H_2S is as shown in Scheme 4.4. The 4-nitrobenzyl group is expected to undergo two electron reduction in the presence of NTR. As a result of reduction, strong electron withdrawing nitro group is converted into an electron donating hydroxylamine or amine group. Upon rearrangement of electrons, a geminal dithiol would be produced. These intermediates have been reported to undergo hydrolysis to produce H_2S as descried earlier.[39]

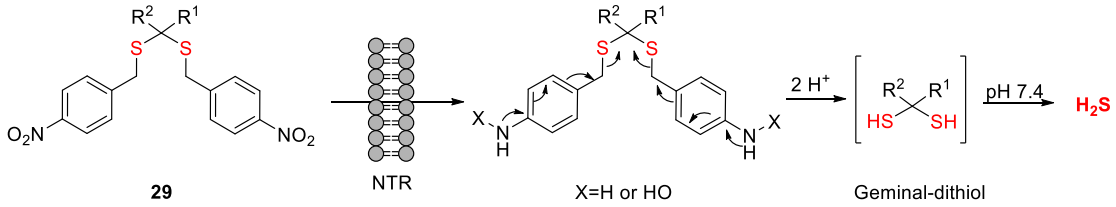

Scheme 4.4. Design and mechanism of NTR-activated H_2S donor **29**; Reduction by NTR results in the formation of an amine or hydroxylamine (X = H or OH); subsequent rearrangement of electrons produces a geminal dithiol that generates H_2S by hydrolysis in buffer.

4.2. Results and Discussion

4.2.1. Synthesis and characterization

To test the hypothesis of NTR activated H_2S generation, we synthesized compounds **29a-29g** in three steps. The readily available 4-nitrobenzyl bromide **26** was reacted with thiourea to afford thiouronium bromide salt **27** in quantitative yield (scheme 4.5). Hydrolysis of **27** in the presence of sodium metabisulfite afforded (4-nitrobenzyl)mercaptan **28** in 94% yield.

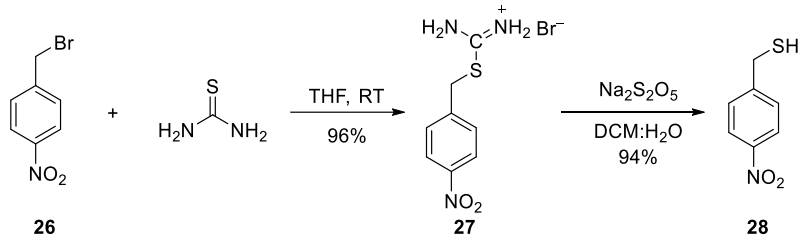

Scheme4.5. Synthesis of (4-nitrobenzyl)mercaptan **28**

Table 4.1. Synthesis of **29a-29g**

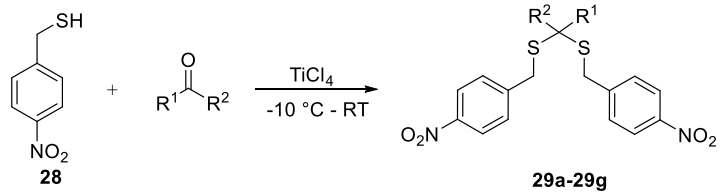

Entry	R^1	R^2	Product	Yield %
1	CH_3	CH_3	**29a**	80
2	Et	Et	**29b**	78
3	Cyclopentyl		**29c**	70
4	Cyclohexyl		**29d**	71
5	Ph	CH_3	**29e**	60
6	4-F-Ph	CH_3	**29f**	42
7	Thiophene	CH_3	**29g**	38

Finally, **28** was reacted with acetone in the presence of catalytic titanium tetrachloride to give compound **29a** in 80% yield (Table 4.1, entry 1). Similarly, a reaction of **28** with diethyl ketone afforded **29b** in 78%yield (Table 4.1, entry 2). A reaction of (4-nitrobenzyl)mercaptan with cyclic ketone such as cyclopentanone and cyclohexanone produced **29c** and **29d** in good yields (Table 4.1, entry 3 & 4). In order to study the possible role of sterics on H_2S release, derivative

29e was synthesized by reacting **28** with acetophenone (Table 4.1, entry 5). The electron withdrawing substituted acetophenone derivative **29f** was synthesized by reacting **28** with 4-fluroacetophenone (Table 4.1, entry 6). (4-nitrobenzyl)mercaptan was also reacted with electron donating substituted acetophenones such as 4'-methoxyacetophenone and 4-methylacetophenone in the presence of titanium tetracholride, but several attempts of isolating the desired products were unsuccessful possible due to decomposition of expected product during purification. However, a reaction of **28** with 2-acetylthiophene proceeded fine and we obtained **29g** in 38% yield (Table 4.1, entry 7). We also synthesized the negative control **30** by esterification of benzoic acid with 4-nitobenzyl alcohol using 1-(3-dimethylaminopropyl)-3-ethylcarbodiimide hydrochloride (EDC-HCl) and 4-dimethylaminopyridine in 84% yield. We predicted that this compound would undergo reduction with NTR but should not produce H_2S (scheme 4.6).

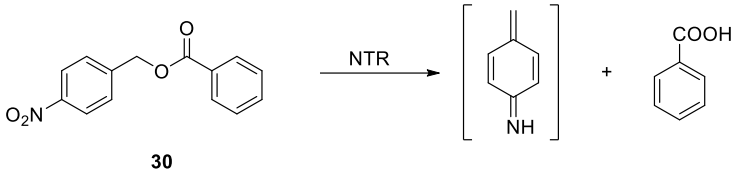

30

Scheme 4.6. NTR-activation of negative control **30**

4.2.2. H_2S release studies

4.2.2.1. H_2S measurement using azide based probe 31a

After synthesis of bis(4-nitrobenzyl)sulfane derivatives **29a-29g**, we studied their ability to undergo metabolism with NTR to release H_2S. However, precise measurement of H_2S concentration is challenging due to high reactivity and volatility of this gaseous species. Methylene blue, the most commonly used method for H_2S detection is not compatible with enzymatic assay and provides erroneous results.

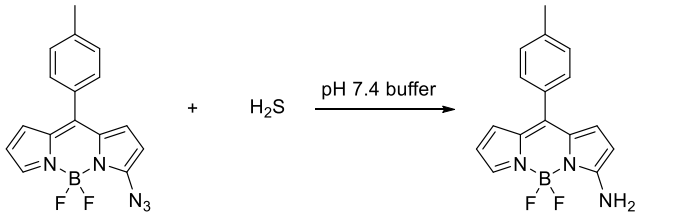

31a **31b**

λ_{ex} - 444 nm, λ_{em} - 515 nm

Scheme 4.7. Reduction of non-fluorescent BODIPY-azide **31a** by H_2S to fluorescent BODIPY-amine **31b**

The fluorescence based assays have also been developed for measurement of low micromolar concentration of H_2S in biological samples in a non-destructive manner.[40] Organic azides are known to undergo reduction with H_2S and this property has been used for the development of H_2S probes. Recently, an azide based **31a** was developed for H_2S detection.[41] H_2S selectively reduces weakly fluorescent azide to produce a highly fluorescent amine **31b** (scheme 4.7). First, the azide-based fluorescent probe **31a** was synthesized using a reported procedure.[41] The azide-based fluorescent probe **31a** was used for the measurement of H_2S generated from bis(4-nitrobenzyl)sulfanes in the presence of NTR. A 96-microwell plate based protocol was developed. When sodium sulphide was incubated with probe **31a** in pH 7.4 buffer, a distinct fluorescence signal was observed at 515 nm (Figure 4.5), confirming the suitability of this probe for H_2S measurement. Next, compound **29a** was co-incubated with **31a** in pH 7.4 buffer, but no evidence of H_2S generation was found suggesting the stability of this compound under these conditions. However, when **29a** was exposed to NTR and cofactor NADH in the presence of **31a**, a distinct fluorescence signal was observed (Figure 4.5), confirming the intermediacy of H_2S. Under similar conditions, when **29b-29g** were independently incubated with NTR, an increase in fluorescence was observed confirming the abilities of these donors to generate H_2S.

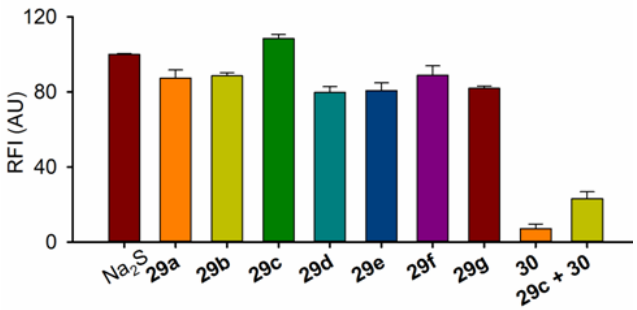

Figure 4.5. Estimation of H_2S generation during incubation of **29a-29g** (50μM) with NTR in HEPES buffer pH 7.4 using BODIPY-based sensor **31a**

Furthermore, fluorescence studies revealed that by changing the steric on gem-dithiol did not significantly affect H_2S generation. In order to confirm the fluorescence signal obtained during incubation of these compounds with NTR was mainly because of H_2S and not due to other reactive species, a similar experiment was conducted with negative control **30**. We expected that this compound would undergo reduction with NTR but should not generate H_2S. Indeed, when **30** was incubated with NTR, as expected no fluorescence signal was observed (Figure 4.5).

Amongst compounds tested, **29c** was found to be the best H_2S donor. In order to confirm the NTR-mediated activation of these compounds to release H_2S, we conducted a control experiment with a competitive substrate. We expected that in the presence of competitive substrate **30**, the H_2S yield from **29c** should diminish. Indeed, when **29c** + NTR was co-incubated with 10 equivalents of **30** in pH 7.4 buffer, diminished fluorescence was observed (Figure 4.5). Together these results confirmed NTR-activated H_2S generation.

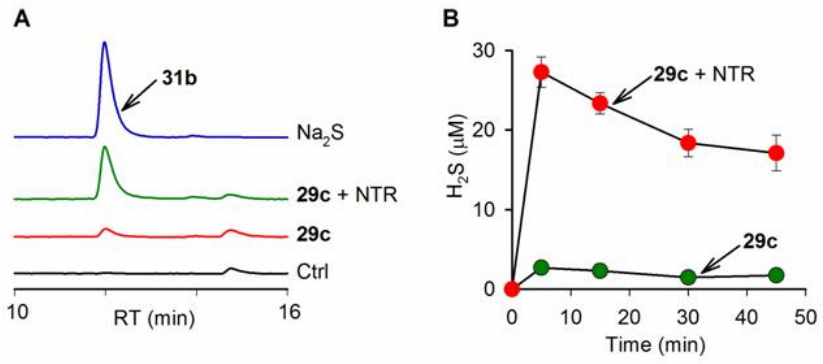

Figure 4.6. (A)HPLC determination of H_2S generation during incubation of **29c** (50 μM) in the presence of NTR and NADH using BODIPY-based sensor **31a** (B) Time course of H_2S generation during incubation of **29c** (50 μM) with NTR in HEPES buffer pH 7.4.

Next, H_2S mediated conversion of **31a** to **31b** in the aforementioned assay was confirmed using HPLC-based assay. The azide-based probe **31a** was incubated with H_2S donor **29c** in pH 7.4 buffer and the resulting mixture was analyzed using HPLC equipped with a fluorescence detector. The formation of **31b** was measured by monitoring fluorescence signal (λ_{ex}-444 and (λ_{em}- 515 nm). The HPLC analysis revealed that no formation of **31b** indicating the stability of H_2S donor under these conditions (Figure, 4.6A). However, when **29c** was exposed to NTR,we observed a new peak at 12 min corresponding to **31b** (Figure, 4.6A) confirming the intermediacy of H_2S. Under similar conditions, when sodium sulfide was reacted with probe **31a**, we observed a similar peak corresponding to **31b** at same retention time (Figure 4.6A). Subsequently, a time course of H_2S generation from **29c** was measured. Unlike hydrolysis-based H_2S donors (i.e., GYY4137 and Na_2S/NaHS), **29c** was found to stable in pH 7.4 buffer. However, in the presence of NTR a gradual increase in H_2S level was observed (Figure 4.6B). The H_2S concentrations started to drop after peak time probably due to volatilization. Thus, this experiment demonstrated the controlled generation of H_2S upon activation with NTR.

4.2.2.2. Hydrogen sulfide measurement using mBBr assay

The precise measurement of H_2S is challenging due to its propensity to undergo oxidation to sulfite, sulfate and polysulfide in the presence of a metal ion under aerobic conditions. Furthermore, other biological thiols such as cysteine and glutathione interfere during the measurement of H_2S. We independently confirmed the H_2S generation from **29c** by another reported protocol using monobromobimane (mBBr) with minor modifications.[42-43] In this method sulfide anion reacts with mBBr and produces a highly fluorescent thioether compound **32b** (Scheme 4.8), which can be detected using HPLC attached with a fluorescent detector.

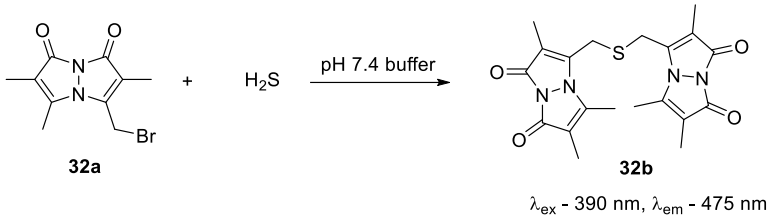

Scheme 4.8. Formation of sulfide-dibimane **32b** during reaction of monobromobimane **32a** with H_2S

When H_2S donor **29c** was incubated with mBBr, no evidence of hydrogen sulfide generation was found in the absence of NTR. However, when **29c** was exposed to NTR, a new peak at 12.8 min corresponding to sulfide-dibimane **32b** was observed (Figure 4.7), confirming the intermediacy of H_2S. Sodium sulfide was used as a positive control in this assay. When sodium sulfide was reacted with mBBr, we observed a similar peak corresponding to **32b** at the same retention time (Figure 4.7). Thus, this experiment also confirmed the H_2S generation from **29c** in the presence of NTR.

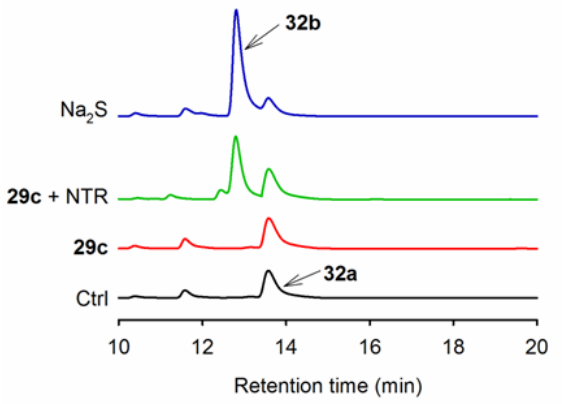

Figure 4.7. Measurement of H_2S generation during incubation of **29c** (50 μM) in the presence of NTR using HPLC based mBBr assay. mBBr (**32a**) reacts with sulfide anion to produce a sulfide-dibimane **32b**, which was monitored using fluorescence channel (λ_{ex} - 390 nm and λ_{em}- 475 nm).

4.2.3. H_2S generation in bacteria

Having demonstrated H_2S generation in buffer, the ability of **29c** to permeate bacterial cells and enhance H_2S was measured by our collaborator using a flow cytometry study. NTR is an enzyme present in bacteria and 4-nitrobenzyl is a well-known substrate for NTR. Thus in order to check, whether bis(4-nitrobenzyl)sulfanes gets activated within bacteria to release H_2S, the azide-based probe **31a** was usedfor intracellular H_2S measurement. The H_2S donor **29c** was used as a representative of bis(4-nitrobenzyl)sulfanes in this assay. Exponentially grown *E. coli* pre-treated with H_2S donor **29c** was incubated with probe **31a** for 5 min and fluorescence was measured using flow cytometry. The flow cytometry analysis revealed an increase in fluorescence (Figure 4.8A), confirming the suitability of this donor to enhance intracellular H_2S level.

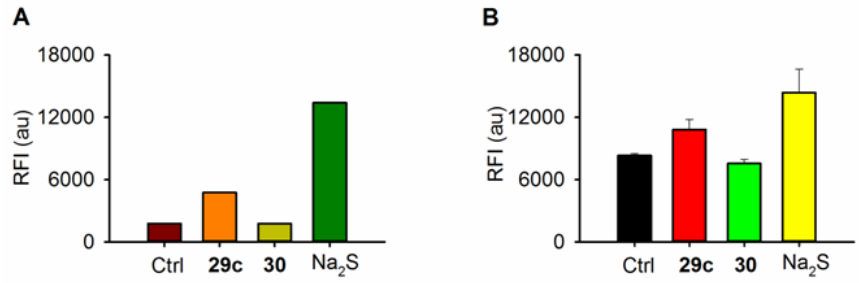

Figure 4.8. Flow cytometry analysis of intracellular H_2S generation by **29c** (50 μM) in (A) *E. coli* and (B) *M.* smegmatis; Na_2S was used as positive control and **30** was used as a negative control compound. (Data provided by Dr. Amit Singh, IISc Bangalore.)

In order to verify that the fluorescence attributed during the incubation of **29c** was due to H_2S, a similar experiment was conducted with a negative control **30**. As expected, we found negligible increase in fluorescence, confirming that H_2S generation from **29c** resulted in an increase in fluorescence. When *E. coli* was incubated with Na_2S, a similar result was observed (Figure 4.8A). To check the ability of **29c** to generate H_2S in *Mycobacterium smegmatis* (*M. smegmatis*), a fast growing and non-pathogenic strain of *Mycobacterium Species*, a flow cytometry analysis was conducted. The results revealed that compound **29c** was capable of enhancing intracellular H_2S level *M. smegmatis* as well (Figure 4.8B). Similarly, negative control **30** did not show an increased fluorescence

in *M. smegmatis*. Together, these experiments confirmed the suitability of this tool to enhance intrabacterial H_2S level.

The ability of **29c** to generate H_2S in bacteria was independently evaluated using a HPLC-based assay. In this assay, *E. coli* cells were co-incubated with probe **31a** and H_2S donor **29c** for 1h. The excessive reagents were removed by discarding supernatant after centrifuging bacterial culture. The bacterial cells were lysed using probe sonicator and the cell lysate was analysed using an HPLC attached with a fluorescence detector. The HPLC analysis revealed the formation of new peak corresponding to **31b** (Figure 4.9A), confirming the H_2S generation in *E. coli*. When similar experiment was conducted in *Bacillus subtilis* (*B. subtilis*), and *M. smegmatis*, similar results were observed (Figure 4.9B and 4.9C, respectively). Thus, these experiments confirmed the ability of this donor to enhance H_2S levels in three different bacteria.

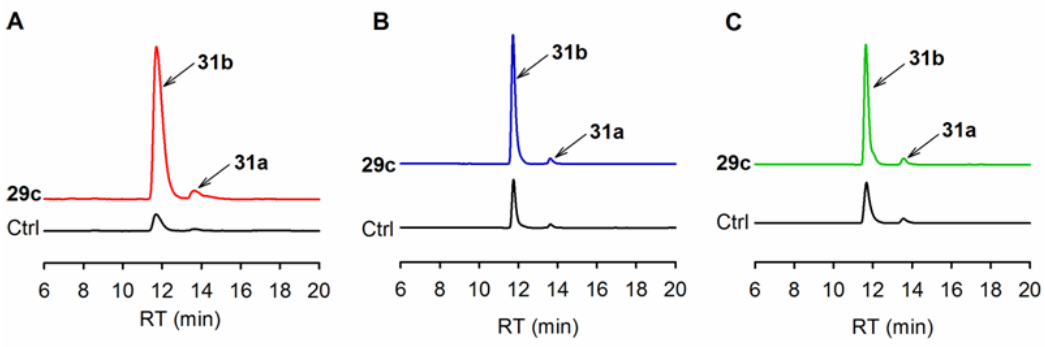

Figure 4.9. Estimation of H_2S generation by **29c** in (A) *E. coli*, (B) *B. Subtilis* and (C) *M. Smegmatis* using HPLC based assay. The formation of **31b** was monitored using HPLC attached with fluorescence detector (λ_{ex}-444 nm and λ_{em}-515 nm).

4.2.4. H_2S generation in macrophages

Methodologies available for H_2S generation, as described in section 4.2.1, do not provide opportunity for selectively enhancing H_2S level in bacterial cells. Macrophages are among the first responders to infection. These cells engulf pathogens and produce fluxes of toxic ROS and RNS.[44-45] It has been proposed that bacteria produces H_2S as a general defense mechanism to counter the stress induced by the host immune cells.[9] In order to study the intrabacterial stress responses during infection, simulating increased H_2S levels within bacteria but not in macrophages is necessary. The enzyme-activated donors have substantial potential of ensuring species selective or cell selective activation of the donor.

As NTR is predominantly present in bacteria but not in mammalian cells, the H_2S donor **29c** must selectively enhance H_2S levels in bacteria but not in mammalian cells. In order to test this hypothesis, human monocytic cells (THP-1) pretreated with **29c** were incubated with probe **31a** and H_2S level was assessed using flow cytometry. The flow cytometry analysis revealed that compound **29c** remained ineffective in enhancing H_2S level (Figure 4.10A). Similarly, when THP-1 cells were treated with a negative control compound **30**, a similar result was recorded. On the other hand, when THP-1 cells were treated with sodium sulfide, an increased fluorescence was observed, confirming its ability to enhance H_2S level in THP-1 cells.

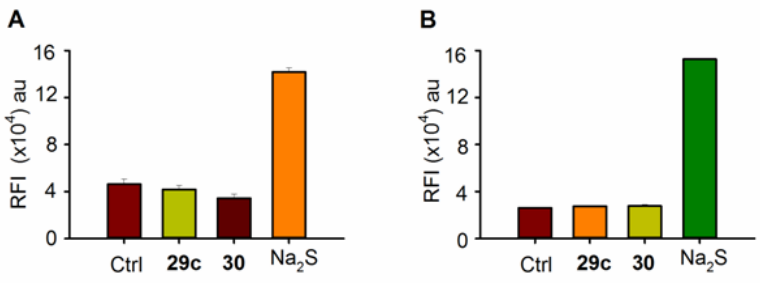

Figure 4.10. Flow cytometry analysis of H_2S generation by **29c** (50 μM) in (A) human monocytic cells (THP-1) and (B) Raw 264.7 cells; Na_2S was used as positive control and compound **30** was used as a negative control compound. (Data is provided by Dr. Amit Singh, IISc Bangalore.)

Next, raw 264.7 cells were incubated with H_2S donor **29c**, but no evidence of H_2S generation was found (Figure 4.10B). Similarly, incubation of negative control compound **30** with raw 264.7 cells did not enhance H_2S level. However, sodium sulfide was able to enhance H_2S levels in raw cells. These experiments suggest that while Na_2S uniformly enhances H_2S levels in both bacterial and mammalian cells, however, **29c** selectively enhanced H_2S levels only in bacterial cells.

The unique feature of these H_2S donors to selectively enhance H_2S levels in bacteria allowed us to investigate role of this gaseous molecule in bacteria and our preliminary investigation reveals that H_2S directly control intracellular redox-balance of bacteria to counter the lethal degree of oxidative stress induced by antibiotics. Further investigation about the precise role of H_2S in antibiotic resistance is currently underway.

4.3. Conclusion

In summary, we have designed and synthesized bis(4-nitrobenzyl)sulfanes as NTR activated H_2S donors. These compounds were found to be stable in pH 7.4 buffer, but upon activation with NTR produced H_2S. We have inferred the H_2S generation from these donors using an azide-based fluorescent probe. The novel H_2S prodrugs that we have developed here provide unique opportunity to selectively enhance H_2S levels within bacterial cells. Using HPLC-based assay, we have demonstrated H_2S generation in *E. coli*, *M. smegmatis* and *B. subtilis*. However, these prodrugs were unable to enhance H_2S levels in macrophages. Thus, we believe that the new class of NTR-activated H_2S donors that we have developed here would be very useful tools for understanding the precise role of H_2S in antibiotic resistance. These studies are presently underway.

4.4. Experimental Section

4.4.1. Synthesis and Characterization

Compounds **28**[46] and **31a**[41] have been previously reported and analytical data that we collected were consistent with the reported values.

General procedure for synthesis of 29a-29g

To a solution of ketone (1 mmol) and *p*-nitrobenzyl mercaptan **28** (2.5 mmol) in chloroform (5 mL) was added 0.5 equivalents of $TiCl_4$ at 0 °C. The resulting reaction mixture was allowed to warm up to RT and stirred overnight or until the consumption of the corresponding ketone (monitored by TLC). To the resulting heterogeneous mixture was then added brine (5 mL) and aqueous layer was extracted with $CHCl_3$ (3×10 mL). The combined organic layer was dried over anhydrous sodium sulfate, filtered and concentrated. The crude material was purified using silica gel column chromatography, eluted with 4-8% EtOAc/pet ether to afford **29a-29g**.

Propane-2,2-diylbis((4-nitrobenzyl)sulfane) (29a)

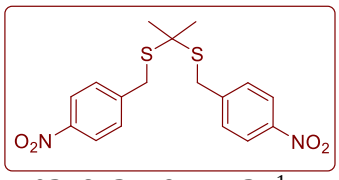

Following the general procedure for the synthesis of bis(4-nitrobenzyl)sulfane **29a** was obtained with an yield of 80% (260 mg). mp 148-150 °C; FT-IR (ν_{max}, cm^{-1}): 3742, 1647, 1596, 1334, 1103, 853, 795, 713; ^{1}H NMR (400 MHz, $CDCl_3$): δ 8.17 (d, *J*= 8.7 Hz, 4H), 7.50 (d, *J*= 8.7 Hz, 4H), 3.92 (s, 4H), 1.60 (s, 6H); ^{13}C NMR (100 MHz, $CDCl_3$): δ 147.1, 145.9, 130.0, 123.9, 58.2, 34.8, 30.9; HRMS (ESI): calcd. For $C_{17}H_{18}N_2O_4S_2$ $[M+Na]^+$: 401.0605; Found: 401.0605

Pentane-3,3-diylbis((4-nitrobenzyl)sulfane)(29b)

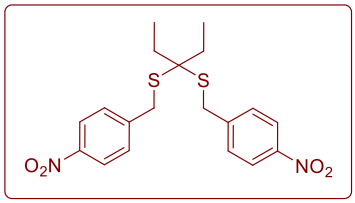

Following the general procedure for the synthesis of bis(4-nitrobenzyl)sulfane **29b** was obtained with an yield of 57% (370 mg). mp 124-126 °C; FT-IR (ν_{max}, cm^{-1}): 1658, 1598, 1559, 1517, 1458, 1342, 1106, 1013, 855; ^{1}H NMR (500 MHz, $CDCl_3$): δ 8.17 (d, *J* = 8.6 Hz, 4H), 7.48 (d, *J* = 8.7 Hz, 4H), 3.87 (s, 4H), 1.67 (q, *J* = 7.3 Hz, 4H), 0.93 (t, *J* = 7.3 Hz, 6H); ^{13}CNMR (50 MHz, $CDCl_3$): δ 147.0, 145.8, 129.9, 123.8, 68.5, 33.4, 28.6, 8.3;HRMS (ESI): calcd. For $C_{19}H_{22}N_2O_4S_2$ $[M+Na]^+$: 429.0919; Found: 429.0921

Cyclopentane-1,1-diylbis((4-nitrobenzyl)sulfane) (29c)

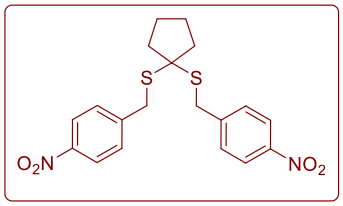

Following the general procedure for the synthesis of bis(4-nitrobenzyl)sulfane **29c** was obtained with an yield of 70% (169 mg). mp 94-96 °C; FT-IR (ν_{max}, cm^{-1}): 3852, 3734, 3674, 3648, 1716, 1597, 1558, 1540, 1508, 1338, 1107, 853, 799; ^{1}H NMR (400 MHz, $CDCl_3$): δ 8.17 (d, *J*= 8.7 Hz, 4H), 7.50 (d, *J*= 8.6 Hz, 4H), 3.92 (s, 4H), 1.87-1.84 (m, 4H), 1.78-1.75 (m, 4H); ^{13}C NMR (100 MHz, $CDCl_3$): δ 147.1, 146.2, 130.1, 123.9, 67.9, 41.6, 35.3, 24.3; HRMS (ESI): calcd. For $C_{19}H_{20}N_2O_4S_2$ $[M+Na]^+$: 427.0761; Found: 427.0762

Cyclohexane-1,1-diylbis((4-nitrobenzyl)sulfane) (29d)

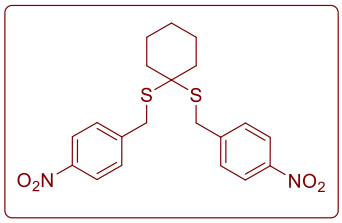

Following the general procedure for the synthesis of bis(4-nitrobenzyl)sulfane **29d** was obtained with an yield of 71% (140 mg). mp 96-98 °C; FT-IR (ν_{max}, cm^{-1}): 3852, 3734, 3674, 3648, 1733, 1716, 1698, 1652, 1508, 1107, 854, 745; ^{1}H NMR (400 MHz, $CDCl_3$): δ 8.17 (d, *J*= 8.6 Hz, 4H), 7.50 (d, *J*= 8.6 Hz, 4H), 3.90 (s, 4H), 1.84-1.81 (m, 4H), 1.62-1.58 (m, 4H), 1.47-1.45 (m, 2H); ^{13}C NMR (100 MHz, $CDCl_3$): δ 147.1, 146.2, 130.0, 123.9, 64.4, 38.0, 33.3, 25.5, 22.5; HRMS (ESI): calcd. For $C_{20}H_{22}N_2O_4S_2$ $[M+Na]^+$: 441.0919; Found: 441.0923.

(1-Phenylethane-1,1-diyl)bis((4-nitrobenzyl)sulfane) (29e)

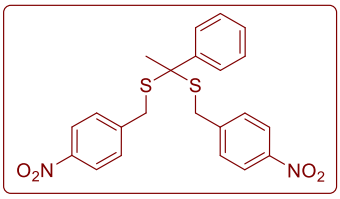

Following the general procedure for the synthesis of bis(4-nitrobenzyl)sulfane **29e** was obtained with an yield of 60% (220 mg). mp 109-111 °C; FT-IR (ν_{max}, cm^{-1}): 3586, 1558, 1396, 974, 857, 803, 767, 752, 699; ^{1}H NMR (400 MHz, $CDCl_3$): δ 8.10 (d, *J*= 8.7 Hz, 4H), 7.69 (d, *J*= 7.6 Hz, 2H), 7.40-7.22 (m, 7H), 3.88-3.77 (m, 4H), 2.04 (s, 3H); ^{13}C NMR (100 MHz, $CDCl_3$): δ 147.0, 145.2, 142.2, 130.0, 128.7, 128.1, 127.1, 123.8, 62.7, 35.4, 30.5; HRMS (ESI): calcd. For $C_{22}H_{20}N_2O_4S_2$ $[M+Na]^+$: 463.0761; Found: 463.0768.

(1-(4-Fluorophenyl)ethane-1,1-diyl)bis((4-nitrobenzyl)sulfane)(29f)

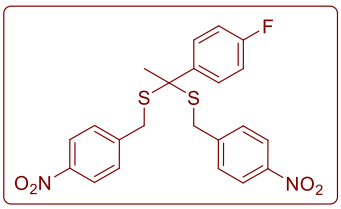

Following the general procedure for the synthesis of bis(4-nitrobenzyl)sulfane **29f** was obtained as a semisolid compound with an yield of 42% (274 mg); FT-IR (ν_{max}, cm^{-1}): 1598, 1518, 1345,

1163, 1065, 858, 841; ^{1}H NMR (500 MHz, $CDCl_3$): δ 8.12 (d, *J*= 8.7 Hz, 4H), 7.69-7.66 (m, 2H), 7.37 (d, *J* = 8.7 Hz, 4H), 7.02 (t, *J* = 8.6 Hz, 2H), 3.89-3.73 (m, 4H), 2.02 (s, 3H); ^{13}C NMR (50 MHz, $CDCl_3$): δ 159.7, 147.0, 144.9, 129.9, 129.0, 128.8, 123.8, 115.6, 115.2, 62.0, 35.4, 30.5; HRMS (ESI): calcd. For $C_{22}H_{29}FN_2O_4S_2$ $[M+Na]^+$: 481.0667; Found: 481.0671.

2-(1,1-Bis((4-nitrobenzyl)thio)ethyl)thiophene (29g)

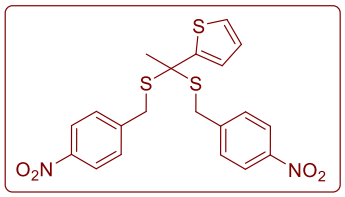

Following the general procedure for the synthesis of bis(4-nitrobenzyl)sulfane **29g** was obtained as a semisolid compound with an yield of 38% (266 mg); FT-IR (ν_{max}, cm^{-1}): 1599, 1522, 1347, 1109, 1077, 857, 803, 739; ^{1}H NMR (500 MHz, $CDCl_3$): δ 8.13 (d, *J*= 8.7 Hz, 4H), 7.40 (d, *J*= 8.7 Hz, 4H), 7.32-7.28 (m, 1H), 7.16 (dd, *J* = 3.16, 1.1 Hz, 1H), 6.94-6.92 (m, 1H), 3.93-3.86 (m, 4H), 2.07 (s, 3H); ^{13}C NMR (50 MHz, $CDCl_3$): δ 148.4, 147.0, 144.9, 130.0, 126.8, 126.3, 126.1, 123.8, 59.5, 35.8, 31.9; HRMS (ESI): calcd. For $C_{20}H_{18}N_2O_4S_3$ $[M+Na]^+$: 469.0326; Found: 469.0327.

4.4.2. H_2S generation from 29a-29g

A stock solution of **29a-29g** (2.5 mM) was prepared in DMSO and 10mM NADH was prepared in HEPES buffer pH 7.4. A stock solution of commercially available *E. coli* nitroreductase (NTR) was prepared using 1 mg of a lyophilized powder dissolved in HEPES buffer (2 mL). A solution of **31a** (1 mM) was prepared in DMSO and stored under dark conditions. The reaction mixture was prepared by adding bis (4-nitrobenzyl)sulphane(4 µL, 2.5 mM), NADH (10 µL, 10mM) and NTR (4µL) in HEPES buffer of pH 7.4 (162µL). The resulting mixture was incubated at 37 °C for 5 min. of **31a** (20 µL,1 mM) was added to the above mixture and incubated for 10 min at 37 °C under dark conditions and fluorescence (excitation 444 nm; emission 520 nm) from reaction mixture was measured using microtiter plate reader. In the control experiment **29c** was co-treated with competitive substrate of NTR **30** (5 µL, 20 mM). Data presented is an average of three independent experiments.

4.4.3. H_2S measurement using HPLC-based assay

A reaction mixture was prepared by adding **29c** (4 µL, 2.5 mM), NADH (10 µL, 10 mM), **31a** (10 µL, 1 mM) and NTR (4µL) in HEPES buffer (172µL) pH 7.4. The resulting mixture was incubated at 37 °C for 5 min under dark conditions. The reaction mixture was filtered (0.22 µm)

and injected (50 μL) in an Agilent high performance liquid chromatography (HPLC) attached with a fluorescence detector (excitation at 444 nm; emission at 520 nm). The column used was Zorbax SB C-18 reversed phase column (250 mm × 4.6 mm, 5 μm), the mobile phase was water: acetonitrile and a gradient starting with 60: 40 % →0 min, 60: 40 to 30: 70 → 0 - 10 min, 30: 70 to 0: 100 → 10 - 17 min, 0: 100 → 17 – 25 min, 0: 100 to 60: 40 → 25 – 28 min was used with flow of 1 mL/min. We independently injected the solution of 50 μM of **31b** (retention time 11.7 min) and confirmed the formation of **31b** from **31a** by H_2S generated from **29c**. Na_2S (100 μM) was reacted with **31a** and served as a positive control.

4.4.4. Calibration curve of Na_2S

A 10 mM Na_2S stock solution was prepared in DI water. The standard solutions of Na_2S (20, 40, 60, 80, 100 μM) were prepared by diluting 20, 40, 60, 80 and 100 μL of 1 mM Na_2S to 1 mL of water, respectively. To standard solution of Na_2S (180 uL), azo-BODIPY **31a** (1 mM, 20 uL) was added in 96-well plate in triplicate. The resulting mixture was incubated at 37 °C for 10 min and fluorescence (excitation 444 nm; emission 520 nm) from reaction mixture was measured using microtiter plate reader.

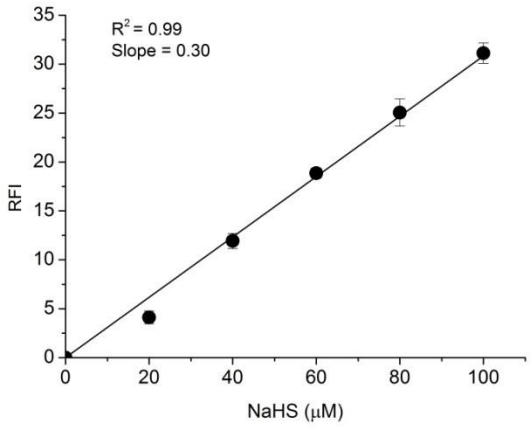

Figure S1. Calibration curve of Na_2S obtained by using azo-BODIPY dye

4.4.5. Time course of H_2S release from 29c

A reaction mixture was prepared by adding **29c** (4 μL, 2.5 mM), NADH (10 μL, 1 mM) and NTR (4μL) in HEPES buffer (162μL) pH 7.4. The resulting mixture was incubated at 37 °C. At different time interval (5, 15, 30 and 45 min) **31a** (20 μL, 1 mM) was added to the above mixture

and incubated under dark conditions for 10 min at 37 °C. The fluorescence (excitation 444 nm; emission 520 nm) from reaction mixture was measured using microtiter plate reader. A calibration curve was used to quantify hydrogen sulfide produced during incubation of **29c** with NTR. In the control experiment **29c** (4 μL, 2.5 mM) was incubated with NADH (10 μL, 10 mM) in HEPES buffer pH 7.4 (166 μL) and at different time interval **31a** (20μL, 1 mM) was added. The fluorescence from reaction mixture was measured. Data presented is an average of three independent experiments.

4.4.6. H_2S measurement using mBBr assay

A 10 mM stock solution of mBBr was prepared in degassed CH_3CN and stored at -20 °C under dark conditions. A 100 mM Na_2S solution was prepared in degassed water and diluted further it to 1 mM in degassed water. Reaction mixture was prepared by adding Na_2S (30 μL, 1 mM), reaction buffer (70 μL, 100 mM Tris-HCl buffer pH 9.5 with 0.1 mM DTPA) and mBBr (50 μL, 0.4 mM) under ambient conditions. The resulting mixture was incubated at RT for 30 min under dark conditions and quenched with 50 μL (1M HCl) solution. In the experiments of **29c** with NTR, the reaction mixture was prepared by adding **29c** (4μL, 2.5 mM), NADH (10 μL, 10 mM) NTR (4μL as prepared previously) in reaction buffer (82μL) pH 9.5. The resulting mixture was incubated for 10 min at 37 °C. To this incubated mixture, mBBr (50 μL, 0.4 mM) was added and incubated at RT for 30 min under dark conditions. The mixture was quenched with 50 μL (1M HCl) solutions. The resulting mixture was filtered (0.22 μm) and injected (10 μL) in an HPLC attached with a fluorescence detector (excitation at 390 nm; emission at 475 nm). The column used was Zorbax SB C-18 reversed phase column (250 mm × 4.6 mm, 5 μm). The mobile phase was water: acetonitrile containing 0.1 % trifluroacetic acid and a gradient starting with 85: 15 →0 min, 85: 15 to 65: 35 → 0 - 5 min, 65: 35 to 45: 55 → 5 - 16 min, 45: 55 to 30: 70 →16 – 23 min, 30: 70 to 10: 90 →23 – 24 min, 10: 90 to 85: 15 →24 – 26 min was used with flow of 0.6 mL/min. Under these conditions, we observed the formation of sulfide dibimane, which elutes at 12.78 min.

4.4.7. FACS analysis

E. coli (ATCC 25922) cells were grown in luria broth (LB) until the OD_{600} of 0.2. *E. coli* cells were washed with 1xPBS and suspended in LB. Cells were pre-treated with **29c** (50 μM) for 20 min followed by addition of **31a** (10 μM) for 5 min. The cells were also treated separately with

30 (50 μM) as a negative control and sodium sulphide (50 μM) as a positive control. The H_2S levels were monitored by measuring mean fluorescence intensity of 30,000 *E coli* cells at an excitation wavelength of 405 nm and emission wavelength of 520 nm using a BD FACS verse flow cytometer (BD Biosciences). Data was analyzed using the FACSuitesoftware. *M. smegmatis* cells were grown in Middlebrook 7H9 broth (Difco) supplemented with 10% OADC (Becton Dickinson), 0.1% Glycerol and 0.1% tween 80 until the mid-log phase (OD_{600} of 0.8) and similar protocol was used for H_2S measurement. This measurement was carried out in Dr. Amit Singh Lab, IISc Bangalore.

4.4.8. Intracellular detection of H_2S from 29c using HPLC

E. coli was cultured in 5 mL of tryptone soya broth (TSB) medium at 37 ºC for 16 h. The cultured bacteria were centrifuged to aspirate out the medium and resuspended to an O.D of 1.0 with fresh TSB medium. This bacterial solution was incubated with **29c** (50 μM) and **31a** (10 μM) for 60 min in dark by covering the falcon tube in an aluminum foil. The suspension was centrifuged to aspirate out any excess of the compound and/or azo-BODIPY in the medium. The bacterial pellete was washed with HEPES buffer pH 7.4 (1 mL × 3) and centrifuged. The collected bacterial pellet was re-suspended with acetonitrile and the cells were lysed by vortexing for 1 min. The cell lysate was then removed by centrifugation and the supernatant acetonitrile (50 μL) was injected in an HPLC attached with a fluorescence detector (excitation at 444 nm; emission at 520 nm). The HPLC method used was as described previously.

4.4.9. H_2S generation in macrophages

The human monocytic cell line THP-1 and raw 264.7 cells were maintained in an atmosphere containing 5% CO_2 at 37 °C in the culture medium recommended by ATCC. The THP-1 and raw 264.7 cells were harvested and washed in 1xPBS and suspended in 1x PBS containing 3% fetal bovine serum. Cells were pre-treated with **29c** (50 μM) for 30 min followed by addition of **31a** (10 μM) for 5 min. The negative control **30** (50 μM) was also incubated with these cells. Sodium sulfide (50 μM) was used as positive control. H_2S generation was monitored by measuring mean fluorescence intensity of 30,000 THP-1 cells at an excitation wavelength of 405 nm and emission wavelength of 520 nm using a BD FACS verse flow cytometer (BD Biosciences). Data was analyzed using the FACSuite software. This measurement was carried out in Dr. Amit Singh Lab, IISc Bangalore.

4.5. Spectral charts

^{1}H NMR Spectrum (400 MHz, $CDCl_3$) of **29a**

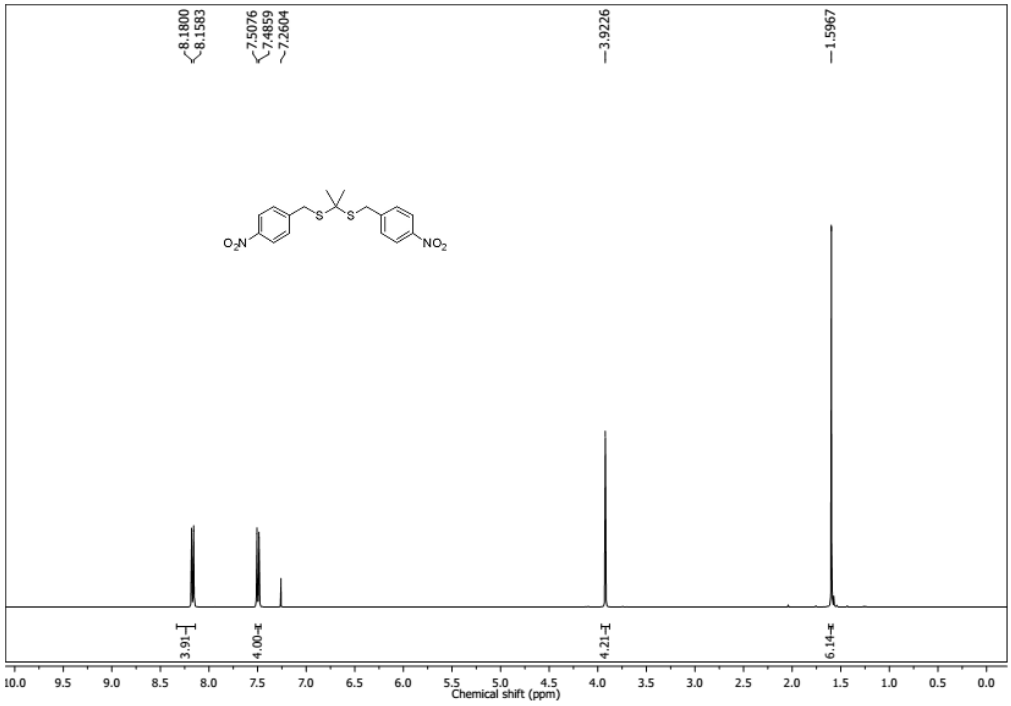

^{13}C NMR Spectrum (100 MHz, $CDCl_3$) of **29a**

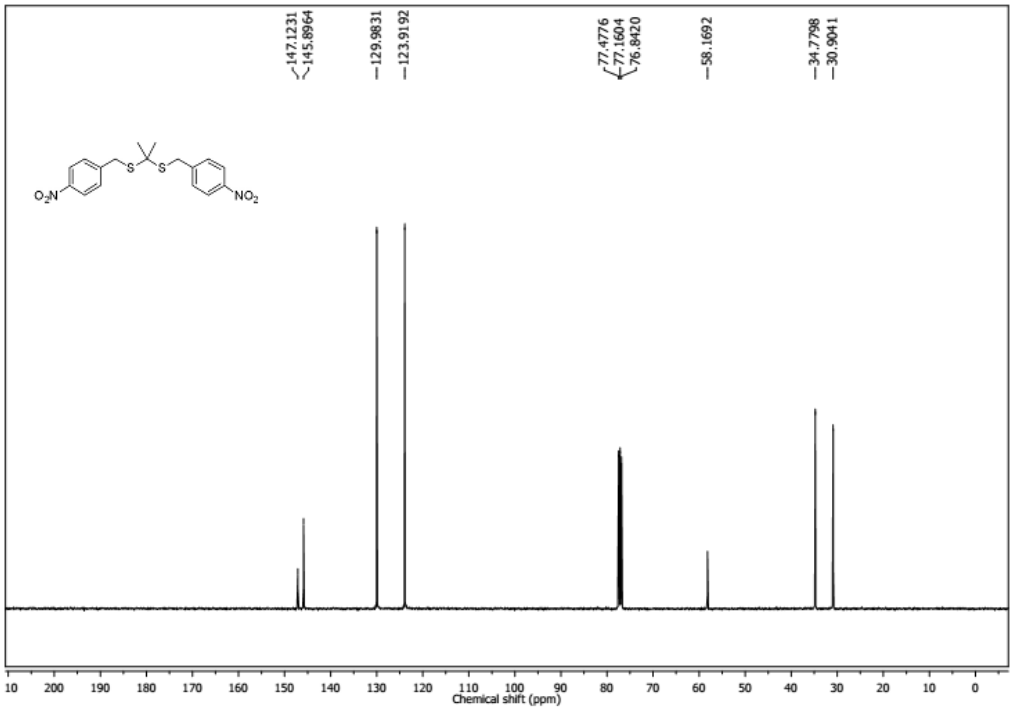

^{1}H NMR Spectrum (500 MHz, $CDCl_3$) of **29b**

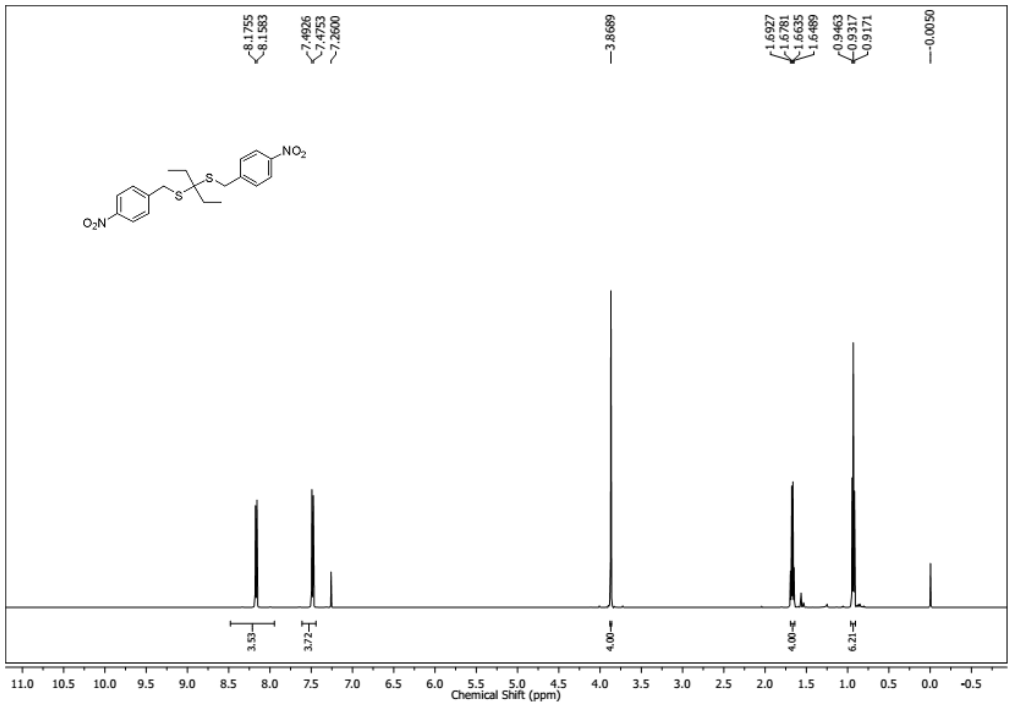

^{13}C NMR Spectrum (125 MHz, $CDCl_3$) of **29b**

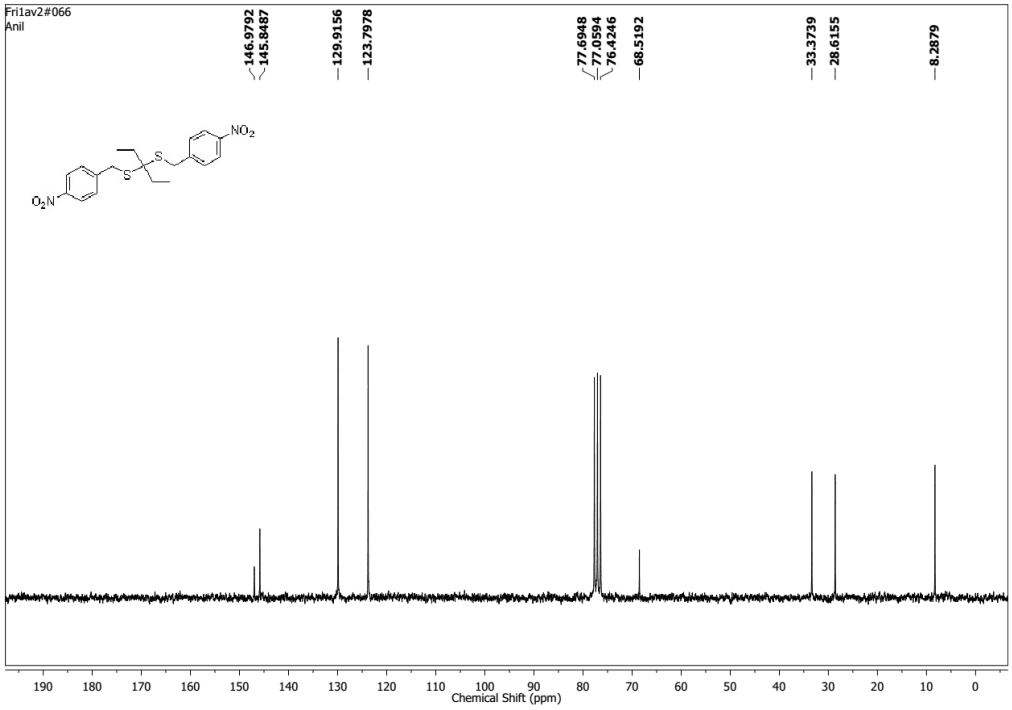

^{1}H NMR Spectrum (400 MHz, $CDCl_3$) of **29c**

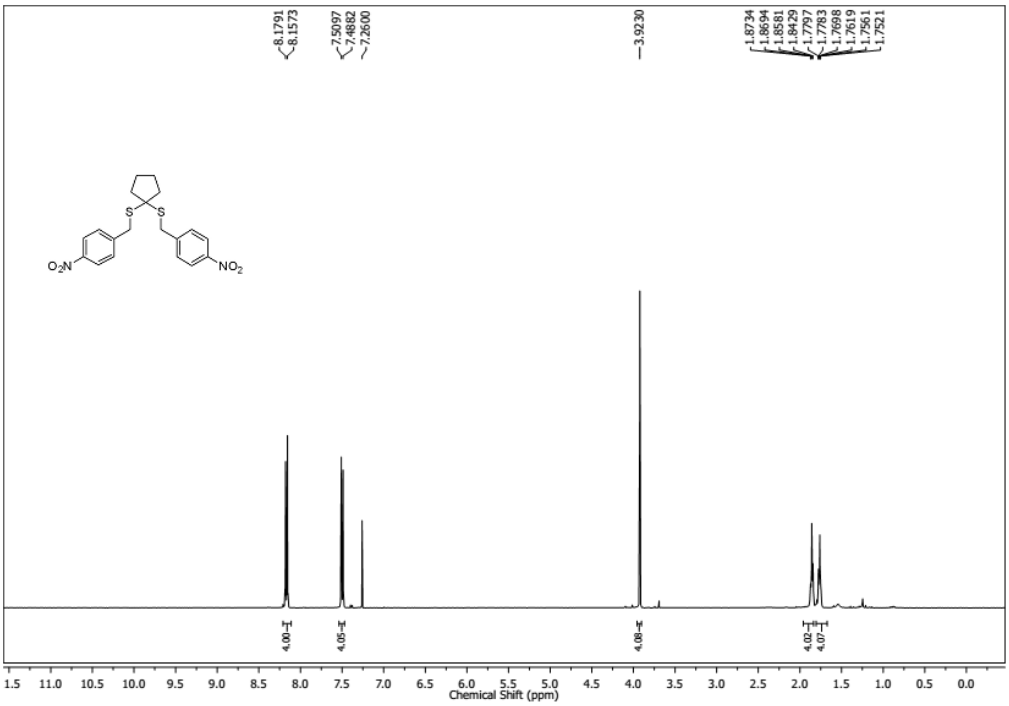

^{13}C NMR Spectrum (100 MHz, $CDCl_3$) of **29c**

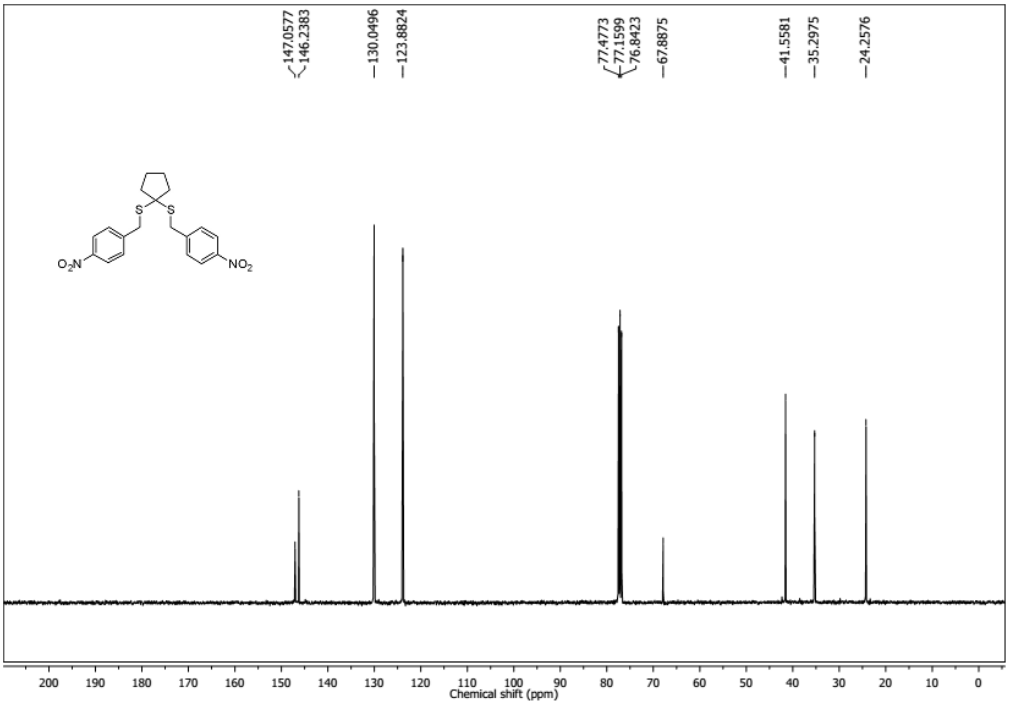

^{1}HNMR Spectrum (400 MHz, $CDCl_3$) of **29d**

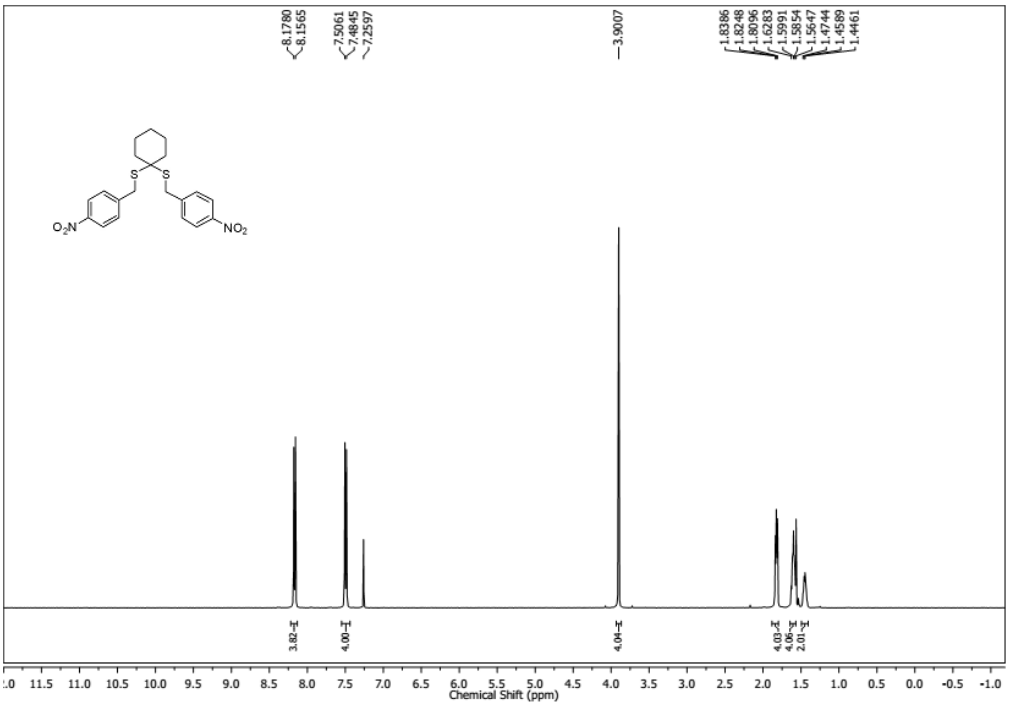

^{13}C NMR Spectrum (100 MHz, $CDCl_3$) of **29d**

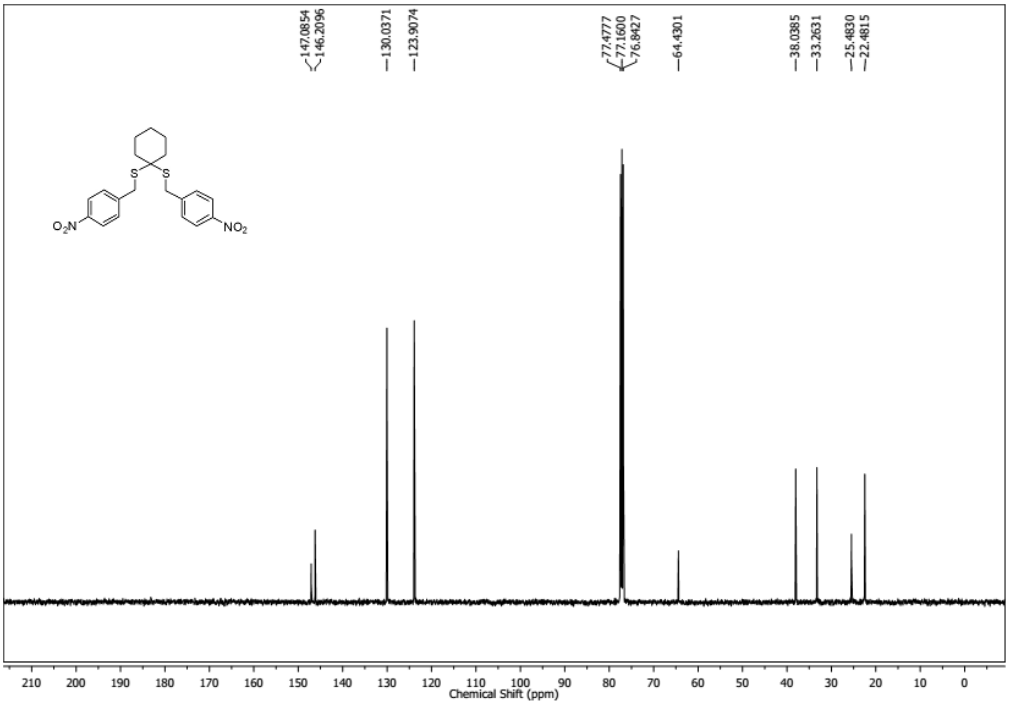

^{1}HNMR Spectrum (400 MHz, $CDCl_3$) of **29e**

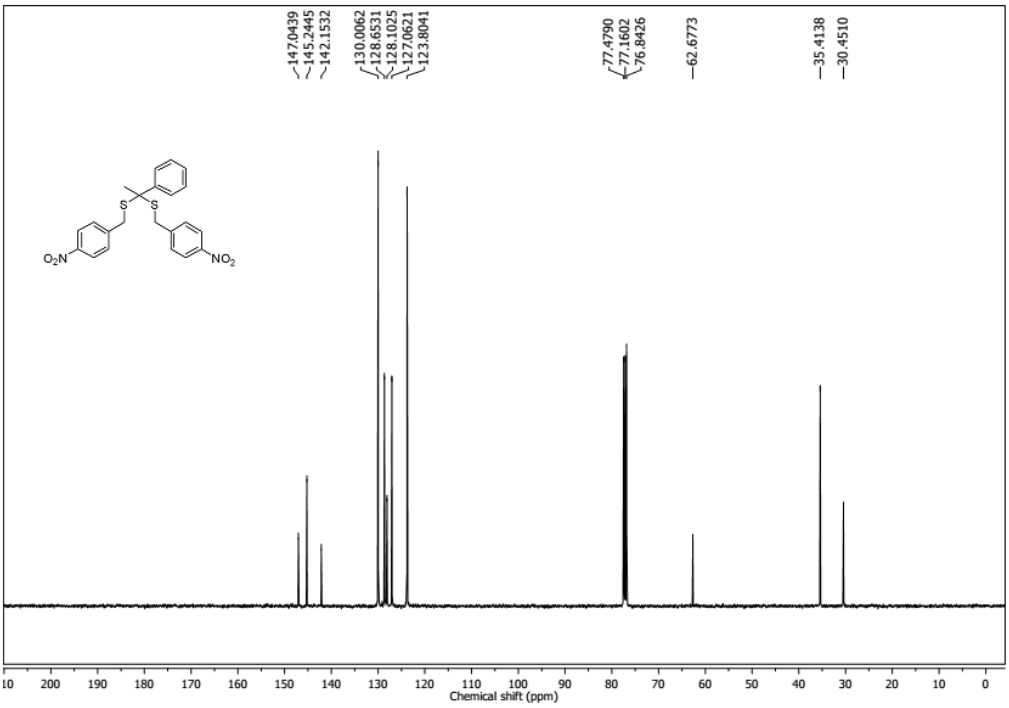

^{13}C NMR Spectrum (100 MHz, $CDCl_3$) of **29e**

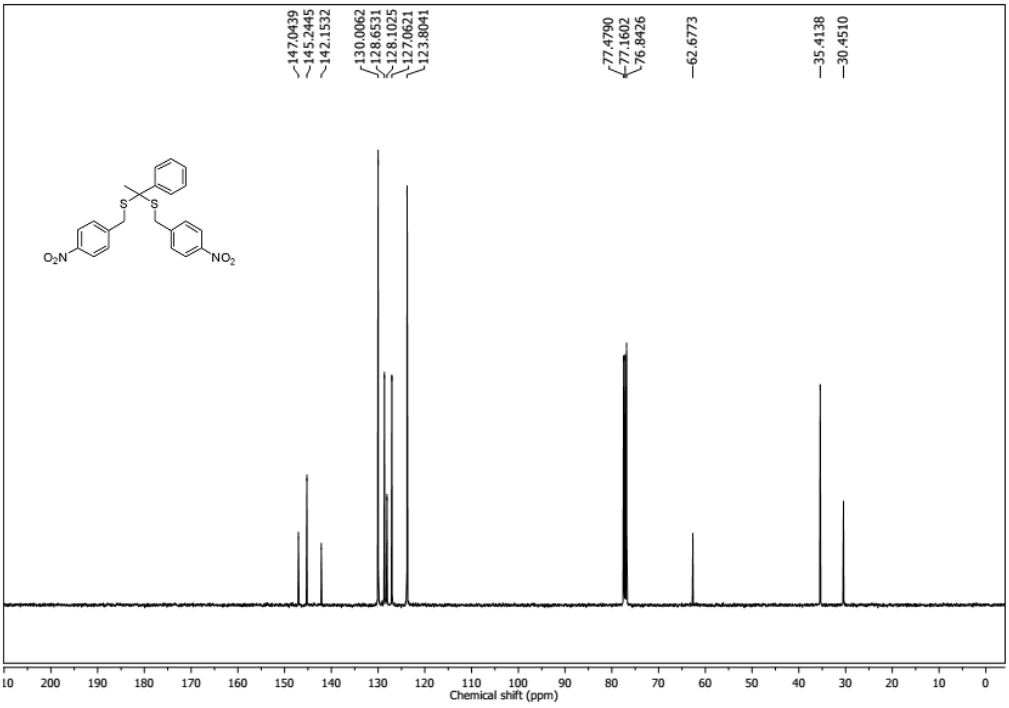

^{1}HNMR Spectrum (500 MHz, $CDCl_3$) of **29f**

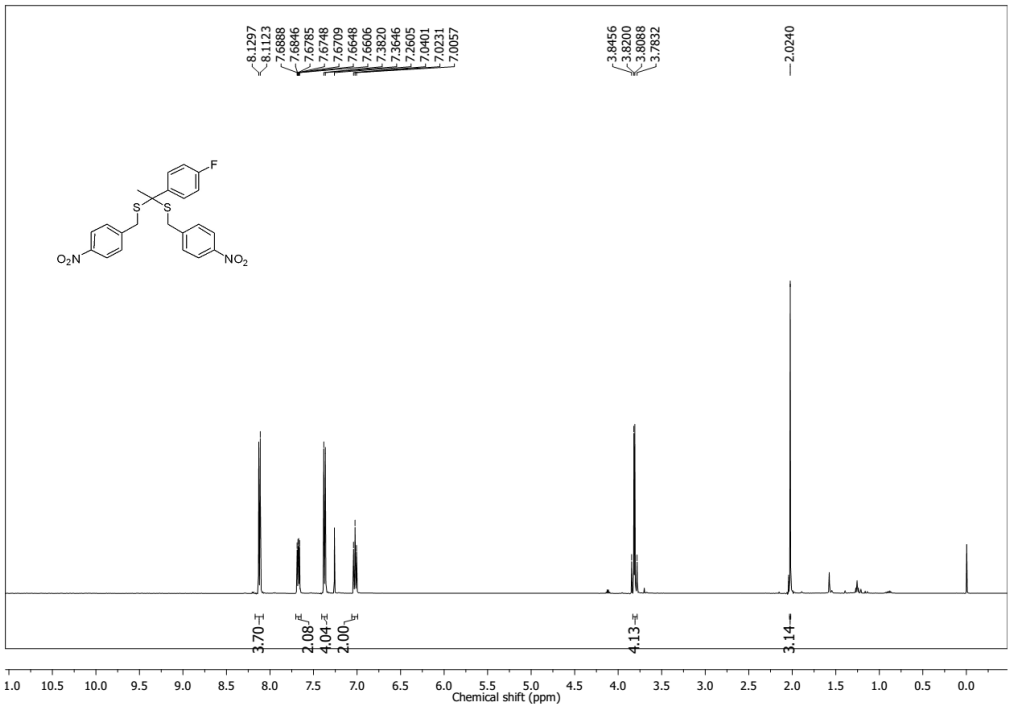

^{13}C NMR Spectrum (125 MHz, $CDCl_3$) of **29f**

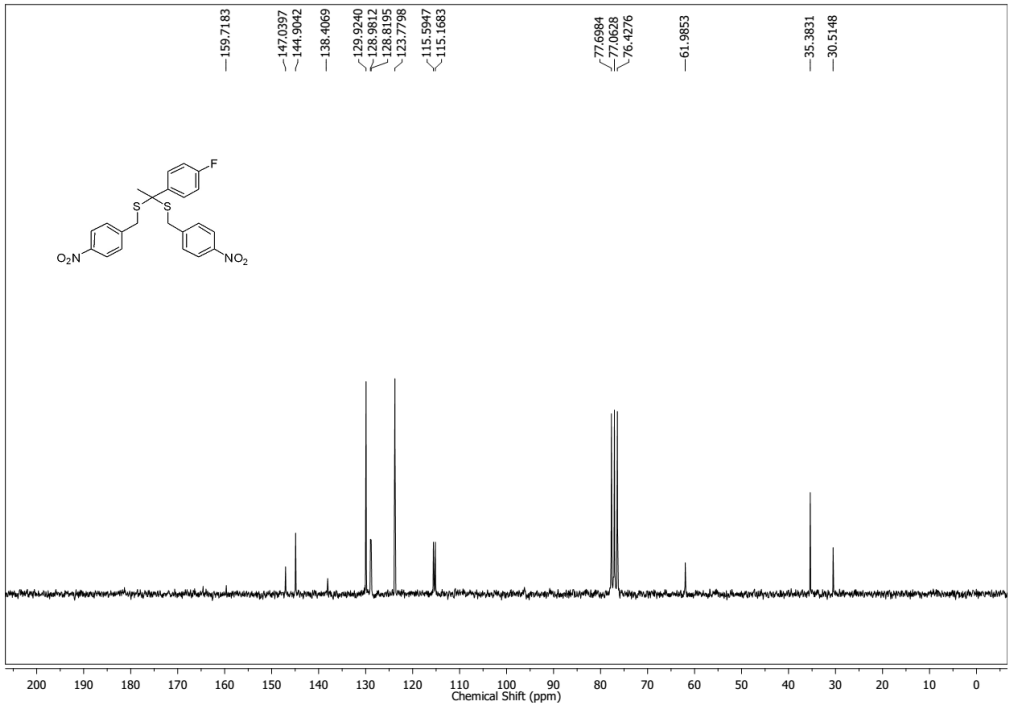

^{1}HNMR Spectrum (500 MHz, $CDCl_3$) of **29g**

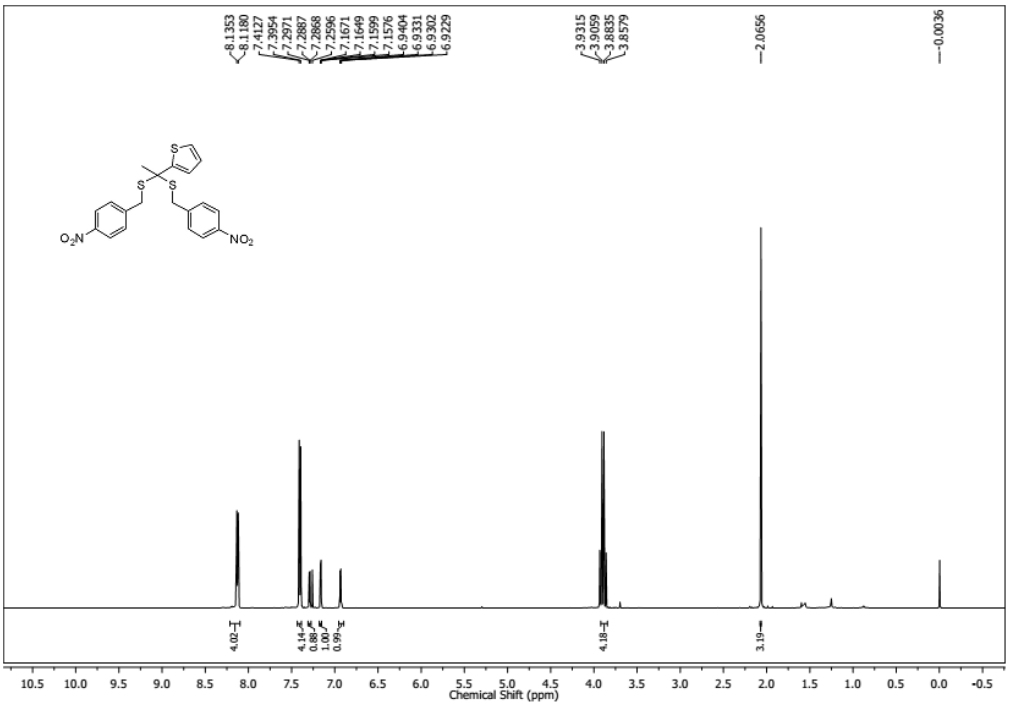

^{13}C NMR Spectrum (125 MHz, $CDCl_3$) of **29g**

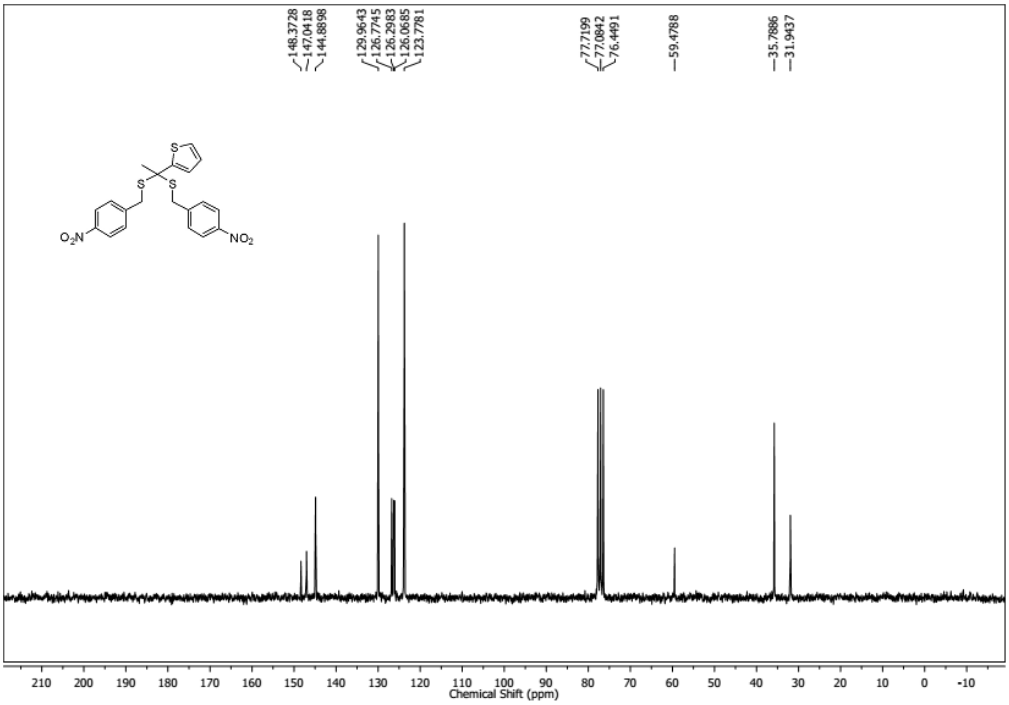

4.6. References

(1) Vandiver, M. S.; Snyder, S. *J. Mol. Med.* **2012**, *90*, 255.

(2) Szabo, C. *Nat. Rev. Drug. Discov.* **2007**, *6*, 917.

(3) Wang, R. *Physiol. Rev.* **2012**, *92*, 791.

(4) Thompson, L. S. *J. Med. Res.* **1921**, *42*, 383.

(5) McMeekin, T. A.; Patterson, J. T. *Appl. Microbiol.* **1975**, *29*, 165.

(6) Clarke, P. H. *Microbiology* **1953**, *8*, 397.

(7) Rivers-Auty, J. *Med. Hypotheses* **2015**, *85*, 612.

(8) Pálinkás, Z.; Furtmüller, P. G.; Nagy, A.; Jakopitsch, C.; Pirker, K. F.; Magierowski, M.; Jasnos, K.; Wallace, J. L.; Obinger, C.; Nagy, P. *Br. J. Pharmacol.* **2015**, *172*, 1516.

(9) Shatalin, K.; Shatalina, E.; Mironov, A.; Nudler, E. *Science* **2011**, *334*, 986.

(10) Großhennig, S.; Ischebeck, T.; Gibhardt, J.; Busse, J.; Feussner, I.; Stülke, J. *Mol. Microbiol.* **2016**, *100*, 42.

(11) Luhachack, L.; Nudler, E. *Curr. Opin. Microbiol.* **2014**, *21*, 13.

(12) Wallace, J. L.; Wang, R. *Nat. Rev. Drug Discov.* **2015**, *advance online publication*.

(13) Kashfi, K.; Olson, K. R. *Biochem. Pharmacol.* **2013**, *85*, 689.

(14) Ono, K.; Akaike, T.; Sawa, T.; Kumagai, Y.; Wink, D. A.; Tantillo, D. J.; Hobbs, A. J.; Nagy, P.; Xian, M.; Lin, J.; Fukuto, J. M. *Free Radic. Biol. Med.* **2014**, *77*, 82.

(15) Li, Q.; Lancaster Jr, J. R. *Nitric Oxide* **2013**, *35*, 21.

(16) Spiller, F.; Orrico, M. I. L.; Nascimento, D. C.; Czaikoski, P. G.; Souto, F. O.; Alves-Filho, J. C.; Freitas, A.; Carlos, D.; Montenegro, M. F.; Neto, A. F.; Ferreira, S. H.; Rossi, M. A.; Hothersall, J. S.; Assreuy, J.; Cunha, F. Q. *Am. J. Respir. Crit. Care Med.* **2010**, *182*, 360.

(17) Pham-Huy, L. A.; He, H.; Pham-Huy, C. *Int. J. Biomed. Sci.* **2008**, *4*, 89.

(18) Caliendo, G.; Cirino, G.; Santagada, V.; Wallace, J. L. *J. Med. Chem.* **2010**, *53*, 6275.

(19) Le Trionnaire, S.; Perry, A.; Szczesny, B.; Szabo, C.; Winyard, P. G.; Whatmore, J. L.; Wood, M. E.; Whiteman, M. *Med. Chem.Commun.* **2014**, *5*, 728.

(20) Zhao, Y.; Wang, H.; Xian, M. *J. Am. Chem. Soc.* **2010**, *133*, 15.

(21) Zhao, Y.; Bhushan, S.; Yang, C.; Otsuka, H.; Stein, J. D.; Pacheco, A.; Peng, B.; Devarie-Baez, N. O.; Aguilar, H. C.; Lefer, D. J.; Xian, M. *ACS Chem. Biol.* **2013**, *8*, 1283.

(22) Roger, T.; Raynaud, F.; Bouillaud, F.; Ransy, C.; Simonet, S.; Crespo, C.; Bourguignon, M.-P.; Villeneuve, N.; Vilaine, J.-P.; Artaud, I.; Galardon, E. *ChemBioChem* **2013**, *14*, 2268.

(23) Martelli, A.; Testai, L.; Citi, V.; Marino, A.; Pugliesi, I.; Barresi, E.; Nesi, G.; Rapposelli, S.; Taliani, S.; Da Settimo, F.; Breschi, M. C.; Calderone, V. *ACS Med. Chem. Lett.* **2013**, *4*, 904.

(24) Song, Z. J.; Ng, M. Y.; Lee, Z.-W.; Dai, W.; Hagen, T.; Moore, P. K.; Huang, D.; Deng, L.-W.; Tan, C.-H. *Med. Chem. Commun.* **2014**, *5*, 557.

(25) Devarie-Baez, N. O.; Bagdon, P. E.; Peng, B.; Zhao, Y.; Park, C.-M.; Xian, M. *Org. Lett.* **2013**, *15*, 2786.

(26) Fukushima, N.; Ieda, N.; Sasakura, K.; Nagano, T.; Hanaoka, K.; Suzuki, T.; Miyata, N.; Nakagawa, H. *Chem. Commun.* **2014**, *50*, 587.

(27) Zheng, Y.; Yu, B.; Ji, K.; Pan, Z.; Chittavong, V.; Wang, B. *Angew. Chem. Int. Ed.* **2016**, *55*, 4514.

(28) Kang, J.; Li, Z.; Organ, C. L.; Park, C.-M.; Yang, C.-t.; Pacheco, A.; Wang, D.; Lefer, D. J.; Xian, M. *J. Am. Chem. Soc.* **2016**, *138*, 6336.

(29) Anlezark, G. M.; Melton, R. G.; Sherwood, R. F.; Coles, B.; Friedlos, F.; Knox, R. J. *Biochem. Pharmacol.* **1992**, *44*, 2289.

(30) Zenno, S.; Koike, H.; Tanokura, M.; Saigo, K. *J. Biochem.* **1996**, *120*, 736.

(31) Race, P. R.; Lovering, A. L.; Green, R. M.; Ossor, A.; White, S. A.; Searle, P. F.; Wrighton, C. J.; Hyde, E. I. *J. Biol. Chem.* **2005**, *280*, 13256.

(32) Friedlos, F.; Denny, W. A.; Palmer, B. D.; Springer, C. J. *J. Med. Chem.* **1997**, *40*, 1270.

(33) Hay, M. P.; Wilson, W. R.; Denny, W. A. *Bioorg. Med. Chem. Lett.* **1999**, *9*, 3417.

(34) Hay, M. P.; Atwell, G. J.; Wilson, W. R.; Pullen, S. M.; Denny, W. A. *J. Med. Chem.* **2003**, *46*, 2456.

(35) Hu, L.; Yu, C.; Jiang, Y.; Han, J.; Li, Z.; Browne, P.; Race, P. R.; Knox, R. J.; Searle, P. F.; Hyde, E. I. *J. Med. Chem.* **2003**, *46*, 4818.

(36) Sharma, K.; Sengupta, K.; Chakrapani, H. *Bioorg. Med. Chem. Lett.* **2013**, *23*, 5964.

(37) Cairns, T. L.; Evans, G. L.; Larchar, A. W.; McKusick, B. C. *J. Am. Chem. Soc.* **1952**, *74*, 3982.

(38) Berchtold, G. A.; Edwards, B. E.; Campaigne, E.; Carmack, M. *J. Am. Chem. Soc.* **1959**, *81*, 3148.

(39) Zhao, Y.; Kang, J.; Park, C.-M.; Bagdon, P. E.; Peng, B.; Xian, M. *Org. Lett.* **2014**, *16*, 4536.

(40) Lin, V. S.; Chen, W.; Xian, M.; Chang, C. J. *Chem. Soc. Rev.* **2015**, *44*, 4596.

(41) Saha, T.; Kand, D.; Talukdar, P. *Org. Biomol. Chem.* **2013**, *11*, 8166.

(42) Shen, X.; Pattillo, C. B.; Pardue, S.; Bir, S. C.; Wang, R.; Kevil, C. G. *Free Radic. Biol. Med.* **2011**, *50*, 1021.

(43) Shen, X.; Kolluru, G. K.; Yuan, S.; Kevil, C. *Methods Enzymol.* **2015**, *554*, 31.

(44) Lambeth, J. D. *Nat. Rev. Immunol.* **2004**, *4*, 181.

(45) Fang, F. C. *Nat. Rev. Microbiol.* **2004**, *2*, 820.

(46) Robins, M. J.; Peng, Y.; Damaraju, V. L.; Mowles, D.; Barron, G.; Tackaberry, T.; Young, J. D.; Cass, C. E. *J. Med. Chem.* **2010**, *53*, 6040.

Synopsis

Synthesis and Evaluation of Small Molecule Generators of Redox-active Reactive Species

Chapter 1: Introduction

Redox-active reactive species such as reactive oxygen species (ROS), reactive nitrogen species (RNS) and reactive sulfur species (RSS) are produced in nearly all living cells. Historically, these reactive species were considered toxic, but recent studies have demonstrated their vital roles in various physiological processes.[1] At moderate concentrations, these reactive species act as important physiological regulators of intracellular signaling pathways.[2-3] However, elevated levels of these reactive species can damage the cellular constituents such as DNA, protein and lipids and irreparable damage can lead to cell death. Therefore, host immune system deploys ROS and RNS as an antimicrobial agent against infectious pathogens (Figure 1).[4]

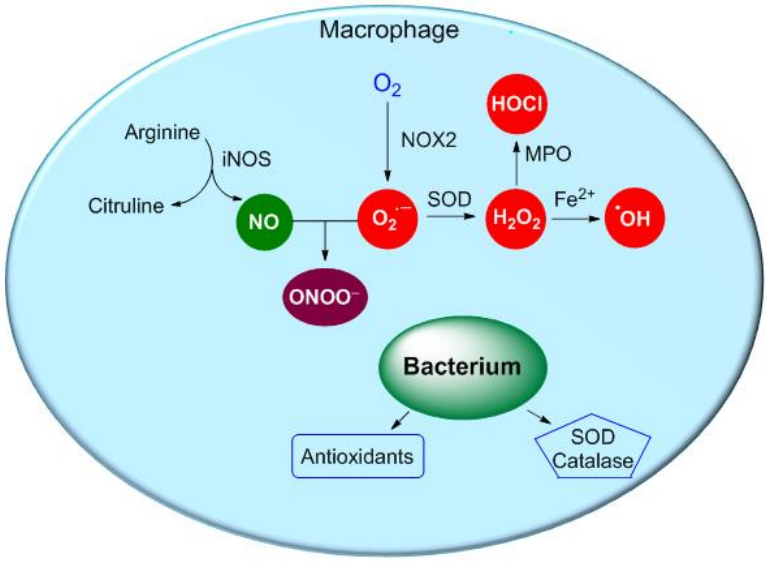

Figure 1. ROS/RNS generation during phagocytosis and defensive mechanism of bacteria

The immune cells such as macrophages and neutrophils engulf the foreign pathogens and activate NADPH oxidase (NOX-2) that catalyzes the formation of superoxide ($O_2^{\bullet-}$) (Figure 1). Under acidic conditions of phagosome, $O_2^{\bullet-}$ is either rapidly dismutated into hydrogen peroxide (H_2O_2) or reacts with nitric oxide (NO) to form peroxynitrite ($ONOO^-$) (Figure 1), both of which are highly cytotoxic molecules. Furthermore, H_2O_2 can form other ROS such as hydroxyl radical

(•OH) and hypochlorus acid (HOCl) (Figure 1). Together, these reactive species can damage the vital cellular constituents of intraphagosomal microorganism and this irreparable damage can lead to cell death.[5] However, certain bacteria have evolved multiple strategies to counter this hostile response. For example, some bacteria express detoxifying enzymes such as SOD, catalase and peroxoredoxin which neutralize the highly reactive ROS and/or RNS, elude phagocytosis. In order to combat infections, several antibiotics were developed to successfully treat the infection. However, bacteria have developed resistance to these antibiotics likely due to misuse and overuse of antibiotics and antibiotic resistance has now become a major concern for global public health.[6-7] Therefore, there is a pressing need for the synthesis of new classes of antibiotics with unique mechanism of action and finding new cellular targets.

In the last decade, the mechanism of antibiotic action has been extensively studied and it has been reported that bactericidal antibiotics induce highly deleterious •OH formation in bacteria, which ultimately contribute to bacterial cell death (Figure 2).[8] Although this view has been challenged,[9-10] recent studies have demonstrated that bactericidal antibiotics induce complex redox alterations that contribute to cellular damage and death.[11-12] These studies demonstrate the importance of ROS in antibiotic mediated bacterial cell death.

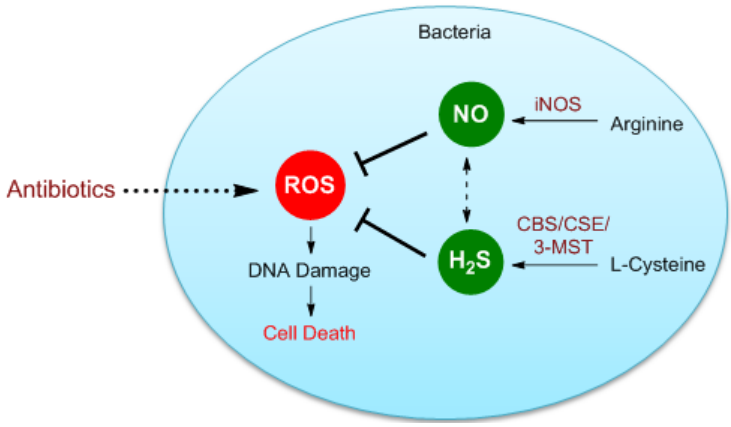

Figure 2. ROS generation during antibiotic action and bacterial protection from oxidative stress by producing H_2S and NO

Recent studies have also demonstrated that bacteria produce NO and H_2S in order to protect bacteria from antibiotics possibly by mitigating oxidative stress induced by antibiotics (Figure 2).[13-14] These studies indicate the cross-talk among NO, H_2S and ROS play critical role during

antibiotics action and protection of bacteria from oxidative stress induced by antibiotics, which, in turn might be linked to resistance. However, cross-talk among these reactive species is not well understood, in part, due to their transient nature under biological system. Therefore, deeper understanding of these redox-active reactive species in bacterial response to antibiotics would be useful for designing new strategies to manage bacterial infections.

In order to precisely study the role of these reactive species in bacteria, their reliable small molecules that can independently generate each of these reactive species are required. Although numerous methodologies for generating ROS, NO, $ONOO^-$ and H_2S have been reported, they are associated with certain limitations such as poor cell permeability, lack of specificity and lack of controlled generation. Therefore, we propose to design and develop new donors of these redox-active reactive species that can independently generate each of these reactive species in bacteria and study their roles in antimicrobial resistance. This thesis contains four chapters. An overview of redox-active reactive species and their various biological roles is presented in Chapter 1. Natural product-inspired benzo[*b*]phenanthridine-5,7,12-trione as bioreductively activated ROS generators is presented in chapter 2.1. Chapter 2.2 describes the structure-activity relationships studies of benzo[*b*]phenanthridine-5,7,12-trione as MRSA inhibitors. In chapter 3, a new small molecule for controlled generation of peroxynitrite is presented. Lastly, in chapter 4, we present synthesis and evaluation of nitroreductase activated H_2S donors that selectively enhance H_2S levels in bacteria, and not in mammalian cells. Altogether, the results presented in this thesis address important problems associated with site-specific generation of redox-active reactive species. Also, these compounds can be used as tools to study roles of these reactive species in antibiotic resistance.

Chapter 2.1: Design, Synthesis and Evaluation of Benzo[*b*]phenanthridine-5,7,12-trione as Reactive Oxygen Species Generators

We designed ROS generators based on the redox-active natural products because these compounds have the ability to induce oxidative stress. For example, jadomycins, produced by *Streptomyces venezuelae*, displayed DNA-damaging activity in the presence of Cu(II) presumably through ROS generation.[15] Deoxynyboquinone, a natural product derivative, has shown potent antitumor activity, and its efficacy is dependent on ROS generation.[16] However, due to complexity of synthesis of these natural products and the presence of multiple functional

groups that can complicate ROS generation mechanism, we proposed to synthesis benzo[*b*]-phenanthridine-5,7,12(6*H*)-triones (**5**) as a potential candidate for ROS generation (Figure 3). This scaffold contained the amide adjoining the quinone of deoxynyboquinone and the aryl ring-like jadomycins.

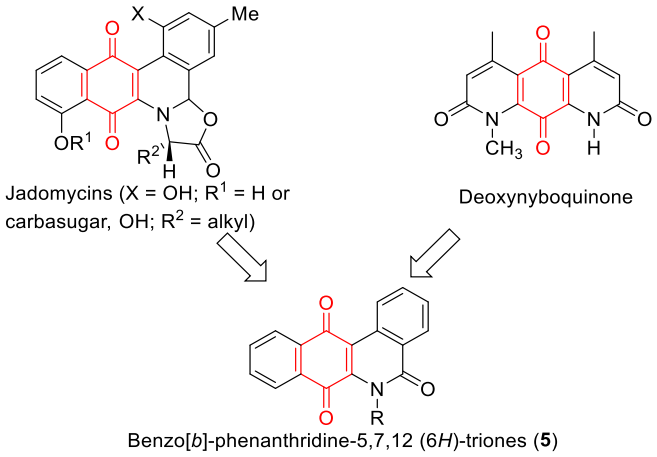

Figure 3. Design of ROS generator **5**

We proposed that **5** can undergo 1e⁻ reduction to from a semiquinone (intermediate I), which then can react with molecular oxygen to produce $O_2^{\bullet-}$ and oxidized quinone. Similarly, **5** can undergo 2e⁻ reduction to from a hydroquinone (intermediate II), which then can react with molecular oxygen to produce two mole $O_2^{\bullet-}$. During this oxidation **5** will be regenerated and would be available for next cycle of ROS generation (Scheme 1).

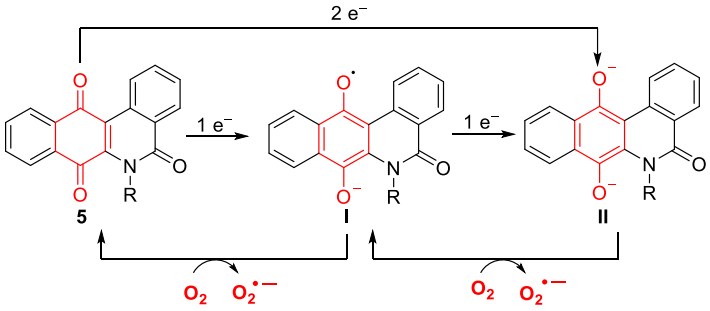

Scheme1. Proposed mechanism of $O_2^{\bullet-}$ generation from **5**

In order to synthesis benzo[*b*]-phenanthridine-5,7,12(6*H*)-trione **5**, a one-pot methodology was developed and a small library of ROS generators **5a-5n** was prepared. The ability of these redox-active compounds to undergo bioreduction to produce $O_2^{\bullet-}$ was measured using luminol based

chemiluminescence assay. These compounds **5a-5n** in the presence of DT-diaphorase (DT-D), a $2e^-$ reductase enzyme, were found to generate $O_2^{\bullet-}$. Next, the inhibitory potential of these ROS generators was tested against methicillin sensitive *Staphylococcus aureus* (MSSA). Interestingly, several analogues were found to inhibit the growth of MSSA with minimum inhibitory concentration (MIC) ranging from 0.5 to 8 μg/mL. Among the derivatives we tested, **5f** was found to be a best MSSA inhibitor with MIC 0.5 μg/mL. **5f** also displayed excellent inhibitory activity against methicillin resistant *S. aureus* (MRSA) with MIC 0.5 μg/mL. The *N*-propargyl derivative, **5f** was identified as the lead compound and selected for further studies.

Next, the potential of **5f** to generate $O_2^{\bullet-}$ was estimated using two independent assays. First, luminol based chemiluminescence assay was used to infer $O_2^{\bullet-}$ generation.[17] When **5f** was incubated in pH 7.4, no evidence of $O_2^{\bullet-}$ generation was found, but when exposed to DT-D, we observed $O_2^{\bullet-}$ generation (Figure 4A). $O_2^{\bullet-}$ generation was also independently confirmed using HPLC based dihydroethidium (DHE) assay (Figure 4B).[18] $O_2^{\bullet-}$ dismutation leads to the formation of H_2O_2 and the potential of **5f** to generate H_2O_2 in the presence of DT-D was confirmed by an Amplex Red fluorescence assay (Figure 4C).[19] From these assay compound **5f** was found to be an efficient ROS generator.

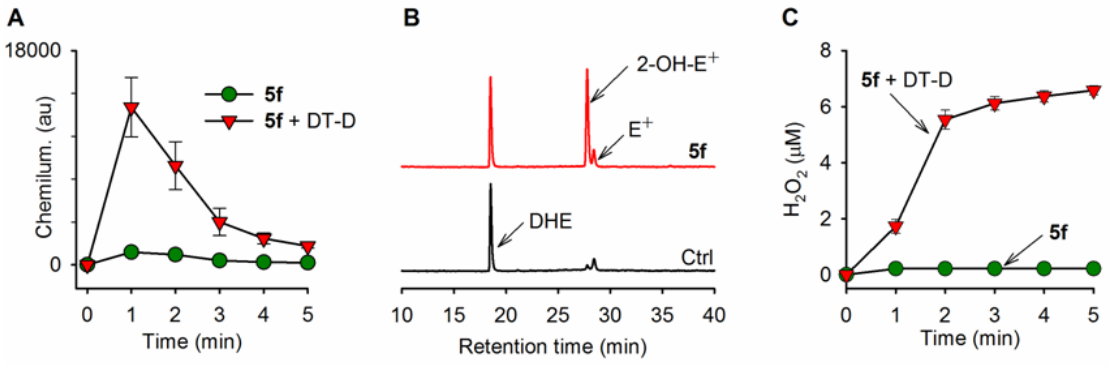

Figure 4. ROS generation by **5f** in pH 7.4 buffer (A) Time course of $O_2^{\bullet-}$ generation was measured using a luminol-based chemiluminescence assay in the presence of DT-D (B) $O_2^{\bullet-}$ generated during incubation of **5f** with DT-D was estimated using a dihydroethidium (DHE) assay. Ctrl is **5f** in pH 7.4 buffer (C) H_2O_2 produced during incubation of **5f** (2 μg/mL) with DT-D was quantified using Amplex Red-based fluorescence assay.

Next, the ability of compound **5f** to permeate bacterial cells and generate ROS was established by DHE, Amplex Red and dichloro-dihydrofluorescein diacetate (H_2DCF-DA) assays. An

enhanced intracellular ROS in *S. aureus* was observed upon incubation with **5f** (Figure 5A, 5B and 5C). Having demonstrated the ROS generation by **5f** in MSSA, next, the ability of **5f** to induce DNA damage in bacteria was tested by measuring expression levels of *RecA*, a repair protein crucial to homologous recombination. The data provided by our collaborator suggests the significant upregulation of *RecA* expression in the presence of **5f**. In order to support the ROS based mechanism contributing to antibacterial activity; the effect of **5f** on the viable colony count of MSSA in the presence thiourea, a ROS quencher, was examined. The growth inhibition of **5f** was reduced in the presence of thiourea, suggesting the contribution of ROS in antibacterial activity of redox-active compound.

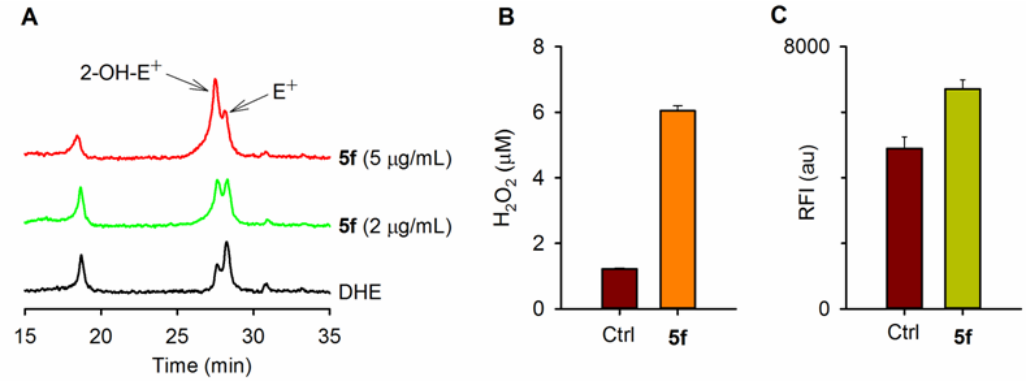

Figure 5. ROS generation by **5f** in *S. aureus* (A) $O_2^{\bullet-}$ generated during incubation of *S. aureus* with 5f was estimated using a dihydroethidium (DHE) assay (B) Estimation of H_2O_2 generated during incubation of *S. aureus* with **5f** (2 μg/mL) was estimated using an Amplex Red fluorescence assay (C) Increase in intracellular oxidative species upon treatment of *S. aureus* with **5f** was determined by a H_2DCF-DA-based fluorescence assay.

Next, the potential **5f** to inhibit the growth of clinical isolates of MRSA was also tested by our collaborator and this compound retained its potency against these MRSA strains. Finally, the cytotoxicity of **5f** was measured against A549, human lung carcinoma cells; however this compound exhibited cytototxicity at comparable concentrations (50% growth inhibitory-8.6 μM), suggesting the necessity of further structural modifications. In summary, Chapter 2.1 describes the development of natural product-inspired redox-active compounds for selectively enhancing intracellular ROS levels in bacteria and their potential to target antibiotic resistance in certain bacteria.

Chapter 2.2: Structure-Activity Relationship Studies of Benzo[*b*]phenanthridine-5,7,12-trione as MRSA Inhibitors

In chapter 2.1, we have demonstrated that the potential of redox-active compounds to target antibiotic resistance in certain bacteria. For example, compound **5f** displayed potent inhibitory activity against MRSA. Although **5f** possessed high inhibitory activity against MRSA, it also exhibited cytotoxicity in mammalian cells. Furthermore, this compound has poor aqueous solubility. In this chapter, we studied the systematic structure activity relationships (SAR) of benzo[*b*]phenanthridine-5,7,12-trione in order to overcome observed challenges without compromising the potency while inhibiting MRSA.

We considered retaining the ROS generating quinone core and systematically modifying the substituents of the parent compound. First, we proposed to synthesize 2-aryl-3-amino-1,4-naphthoquinone **8** for understanding the importance of amide adjoining quinone and aromatic ring-A for anti-MRSA activity (Figure 6). In order to investigate the role of aromatic rings A and D for their participation in anti-MRSA activity, the scaffold **13** was proposed in which aromatic ring-A was replaced with 4-methyl group and aromatic ring-D was replaced with bridged bicyclic ring. Lastly, we wanted to determine the importance of aromatic ring A for anti-MRSA activity. Therefore, compound **18** was proposed in which the aromatic ring A was retained and aromatic ring D was replaced with bicyclic ring.

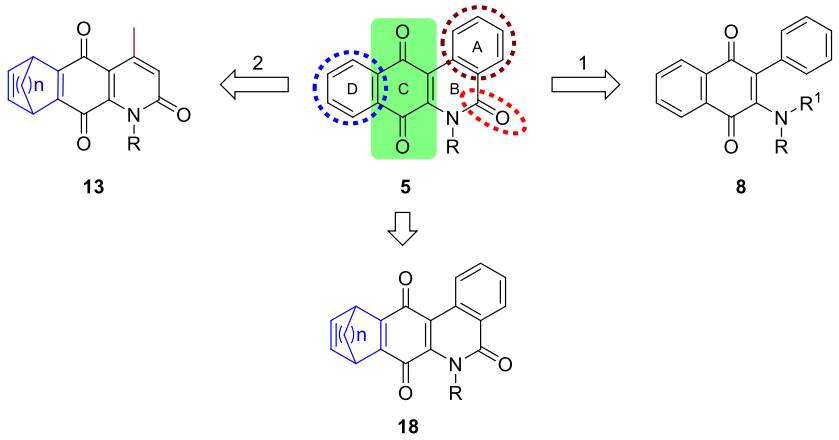

Figure 6. Schematic representation of the systematic structural modifications to the benzo[*b*]phenanthridine-5,7,12-trione (**5**)

A series of 2-aryl-3-amino-1,4-naphthoquinones **8a-8m** were synthesized following a two-step synthetic protocol in moderate to good yields. Next, a series of *N*-alkyl-4-methyl-6,9-dihydro-6,9-ethano-benzo[*g*]quinoline-2,5,10(1*H*)-triones (**13a**,**13b** and **13e**) were synthesized in order to investigate the role of aromatic ring A and D for anti-MRSA activity (Figure 7). During the synthesis of **13** analogues, we obtained *O*-alkyl intermediates **12a-12e** as byproducts. Using these intermediates, we synthesized *O*-alkyl-derivatives **14b-14e** and **15b-15e** to test whether by changing the electron withdrawing amide group to electron donating 2-alkoxy group has any effect on antibacterial activity. Finally, compounds **18a-18c** were synthesized in order to investigate the importance of aromatic ring-D on MRSA activity (Figure 7).

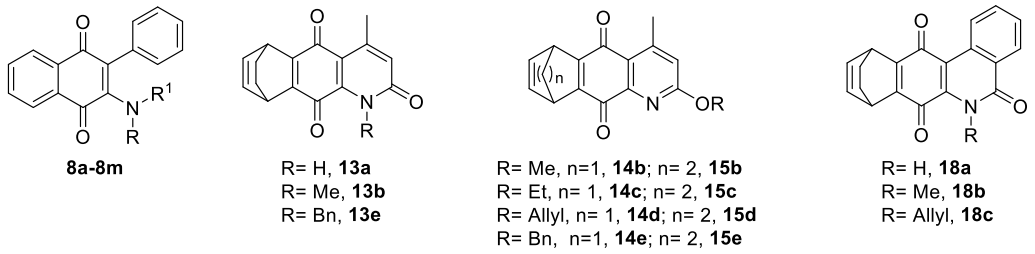

Figure 7. Structures of analogues of benzo[*b*]phenanthridine-5,7,12-trione (**5**)

Next, these compounds were tested for their inhibitory potential against MSSA. 2-aryl-3-amino-1,4-naphthoquinones **8a-8m** were found to be inactive against MSSA, suggesting the necessity of amide group between quinone and aromatic ring A for anti-bacterial activity. The *N*-alkyl derivatives **13a**, **13b** and **13e** exhibited moderate to good inhibitory activity (MICs 2, 1 and 8 μg/mL, respectively). The *O*-alkyl derivatives **14b** and **14c** also exhibited high inhibitory activity against MSSA (MICs 1 and 2 μg/mL, respectively). However, compound **14d-14e** and **15b-15e** were found to be inactive against MSSA, suggesting that introducing the bulky substituent at the 2-position markedly diminishes the potency. Compound **18a** exhibited excellent inhibitory activity against MSSA with MIC 0.12 μg/mL, superior than vancomycin, a clinically used antibiotic. Similarly, derivatives **18b** and **18c** also showed high inhibitory activity against MSSA. The correlation between ClogP, a measure of cell permeability and antibacterial activity was studied and we found that the compound having low lipophilicity (ClogP value < 4) exhibited good inhibitory activity against MSSA. We identified **18a** as the lead compound and used it for further studies. Using DHE and amplex red fluorescence assays, we observed intracellular generation of $O_2^{\bullet-}$ and H_2O_2 in *S. aureus* upon incubation with **18a** (Figure 8).

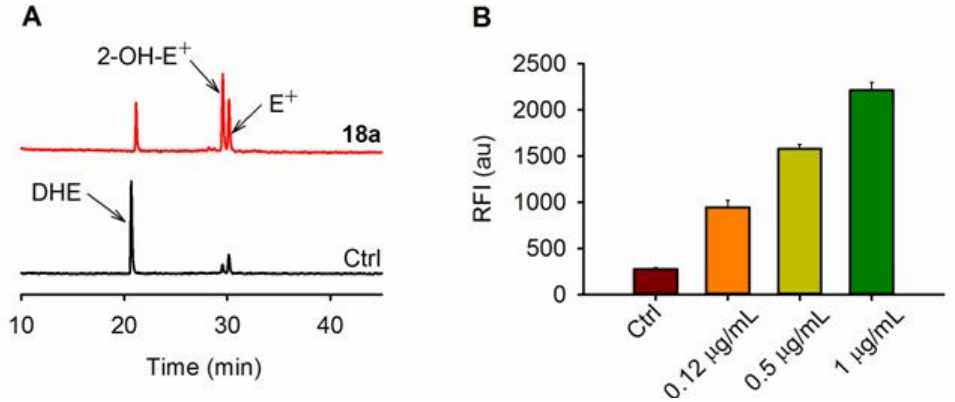

Figure 8. ROS generation by **18a** in *S. aureus* (A) $O_2^{\bullet-}$ generated during incubation of **18a** (0.5 µg/mL) with *S. aureus* was estimated using a dihydroethidium (DHE) assay. (B) Measurement of H_2O_2 generated during incubation of *S. aureus* with **18a** (0.12, 0.5, and 1 µg/mL) was estimated using an Amplex Red fluorescence assay.

As determined by our collaborator, the lead compound **18a** also retained excellent inhibitory activity against clinical strains of MRSA with MIC values in the range of 0.015–0.5 µg/mL. Furthermore, **18a** also showed excellent potency against vancomycin resistant *S. aureus* (VRSA) strains with MIC values of 0.01–0.03 µg/mL. Finally, the cytotoxicity of **18a** was evaluated against vero cells (kidney epithelial cells) and the growth inhibitory concentration (GI_{50}) was found to be 9.7 µg/mL. The selectivity index of **18a** against MRSA NR129 was found to be > 161, which was superior to **5f**. Further, this compound was minimally cytotoxic against mammalian cells and possessed essentially no hemolytic activity.

On the basis of the structural features and the antibacterial activity data, the SARs are summarized as below. The removal of amide adjoining quinone and aromatic ring-A resulted in a loss of anti-MSSA activity. Replacing aromatic ring-A by methyl group and aromatic ring-D with bicyclic ring was tolerated but did not improve anti-bacterial activity. Bulky group at *N*-1 position of **13**-series was not tolerated. Similarly, *O*-alkyl derivatives **14c**-**14d** and **15a**-**15d** were found to be inactive against MSSA suggesting that changing the electron withdrawing amide ring to electron donating 2-alkoxy group and increasing steric reduces biological activity. Retaining aromatic ring A and replacing aromatic ring D with bicyclic ring was found to be beneficial in terms of potency. Thus, together these results suggest that modification of redox-active natural product is a simple and feasible approach for developing novel antimicrobial agents.

Chapter 3: Design, Synthesis of Evaluation a Small Molecule for Controlled generation of Peroxynitrite

In chapter 2, we have described the development of natural product-inspired efficient $O_2^{\bullet-}$ generators. The mechanism for $O_2^{\bullet-}$ generation from these compounds involved reaction of molecular oxygen with semiquinones or hydroquinones, which in turn are produced during bioreduction of quinones. Under physiological conditions, $O_2^{\bullet-}$ either rapidly dismutated into H_2O_2 or reacts with NO at diffusion controlled-rate to produce $ONOO^-$, a short-lived RNS. $ONOO^-$ is a highly reactive species that gives rise to both oxidative and nitrosative stress in bacteria. Hence $ONOO^-$ is deployed by the immune system as an antimicrobial agent against infectious pathogens.[4] Although a number of *in vitro* studies have demonstrated the microbicidal role of $ONOO^-$, assessing its cellular effects *in vivo* is challenging due to the transient nature of this reactive species. Furthermore, recent studies have demonstrated the importance of peroxynitrite-mediated cell signaling, which occurs at sub-lethal concentrations.[20-21] However, this transition of $ONOO^-$ from signaling to toxicity is poorly characterized, in part, due to the difficulty associated with controlled generation of $ONOO^-$ within cells. A number of methodologies have been developed to deliver $ONOO^-$ in cells,[22-23] but they are often associated with various limitations such as poor cell-permeability, poor bioavailability, lack of site-specificity and lack of controlled generation of $ONOO^-$.

In order to produce $ONOO^-$, we hypothesized that a small molecule that can be activated within cells to generate $O_2^{\bullet-}$ as well as release NO would be ideal. Once produced, NO and $O_2^{\bullet-}$ are known to react at a nearly diffusion-controlled rate to generate $ONOO^-$.

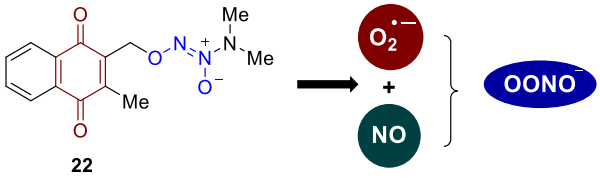

Scheme 2. Peroxynitrite donor **22**, where a NO generating diazeniumdiolate is linked to a $O_2^{\bullet-}$ generating 1,4-naphthoquinone group.

In aerobic buffer, $O_2^{\bullet-}$ is generated during the reaction of O_2 with semiquinones or hydroquinones, which in turn are produced during bioreduction of 1,4-benzoquinones. For

reliably generating NO within cells, diazeniumdiolates and their protected forms are frequently used.[24] Based on this, we designed **22** as potential candidate that produces both $O_2^{\bullet-}$ as well as NO upon entry into cells (Scheme 2).

In order to tests this hypothesis, compound **22** was synthesized in three steps. In addition, negative control compound **25** was also synthesized as $O_2^{\bullet-}$ generator (Figure 9). Next, the ability of **22** to generate $O_2^{\bullet-}$ was tested using DHE assay. In the presence of DT-D, we found evidence for 2-OH-E^+, which is indicative of $O_2^{\bullet-}$ generation. Next, the ability of **22** to produce NO was assessed by a chemiluminescence assay.[25] When the reaction mixture of **22** + DT-D was incubated in pH 7.4 buffer, we find the signal for NO generation. Having established NO and $O_2^{\bullet-}$ generation from **22**, next we verified the $ONOO^-$ generation using $ONOO^-$ probe 3-methyl-coumarin-7-(pinacol boronate ester) **23a**, a weakly fluorescent compound that is reported to rapidly react with $ONOO^-$ to produce highly fluorescent compound **23c**.

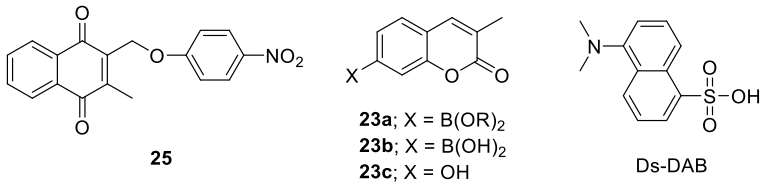

Figure 9. Structures of $O_2^{\bullet-}$ generator and peroxynitrite probes

When **22** was incubated in the presence of DT-D, a significant increase in fluorescence signal was recorded (Figure 10A), confirming the $ONOO^-$ generation. The formation of $ONOO^-$ was independently verified using $ONOO^-$ probe *N*-(2-aminophenyl)-5-(dimethylamino)-1-naphthalene sulfonic amide (Ds-DAB).[26] When Ds-DAB was incubated with authentic $ONOO^-$, a characteristic fluorescence emission at 505 nm was observed (Figure 10B). A similar shift in fluorescence was seen during incubation of **22** and DT-D confirming the production of $ONOO^-$ (Figure 10B).

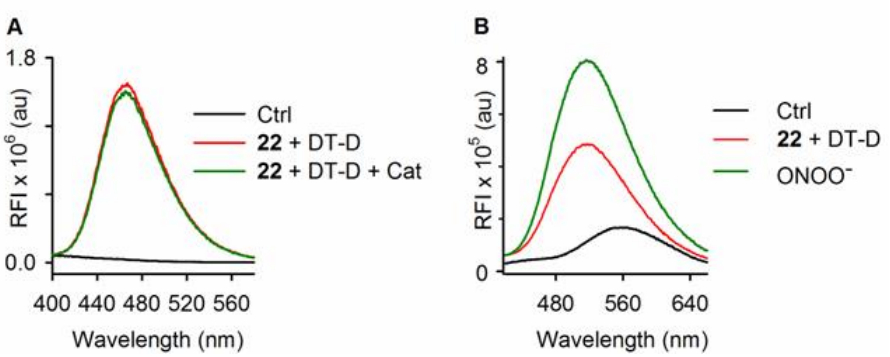

Figure 10. $ONOO^-$ generation from **22** (A) Fluorescence emission spectra during incubation of **23a** (100 μM) with **22** (100 μM) + DT-D in PB pH 7.4, (λ_{ex} = 315 nm); In case of an H_2O_2 scavenger, **22** + DT-D was co-incubated with catalase (100 U/mL); Ctrl is **23a** incubated with **22**. (B) Fluorescence emission spectra of Ds-DAB (10 μM) during incubation with **22** (100 μM) + DT-D in pH 7.4 buffer (λ_{ex} = 350 nm); Authentic $ONOO^-$ (100 μM) was reacted with Ds-DAB and served as a positive control; Ctrl is Ds-DAB (10 μM) in pH 7.4 buffer.

The ability of **22** to permeate cells and generate $ONOO^-$ was demonstrated using Ds-DAB. Using colorectal cancer cells (DLD-1) pre-incubated with Ds-DAB, confocal microscopy revealed a significant and dose-dependent enhancement in fluorescence signal at 505 nm (Figure 11). Under similar conditions, SIN-1 had diminished capacity to enhance peroxynitrite in DLD-1 cells. Furthermore, the suitability of **22** to enhance $ONOO^-$ in a variety of cell lines including SW 480 colon cancer cells, A549 lung cancer cells and primary corneal fibrolast cells was also demonstrated.

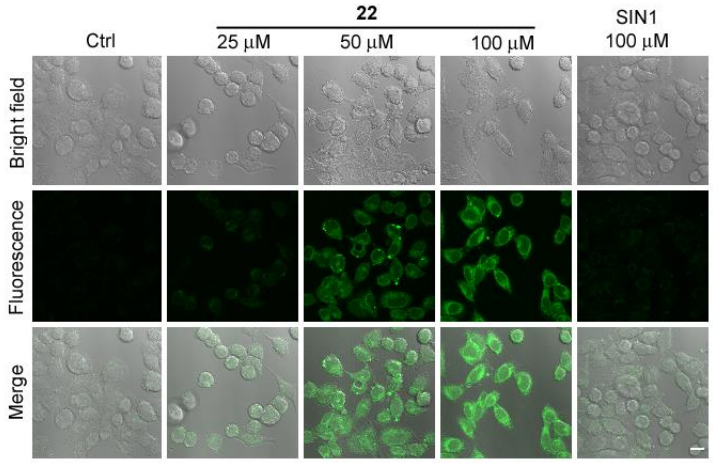

Figure 11. $ONOO^-$ generation in DLD-1 cells treated with **22** at 25, 50, 100 μM and SIN-1 (100 μM) for 1 h using Ds-DAB; Ctrl is untreated DLD-1 cells; scale bar: 10 μm.

The mechanism for $ONOO^-$ generation from **22** involving enzyme-triggered generation of NO as well as $O_2^{\bullet-}$ was proposed (Scheme 3). Reduction of **22** by $1e^-$ reductases can generate a highly reactive semiquinone intermediate **I**, which can react with molecular oxygen to produce $O_2^{\bullet-}$ or undergo further reduction to produce **II**.

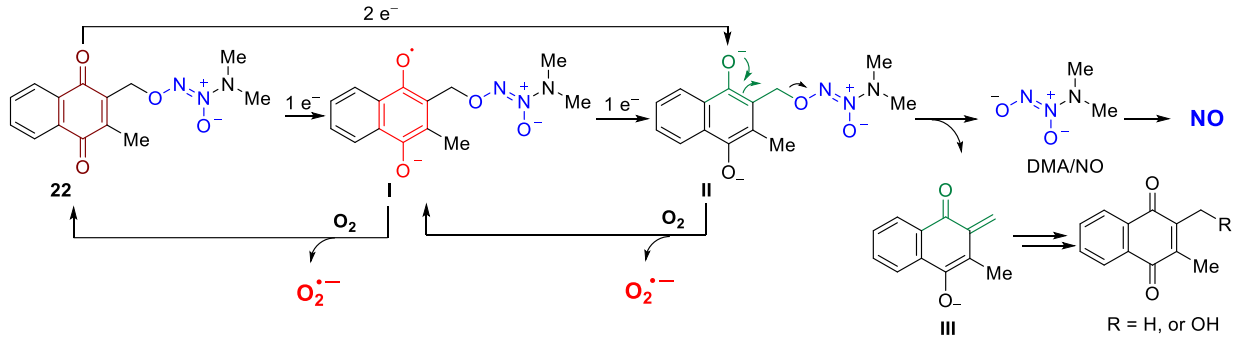

Scheme 3. Proposed mechanism for $O_2^{\bullet-}$ and NO generation during incubation of **22** with a bioreductive enzyme

Alternatively, **II** can be produced by $2e^-$ reductases such as DT-D and this intermediate can also generate 2 mol of $O_2^{\bullet-}$. Furthermore, **II** can trigger the rearrangement of electrons that result in departure of diazeniumdiolate, which is known to undergo hydrolysis in buffer to produce NO. The observation of enhanced NO formation during incubation of **22** + DT-D indicated the formation of intermedaite **II**. Furthermore, $O_2^{\bullet-}$ generation from **22** in the presence of DT-D was supported by the formation of intermediate **II**. Additionally, the proposed mechanism of $ONOO^-$ generation was supported by HPLC decomposition studies of **22** and **25**.

Lastly, we tested the cytotoxicity of this $ONOO^-$ generator against both Gram-positive as well as Gram-negative bacteria. $ONOO^-$ generator, **22** exhibited potent inhibitory activity against gram positive bacterium *S. aureus*, but gram-negative bacteria *E. coli* tolerated this compound, suggesting sensitivity of *S. aureus* toward $ONOO^-$. In summary, we have developed a novel small molecule that reliably generates $ONOO^-$ within cells.

Chapter 4: Design, Synthesis and Evaluation of Nitroreductase Activated Hydrogen Sulfide Donors

In order to address the global antibiotic-resistance concern, several approaches including developing new classes of antibiotics, identification of novel targets and use of different

antibiotic combinations have been considered. In chapter 2, we have demonstrated that antibiotic resistance in certain bacteria can be targeted using redox-active compounds. Recently, H_2S has been reported to protect bacteria from the oxidative stress induced by antibiotics, suggesting its role in antibiotic resistance.[14] However, the precise mechanisms by which H_2S acts remain to be completely understood. In order to understand the role of H_2S in bacteria developing drug resistance, a methodology for controlled generation of H_2S is necessary. Due to the difficulty in producing gaseous species in cells in a controlled manner, exogenous sources that dissociate to generate H_2S are routinely used. Inorganic salts such as sodium sulfide (Na_2S) or NaHS are frequently used but suffer from volatility of the gas as well as a lack of control of site of H_2S generation. Although a number of H_2S donors have been developed recently,[27-29] they are associated with various disadvantages such as poor cell permeability, lack of control on its generation and lack of trigger that can selectively release H_2S in bacteria without affecting the cellular redox-balance.

In order to achieve specificity, we propose the synthesis of H_2S donors that can be activated by an enzyme which is specifically found in bacteria. We considered bis(4-nitrobenzyl)sulfanes with general structure **29** as candidates for enzyme activated H_2S donors (Scheme 4). The nitro group of **29** can be used as a functional group for metabolism by a bacterial enzyme such as nitroreductase (NTR), which is expressed in bacteria. The 4-nitrobenzyl group is expected to undergo two electron reduction in the presence of NTR. As a result of reduction, strong electron withdrawing nitro group is converted into an electron donating hydroxylamine or amine group. Upon rearrangement of electrons, a geminal dithiol would be produced; these intermediates have been previously proposed to undergo hydrolysis to produce H_2S.[30]

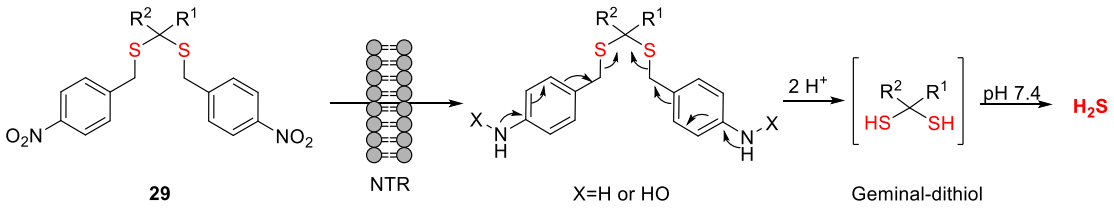

Scheme 4. Proposed design and activation of NTR-activated H_2S donors

In order to test the hypothesis of NTR-activated H_2S generation, we synthesized bis(4-nitrobenzyl)sulfanes **29a-29g** in three steps with moderate to good yields. A negative control **30**, which is a substrate for NTR but not a source of H_2S, was also synthesized.

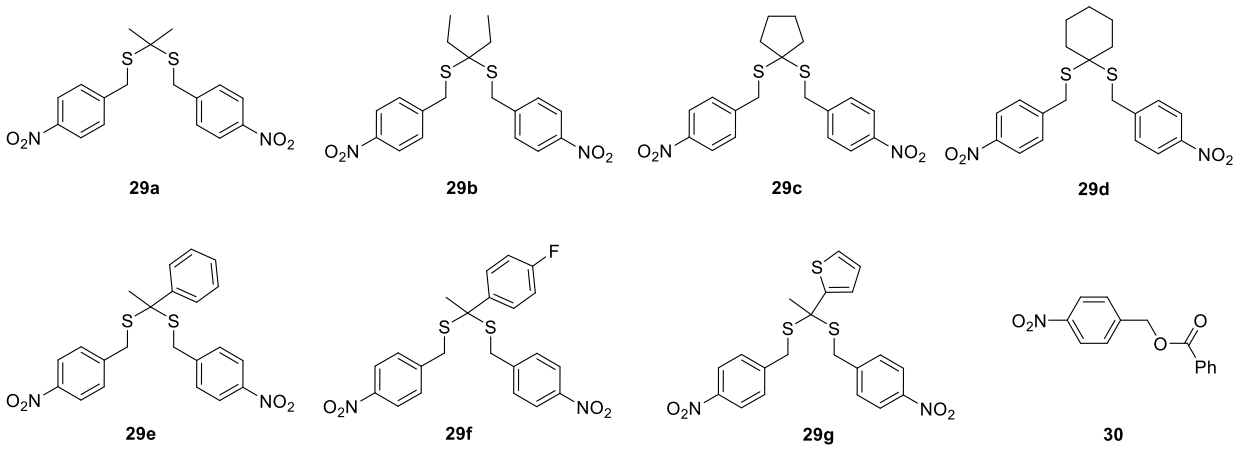

Figure 12. Structures of H_2S donor **29a-29g** and negative control compound **30**

Next, we evaluated **29a-29g** for their ability to undergo metabolism with NTR to release H_2S. An azide based fluorescence probe **31a**, that is reported to be selectively activated by H_2S to produce a highly fluorescent amine **31b** (Figure 13), was used for H_2S detection.[31] When **29a** was incubated alone in pH 7.4 buffer, no evidence of H_2S generation was found. However, when **29a** was exposed to NTR in the presence of NADH, a significant increase in fluorescence was observed, confirming the H_2S generation (Figure 14). Under similar conditions, **29b**-**29g** were independently incubated in the presence of NTR and **29c** was found to be the best source of H_2S and was chosen for further evaluation (Figure 14).

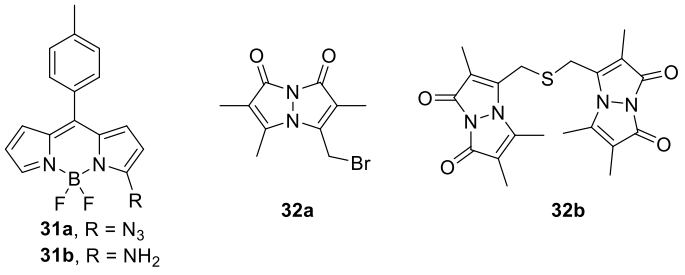

Figure 13. Structures of H_2S probes and their products upon reaction with H_2S

Next, **29c** was co-incubated with 10 eq. of 4-nitrobenzylbenzoate **30**, which is a substrate for NTR, but does not generate H_2S. As expected we find nearly complete abrogation in fluorescence attributable to generation of H_2S (Figure 14).

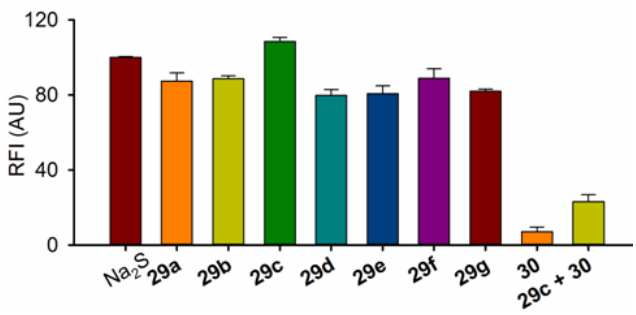

Figure 14. Estimation of H_2S generation during incubation of **29a-29g** (50 μM) with NTR in HEPES buffer ph 7.4 using BODIPY-based sensor **31a**

NTR-mediated activation of **29c** to release H_2S was independently confirmed by HPLC based monobromobimane (mBBr) assay.[32] In this assay, mBBr reacts with sulfide anion to produce a highly fluorescent sulfide-dibimane **32b** (Figure 13) and the presence of this product can be confirmed by HPLC analysis.[32] **29c** in the presence of NTR was found to produce **32b** (Figure 15), confirming H_2S release. Together these experiments confirmed the H_2S generation from **29c** in the presence of NTR.

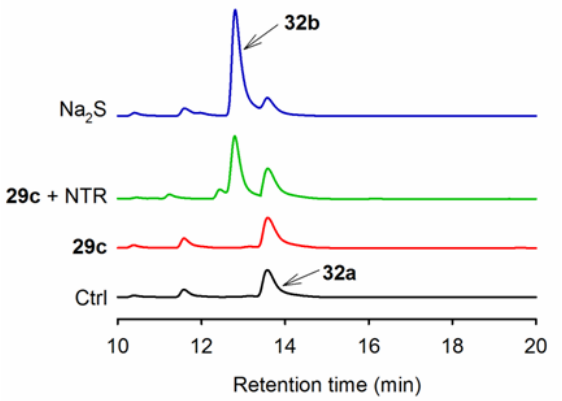

Figure 15. An HPLC based mBBr assay was performed to infer H_2S generation during incubation of **29c** (50 μM) in the presence of NTR. mBBr (**32a**) reacts with sulfide anion to produce a sulfide-dibimane **32b**, which was monitored using fluorescence channel (λ_{ex} - 390 nm and λ_{em}- 475 nm).

Next, the ability of **29c** to permeate bacterial cells and release H_2S was monitored in *E. coli* by flow cytometry study. The incubation of *E. coli* with **29c** resulted in intracellular release of H_2S (Figure 16A), suggesting that synthesized bis(4-nitrobenzyl)sulfanes are capable of enhancing H_2S in bacterial cells. The ability of **29c** to release H_2S was also demonstrated *Mycobacterium smegmatis* (*M. smegmatis*). On the other hand, **29c** remained completely ineffective in increasing H_2S levels in human monocytic cells (THP-1) (Figure 16B), confirming its ability to enhance H_2S levels only in bacteria and not in macrophages. Thus, this study lays the foundation for novel methodologies for site-specific enhancement of H_2S using this new class of H_2S donors.

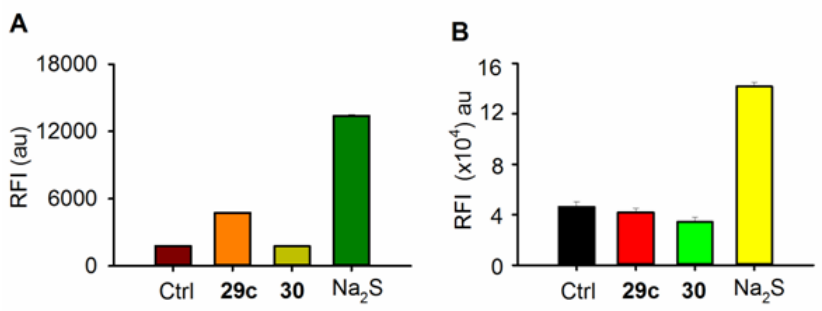

Figure 16. Flow cytometry analysis of intracellular H_2S generation by **29c** (50 μM) in (A) *E. coli* and (B) human monocytic cells (THP-1); Na_2S was used as positive control and **30** was used as a negative control compound. (Data provided by Dr. Amit Singh, IISc Bangalore.)

The unique feature of these H_2S donors to selectively enhance H_2S levels in bacteria allowed us to investigate role of this gaseous molecule in bacteria and our preliminary investigation reveals that H_2S directly control intracellular redox-balance of bacteria to counter the lethal degree of oxidative stress induced by antibiotics. These finding suggests that regulating bacterial H_2S levels by inhibiting H_2S biosynthesis pathways could be potential strategy to alter the resistance toward conventional antibiotics.

Taken together, we have developed novel small molecules that can independently generate ROS, $ONOO^-$ and H_2S within cells. Using these redox-active compounds, we demonstrate that antibiotic resistance in certain bacteria can be targeted by perturbing bacterial redox-homeostasis. Furthermore, we anticipate that these H_2S donors would be useful in future studies aimed towards a better understanding of this gas on redox homeostasis and antibiotic resistance.

References

(1) Dröge, W. *Physiol. Rev.* **2002**, *82*, 47.

(2) Finkel, T. *J. Cell Biol.* **2011**, *194*, 7.

(3) Li, L.; Rose, P.; Moore, P. K. *Annu. Rev. Pharmacol. Toxicol.* **2011**, *51*, 169.

(4) Fang, F. C. *Nat. Rev. Microbiol.* **2004**, *2*, 820.

(5) Flannagan, R. S.; Cosio, G.; Grinstein, S. *Nat. Rev. Microbiol.* **2009**, *7*, 355.

(6) Laxminarayan, R.; Duse, A.; Wattal, C.; Zaidi, A. K. M.; Wertheim, H. F. L.; Sumpradit, N.; Vlieghe, E.; Hara, G. L.; Gould, I. M.; Goossens, H.; Greko, C.; So, A. D.; Bigdeli, M.; Tomson, G.; Woodhouse, W.; Ombaka, E.; Peralta, A. Q.; Qamar, F. N.; Mir, F.; Kariuki, S.; Bhutta, Z. A.; Coates, A.; Bergstrom, R.; Wright, G. D.; Brown, E. D.; Cars, O. *Lancet Infect. Dis.* **2013**, *13*, 1057.

(7) Rossolini, G. M.; Arena, F.; Pecile, P.; Pollini, S. *Curr. Opin. Pharmacol.* **2014**, *18*, 56.

(8) Kohanski, M. A.; Dwyer, D. J.; Hayete, B.; Lawrence, C. A.; Collins, J. J. *Cell*, *130*, 797.

(9) Keren, I.; Wu, Y.; Inocencio, J.; Mulcahy, L. R.; Lewis, K. *Science* **2013**, *339*, 1213.

(10) Liu, Y.; Imlay, J. A. *Science* **2013**, *339*, 1210.

(11) Dwyer, D. J.; Belenky, P. A.; Yang, J. H.; MacDonald, I. C.; Martell, J. D.; Takahashi, N.; Chan, C. T. Y.; Lobritz, M. A.; Braff, D.; Schwarz, E. G.; Ye, J. D.; Pati, M.; Vercruysse, M.; Ralifo, P. S.; Allison, K. R.; Khalil, A. S.; Ting, A. Y.; Walker, G. C.; Collins, J. J. *Proc. Natl. Acad. Sci. U.S.A.* **2014**, *111*, E2100.

(12) Foti, J. J.; Devadoss, B.; Winkler, J. A.; Collins, J. J.; Walker, G. C. *Science* **2012**, *336*, 315.

(13) Gusarov, I.; Shatalin, K.; Starodubtseva, M.; Nudler, E. *Science* **2009**, *325*, 1380.

(14) Shatalin, K.; Shatalina, E.; Mironov, A.; Nudler, E. *Science* **2011**, *334*, 986.

(15) Cottreau, K. M.; Spencer, C.; Wentzell, J. R.; Graham, C. L.; Borissow, C. N.; Jakeman, D. L.; McFarland, S. A. *Org. Lett.* **2010**, *12*, 1172.

(16) Bair, J. S.; Palchaudhuri, R.; Hergenrother, P. J. *J. Am. Chem. Soc.* **2010**, *132*, 5469.

(17) Trung Pham, H.; Marquetty, C.; Pasquier, C.; Hakim, J. *Anal. Biochem.* **1984**, *142*, 467.

(18) Zielonka, J.; Vasquez-Vivar, J.; Kalyanaraman, B. *Nat. Protoc.* **2008**, *3*, 8.

(19) Zhou, M.; Diwu, Z.; Panchuk-Voloshina, N.; Haugland, R. P. *Anal. Biochem.* **1997**, *253*, 162.

(20) Sawa, T.; Zaki, M. H.; Okamoto, T.; Akuta, T.; Tokutomi, Y.; Kim-Mitsuyama, S.; Ihara, H.; Kobayashi, A.; Yamamoto, M.; Fujii, S.; Arimoto, H.; Akaike, T. *Nat. Chem. Biol.* **2007**, *3*, 727.

(21) Rawet-Slobodkin, M.; Elazar, Z. *Mol. Cell* **2013**, *52*, 767.

(22) Ieda, N.; Nakagawa, H.; Peng, T.; Yang, D.; Suzuki, T.; Miyata, N. *J. Am. Chem. Soc.* **2012**, *134*, 2563.

(23) de Boer-Maggard, T. R.; Resendez, A.; Mascharak, P. K. *Chem. Bio. Chem.* **2013**, *14*, 2106.

(24) Sharma, K.; Chakrapani, H. *Nitric Oxide* **2014**, *43*, 8.

(25) Dharmaraja, A. T.; Ravikumar, G.; Chakrapani, H. *Org. Lett.* **2014**, *16*, 2610.

(26) Lin, K.-K.; Wu, S.-C.; Hsu, K.-M.; Hung, C.-H.; Liaw, W.-F.; Wang, Y.-M. *Org. Lett.* **2013**, *15*, 4242.

(27) Zhao, Y.; Biggs, T. D.; Xian, M. *Chem. Commun.* **2014**, *50*, 11788.

(28) Kang, J.; Li, Z.; Organ, C. L.; Park, C.-M.; Yang, C.-t.; Pacheco, A.; Wang, D.; Lefer, D. J.; Xian, M. *J. Am. Chem. Soc.* **2016**, *138*, 6336.

(29) Zheng, Y.; Yu, B.; Ji, K.; Pan, Z.; Chittavong, V.; Wang, B. *Angew. Chem. Int. Ed.* **2016**, *55*, 4514.

(30) Zhao, Y.; Kang, J.; Park, C.-M.; Bagdon, P. E.; Peng, B.; Xian, M. *Org. Lett.* **2014**, *16*, 4536.

(31) Saha, T.; Kand, D.; Talukdar, P. *Org. Biomol. Chem.* **2013**, *11*, 8166.

(32) Shen, X.; Pattillo, C. B.; Pardue, S.; Bir, S. C.; Wang, R.; Kevil, C. G. *Free Radic. Biol. Med.* **2011**, *50*, 1021.

List of Figures

List of Tables

List of Schemes

List of Publications

1. **Khodade, V. S.**; Dharmaraja, A. T.; Chakrapani, H., "Synthesis, Reactive Oxygen Species Generation and Copper-Mediated Nuclease Activity Profiles of 2-Aryl-3-amino-1,4-naphthoquinones" *Bioorg. Med. Chem. Lett.* **2012**, *22*, 3766-3769.

2. **Khodade, V. S**.; Sharath Chandra, M.; Banerjee, A.; Lahiri, S.; Pulipeta, M.; Rangarajan, R.; Chakrapani, H. "Bioreductively Activated Reactive Oxygen Species (ROS) Generators as MRSA Inhibitors" *ACS Med. Chem. Lett*.,**2014**, *5*, 777-781.

3. **Khodade, V. S.**, Kulkarni, A.; Gupta, A. S.; Sengupta, K.; and Chakrapani, H. "A Small Molecule for Controlled Generation of Peroxynitrite" *Org. Lett.* **2016**, *18*, 1274-1277.

4. **Khodade, V. S**.; Shukla, P.; Sharath Chandra, M.; Singh A.; Chakrapani, H. "Design and Development of an Enzyme Activated Hydrogen Sulfide (H_2S) Donor Reveals a Key Role for this Gas in Antibiotic Resistance" *Manuscript under preparation*.

5. **Khodade, V. S**.; Soni, I.; Chopra, S.; Chakrapani, H. "Synthesis and Evaluation of Redox-active Small Molecules as Vancomycin Resistant *S. aureus* Inhibitors" *Manuscript under preparation*.